https://doi.org/10.15388/vu.thesis.1020
https://orcid.org/0000-0003-3111-2702

VILNIUS UNIVERSITY

Justinas Babinskas

Development of Synthetic Substrates for Laccase and Carbonic Anhydrase Functional Characterisation

DOCTORAL DISSERTATION

Technological Sciences,
Chemistry Engineering (T 005)

VILNIUS 2026

The dissertation was prepared between 2020 and 2024 during doctoral studies at Vilnius University and is being defended externally.

Academic Advisor – Dr. Inga Matijošytė (Vilnius University, Technological Sciences, Chemical Engineering – T 005).

The doctoral dissertation will be in a public meeting of the Dissertation Defence Panel:

Chairman – Assoc. Prof. Dr. Audrius Gegeckas (Vilnius University, Technological Sciences, Chemical Engineering – T 005).
Members:
Assoc. Prof. Dr. Arita Dubņika (Riga Technical University (Latvia), Technological Sciences, Chemical Engineering – T005),
Prof. Dr. Renata Gudiukaitė (Vilnius University, Natural Sciences, Biology – N010),
Dr. Nina Urbelienė (Vilnius University, Technological Sciences, Chemical Engineering – T005),
Dr. Asta Zubrienė (Vilnius University, Technological Sciences, Chemical Engineering – T005).

The dissertation shall be defended at a public meeting of the Dissertation Defence Panel at 13:00 on 8th of December 2026 in Room R401 of the Life Sciences Center, Vilnius University.
Address: Saulėtekis av. 7, Vilnius, Lithuania
Tel. +37052234419; e-mail: info@gmc.vu.lt

https://doi.org/10.15388/vu.thesis.1020
https://orcid.org/0000-0003-3111-2702

VILNIAUS UNIVERSITETAS

Justinas Babinskas

Sintetinių substratų, skirtų lakazių ir karboanhidrazių funkciniam charakterizavimui, kūrimas

DAKTARO DISERTACIJA

Technologijos mokslai,
Chemijos inžinerija (T 005)

VILNIUS 2026

Disertacija rengta 2020 – 2024 metais studijuojant doktorantūroje Vilniaus Universitete ir ginama eksternu.

Mokslinė konsultantė – dr. Inga Matijošytė (Vilniaus universitetas, technologijos mokslai, chemijos inžinerija – T005).

Gynimo taryba:
Pirmininkas – doc. dr. Audrius Gegeckas (Vilniaus universitetas, technologijos mokslai, chemijos inžinerija – T005).
Nariai:
doc. dr. Arita Dubņika (Riga Techical University (Latvia), technologijos mokslai, chemijos inžinerija – T005),
prof. dr. Renata Gudiukaitė (Vilniaus iniversitetas, gamtos mokslai, biologija – N010),
dr. Nina Urbelienė (Vilniaus universitetas, technologijos mokslai, chemijos inžinerija – T005),
dr. Asta Zubrienė (Vilniaus universitetas, technologijos mokslai, chemijos inžinerija – T005).

Disertacija ginama viešame Gynimo tarybos posėdyje 2026 m. gruodžio mėn. 8 d. 13:00 val. Vilniaus universiteto, Gyvybės mokslų centro R401 auditorijoje. Adresas: Saulėtekio al. 7, Vilnius, Lietuva, tel. +37052234419; el. paštas info@gmc.vu.lt

CONTENTS

ABBREVIATIONS 7
INTRODUCTION 9
1. **LITERATURE OVERVIEW** 13
1.1. Functional Characterisation of Biocatalysts 13
1.2. Functional Characteristics of Laccases 17
1.2.1. Conventional Substrates for the Functional Characterisation of Laccases ... 21
1.2.2. Alternative Substrates for the Functional Characterisation of Laccases 24
1.3. Functional Characteristics of Carbonic Anhydrase 30
1.3.1. Structure-Function Relationships in Carbonic Anhydrases 31
1.3.2. Hydration-Based Assays for the Measurement of Carbonic Anhydrase Activity 35
1.3.3. Hydrolysis-Based Assays for the Measurement of Carbonic Anhydrase Activity 42
2. **RESULTS AND DISCUSSION** 45
2.1. Ferbamine Development and Application for Laccase Functional Analysis 45
2.1.1. Analysis of Ferbamine Synthesis Mechanism 47
2.1.2. Thermal and pH Stability of Ferbamine 52
2.1.3. Application of Ferbamine in Agar Plates for Laccase Activity Screenings .. 53
2.1.4. Screening of Wild-Type Microorganisms from Dinaric Caves 58
2.2. Development of the Carbonic Anhydrase Substrates 62
2.2.1. Phenyl Azo Dye Carbonate Substrates: Synthesis and Activity Evaluation . 63
2.2.2. Thiocarbonate Ester Substrates: Synthesis and Evaluation 78
2.2.3. In Silico Evaluation of Carbonate and Thiocarbonate Ester Substrates 82
2.2.4. p-Nitrophenyl Carbamate and Carbazate Substrates: Synthesis and Evaluation 87
2.2.5. Phenyl Azo Dye Carboxylic Ester Substrates: Synthesis and Evaluation 89
2.2.6. Development of an E-C-B-Based method for Ad Hoc Identification of Outlying Data Points 96
2.2.7. Comparative Evaluation of the HABSA-Ac Assay with p-Nitrophenyl Acetate and Indoxyl Acetate Assays 102
3. **MATERIALS AND METHODS** 105
3.1. General Procedures 105
3.2. Materials 105
3.3. Synthesis Methods 106
3.3.1. Ferbamine Using Optimised Conditions 106
3.3.2. Phenyl Azo Dyes 107
3.3.3. Phenyl Azo Dye Carbonates 108
3.3.4. Thiocarbonates 110
3.3.5. Carbamates and Carbazates 111
3.3.6. 4-(4-hydroxyphenylazo)benzenesulfonic acid acetate (HABSA-Ac) 114
3.4. Characterisation of Dyes and Substrates 115

3.4.1. UV-VIS Spectroscopy of Ferbamine Solutions 115
3.4.2. Thermal and pH Stability of Ferbamine 115
3.4.3. ATR-FTIR Analysis of Ferbamine Synthesis Products 115
3.4.4. Determination of pK_as for Phenyl Azo Dyes 115
3.4.5. UV-VIS Spectra of HABSA and AO6 116
3.4.6. Determination of Molar Extinction Coefficients 116
3.4.7. Stability of HABSA-Ac in DMSO 116
3.5. Assays 117
3.5.1. UV-VIS Spectroscopic Laccase Activity with Metol 117
3.5.2. Bis(HABSA)c Assays with Amino Acids 117
3.5.3. Esterase Activity Assay with pNPA as the Substrate 118
3.5.4. Esterase Activity Assay with Indoxyl Acetate as the Substrate 118
3.5.5. Lipase Activity Assay with p-Nitrophenyl Palmitate as the Substrate 118
3.5.6. Bradford Protein Assay 119
3.6. Agar Plates for Cultivation and Laccase Activity Screening 120
3.6.1. Ferbamine-Agar Plate With Wells 120
3.6.2. Medium-Agar Plates With Various Ferbamine Concentrations for Cultivation and Screening of Microorganisms 120
3.7. Cave Sampling Sites and Their Physical Parameters 121
3.8. Development of Carbonic Anhydrase Assay With HABSA-Ac as the Substrate 122
3.9. Determination of Carbonic Anhydrase Catalysis Parameters 123
3.9.1. Thermodynamic Parameter Analysis Using Arrhenius and Transitional State Theory (TST) Plots 123
3.9.2. Kinetic Parameter Analysis Using Linewaever-Burk (L-B), Eadie-Hostee (E-H) and Hanes-Wolf (H-W) Plots 124
3.9.3. Kinetic Parameter Analysis Using Eisenthal-Cornish-Bowden (E-C-B) Plot 125
3.9.4. Adaptation of the E-C-B Plot for Outlier Identification in Kinetic Measurement Data 125
3.9.5. Inhibition Data Analysis 125
3.10. Statistical Analysis 126
3.11. *In silico* Methods 126
3.11.1. Amber24 Molecular Dynamics Simulations 126
3.11.2. Semiempirical Extended Tight Binding (xTB) Computations 127
3.11.3. Gamess DFT Computations 127
CONCLUSIONS 128
REFERENCES 129
SUPPLEMENTARY MATERIALS 145
SANTRAUKA 150
ACKNOWLEDGEMENTS 179
LIST OF PUBLICATIONS 180
CONFERENCE LIST 181
CURRICULUM VITAE 183

ABBREVIATIONS

ABTS – 2,2'-azino-bis(3-ethylbenzothiazoline-6-sulfonic acid)
Ac – acetyl group
AcCl – chloroacetyl group
ACN – acetonitrile
AMPD – 2-amino-2-methyl-1,3-propanediol
AO6 – 4-(2,4-dihydroxyphenylazo)benzenesulfonic acid
ARIPA – 5-(2,4-dihydroxyphenylazo)isophthalic acid
ATR-FTIR – attenuated total reflectance Fourier-transform infrared spectroscopy
bCAII – bovine carbonic anhydrase II
bis(AO6)c – bis[4-(2,4-dihydroxyphenylazo)benzenesulfonic acid] carbonate
bis(ARIPA)c – bis[5-(2,4-dihydroxyphenylazo)isophthalic acid] carbonate
bis(HABSA)c – bis[4-(4-hydroxyphenylazo)benzensulfonic acid] carbonate
bis(HPDIA)c – bis[5-(4-hydroxyphenylazo)isophthalic acid] carbonate
BNPC – bis(4-nitrophenyl) carbonate
BSA – bovine serum albumin
C-B – Cornish-Bowden
C-PCM – conductor-like polarizable continuum model
CA – carbonic anhydrase
cHex – cyclohexane
DABCO – 1,4-diazabicyclo[2.2.2]octane
DBU – 1,8-diazabicyclo[5.4.0]undec-7-ene
DCM – dichloromethane
DDAN – 7-hydroxy-9H-(1,3dichloro-9,9-dimethylacridin-2-one)
DET – direct electron transfer
DFT – density functional theory
DHPPA – 3,4-dihydroxyhydrocinnamic acid
DMF – *N*,*N*-dimethylformamide
DMP – 2,6-dimethoxyphenol
DMPD – *N*,*N*-dimethyl-*p*-phenylenediamine
DMSO – dimethylsulfoxide
E-C-B – Eisenthal-Cornish-Bowden
E-H – Eadie-Hofstee
EPR – electron paramagnetic resonance
Et_3N – triethylamine
Et_2O – diethyl ether
EtOAc – ethyl acetate
EtOH – ethanol
H-W – Hanes-Woolf
HABSA – 4-(4-hydroxyphenylazo)benzensulfonic acid
HABSA-Ac – 4-(4-acetoxyphenylazo)-benzenesulfonic acid
hCAIX – human carbonic anhydrase IX
HPDIA – 5-(4-hydroxyphenylazo)isophthalic acid

HPLC – high-performance liquid chromatography
(HR)MS – (high-resolution) mass spectrometry
IRC – intrinsic reaction coordinates
L-B – Lineweaver-Burk
L-DOPA – L-3,4-dihydroxyphenylalanine
LB – Luria-Bertani broth
MBTH – 3-methyl-2-benzothiazolinone-hydrazone hydrochloride
MD – molecular dynamics
MeOH – methanol
mHM – modified Mueller-Hinton
NMR – nuclear magnetic resonance
PAGE – polyacrylamide gel electrophoresis
PDA – potato-dextrose agar media
PhOCS-Cl – *O*-phenyl thionochloroformate
PhOCS-HABSA – 4-(4-hydroxyphenylazo)benzenesulfonic acid phenyl thiocarbonate
pNP – *p*-nitrophenol
pNPA – *p*-nitrophenyl acetate
psCA1 and psCA2 – *Pseudomonas aeruginosa* carbonic anhydrase 1 and 2
Py – pyridine
QM – quantum mechanics
QM/MM – quantum mechanics and molecular mechanics
RBBR – Remazol brilliant blue R
SDS – sodium dodecyl sulfate
T1 – type 1 copper centre
T2/T3 – type 2 and type 3 copper cluster
TCDI – 1,1-thiocarbonyldiimidazole
THF – tetrahydrofuran
TLC – thin-layer chromatography
TOL – toluene
Tris – 2-amino-2-(hydroxymethyl)propane-1,3-diol
TS – trypticase soy broth
TS1 and TS2 – transition state 1 and 2
WA – Wilbur-Anderson
xTB – extended tight-binding
YEPG – yeast extract-peptone-glycerol

INTRODUCTION

The identification and characterisation of novel biocatalysts, as well as their investigation, development and validation in technological applications, rely on functional analysis. Functional analysis methods detect differences in chemical or physical properties between the substrate and the product of the catalytic process (Reymond, 2008). These differences may include oxidation potential, light absorption, electron density, vibrational modes and more. The analysis can also cover observations of physical phenomena induced by the reaction, such as chemiluminescence or changes in free energy (heat). Some of these methods evaluate biocatalytic activity qualitatively, while others use specialised equipment to quantify it numerically (Babinskas and Matijošytė, 2025). Thus, regardless of the techniques used, the substrate is an intrinsic component of biocatalyst functional analysis.

Laccases are multi-copper oxidases (EC 1.10.3.2) that contain T1, T2, and T3 copper sites. Over the years of research on various laccases, a wealth of information has been gathered regarding their catalytic mechanisms, redox potentials, enzyme sources, and potential applications. These enzymes catalyse the unique oxidation of phenols, aromatic amines, and thiols by utilising oxygen as a co-substrate and producing water as a by-product (Jones and Solomon, 2015). This process holds significant potential for industries such as food, textiles, paper, biofuels, cosmetics, paints, furniture, organic synthesis, nanobiotechnology, and bioremediation (Mate and Alcalde, 2017). By employing laccase-mediator systems, the substrate range can be expanded, allowing them to potentially replace hydrogen peroxide and other chemical oxidisers on an industrial scale. However, the practical application of laccases is currently limited by several unresolved challenges, including poor stability, lack of commercial availability, inefficient expression systems, and low immobilisation yields. One limitation to the discovery of laccases with new and novel features is the scarcity of substrates that are suitable for high-throughput screening. Currently, the most common compound used for laccase functional analysis is 2,2'-azino-bis(3-ethylbenzothiazoline-6-sulfonic acid) – ABTS (Babinskas and Matijošytė, 2025). Although spectrophotometric activity assays with this substrate yield acceptable results, ABTS has poor stability, low specificity, and is relatively expensive. Its use in high-throughput screening on agar plates is significantly hindered due to its thermal and pH instability.

Carbonic anhydrases (CAs) are a family of metalloenzymes (EC 4.2.1.1) that catalyse the reversible hydration of CO_2. These enzymes are widely prevalent in nature due to their crucial roles in CO_2 transport and pH

homeostasis. For several decades, CAs have been recognised as pharmacological targets in the study of various human diseases (Aspatwar et al., 2022). Recently, they have gained significant attention as potential biocatalysts for CO_2 capture and collection. Their remarkable speed in CO_2 to bicarbonate conversion is considered one of the fastest enzymatic reactions, making them particularly appealing for CO_2 sequestration (Effendi and Ng, 2019). However, the use of currently available enzymes or their modified versions is often limited by their inherent instability under industrial conditions. To address this issue, researchers are exploring various strategies, such as genetic engineering and enzyme immobilisation. Nevertheless, the effectiveness of these strategies is constrained by the methods used to evaluate enzymatic activity.

The aim of this work was to develop novel synthetic substrates and analytical methodologies for the functional characterisation of enzymes, using laccases and carbonic anhydrases as model biocatalysts.

Research objectives were:

1. To develop and optimise the synthesis of Ferbamine and establish its application in agar plate-based assays for the high-throughput screening of laccase activity.
2. To evaluate the suitability of Ferbamine for detecting laccase activity in diverse biological and environmental sample matrices.
3. To synthesise and structurally characterise a series of phenol azo dye derivatives.
4. To develop synthesis approaches for the preparation of activated phenol azo dye carbonate and thiocarbonate ester substrates.
5. To investigate the applicability of phenol azo dye carbonate, thiocarbonate, acetate, and related ester substrates as functional probes for the characterisation of carbonic anhydrases.

Scientific Novelty

This work addresses a long-standing limitation in high-throughput laccase screening by introducing **Ferbamine as a novel phenazine-based substrate** for agar plate assays. Unlike conventional laccase substrates, Ferbamine was specifically developed to enable rapid, visual, and high-throughput detection of laccase activity in microbial colonies and crude biological samples. A **new synthetic strategy** for Ferbamine was established by modifying the classical methylene blue synthesis based on *N,N*-dimethyl-*p*-phenylenediamine (DMPD). Subsequent optimisation of the reaction conditions resulted in a reproducible synthetic procedure with an increased product yield of up to

0.92%. Furthermore, comprehensive structural characterisation of the reaction intermediates and products by HRMS, NMR, and ATR-FTIR enabled the proposal of **a previously undescribed reaction mechanism** for Ferbamine formation. Beyond explaining the synthesis of a single compound, this mechanism advances the understanding of phenylenediamine oligomerisation chemistry and provides a rational framework for the future design of phenazine-derived amine substrates with improved analytical performance. The applicability of Ferbamine as a laccase substrate was comprehensively validated through physicochemical characterisation, biological evaluation, and large-scale screening. The substrate exhibited high stability under acidic conditions and demonstrated excellent agreement with an established spectrophotometric Metol assay. Its performance was further confirmed using 65 fungal protein extracts representing 42 species, including 26 species that had not previously been investigated for laccase activity. Moreover, the substrate enabled high-throughput screening of 207 environmental isolates from Dinaric caves, leading to the identification of a *Pseudomonas chlororaphis* strain exhibiting pronounced laccase-like activity. These findings demonstrate the suitability of Ferbamine for enzyme discovery and microbial bioprospecting applications.

For the functional characterisation of carbonic anhydrases (CAs), this work explored the **largely underutilised class of carbonate and thiocarbonate ester substrates**, expanding the range of synthetic probes available for studying CA catalysis. Novel transcarbonation methodologies were developed and optimised to synthesise a series of activated azo dye carbonate esters. Among these, bis(HABSA)c emerged as a promising chromogenic substrate for spectrophotometric assays. However, its unexpected interaction with protein structures uncovered **a previously unrecognised limitation** of activated carbonate esters for enzyme activity measurements. To overcome this challenge, a **new experimental strategy** based on selective enzyme inhibition with acetazolamide was established, enabling the catalytic component of substrate hydrolysis to be distinguished from non-catalytic processes and providing a more accurate evaluation of enzyme activity. This work also presents the **first systematic investigation** of azo dye thiocarbonate esters as substrates for carbonic anhydrases. Following the development of three synthetic approaches, a successful route to phenyl HABSA thiocarbonate was established, yielding a substrate that exhibited substantially improved catalytic hydrolysis compared with its carbonate analogue and demonstrating the potential of thiocarbonate esters as an alternative substrate platform for CA functional studies. To further interpret the experimental observations, molecular modelling was employed, revealing

important limitations of current computational approaches for metalloenzyme simulations and providing insights that extend beyond the scope of the experimental system. In parallel, carbamate and carbazate derivatives were synthesised and evaluated as potential CA substrates, demonstrating that these compound classes are not suitable for CA-catalysed hydrolysis and thereby refining substrate selection criteria for future assay development. The major methodological advance of this work was the development of **an acetylated HABSA substrate**, which overcame the limitations observed with carbonate-based compounds. This substrate exhibited superior performance in kinetic, thermodynamic, and inhibition studies compared with the conventional CA substrates *p*-nitrophenyl acetate and indoxyl acetate, representing **a new and improved analytical tool for carbonic anhydrase functional characterisation**. Furthermore, a novel *ad hoc* statistical approach for identifying erroneous kinetic data points was developed, improving the robustness and reliability of Michaelis-Menten analyses and contributing to more accurate enzymatic characterisation.

Statements to be defended:

1. Ferbamine represents a novel phenazine-based substrate for laccase activity detection, combining high thermal stability, low toxicity, and suitability for long-term, high-throughput screening in diverse biological and environmental matrices.
2. The proposed mechanism of Ferbamine formation expands the understanding of phenylenediamine oligomerisation and provides a framework for the rational design of new phenazine-derived substrates.
3. The structure of the carbonyl functional group is a key determinant of susceptibility to carbonic anhydrase-catalysed hydrolysis, with carbonate and thiocarbonate esters serving as enzymatically cleavable substrates, whereas carbamate and carbazate analogues remain resistant to catalysis.
4. 4-(4-Hydroxyphenylazo)benzenesulfonic acid acetate (HABSA-Ac) represents a new generation of carbonic anhydrase substrate, providing superior thermodynamic stability, minimal non-enzymatic autohydrolysis, and enhanced selectivity compared with conventional ester-based assays.
5. The functional performance of synthetic carbonic anhydrase substrates is governed not only by their intrinsic chemical reactivity but also by their interactions with protein structures, demonstrating that substrate design must simultaneously consider catalytic susceptibility and non-catalytic protein binding.

1. LITERATURE OVERVIEW

In 1998, P. Anastas and J. Warner published their most influential work titled "Green Chemistry: Theory and Practice“, outlining the main 12 green chemistry principles (Anastas and Warner, 2000). Ever since then, these guiding principles have become the cornerstones of chemical process development, including the use of catalysts to enhance efficiency, the adoption of alternative organic solvents, the recovery of reagents and solvents, process intensification to reduce resource consumption, and the utilisation of bio-based or renewable raw materials. However, many chemical processes still cannot adhere to all the principles for a variety of reasons: incompatible or expensive solvents, equilibrium reactions, the need for high temperatures or pressures, inefficient catalysts, side or nonspecific reactions, and unrecyclable side-reaction products.

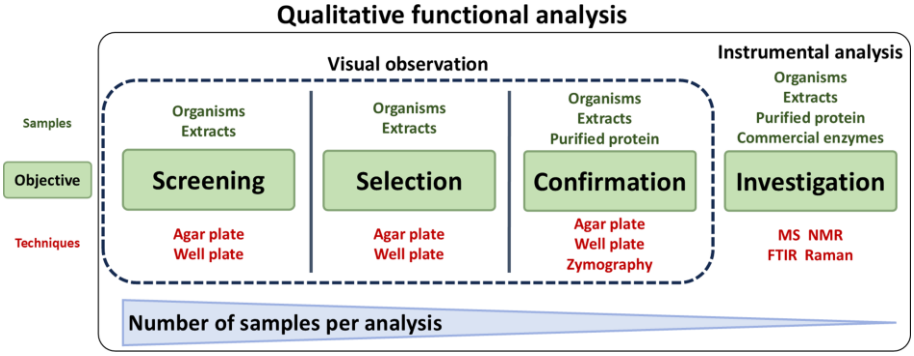
As an alternative to chemical processes, biocatalysis uses enzymes, protein complexes, parts of cells, whole cells, or even multiple strains simultaneously to drive chemical transformations. Biocatalysis has numerous advantages compared to chemical processes: better stereo-, iso-, enantio-selectivity; reactions at atmospheric pressure and minimal heating; water as the most common solvent; minimal side reactions; better usage of bio-based materials; low levels of dangerous reagents; biodegradability and biocompatibility of catalysts. For these reasons, biocatalysis adheres more closely and effectively to the 12 principles of green chemistry. Unfortunately, the application of enzymes is still plagued by the common drawbacks of the biocatalytic process development: commercial unavailability or lack of suitability, high production costs, low activity, stability, or immobilisation yields, and insufficient methods or substrates for their analysis.

1.1. Functional Characterisation of Biocatalysts

To implement biocatalysis processes effectively, it is imperative to analyse the biocatalyst's (enzyme) functionality. Functional analysis involves examining an enzyme’s properties by leveraging the catalytic reaction it catalyses. This process encompasses a wide range of activities, from identifying new enzymes through screening methods to refining engineered biocatalytic processes. A significant challenge is the lack of suitable methods to monitor the activity of many enzymes with high industrial potential. Functional analysis is only feasible when there is a detectable difference between the substrate and the product, and such differences may involve changes in spectral properties, electrochemical signals, physical states, or other measurable attributes (Reymond, 2008). However, highly selective

enzymes often face limitations when interacting with natural substrates, including a lack of detectable responses, instability, low sensitivity, insolubility in the reaction medium, slow reaction rates, or restricted operating conditions (Jonas and Hollfelder, 2008). Synthetic compounds offer alternative options but may not accurately mimic natural catalytic processes. Enzymes with high substrate promiscuity can interact with a broader range of substrates, making them compatible with a wider range of methods and assay conditions.

Enzyme functional analysis approaches can be broadly categorised into two types based on the results they procure: qualitative (**Scheme 1.1**) and quantitative (**Scheme 1.2**).



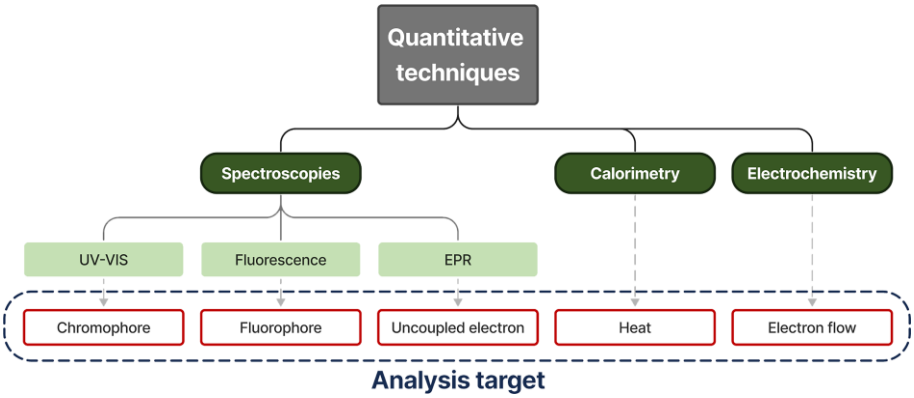
Scheme 1.1 Types of samples, objectives and techniques used in qualitative functional analysis (Babinskas and Matijošytė, 2025).

Qualitative methods primarily rely on visual observations to assess enzyme activity. Agar plates are the most versatile technique in qualitative functional analysis. It is used to identify, select and confirm organisms capable of producing the targeted enzymes. This technique works by observing a colour change around the microorganisms when they are incubated on an agar medium supplemented with nutrients and an enzymatic substrate. Generally, well-plate methods are associated with UV-Vis spectroscopy using plate readers. Still, in complex matrices, with unidentified or nontransparent samples, qualitative analysis can provide rapid screening, selection, confirmation, rough estimation, or comparison of enzymatic activities (Choolaei et al., 2021). The zymogram technique is based on performing polyacrylamide gel electrophoresis (PAGE) under native conditions – proteins maintain their structural and catalytic properties while trapped in the gel. It visualises the targeted enzymes by incubating the PAGE gel in a selective substrate solution. Zymography is primarily used to confirm enzyme catalytic activity after production or purification (Cen et al., 2022; Gao et al., 2024). In some cases, instrumental analysis is also employed to study the biocatalytic

process or the produced compounds. The qualitative data obtained from these techniques can provide information on molecular weight distribution (mass spectrometry [MS]), chemical shifts (nuclear magnetic resonance [NMR]), or vibrational modes (infrared [FTIR] or Raman spectroscopy). Although these methods do not generate numerical data, they provide valuable insights into the enzyme‘s functionality (Jain et al., 2020). The appeal of qualitative techniques stems from their simplicity: most methods do not require complex equipment, support parallel analysis of a large number of samples without robotics or automation, have protocols that are relatively easy to use and replicate, and are often flexible enough to accommodate a wide range of working conditions.

The above-mentioned techniques are typically associated with qualitative information; there are ways to obtain (semi)quantitative results. Examples include agar plates, where the radius of colour change around colonies is measured to estimate and compare catalytic activities among colonies (Mallerman et al., 2019). Results from well plates containing non-transparent samples can be correlated with a series of positive controls that exhibit gradual outcomes (Labus and Maniak, 2023). Easy-to-use, license-free software can process zymography gels from photos and provide relative response strengths, create calibration curves, and much more (National Institutes of Health, 2010). Additionally, instrumental analyses, such as MS or NMR, can utilise compounds with predetermined concentrations and properties as internal standards.

Quantitative functional techniques use specialised equipment to directly measure the substrate‘s depletion or product formation to assess the catalytic activity and provide numerical data (**Scheme 1.2**) (Bisswanger, 2014).



Scheme 1.2 Quantitative functional analysis techniques and their analysis targets (Babinskas and Matijošytė, 2025).

The enzymatic activity, expressed numerically, enables easy analysis and comparison of results. By far, the most applied quantitative analysis technique is UV-Vis spectroscopy. It measures changes in light absorption over time to quantify enzymatic activity as the amount of substrate converted (μmol) per minute at the defined pH and temperature. Additionally, spectroscopy provides a convenient means of performing kinetic measurements, which are essential for elucidating catalytic mechanisms. The majority of published or commercially available enzymatic assays use UV-Vis spectroscopy. Fluorescence spectroscopy is a technique that measures the intensity of light emitted by excited compounds. Although it is a popular technique for some enzyme activity assays (Mogalisetti and Walt, 2016), the simplicity and convenience of UV-Vis spectroscopy make fluorimetry less appealing. Electron paramagnetic resonance (EPR) spectroscopy is a technique that records the energy absorption behaviour of unpaired electrons in external magnetic fields. It is primarily used to analyse chemical moieties such as transition-metal complexes and inorganic and organic radicals (Jones and Solomon, 2015). Calorimetry refers to techniques that measure the heat absorbed or released during enzyme-ligand interactions or catalytic processes. In the study of enzymatic catalysis, calorimetric techniques are mainly used to measure thermodynamic or kinetic parameters such as total molar enthalpy, Michaelis-Menten parameters, enzymatic activity, or inhibition parameters. Calorimetry has an advantage over spectrophotometric methods because it directly measures reaction processes rather than changes in substrate or product concentration. This makes it more sensitive and requires lower concentrations of the enzyme or substrate than spectroscopy, although the enzyme and other components must be of higher quality as well. Electrochemical analysis is a fundamental method for studying enzymes that catalyse redox reactions. This especially applies to enzymes that operate via the outer-sphere oxidation mechanism. The probability and rate of substrate oxidation depend not only on the substrate coordination in the active site but also on the difference in redox potential between the substrate and the enzyme (Glazunova et al., 2018). Electrochemical methods permit the measurement of potential differences in enzyme-substrate systems and the analysis of the substrate-catalysis mechanism. Also, reaction rates or substrate concentration are measured as electrical current between the enzyme and electrode in direct electron transfer (DET) or by detecting changes in current generation due to electroactive compounds (Palanisamy et al., 2017; Jamshidinia et al., 2017).

In rarer cases, functional analysis is used to study the formed products rather than the enzyme's activity. It helps to determine catalysis mechanisms, secondary processes following catalysis, and enzyme selectivity towards

substrates (Wang et al., 2022; Peng et al., 2021). To achieve this, robust techniques such as MS, NMR, FTIR or Raman spectroscopy are used. They are widely employed in organic chemistry to determine molecular structures and provide information about the processes occurring.

In conclusion, enzyme functional analysis relies on a range of complementary methods rather than a single universal technique. Selecting the right approach depends on the substrate and the properties under investigation, while ongoing methodological advances continue to improve speed, sensitivity, and compatibility with throughput strategies.

1.2. Functional Characteristics of Laccases

Laccase is an enzyme that belongs to the family of blue oxidases (EC. 1.10.3.2). It catalyses a mono-electronic oxidation reaction, coupled with oxygen reduction to water. Although it is classified as a benzendiol oxidoreductase, its substrate range is much broader, encompassing aromatic hydroxyls, thiols, and amines. Laccase is also attributed to multi-copper oxidases as its active site contains four Cu(II) ions in three copper centers – T1, T2 and T3 (**Figure 1.1**) (Enguita, 2011).

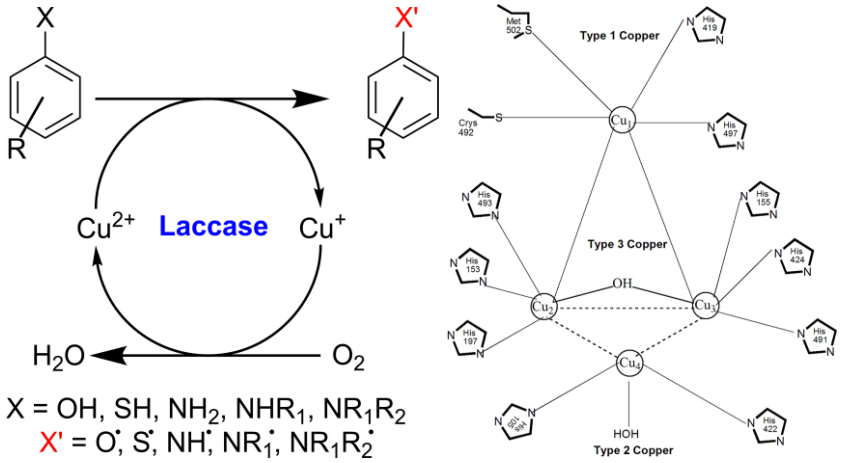


Figure 1.1 Simplified laccase catalysis reaction and the active site of *Trameter versicolor* laccase (Enguita, 2011; Christopher et al., 2014).

These centre-complexes are classified into types according to the number of copper ions and their spectroscopic properties. T1 is made of one copper ion and is complexed by two His and one Cys amino acids. Axial (fourth) amino acid may be Met, Phe, Leu or may be absent depending on the origin of the enzyme (Ducros et al., 1998). The T1 center exhibits an intense absorption band at ~600 nm (ε ~5000 M^{-1} cm^{-1}) due to charge transfer (Cys)S^{-}→Cu(II). Another characteristic of the T1 is its EPR signal of parallel hyperfine

coupling (A_{II} 40-90 × 10^{-4} cm^{-1}) (Jones and Solomon, 2015). The redox properties of the laccase are determined by the T1 redox potential, strongly influenced by its axial ligand and geometry (Palmer et al., 1999), which can range from ~0.4 V to ~0.8 V vs NHE (Zimbardi et al., 2016). T2 centre also contains one Cu(II) ion with two His amino acids, but its third ligand is a water molecule. Lacking a ligand with a strong charge transfer capability, T2 does not exhibit UV-Vis absorption, but has a parallel hyperfine coupling constant A_{II} 140-200 × 10^{-4} cm^{-1} (Jones and Solomon, 2015). T3 is a binuclear Cu(II) centre where each ion is complexed by three His and connected by a bridging OH^- ligand. Charged ligand exhibits a charge transfer to the Cu(II) ions, which is observed as an absorption band at ~330 nm, but it also creates an antiferromagnetic coupling, which makes T3 undetectable in EPR (Jones and Solomon, 2015). In laccase, T2 and T3 are commonly referred to as the T2/T3 trinuclear cluster due to their combined participation in catalysis.

The laccase catalytic mechanism comprises three main steps: substrate oxidation, electron transfer, and oxygen reduction. It is classified as a ping-pong-type mechanism because the enzyme catalyses reactions on more than one substrate and passes through intermediate forms (Arregui et al., 2019). Currently, the mechanism of catalysis is still not fully understood, but the main principles are well known. The first step is the oxidation of the substrate and the reduction of T1. T1 centre is located near the surface of the enzyme. It binds the substrate and catalyses a mono-electron oxidation, producing a substrate radical (Mehra et al., 2018). At the same time, T1 accepts one electron and is reduced from Cu(II) to Cu(I) ($T1_{red}$). The second catalysis step involves electron transfer from $T1_{red}$ to the T2/T3 cluster. They are connected by a Cys-His chain with a supplementary hydrogen bond network. This connection creates a super-exchange pathway for electron transfer between the copper centres (Jones and Solomon, 2015). Electron transfer oxidises the $T1_{red}$ back to Cu(II) while one of the T2/T3 cluster copper ions accepts the electron and is reduced to Cu(I). The T1 Cu(II) regeneration allows it to catalyse substrate oxidation again. Then, electron transfer between $T1_{red}$ and T2/T3 reduces another copper ion in the cluster. This loop, in total, is repeated three times until T2/T3 coppers are fully reduced to Cu(I) – $T2/T3_{red}$. The fourth substrate oxidation also reduces the T1, but the $T2/T3_{red}$ cannot accept more electrons – laccase enters a fully reduced state. The third step of catalysis is the reduction of molecular oxygen. $T2/T3_{red}$ can coordinate a co-substrate – molecular oxygen. Four electrons, which are stored in the four Cu(I) complexes, together with four H^+, are used to reduce the oxygen molecule to two water molecules (Jafari et al., 2020). This step of the catalysis mechanism is the most investigated, as the intermediate changes in the $T2/T3_{red}$-O_2 are not

completely clear. A plethora of investigations using mutagenesis (Gabdulkhakov et al., 2019), crystallography and inhibition (Polyakov et al., 2019), spectroscopies (Yu et al., 2024) and computational methods (Jafari et al., 2020) have produced several possible scenarios. A few more accepted pathways are presented in **Figure 1.2**.

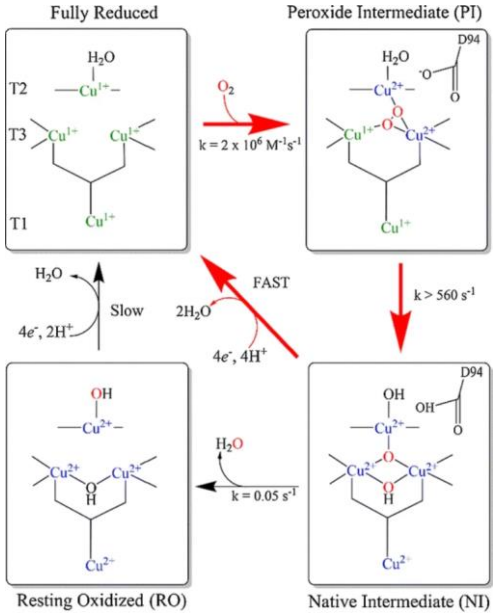


Figure 1.2 Proposed O_2 reduction pathways. Reaction starts from the fully reduced state (Jones and Solomon, 2015).

It has been suggested that during regular catalytic activity (red arrows), two water molecules are released in a single step. However, the enzyme can enter a resting, oxidised state (black arrows), releasing water molecules in a series and exhibiting lower catalytic activity (Jones and Solomon, 2015).

Laccase can be found in various organisms, including insects, bacteria, higher plants, and fungi. In most species of insects, laccase is an integral part of the cuticle formation. It catalyses the oxidation of L-DOPA and its derivatives to the appropriate *o*-quinones (Arakane et al., 2009). After further modification by other enzymes and laccase, these compounds react to form melanin, yellowish pigments, and participate in sclerotisation – the hardening of the insect cuticle (Asano et al., 2019). In plants, laccase is a commonly found enzyme whose primary function is lignin polymerisation, with additional roles in wound healing and iron oxidation (Dwivedi et al., 2011). It has been reported that some plant species even express multiple laccase genes (Ranocha et al., 1999). Laccase has been found in almost every wood-rotting fungi and is best known for its function in lignin degradation (Hoegger et al.,

2006). Brown-rot and white-rot fungi families are the best characterised and investigated sources of lignin-modifying and laccase-like enzymes. One of the best commercially available laccases is derived from the white-rot fungus *Trametes versicolor* and is available from well-known distributors such as Sigma-Aldrich. Laccase has also been linked to melanin biosynthesis in fungi, which is essential for their survival (Eisenman and Casadevall, 2012). Bacterial laccases are the latest addition to the laccase family. In *Bacillus subtilis*, CotA laccase functions as a catalyst for the biosynthesis of brownish pigment during sporulation. The pigment acts as a UV shield, protecting the bacteria from oxidising compounds (Hullo et al., 2001). Additionally, laccase-like enzymes are associated with bacterial degradation of humic substrates in polar soils (Park et al., 2021). Bacterial laccases have been shown to exhibit higher thermal stability and to function at alkaline pH (Gunne and Urlacher, 2012), which is uncharacteristic for this family of enzymes. High salt resistance is also a key feature of bacterial laccases (Arregui et al., 2019). Laccases can also be classified according to their redox potential. Fungal laccases generally exhibit higher oxidation potential, typically between ~400 mV and ~800 mV vs NHE. Bacterial, plant, and insect laccases fall under the low redox potential category, ranging from ~100 mV to ~450 mV (Jones and Solomon, 2015).

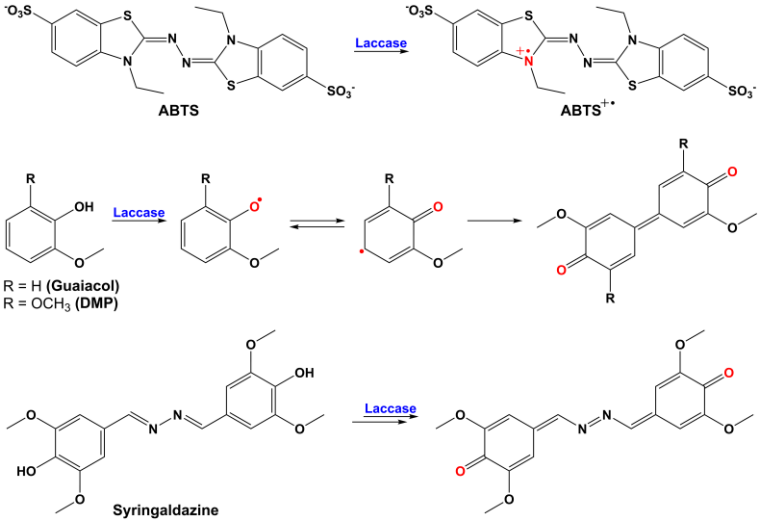
Lignin is an amorphous polyphenol and the second most abundant biopolymer in nature by mass. It is found in all lignocellulosic biomass, the main constituent of plant life. In many industries, lignin is an unwanted by-product that must be removed during manufacturing to produce higher-quality products. For example, most of the cost of paper manufacturing is due to lignin removal in the Kraft process. This process uses a $NaOH/Na_2S$ mixture at high temperatures to break down lignin into water-soluble oligomers (Argyropoulos et al., 2023). Laccase belongs to the family of lignin-modifying enzymes. This family comprises oxidoreductases, which catalyse reactions that modify lignin structure – creating, altering, or breaking chemical bonds found in lignin. Most of these enzymes are peroxidases – manganese peroxidase, lignin peroxidase, unspecific peroxidase, and more (da Silva Vilar et al., 2022). Peroxidases use hydrogen peroxide as a co-catalyst for oxidation, whereas laccase uses molecular oxygen. Lignin is highly resistant to chemical modification and processing, making it almost unusable. Lignin-modifying enzymes could serve as an alternative to chemical processes for lignin removal. Unfortunately, using a large amount of hydrogen peroxide in large-scale manufacturing is unfavourable; thus, laccases are considered a better option. In addition, laccases can oxidise redox mediators – small molecules which participate in redox reactions as electron carriers between reactants

(Brogioni et al., 2008). Some mediators not only increase the rate of substrate oxidation but also expand the substrate range and even allow the oxidation of non-aromatic substrates, such as benzyl alcohol (Marjasvaara et al., 2004). The promiscuity of laccases and laccase-mediator systems makes these enzymes very attractive for bioremediation, organic synthesis, textiles, paper, food, dyes, cosmetics production, and biofuel cells (Mate and Alcalde, 2017).

1.2.1. Conventional Substrates for the Functional Characterisation of Laccases

There are many methods for the functional analysis of laccases, which typically involve aromatic compounds. However, four particular substrates are more frequently utilised in laccase studies than any other compounds (**Table 1.1**).

Table 1.1. The catalysis of the conventional substrates, and their main advantages and disadvantages in the application of laccase functional analysis.



Name	Advantages	Disadvantages	Ref.
ABTS	High sensitivity Easily discernible colour Fast catalysis rate	Low selectivity Low stability Expensive	Labus and Maniak, 2023; Mander et al., 2006
Guaiacol	High sensitivity Fast catalysis rate Easily discernible colour Inexpensive	Low stability	Moshtaghioun et al., 2011; Agrawal and Verma, 2019
DMP	Inexpensive	Low sensitivity	Kontro et al., 2020
Syringaldazine	High stability	Low sensitivity Expensive Low water solubility	Ali et al., 2020

Of the four, ABTS (2,2'-azino-bis(3-ethylbenzothiazoline-6-sulfonic acid)) is the most widely used in laccase research. It is highly sensitive to laccase activity, and its mono-oxidation product ($ABTS^{\bullet+}$) exhibits an intense and easily discernible green colour (Mander et al., 2006). Guaiacol (2-methoxyphenol) and DMP (2,5-dimethoxyphenol) are phenol-type substrates similar to the monomers of the natural laccase polyphenol substrate, lignin (Kontro et al., 2020). Their oxidation products are phenoxy radicals, which undergo further coupling reactions to produce dark brown-coloured compounds (Dawel et al., 1997; Schirmann et al., 2018). Syringaldazine (4-hydroxy-3,5-dimethoxybenzaldehyde azine) is also a standard option (Hullo et al., 2001), but due to its lower water solubility, it is less applied than ABTS, guaiacol, or DMP.

The four compounds mentioned are quintessential substrates for analysing laccase functional properties; nonetheless, they have a few shortcomings. ABTS oxidation is catalysed not only by laccases but also by phenol oxidases (Bach et al., 2013), bilirubin oxidases (Kimura and Kamagata, 2016), peroxidases (Liberato et al., 2018), and more (Kocabas et al., 2008). Guaiacol, DMP and syringaldazine are also catalysed by enzymes other than laccase (Pieczul et al., 2020; Solano et al., 2001; Bala et al., 2016). In short, these substrates are sensitive to oxidoreductase catalytic activities but not specifically to laccases. Consequently, they are primarily employed to confirm or measure laccase activity in organisms capable of producing the enzyme (Toker et al., 2021), or after production *via* expression systems (Itoh et al., 2021), fermentation (Jutinico-Shubach et al., 2022), or chromatographic purification (La et al., 2023), rather than to observe it in completely unexplored or unknown samples. Usually, only one of these substrates is used to confirm the activity, assuming that laccases have the same selectivity towards the substrates, or further differentiation is performed (Jordaan and Leukes, 2003). However, zymography showed that three fungal laccases preferred ATBS and guaiacol, followed by DMP, with syringaldazine showing the lowest preference (Agrawal and Verma, 2019). For other types of laccases, such as bacterial, plant, or insect laccases, substrate sensitivity has been observed on a case-by-case basis but has not been explored systematically. Another drawback of these general substrates is their susceptibility to autooxidation induced by external factors. It is well known that ABTS has limited stability in solution and is vulnerable to autoxidation induced by oxygen in air, thermal effects, irradiation, or impurities (Tsujimura et al., 2001; Lee and Yoon, 2008; Peng et al., 2023). Guaiacol and DMP are considered to be more stable but still exhibit similar inadequacies (Li et al., 2023).

Despite the listed shortcomings, the use of these general substrates is particularly prominent in agar plates, well plates, zymography and UV-Vis spectroscopy assays. Among these, ABTS and guaiacol are the most frequently used substrates in the agar technique. Syringaldazine, 1-naphthol, DMP and other phenols are also used (Mallerman et al., 2019; More et al., 2011; Zavarzina et al., 2018; Batista-García et al., 2017) but to a lesser extent. That is to say, the use of ABTS and guaiacol, along with reports of their stability, creates a discrepancy. It is rarely stated in published research, but many authors could attest to the problematic nature of ABTS autooxidation. Sigma-Aldrich®, one of the distributors of ABTS, in the product description issued warnings about the stability of ABTS solution: "is sensitive to heavy metal ions", "should be prepared fresh each day", "at room temperature, exposed to oxygen and light may turn dark green within an hour or two" (ABTS Sigma-Aldrich®). Meanwhile, the substrate-agar preparation and application directly contradict these warnings: the substrate is added to warm, salt-containing agar, and the plates are then incubated for days at elevated temperatures. This disagreement raises fundamental and practical questions.

Well-plate techniques and general substrates cover both qualitative screening and quantitative UV-Vis assays. The former approach uses conventional substrates, mainly ABTS (Jia et al., 2022), in a rather unique setup. For instance, Labus and Maniak (2023) extended the ABTS stability in solution at 4 °C from ~5 days to more than 20 days by immobilising it in a gelatine-based hydrogel within the wells of a 96-well plate. Dias and co-workers (2017) produced ABTS-impregnated paper discs for a quick (10-minute) screening of collected fractions in a well-plate after chromatographic purification.

The quantitative approach utilises the fact that the oxidation of conventional substrates catalysed by laccase produces compounds with high molar extinction coefficients in the visible spectrum: $ABTS^{\bullet+}$ (ε_{420} 36000 M^{-1} cm^{-1}) (Baltierra-Trejo et al., 2015), $guaiacol_{ox}$ (ε_{470} 6400 M^{-1} cm^{-1}) (Kenzom et al., 2014), DMP_{ox} (ε_{470} 27500 M^{-1} cm^{-1}) and $syringaldazine_{ox}$ (ε_{530} 65000 M^{-1} cm^{-1}) (Ali et al., 2020). Their oxidation processes can be measured at short intervals (1-10 min) using a standard spectrophotometer or a well-plate reader. UV-Vis assays are typically conducted alongside blank and control reactions to account for inaccuracies caused by substrate autooxidation or by sample effects. However, it is essential to note that $ABTS^{\bullet+}$ is generally used to measure the antioxidant properties of compounds and mixtures by observing its reduction (Ilyasov et al., 2020; Dong et al., 2015); thus, any compound with reduction potential can influence ABTS assays. Terron et al. (2004) demonstrated that tannic acid, a common polyphenol found in wood biomass,

directly interferes with the laccase-ABTS assay by reducing the $ABTS^{\bullet+}$, but not DMP oxidation products.

To summarise, the general substrates are and will remain the most commonly used choice for laccase functional analysis. This is because they are well-investigated, readily available, and have thoroughly optimised protocols. Yet, some of their drawbacks become evident across various analytical methods; thus, most functional analysis methods require more specialised compounds or approaches that can provide superior alternatives to general substrates.

1.2.2. Alternative Substrates for the Functional Characterisation of Laccases

In this section, a discussion of non-conventional (alternative substrates for choice), approaches and strategies for individual techniques will cover their applications, limitations, and recommendations (**Table 1.2**). The *agar plate* technique is commonly used to screen microorganisms for potential biocatalytic activity. Laccases, enzymes capable of oxidising xenobiotic compounds such as dyes, are often studied in this context if they are biocompatible and soluble in an agar medium (Fernández-Remacha et al., 2022; Juárez-Hernández et al., 2021; Martorell et al., 2012; Eichlerová et al., 2006). The only downside of this approach is that data on the dye's toxicity to a particular organism may not be available in advance, or that biodegradation is not catalysed by a laccase. Although the catalytic mechanism of action in the nature of laccase has not been fully elucidated, lignin is attributed to it as one of its natural substrates (Kameshwar and Qin, 2017). Due to its high potential for industrial applications, lignin is widely researched. Lignin is a vital substrate in the agar plate technique for identifying lignin-modifying microorganisms. It is utilised in two ways: direct observation or staining with a solution. In the direct observations, lignin is added to agar as the sole or primary carbon source. That way, only the organisms capable of lignin degradation and absorption can grow on the medium (Ahmed et al. 2018; Dev et al. 2023). It is a straightforward and accessible way to identify the lignin-degrading microorganisms. The second approach uses a staining solution ($FeCl_3$ and $K_3[Fe(CN)_6]$) after the organism has been cultivated for a specific time. The redox reaction between phenols in lignin and the staining mixture produces Prussian blue ($Fe_4[Fe(CN)_6]_3$), while the area with degraded lignin stays clear (Paramjeet et al., 2018). This method is suitable for screening organisms that may not be particularly efficient or naturally participate in lignin degradation but produce functional enzymes. Lignin-agar methods are one of the best ways to identify and screen lignin-degrading organisms, but

Table 1.2 Non-conventional substrates for laccase functional analysis: techniques, applications and limitations (Babinskas and Matijošytė, 2025).

Substrates	Technique	Application	Limitations	Ref.
Poly R-787, RBBR (dyes) Lignins/Prussian blue staining	Agar plates	Microorganism screening for lignin, dye degradation	Non-natural substrates Low selectivity Substrate toxicity	Kiiskinen et al., 2004; Fernández-Remacha et al., 2022
1,8-diaminonaphalene, benzidine, *o*-tolidine, *p*-anisidine (aromatic amines) DHPPA/MBTH co-staining mixture RBBR, Reactive Blue 4, Indigo carmine, Bromophenol blue, Brilliant green (dyes)	Zymography	Identification of targeted enzyme in protein mixtures	Protein denaturation or loss of activity under PAGE conditions	Agrawal and Verma, 2019; Rühl et al., 2013; Zeng et al., 2011
BRRB, Poly R-787 (dyes) Phenols/amines Lignins/Folin-Ciocalteu reagent	UV-Vis spectroscopy	Mechanism investigations Catalysis kinetics Activity characterisation	Low catalysis rates	Pardo et al., 2013; Areskogh et al., 2010; Xu et al., 2018
Amplex red, DDAN, phenylacetic acids, *N*-benzoyl leucomethylene blue, L-DOPA-g-C_3N_4	Fluorescence spectroscopy	Activity measurements in complex media	Expensive substrates General substrates are not employable	Wang et al., 2017; Tian et al., 2019
Lignins 2,6-dimethoxyphenols, violuric acid, 4-aminodiphenylamine, tyrosine Prussian blue	EPR spectroscopy	Mechanistic investigations Catalysis kinetics	Applicable only for molecules with unpaired electrons	Munk et al., 2017; Perna et al., 2019
Lignins, lignin monomers and structurally similar compounds Amines	Calorimetry	Thermodynamic parameters Catalysis kinetics	Require high-grade enzymes and substrates	Wang et al., 2000; Islam et al., 2022
Oxygen (O_2) Phenols	Electrochemistry	Electrochemical characterisation Activity assays	Enzyme immobilisation or use of mediators	Palanisamy et al., 2017; Shleev et al., 2005; Lopes et al., 2019
Natural materials Pollutants, dyes Amines/phenols	Mass spectrometry	Mechanistic investigations Product analysis	Expensive equipment	Saito et al., 2005; Sousa et al., 2014
Catechols Lignin phenols	NMR spectroscopy	Mechanistic investigations Product analysis	Expensive equipment Analyte isolation Complex results	Deshaies et al., 2021
Lignins Amines Pollutants	FTIR/Raman spectroscopy	Mechanistic investigations Product analysis	Insufficient information	Lähdetie et al., 2009; Feng et al., 2023

they have several drawbacks. Firstly, the lignins used in these methods are chemically altered, alkaline or Kraft-type lignins, because they are water-soluble (Sharan et al., 2024; Umashankar et al., 2018). Native lignin is insoluble and more recalcitrant, so using altered lignins may not represent the occurring processes. Secondly, laccase is not the only enzyme capable of lignin degradation. Several other enzymes, primarily peroxidases, participate in lignin degradation and are found in lignin-modifying organisms (Ambatkar et al., 2021; Nurul-Aliyaa et al., 2023). Thirdly, the Prussian blue method is not a continuous assay – adding the staining mixture impedes further growth of the organisms. Therefore, it is unsuitable for monitoring lignin degradation. Lastly, Pointing (1999) has noted that staining only indicates the degradation of phenolic components and should not be used to suggest complete degradation. In conclusion, the agar plate technique can employ general substrates, or lignin and dyes as viable alternatives, but there are limitations regarding assay conditions or enzyme specificity. For routine confirmation of activity, the agar-plate technique lacks substrates specifically designed and biocompatible with high resistance to environmental effects.

The first substrates for laccase *zymography* were the amine compounds, such as benzidine (Prillinger and Molitoris, 1979), 1,8-diaminonaphthalene (Hoopes and Dean, 2001), *o*-tolidine (Sun et al., 2004) and *p*-anisidine (Téllez-Téllez et al., 2005). Recently, the amine substrates were phased out in favour of general substrates, and their performance was satisfactory if the enzyme concentration or activity was substantial. Otherwise, a method using DHPPA (3,4-dihydroxyhydrocinnamic acid) as a substrate, in which the two-electron oxidation product reacts with the coupling reagent MBTH (3-methyl-2-benzothiazolinone-hydrazone hydrochloride) to form a brown-coloured adduct, is a better option (Rühl et al., 2013; Schulze et al., 2019). The advantage of this approach is that the gel is incubated "until protein bands show up"(Rühl et al., 2013), which is not recommended for general substrates due to their autooxidation. Another approach for zymography is to use coloured compounds to observe their discolouration. For this reason, dye solutions are used in gel staining to identify laccases capable of discolouring them (Jutinico-Shubach et al., 2022; Zeng et al., 2011; Iracheta-Cárdenas et al., 2016). It should be noted that dye degradation is not a laccase-specific process and can be catalysed by other enzymes (Liu et al., 2009). In summary, the general substrates are well-versed compounds for zymography. In case of their ineffectiveness, methods using synthetic dyes or co-staining with DHPPA/MBTH mixture are available. Still, the co-staining approach is underutilised in zymography, which enables the observation of a broader

range of typically inapplicable compounds (Hilgers et al., 2018; Sherif et al., 2013).

In addition to conventional substrates, *UV-Vis spectrophotometric* laccase activity assays rarely use other substrates. Various methoxy-, hydroxy-, and amine phenols are used to characterise enzyme properties against different substrates (Xu, 1996) or to investigate the application of laccase (Sun et al., 2013). These compounds, like general substrates, are characterised by the observation of oxidation products. Another approach in UV-Vis spectroscopy assays is to observe a decrease in absorbance. This principle is widely used to assess the efficiency of dye biodegradation. Dye compounds are ideal for this purpose because they are generally stable, have high molar extinction coefficients, and are readily available. Some commonly used dyes include Poly R-478 (Alcalde et al., 2002) and RBBR (Xu et al., 2018), but laccase-dye assays can involve any soluble dye. Areskogh and co-authors (2010) published noteworthy work in which they adapted the Folin-Ciocalteu reagent for phenol content determination to investigate laccase-catalysed polymerisation of lignosulfonates. Polymerisation is evaluated by the decrease in phenolic content of lignosulfonate. Building on this concept, a high-throughput screening method for the spectrophotometric well-plate technique was developed by Rodriguez-Escribano et al. (2017). The authors concluded that this method could also be used to screen for lignosulfonate depolymerisation. To summarise, UV-Vis spectrophotometry employs the general substrate for laccase activity measurements. However, some studies have found that they can lead to inaccurate results due to longer assay times or side reactions with other compounds. To avoid these issues, Moshtaghioun and colleagues (2011) suggest developing novel substrates that monitor substrate depletion rather than analysing unstable products. Though dye compounds or lignins could be considered, their oxidation rates are too low to be viable for enzymatic activity assays.

Specialised substrates, such as *N*-benzoyl leucomethylene blue (Ren et al., 2023), Amplex Red (10-acetyl-3,7-dihydroxyphenoxazine) (Wang et al., 2017), 4-hydroxyphenylacetic acid, DDAN (7-hydroxy-9H-(1,3-dichloro-9,9-dimethylacridin-2-one)) (Tian et al., 2019), (3-methoxy-4-hydroxyphenyl)acetic acid (Lonergan et al., 1997), and L-dopa-(carbon nitride) (Arabi et al., 2020) are used to determine the level of laccase activity using *fluorescence spectroscopy*. The use of this approach provides an alternative to UV-Vis spectroscopy, while supporting higher sensitivity and lower enzyme consumption. Nonetheless, the narrow selection of substrates combined with their cost makes fluorometry less applied than other spectroscopies.

EPR spectroscopy is not commonly used to observe substrates because most organic radicals quickly undergo a second oxidation or recombination reaction (**Table 1.2**). Still, it is suitable for analysis when oxidation of the substrate yields detectable moieties. Munk et al. (2017) have demonstrated that it is possible to directly assess the dynamics of radical formation in lignin catalysis by laccase. Building on that, Perna and others (2019) developed a method to determine the kinetic parameters of the laccase-lignin reaction and to calculate Michaelis-Menten parameters. EPR is also applicable to investigating catalytic mechanisms and secondary reactions (Zippilli et al., 2021; Martorana et al., 2014), the generation or decay of radicals (Felby et al., 1997; Spulber et al., 2014), and the materials produced (Carić et al., 2015; Mattinen et al., 2005). In brief, EPR is a highly specialised technique with a limited range of applications. Nonetheless, it enables direct observation of the lignin-laccase reaction and provides invaluable data on reaction rates and process parameters.

Calorimetry is not commonly used in laccase investigations, and the range of substrates employed is mainly limited to general substrates or simple phenols and amines (Wang et al., 2000; Ebrahimi et al., 2015; Volkova et al., 2012). Though recently, Islam et al. (2022) demonstrated that calorimetry could be used to measure the Michaelis-Menten kinetics of Kraft lignin conversion and reaction molar enthalpy. Currently, the only other technique capable of measuring the kinetic parameters of the laccase-lignin reaction is EPR. Still, the calorimetric approach is underused, especially in investigating the enzymatic catalysis of lignin. One reason it may be overshadowed by other established methods, such as UV-Vis assays, is their wider availability.

Electrochemistry is a unique approach for laccase functional analysis because it directly uses molecular oxygen as a substrate to determine the enzyme's redox potential. This analysis measures the electric potential required for the laccase to accept electrons via the DET mechanism from the electrode to the T1 copper site, reducing molecular oxygen (Lopes et al., 2019; Aleksejeva et al., 2019). These experiments require that laccases be immobilised on the electrode surface, which presents its own challenges (Tominaga et al., 2023). In another approach, using mediators, small molecules acting as electron transporters between the enzyme and electrode, allows for the avoidance of enzyme immobilisation (Cui et al., 2021), but can be limited by the mediator diffusion or degradation rates (Saha and Mukhopadhyay, 2022). In addition to redox potential, the rate of oxygen reduction by laccase is also used to measure its enzymatic activity (Shleev et al., 2005). Less common approaches to electrochemical investigations involve oxidising the usual substrate. Compound oxidation by laccase generates a

current proportional to the oxidised compound's concentration. As a result, their application enables them to characterise the laccase catalysis process, measure kinetic parameters, and develop enzymatic assays (Mattos et al., 2022; Sýs et al., 2017).

The techniques, methods, and approaches discussed previously focused on detecting and confirming laccase activity as closely as possible in real time. However, functional analysis is used to study the products formed rather than the enzyme's activity when laccase is applied in various processes. This helps to determine catalysis mechanisms, secondary processes following catalysis, and enzyme selectivity towards substrates (Wang et al., 2022; Peng et al., 2021). Robust techniques such as *MS*, *NMR*, *FTIR* or *Raman spectroscopy* are used to achieve this. Unlike the methods mentioned above, these techniques are only partially dependent on substrates; therefore, the discussion will focus more on their applications than on the substrates used. In laccase research, MS is mainly used to examine substrates whose oxidation produces mixtures or oligomeric compounds. It is widely used to analyse reaction products and predict reaction mechanisms in studies of biodegradation pathways involving synthetic polymers (Tiwari et al., 2024), xenobiotic compounds (Beck et al., 2018), dyes (Mao et al., 2015), and natural materials (Zhang et al., 2022). Saito et al. (2005) conducted a notable investigation that served as a basis for exploring lignin modifications and degradation by laccase using MS (Goacher et al., 2018; Sharan et al., 2024). On rare occasions, laccase is investigated as a biocatalyst for the synthesis of low-molecular-weight amine/phenol oligomers (Jia et al., 2023). The reaction mechanism and degree of oligomerisation are analysed using MS, as illustrated by the works of Sousa and co-workers (2013; 2014). NMR is a powerful technique that, in simple terms, shows the positions of atoms in a molecular structure based on the electron shielding around their nuclei. It is highly sensitive to the slightest differences in the environments of atoms; thus, its use focuses on identifying specific isomers in laccase-catalysed addition and polymerisation (Deshaies et al., 2021; Hajdok et al., 2009) or in degradation reactions (Xia et al., 2003). The downside is that analysis requires isolating the targeted compounds. In addition, the multitude of NMR signals, chemical shifts, and splitting patterns produces an intricate spectrum that requires considerable skill and expertise to interpret correctly. FTIR and Raman spectroscopy are analytical techniques that help identify molecular moieties or groups based on their vibrational modes. They are rarely applied in isolation in enzyme functional analysis since they do not provide sufficient information about the entire molecule. Instead, they are used to complement the results of other analysis methods. In laccase investigations, these spectroscopies are employed to observe changes during

the degradation of xenobiotic compounds (Feng et al., 2023; Coman et al., 2023), synthetic polymers (Ray et al., 2023), lignin phenolic units (Lähdetie et al., 2009; Senthilvelan et al., 2017) or laccase-catalysed polymerisation (Kashima et al., 2019). In summary, MS, NMR, and vibrational spectroscopies are peerless tools for studying the process and products of laccase catalysis. MS, FTIR, and Raman are particularly robust and can be employed for mixtures, whereas NMR measurements are typically performed on pure compounds. Factors such as equipment costs, time consumption, the complexity of the results, and the expertise required for accurate interpretation make these analytical techniques less appealing for enzyme functional analysis.

In conclusion, laccase functional analysis has utilised a diverse array of compounds containing phenolic moieties. The most widely used substrates are ABTS, DMP, guaiacol, and syringaldazine, as they are used in nearly every functional analysis method discussed. However, these conventional substrates are plagued by numerous drawbacks that limit their applicability and potential for modification. In some instances, compounds labelled as non-conventional substrates can address these shortcomings, yet a knowledge gap persists.

1.3. Functional Characteristics of Carbonic Anhydrase

The rapid acceleration of global warming is primarily attributed to carbon dioxide (CO_2) emissions from industrial processes, power plants, and transport. A potential solution to this problem is the utilisation of CO_2 as a novel primary raw material for conversion into high-value-added products (Talekar et al., 2022). The technologies currently under investigation include converting CO_2 into valuable compounds and products via biocatalysis, electrocatalysis, photocatalysis, and thermocatalysis. Among these, biocatalytic methods offer a sustainable, efficient, cost-effective alternative to traditional chemical processes, positioning them as a vital component in the future of industrial chemistry.

Carbonic anhydrase (CA) enzymes (EC 4.2.1.1), which catalyse the hydration of CO_2 at high turnover rates in living organisms, can be employed to accelerate CO_2 capture, conversion, and utilisation, thereby contributing to carbon neutrality efforts. CAs have been observed in most organisms across all three domains of life. To date, eight distinct structural CA classes have been identified (α, β, γ, δ, ζ, η, θ, and ι) (Jensen et al., 2019). Most CAs are metalloenzymes, and metal ions play a crucial role in the catalytic cycle. The current research on CA in medicine is well developed and advanced, but its application in industrial biotechnology to reduce CO_2 emissions remains in its

early stages. One factor influencing, and possibly limiting, the discovery of new CA and/or the optimisation of existing ones is methodological limitations in enzymatic activity measurement assays, including challenges with high-throughput screening, ease of operation, and analytical method variability. While various methods exist for measuring carbonic anhydrase activity, each has inherent limitations that can affect accuracy and reliability, impacting daily lab use.

CA catalyses a reversible CO_2 hydration reaction to hydrogen carbonate anion (HCO_3^-) and a proton (H^+), as shown in **Figure 1.3**, and this process is exclusively observed in CAs. Some members of the CA family also exhibit catalytic activity as carboxylic-, phosphate-, and sulphate-ester-hydrolysing enzymes.

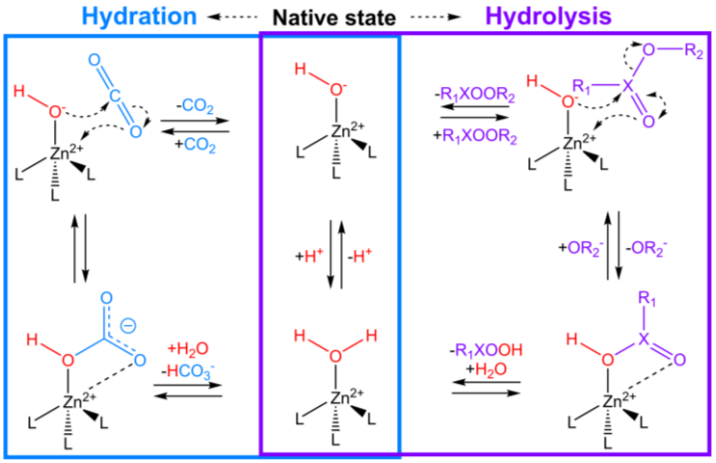


Figure 1.3 Simplified reaction mechanisms of hydration and hydrolysis catalysed by the CAs.

In the native state, CA coordinate a hydroxyl ion (OH^-) in equilibrium with its protonated state, H_2O. Then, a CO_2 or ester molecule enters the active site, and the Zn^{2+} ion acts as a Lewis acid for the entering oxygen atom. Coordination between zinc and oxygen increases the C=O (where X = C, P, or S) bond polarisation, making the carbon atoms more susceptible to a nucleophilic attack from the OH^- ion in the vicinity. The formed products undergo an exchange with a free water molecule, returning the enzyme to its native state.

1.3.1. Structure-Function Relationships in Carbonic Anhydrases

CAs are enzymes that catalyse the reversible hydration of carbon dioxide. As CAs are widespread within all living organisms, these enzymes differ in structure, catalytic activity, and distribution (**Table 1.3**). Out of the currently

Table 1.3 Comparative analysis of CAs.

Class	Occurrence	Structural features	Biochemical properties	Confirmed catalytic activity	Ref.
α	Vertebrates, some bacteria	Monomeric; Zn^{2+} coordinated by three His	Broad versatility; thermolabile	Hydratase Esterase, phosphatase, sulphatase, carbonate hydrolase	Boone et al., 2014; Supuran, 2016
β	Bacteria, archaea, plants, fungi, algae	Oligomeric (dimer, tetramer, octamer); Zn2+ coordinated by three Cys/His	Thermostable; pH-dependent activity	Hydratase	Akocak and Supuran, 2019; Supuran, 2016
γ	Archaea	Trimetic; Zn^{2+} coordinated by three His; can coordinate other ions (Fe^{2+}, Co^{2+})	Highly thermostable, primitive fold	Hydratase	Akocak and Supuran, 2019; Aspatwar et al., 2022
δ	Diatoms	Zn^{2+} in the active site	Likely similar to ξ-CA in metal adaptation	Hydratase	Aspatwar et al., 2022; Boone et al., 2014
ξ	Diatoms	Repeated Zn-binding domains; can coordinate other ions (Cd^{2+}, Co^{2+})	Adapted to low Zn^{2+} environments; metal substitution	Hydratase	Aspatwar et al., 2022
η	Protozoa, bacteria	Zn^{2+} in the active site	Activated by amines/amino acids	Hydratase Esterase	Akocak and Supuran, 2019
θ	Unicellular eukaryotes	Zn^{2+} in the active site	N.d.	Hydratase Esterase	Aspatwar et al., 2022; Kikutani et al., 2016
ι	Diatoms, algae	Metal-independent activity	Functions without metal ion; characterised with Mn^{2+}	Hydratase Esterase	Aspatwar et al., 2022; Jensen et al., 2019

known eight distinct classes of carbonic anhydrases found in nature (α, β, γ, δ, ζ, η, θ, and ι) (Jensen et al., 2019), animals possess only the α-CA class. In addition, this class is also found in plants, algae, and protozoa, while bacteria, fungi, and archaea have β-CAs, and bacteria, cyanobacteria, and archaea have γ-CAs. Marine diatoms have been found to contain the δ, ζ, and θ classes (Aspatwar et al., 2022). Typically, the active site of CAs contains zinc as the most frequently observed metal ion in α, β, γ, and δ-class CAs (Rowlett, 2010). θ-class CA is less well described, but it has been shown to contain a zinc ion in its active centre (Kikutani et al., 2016). The γ-class can coordinate various

metal ions, including Fe^{2+} or Co^{2+}. Meanwhile, ζ-CAs are capable of being active with either Zn^{2+} or Cd^{2+} ions and appear to be coordinated in a fashion similar to certain *β*-CAs (Amata et al., 2011). *η*-CAs are reported to coordinate Zn^{2+} metal ions (De Simone et al., 2015). Most recently, *ι*-CAs have been characterised to have Mn^{2+} (Jensen et al., 2019). Variation of CAs that can operate without a metal ion has also been described (Hirakawa et al., 2021). While the *α*-, *β*-, and *γ*-CAs regulate fundamental processes such as respiration (*α*), photosynthesis (*β*), and archaeal metabolism (*γ*), the more recently evolved *δ*-, ζ-, and *ι*-CAs have specialised in marine carbon fixation. The *δ*- and ζ-CAs optimise CO_2 acquisition in diatoms through surface-associated activity and alternative metal cofactors, respectively. While *ι*-CA operates independently of metals, it provides ecological adaptability for phytoplankton. Together, these variations highlight how CA classes have evolved to meet the specific environmental demands of their host organisms, underscoring the potential for discovering new CA variants with unique properties and promising biotechnological applications.

The presented comparison shows that all CAs classes are structurally distinct but unified by a single factor: the catalysis of CO_2 hydration. The *α*, *η*, *θ*, and *ι* classes have been confirmed to display esterase-like activity, while the first identified and most studied *α*-CAs have been described as catalysing the hydrolysis of specific phosphate, sulphate, and carbonate esters. Other classes lack these activities or have not been thoroughly tested for them. Therefore, the most commonly used methods for CA characterisation encompass CO_2 as the substrate, such as spectrophotometric CO_2 hydration assays employing stopped-flow instrumentation (Khalifah, 1971), exchange of ^{18}O between carbon dioxide and water determined by membrane inlet mass spectrometry (Li et al., 2011; Silverman, 1982), and assays based on the hydrolysis rate of *p*-nitrophenyl acetate as a surrogate (Colombo and Pinelli, 1981). CAs are confirmed as drug targets for various diseases and disorders linked to pH and electrolyte balance, including glaucoma, oedema, acute mountain sickness, epilepsy, cancer, and obesity (Chegwidden, 2021). Therefore, a primary application of CA enzymatic activity assays in drug design is to evaluate the inhibitory properties of new compounds or antibodies. These experiments are conducted under conditions closely mimicking physiological environments, typically at pH 7.0 to 7.5 and with added salts to maintain a constant ionic strength. The discovery and investigation of CAs catalytic properties now span nearly a century. Over this period, a few key studies broadened the pool of methods for CAs investigations. Starting with the first documentation of CA's catalytic properties (Meldrum and Roughton, 1933), authors used manometric CO_2 pressure measurements to examine

proteins isolated from mammalian blood. In 1948, Wilbur and Anderson developed a potentiometric method involving CO_2-saturated water and a standard pH electrode. Another breakthrough came from Thorslund and Lindskog in 1967, when they proved that some CAs can catalyse the hydrolysis of carboxylic esters, opening the possibility of employing esters as a substitute for CO_2. The last major addition to the CAs toolbox was the employment of MS to observe isotope exchange rates between different chemical species (Silverman, 1973). Each technique is distinguished by its specific detection method, experimental requirements, and suitability for different reaction types, including both CO_2 hydration and various hydrolytic activities.

Despite the application of genetic engineering to improve existing CAs (Alvizo et al., 2014; Parra-Cruz et al., 2020), there is a high demand for the discovery of novel carbonic anhydrases, particularly those derived from extremophiles. Organisms living in extreme ecological niches often produce proteins that have evolved to maintain functionality under harsh conditions. Hydrothermal vents, hypersaline or soda-alkaline lakes and pools, deserts, and volcanic areas are the primary locations for the discovery of extremophiles (Mesbah and Sarmiento, 2016). However, more than 99% of extremophilic microorganism species cannot be cultured in laboratories using standard protocols (Papudeshi et al., 2017). Thus, metagenomic analyses using high-throughput bioinformatic approaches enable screening for billions of potential enzyme-encoding genes in vast metagenomic datasets (Guazzaroni et al., 2010). However, bioinformatic techniques are usually unable to determine enzyme activity. Currently, most approaches for measuring CA enzymatic activity rely on solution-based colourimetric methods, which are typically used to assess protein extracts from cultured organisms rather than for initial screening. One of the most frequently mentioned methods in the literature for the functional screening of CA-positive organisms is the use of agar plates containing *p*-nitrophenyl acetate (pNPA). However, methods that use pNPA rely on esterase activity, which is not present in all CA classes and isoforms (Innocenti and Supuran, 2010). The method for assessing CA hydratase activity was introduced by Ferrer and colleagues (2020), who developed a rapid screening assay to directly detect CA-positive microorganisms in environmental samples. The method uses pH-sensitive strips in microcentrifuge tubes that change colour in response to CO_2 gas produced during the CA reaction. Nonetheless, the environmental inferences significantly limit the utility of this method and should be used only as a preliminary indicator, given the lack of alternatives for detecting CA activity. Despite the chosen activity-based measurement method, no single assay is

universally suitable for screening CA-positive microorganisms. **Table 1.4** outlines a range of established analytical approaches for probing the catalytic performance of CAs. Each technique is distinguished by its specific detection method, experimental requirements, and suitability for different reaction types, including both CO_2 hydration and hydrolytic activities. The table compares the operational advantages and limitations of each method. The overview of techniques used for CA activity measurements presents a wide range of methods with different levels of complexity, sensitivity, and methodological challenges. It also highlights two significant shortcomings that could hinder and frustrate researchers: most assays rely on CA hydration-catalytic activity and are not suitable for high-throughput screening. The substrate in hydration-based methods is the CO_2-saturated water. While its preparation is relatively simple and inexpensive, CO_2's gaseous properties may affect measurement reproducibility and accuracy. High-throughput techniques often rely on methods that allow fast scanning of samples in series or single measurements in parallel, e.g., a UV-Vis plate reader. The rapid turnover of CO_2 as a substrate, along with techniques that either do not support it or are heavily constrained by analysis time or detection mode, leaves only CAs with hydrolytic activity compatible with high-throughput functional analysis. The presented advantages, disadvantages, limitations and proposed new strategies will be examined in more detail in the following sections.

1.3.2. Hydration-Based Assays for the Measurement of Carbonic Anhydrase Activity

Medical and pharmacological investigations use CAs as targets to control pH and fluid-balance-related diseases. Non-medical investigations mainly involve CO_2 fixation and subsequent utilisation (Nguyen et al., 2024). Therefore, it is not surprising that most available activity assays observe and measure the CO_2 hydration process. However, one of the main issues in activity experiments is CO_2, which is weakly soluble in water (Carroll et al., 1991). To prepare the substrate solution for measurements, dry ice is added or CO_2 gas is bubbled into the water, a process that can take up to 3 h to achieve a fully CO_2-saturated solution. The substrate concentration in a solution can be estimated from phase diagrams, but the actual CO_2 saturation and concentration remain unknown because of the dynamic CO_2 equilibrium shown in **Figure 1.5**. Zeebe and Wolf-Gladrow (2001) have summarised the factors affecting CO_2 equilibrium in their work on CO_2 in seawater. They used kinetic models to show that not only the instantaneous pH but also the solution ionic strength, temperature, other gases, and atmospheric pressure influenced CO_2 solubility and hydration. Furthermore, $CO_{2(aq)}$, the substrate for CAs,

Table 1.4 Techniques for CA functional analysis: assay principles and limitations (Babinskas et al., 2026).

Technique	Activity type	Assay principles	Advantages	Disadvantages	Limitations	Equipment	Ref.
Manometry	Hydration	Changes in CO_2 gas volume/pressure	• Simple procedure • Inexpensive equipment • Simulation of industrial conditions	• Low sensitivity • High enzyme consumption • Laborious setup	• No high-throughput support	• Manometer • Differential pressure transducer	Karler and Woodbury, 1963
Gravimetry	Hydration	Mass of $(H)CO_3$ salt precipitate	• Simple procedure • Inexpensive equipment • Simulation of industrial conditions	• Low sensitivity • High enzyme consumption • Laborious setup • Long analysis time	• No high-throughput support • Metal ion interference	• Analytical balance	Caulfield et al., 2022
Protonography	Hydration	Colour change of bromophenol blue indicator	• Standard SDS-PAGE equipment • Complex samples • Assessment of enzyme size and oligomerisation • High sensitivity	• Laborious setup • Qualitative results • Short documentation window • Long analysis time	• Inactivation by SDS-PAGE components or procedure • Restricted high-throughput support	• Electrophoresis system • SDS-PAGE documentation system	Del Prete, De Luca, Landolo, et al., 2015
Potentiometry	Hydration	Changes in pH values	• Simple procedure • Inexpensive equipment • High sensitivity • Fast analysis	• High enzyme consumption • Specialised setup	• pH meter response time • Protein adsorption on electrode	• pH meter • Wilbur-Anderson method setup	Wilbur and Anderson, 1948

Table 1.4 Continuation

UV-Vis spectrophotometry	Hydration Hydrolysis	Change in light absorption values	• Simple procedure • Fast analysis • Supports high-throughput screening	• Hydration – cost of stopped-flow setup • Hydrolysis – organic solvents	• Hydration – linear only in indicator transition range • Hydrolysis – not applicable to all CA classes	• UV-Vis spectrophotometer • Plate reader • Stopped-flow setup	Smirnovienė et al., 2017; Uda et al., 2015
Isotope exchange	Hydration	Changes in isotope distribution between chemical species	• Complex samples • Wide range of conditions • Extreme sensitivity	• Complex results • Expensive equipment and consumables	• NMR – only end-point measurements • Restricted high-throughput support	• Mass spectrometer • Membrane inlet • Nuclear magnetic resonance spectrometer	Silverman, 1982
Gas chromatography	Hydration	Gas detection	• Complex samples • High sensitivity	• Specific equipment	• No high-throughput support	• Gas chromatographer • Gas sample injection system	Iizuka et al., 2024
Gas FTIR	Hydration	Gas identification through vibration modes	• Simple procedure	• Low sensitivity • Specific equipment	• Moisture interference • No high-throughput support	• FTIR spectrophotometer • Specialised gas cell	Stimler et al., 2012

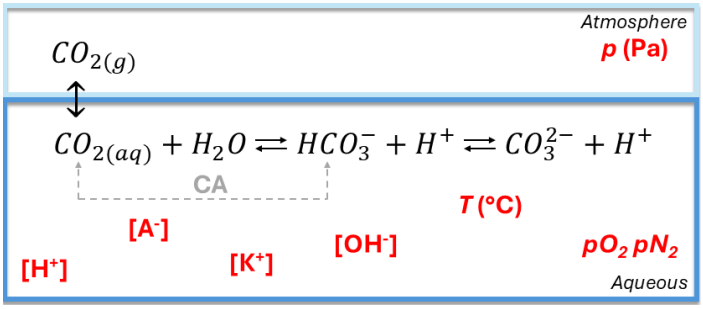


Figure 1.5 CO_2 exchange and equilibrium in an air-aqueous biphasic system.

accounts for only up to 1% of the equilibrium. On top of that, even pressurised solutions slowly leak gas, resulting in a continuously decreasing substrate concentration and a shift in the equilibrium. It is especially problematic in experiments measuring kinetic and inhibition constants for high-affinity compounds. Another challenge with a CO_2-saturated solution comes in when the enzyme is immobilised. Depending on the immobilisation method, the substrate has to cross several additional barriers between phases, such as the bulk liquid-to-liquid film on the carrier surface, to access the enzyme's active sites, as outlined in a review on immobilised CA application by Molina-Fernandez and Luis (2021). If the immobilised CA retains its high turnover number, mass transfer may become the rate-limiting step, distorting the activity results. To overcome these issues, a possible strategy would be to develop an inert additive that increases CO_2 solubility in water or to use non-aqueous systems such as ionic liquids or deep eutectic solvents, which exhibit better CO_2 equilibrium stability (Trivedi et al., 2016). An often-overlooked alternative is to use carbonate salts instead of CO_2 to observe the dehydration reaction by monitoring changes in pH (Alvizo et al., 2014). Despite the listed limitations, most routine CA assays use CO_2 as the substrate, ranging from simple gas-volume measurements to sophisticated isotope-exchange analyses.

Physical measurement is the most direct way to observe changes in gas volume or mass. Manometry, which involves measuring gas pressure in a closed system, can be applied to measuring CO_2 consumption in reactions (Dilmore et al., 2009). It was one of the first techniques used to identify CA in human blood and had an intrinsic role in studying CO_2 metabolism and CA's role in mammalian biochemistry (Karler and Woodbury, 1963). Although this method has become less popular due to its laborious setup and the need for higher precision, especially in biomedical fields, it is still employed in a similar fashion for CO_2 capturing or immobilised CA research. The enzyme is placed in a flow-through system, such as a bubble or packed-bed reactor, and then a known-composition gas mixture is injected. Changes in effluent

pressure, volume, or CO_2 fraction during gas-IR analysis enable estimation of the kinetics of CO_2 absorption and catalysis in systems that mimic real-world conditions (Alvizo et al., 2014; Peirce et al., 2018; Yadav et al., 2010). Similarly, gravimetry can be used to measure the mass of absorbed CO_2 (Trivedi et al., 2016). By conducting the reaction in a solution containing Ca^{2+}, Mg^{2+}, or Ba^{2+} ions, the amount of CO_3^{2-} formed can be estimated from the mass of the precipitated carbonate salt (Caulfield et al., 2022; Uygun et al., 2015). This method is often employed to investigate the role and potential applications of CA in biomineralisation and sequestration processes (Mirjafari et al., 2007; Power et al., 2016).

During catalytic CO_2 hydration, a single H^+ ion is produced, changing the solution's pH; therefore, an electrometric pH electrode can directly measure the change in pH. In fact, in 1948 Wilbur and Anderson published a method now known as the Wilbur-Anderson assay. It has been highly successful, to the point that hydration activity units (WA units) are now named after the authors and are the standard descriptor of CA catalytic efficiency. Even spectrophotometric assays, discussed later, sometimes express the enzymatic activity through WA units. Nonetheless, a few aspects need to be taken into consideration. Firstly, the Wilbur-Anderson assay requires a specialised setup and laborious preparation, as measurements are performed at 0 °C using CO_2-saturated water. Additionally, the pH meter's slow response time can make it difficult to obtain highly reproducible results. Secondly, this method needs a relatively large quantity of enzyme because the reaction volume for common pH electrodes is 5-10 ml. Thirdly, protein adsorption on the surface of a typical glass-membrane pH electrode might interfere with measurements. Lastly, measurements of immobilised CA require vigorous mixing to minimise the lag between H^+ diffusion from the enzyme to the electrode surface. In spite of that, the description of CA with WA units is the industry standard and will remain that way for the foreseeable future.

There is only one qualitative method available for exploring CO_2 hydration – *protonography*. It is a specialised technique used to detect enzymatic activities that shift the pH in the presence of a substrate; i.e., catalysis changes the H^+ concentration. To perform protonography, SDS-PAGE electrophoresis is carried out using a standard protocol with a minor difference: the protein samples are not treated with 2-mercaptoethanol and temperature to avoid denaturation (Del Prete et al. 2015a). For the detection of CAs activity, the SDS-PAGE gel is incubated in a buffer supplemented with bromothymol blue pH indicator, then in CO_2-saturated deionised water. The indicator, once absorbed, undergoes a colour transition from blue (alkaline) to yellow (acid) near pH 7. In the gel, the CA catalysis process accelerates the release of H^+

ions, resulting in a green-yellow colour at the enzyme bands. This method provides a simple way to identify CA in protein mixtures, determine their molecular size or oligomerisation state, and even provide a rough comparison of activities. However, protonography has a few minor drawbacks. For instance, a sample treated without 2-mercaptoethanol or without boiling does not necessarily retain its activity. Furthermore, the catalytic activity of CA can be reversibly inhibited by SDS, and the inhibition can be reversed by incubating the gel in a Triton X-100 solution (Del Prete et al. 2015a; Del Prete et al. 2015b). The indicator colour shift is a rapid process and must be documented within 10-30 s after the gel is placed in CO_2-saturated water. Otherwise, the CA bands begin to blur due to H^+ diffusion, lowering the overall pH and causing a colour transition in bromothymol blue throughout the gel (De Luca et al., 2015). In summary, protonography is a unique method that readily provides valuable information about CAs; however, the lengthy preparation and electrophoresis times, combined with a short time window for obtaining decent results, require some practice and experience.

Spectrophotometric methods have been developed to measure CA activity using pH indicators as chromophores. The basic procedure involves mixing a buffer solution with an indicator and the enzyme. The reaction is initiated by adding CO_2-saturated water to the mixtures, which catalyses the release of H^+ ions. The spectrophotometric measurement monitors the change in absorbance at the appropriate wavelength as pH decreases. The main drawback of this principle is that colour changes in indicators occur over narrow ranges. For an activity assessment over a wide pH range, multiple indicators are required, as illustrated by Smirnovienė and colleagues (2017). Khalifah (1971) investigated the use of *p*-nitrosophenol, *p*-nitrophenol, *m*-cresol purple, and chlorophenol red as indicators, but phenol red is the most common (Anandabaskar, 2022). It should be noted that each indicator has a unique molar extinction coefficient; thus, their characterisation must be conducted to normalise the hydration activity results across different indicators. Most spectrophotometric assays employ stopped-flow systems, an automated, extremely accurate and efficient mixing setup with measurement dead time as low as milliseconds, due to the CO_2 hydration catalysis rate exceeding 1 M s^{-1} (Wistrand, 1981). Furthermore, stopped-flow systems are well-suited for investigating the kinetics and mechanisms of inhibition. For more routine activity measurements, Kim and Jo recently (2022) developed a spectrophotometric method that uses real-time measurements in a cuvette, with phenol red as an indicator. Briefly, despite the cost of stopped-flow equipment, spectrophotometric methods are essential for CA investigations and research but are limited by the indicators used.

Both spontaneous and CA-catalysed hydration reactions are reversible, meaning that the formed HCO_3^- is exchanged into CO_2 and *vice versa*. *Isotope analysis* works by calculating the exchange rates for non-catalysed reactions *vs* catalysed reactions. For example, Simonsson et al. (1979) developed a method to generate $^{13}CO_2$ from $Ba^{13}CO_3$ in a controlled and sealed system. The catalysed exchange rates of ^{13}C atoms at various pH values and in different buffers were measured by ^{13}C NMR spectroscopy. Such feats are not possible for spectrophotometric methods, as pH indicators are only effective in limited pH ranges (Gurd et al., 1974). Similarly, Silverman (1982) described an approach in which ^{18}O-labelled water was used in isotope-exchange experiments. The analysis was performed using mass spectrometry (MS) to differentiate between and measure the levels of CO_2, $CO^{18}O$, and $C^{18}O_2$ (Delacruz et al., 2010). Of course, the specific isotopes are not limited to the techniques presented and can be used in a variety of ways – for example, ^{13}C for MS (McConnell et al., 2007) or ^{17}O for NMR (Rose and Bryant, 1980). In 2020, the first *in vivo* application of ^{13}C NMR on CA catalytic activity in the brain was reported by Tomar and Shen, marking a milestone not only in the medical field but also in enzyme functional analysis. In summary, NMR and MS are standard techniques for analysing enzyme catalysis with high sensitivity and are not restricted by buffers or pH. However, the requirements and cost of isotope-labelled compounds and specialised equipment make them less accessible for CA investigations than other methods.

CO_2 is the primary molecule involved in the CA catalytic cycle, but there are a few other molecules that can also participate in the same hydration reaction. Carbonyl sulfide (COS) and carbon disulfide (CS_2) are two such molecules that are structurally similar to CO_2 but with oxygen atoms substituted for sulphur (**Figure 1.6**).

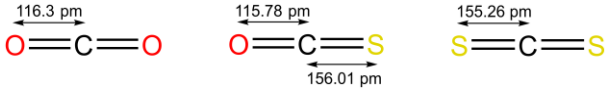


Figure 1.6 Molecular structures and bond lengths of CO_2, COS and CS_2.

When these molecules undergo hydration, they produce CO_2 and H_2S. The formation of CO_2 can be monitored using gas IR spectroscopy (Stimler et al., 2012), while H_2S is observable in gas MS (Miller et al., 1989), gas chromatography (Iizuka et al., 2024), qualitative PbS precipitate gravimetry (Alterio et al., 2021) or Methylene blue formation (Haritos and Dojchinov, 2005). The exact biological function of this activity has not yet been determined; therefore, a broader range of methods is required for further research.

1.3.3. Hydrolysis-Based Assays for the Measurement of Carbonic Anhydrase Activity

The second type of catalytic activity expressed by CAs is hydrolytic activity. It covers the hydrolysis of esters containing -OH functional groups and of carboxylic acids for esterase-like activity, of phosphate for phosphatase-like activity, of sulfate for sulphatase-like activity, or of carbonic acid for carbonate esterase activity. The CA's esterase-like activity is best characterised by using *p*-nitrophenyl acetate (pNPA). Its assay utilises UV-Vis spectroscopy to monitor the liberation of the *p*-nitrophenolate (pNP) anion at 400-405 nm (Peng et al., 2016). Research has shown that the substrate hydrolysis rate strongly correlates with the alcohol group pK_a: a lower pK_a results in a higher catalytic rate (Lopez et al., 2011). Because pNP has one of the lowest pK_a values for a simple phenol (pK_a 7.14) and exhibits a high molar extinction coefficient above pH 7.5 ($\varepsilon > 10$ mM^{-1} cm^{-1}), it is one of the best chemical moieties for the UV-Vis assay. Longer acid alkyl chains result in slower hydrolysis rates, as demonstrated by investigations on other pNP esters, such as propionate, butyrate, valerate, and caproate (Höst et al., 2006). Unlike CO_2, the typical pNPA hydrolysis turnover is usually within the 10^1-10^3 s^{-1} range (Verpoorte et al., 1967), making it easy to handle in a standard spectrophotometer cuvette or plate reader, and to work with immobilised proteins (Yoshimoto et al., 2018). Therefore, pNPA is an excellent choice for investigating and screening potential inhibitors (Uda et al., 2015). On the other hand, pNPA hydrolysis can be catalysed by a variety of esterases (Li et al., 2020), lipases (De Caro et al., 1986) and other proteins (Schoonen et al., 2017; Taylor et al., 1963; Verma and Ghosh, 2010). Furthermore, due to its low water solubility, organic co-solvents, such as acetonitrile or dimethyl sulfoxide, are employed in the assays, which can interfere with enzymatic catalysis. Other substrates, like indoxyl acetate, have also been used for high-throughput screening in well plates (Baliukynas et al., 2020). Meanwhile, mandelic acid esters have been used to explore CA enantioselectivity (Chênevert and Létourneau, 1990). Interestingly, research has also shown that human CA hydrolyses potential inhibitors containing acetylated carbohydrate sulfamates (Lopez et al., 2011). In summary, pNPA is one of the best-known substrates used in esterase assays, including CAs that express ester-hydrolysis activity. Its wide applicability, low cost, and established methodologies make it an excellent choice for assessing CA activity; however, pNPA may be a limiting substrate in thermostable or highly alkaline enzyme research due to its high rate of autohydrolysis (Fredslund et al., 2018).

In addition to CO_2 hydration, some lesser-known CA activities involve the hydrolysis of substrates such as phosphate, sulfate, or carbonate esters (**Figure 1.7**).

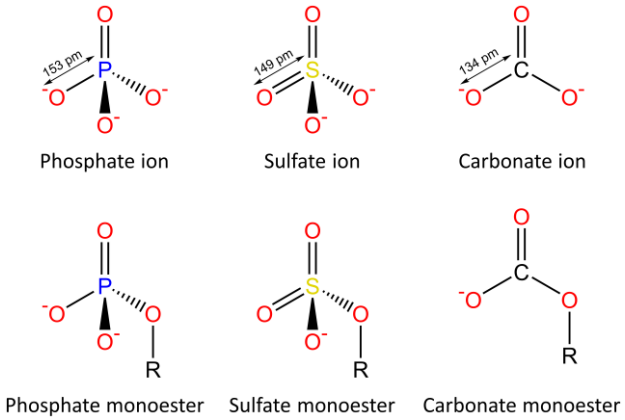


Figure 1.7 Molecular structure of phosphate, sulfate and carbonate ions, and their corresponding monoesters.

In 1978, Pocker and Sarkanen demonstrated that CA can exhibit phosphatase-like activity (Pocker and Sarkanen, 1978). They compared the hydrolysis kinetics of dimethyl 2,4-nitrophenyl phosphate and 2,4-dinitroacetate. Following this, Koester et al. (1981) investigated this activity of human CAIII using *p*-nitrophenyl phosphate as a substrate. Carbamoyl phosphate was used to examine differences in mammalian CA phosphatase activities (Nishita and Deutsch, 1986). Additionally, it has been demonstrated that the α, but not *β*, *γ,* or *ζ* class CAs exhibit this activity, using pNP phosphate and diethyl pNP phosphate as substrates (Innocenti and Supuran, 2010). Despite these findings, the overall biological role and the mechanisms underlying CA phosphate activity remain poorly understood.

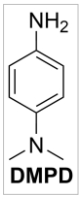
CA also exhibits a sulfatase-like activity, as evidenced by its ability to hydrolyse a variety of methanesulphonates (Kazancıoğlu et al., 2012) and cyclic diol monosulphonates (Çavdar et al., 2012). Interestingly, CAs have been shown not to catalyse the hydrolysis of pNP sulphate (Innocenti et al., 2008). Not much else is known or explored about CA's sulfatase activity.

The bicarbonate ion produced by CA catalysis participates in an acid-base equilibrium and has a structure similar to that of the carbonate ion. While their esters would be great for enzyme activity measurements, both bicarbonate and carbonate monoesters are highly unstable. Even the synthesis of a simple ester, like monoethyl carbonic acid, requires complex, multi-step, and air-sensitive reactions (Bernard et al., 2017), making these compounds commercially unavailable and practically inapplicable. Additionally, there is evidence of CA

inhibition by mono-alkyl carbonates (Pocker and Deits, 1984). This leaves only diesters of carbonic acid, referred to as carbonate esters, as suitable substrates. Pocker and Guilbert conducted monumental kinetic studies in 1972 and 1974 on CA-catalysed carbonate decomposition. They used methyl pNP carbonate, bis-(pNP) carbonate, and three isomers of pyridine methyl carbonates to gain insights into the catalytic properties of CA, including inhibition mechanisms (Pocker and Guilbert, 1972, 1974). Surprisingly, no further works have been published on CA characterisations involving carbonate esters. This catalytic property appears to have fallen into obscurity to the point that even more recent publications listing CA-catalysed reactions, including single instances, do not mention carbonate ester hydrolysis (Kazancıoğlu et al., 2012). There could be a few reasons, such as the absence of suitable compounds. In addition, the primary synthesis methods for these esters rely on phosgene, an extremely toxic and dual-use gas, which complicates the production of tailor-made substrates, even on a laboratory scale.

In essence, most CA activity assays focus on the CO_2 hydration reaction, while several methods also evaluate hydrolytic activity, each presenting distinct advantages and limitations in terms of sensitivity, instrumentation requirements, and compatibility with different CA isoforms and reaction conditions. Together, these approaches constitute a valuable toolkit for CA functional characterisation, although their limitations highlight the need for more sensitive, selective, scalable, and high-throughput methodologies.

2. RESULTS AND DISCUSSION



During the initial screening of potential aromatic amines, phenol amines and phenylenediamines for laccase functional analysis, *N*,*N*-dimethyl-*p*-phenylenediamine (DMPD) was identified as a highly promising building block. It contains two amine groups – the primary (-NH_2) and tertiary (-*N*-$(CH_3)_2$) – and belongs to the class of phenylenediamine compounds. This class's ortho and para variants exhibit similar properties to *p*- or *o*-hydroquinones. One of them is being easily oxidised under mild conditions. The product of phenylenediamine oxidation is benzoquinone diimine. The latter is readily reactive toward nucleophilic addition-type reactions with starting phenylenediamine or supplemented nucleophiles (Coulter et al., 2007; Sousa et al., 2014). DMPD oxidation can be easily catalysed by laccase but lacks the stability required for long-term agar plate incubations. In the initial experiments, oxidation followed by nucleophilic addition was applied to oligomerise DMPD to a more suitable phenazine-type compound. Four constituents were prospected in the development and analysis of the substrate: i) synthesis reproducibility and yield; ii) pH and thermal stability; iii) sensitivity to laccase activity; iv) biocompatibility with microorganisms. Overall, the aim was to develop a substrate which is easy to synthesise, stable over a wide pH range and at elevated temperatures and exhibits low toxicity to microorganisms.

2.1. Ferbamine Development and Application for Laccase Functional Analysis

The initial Ferbamine synthesis step was derived from the synthesis of methylene blue by removing a secondary thiosulfate nucleophile (Berneth, 2008). The reaction entailed oxidation of DMPD, followed by its oligomerisation with the unoxidised form. After the initial oxidation step, the mixture was refluxed to generate Ferbamine. The overall yield was about 0.27%; therefore, adjustments to the synthesis process were made to increase it.

One reason the initial oxidation might have been inefficient was either an insufficient amount of oxidising agent or an excess of it. So, the synthesis improvements began with the oxidising agent, ammonium persulfate ($(NH_4)_2S_2O_8$), to the DMPD ratio (*3.3.1*). It was changed from 0.90 to 1.1 by a 0.05 step increase to analyse the yield and its composition using thin-layer chromatography (TLC). It was established that a 1.0 equivalent is optimal, as using 1.05 or higher equivalents increased by-product formation. Less than

1.0 equivalents resulted in decreased yields. Hydrogen peroxide was also tested as an oxidising agent, but it formed new derivatives as by-products.

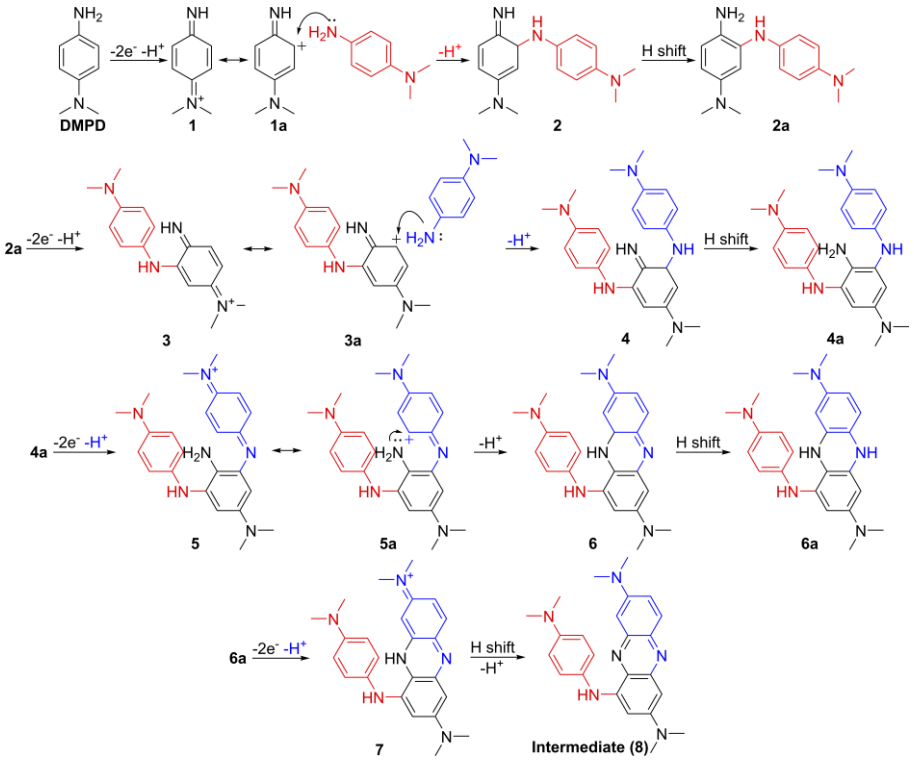
The initial oligomerisation of DMPD produced a precipitate containing a variety of oligomers and their isomers, most of which were by-products. Thus, refluxing the precipitate in organic solvents was selected for the study as the best method to remove unwanted compounds. A 50 mg of the precipitate was refluxed with 10 ml of a selected organic solvent: EtOAc, Et_2O, toluene, cHex, THF or $CHCl_3$. TLC analysis indicated that, among the six solvents tested, EtOAc was the most effective in removing the by-products. Flash and gravity silica gel chromatography were employed to achieve complete removal of unwanted compounds, but most compounds exhibited pronounced tailing even at low concentrations, preventing the removal of by-products. It was attributed to the compound's basic properties stemming from the presence of multiple amine groups. Chromatographic separation of these compounds may require specialised silica gel, retention modifiers, or other mobile-phase components (Bidlingmeyer et al., 1982), which were not pursued in this work. The second step of the overall synthesis process was carried out by refluxing 50 mg of the dry precipitate obtained in the first part of the synthesis with 100 ml of dH_2O for 1-5 h at 100 °C. The data obtained revealed that the highest yield was achieved after 4 h.

The enabled pathway for Ferbamine synthesis was readily performed and reproducible; however, the overall conversion of DMPD to Ferbamine remained insufficient. It was assumed this might be related to the limited solubility of the precipitate in dH_2O. Therefore, a strategy to increase solubility was explored using organic solvents (MeOH, EtOH, DMF, or DMSO) alone or in combination with dH_2O (*3.3.1*). Their volume in mixtures with dH_2O was 1%, 3%, 5%, 10%, 50% and 90% (*v/v*). The reactions were carried out for 4 h at 100 °C. When the solvent's boiling point was below 100 °C, the reaction was carried out at the solvent's boiling point. The TLC analysis results indicated that Ferbamine did not form in mixtures with organic solvents at concentrations above 5%. The best overall yield (0.92%) was achieved using 5% MeOH (*3.3.1*). Analytical high-performance liquid chromatography (HPLC) with the help of Dr. Andrius Sakalauskas (Sector of Amyloid Research, Institute of Biotechnology, Life Sciences Center, Vilnius University) was employed to ascertain the Ferbamine composition. It showed three compounds with similar relative intensities and low impurity levels ($\leq$ 5%). This synthesis outcome was satisfactory, as the substrate was intended for use in agar plates rather than qualitative methods. Subsequently, these compounds and the products of the initial oxidation step were identified and characterised using liquid chromatography coupled to quadrupole time-of-

flight mass spectrometry (LC-HRMS), which was performed by PhD student Martynas Malikėnas (Department of Organic Chemistry, Faculty of Chemistry, Vilnius University).

2.1.1. Analysis of Ferbamine Synthesis Mechanism

The oxidation of phenylenediamines, followed by addition reactions, is well known and of significant importance for the production of dyes on an industrial scale (Berneth, 2008), the formation of Bandrowski's bases (Coulter et al., 2007) and polymerisation (Li et al., 2013). However, despite numerous attempts (Sousa et al., 2014; Meyer and Fischer, 2015), the oxidation of phenylenediamines and the subsequent processes remain incompletely understood. To advance understanding of aromatic diamine oligomerisation, we have proposed mechanisms (**Scheme 2.1** and **Scheme 2.2**) for the synthesis of the intermediate (oxidation product), and finally Ferbamine. The mechanisms were constructed based on obtained LC-HRMS data (**Table S1 and S2**), measurements by NMR (*3.3.1*) and ATR-FTIR (*3.4.3*), and supported by the results of electrochemical DMPD oxidation reported by Modestov et al. (2004) and Jiang et al. (2020) on electrochemical *o*-phenylenediamine oligomerisation. The pivot of this mechanism is the



Scheme 2.1 Proposed Ferbamine intermediate synthesis mechanism.

oligomerisation of DMPD, which entails three-step cycles: 1) oxidation of the DMPD structural unit; 2) 1,4-nucleophilic addition; 3) H shift driven by molecule aromatisation. The reaction starts with the 2-electron oxidation of DMPD to compound **1**. This compound has a positive charge on the *N*,*N*-dimethyliminium group and a resonance form **1a**. It undergoes a 1,4-nucleophilic addition reaction with another DMPD molecule, which acts as the nucleophile. The shown addition position is preferred due to the partial positive charge. Furthermore, this synthesis step is performed at low temperatures (0-5 °C), which directs the reactions towards thermodynamic instead of kinetic products. Resulting compound **2** undergoes the H shift to compound **2a**. This process is driven by a thermodynamically favourable increase in the size of the delocalized electron system – aromatisation. **2a** undergoes the same repetitive oligomerisation of DMPD, resulting in **4a**, and further continues to form compound **6a**. This repetitive reaction pattern has been reported by Jiang and colleagues (2020) in the electrochemical oxidation of *o*-phenylenediamine. **6a** undergoes further oxidation to **7**, and a H shift to produce the intermediate (**8**). We suggest that oligomerisation slows after 1,4-addition steps due to the formation of a larger aromatic system, thereby allowing better positive charge delocalisation upon oxidation. Furthermore, the expansion of the aromatic ring system yields larger molecules that lack water-solubility. It results in the intermediate (**8**) precipitating from the reaction solution. Nonetheless, some of the intermediates remain dissolved and participate in further oligomerisation, as evidenced by minor amounts of higher-mass oligomers observed in HRMS analysis (**Table S1**).

In addition to HRMS of the reaction products, ATR-FTIR was used to monitor vibrational band shifts during the intermediate synthesis. Spectra were measured of the neutralised DMPD solution, and at every 0.2 eqv increment of oxidiser added to the reaction mixture (**Figure 2.1**). Data displayed the gradual disappearance of the 3100-3500 cm^{-1} primary amine N-H stretching bands and emergence of protonated amine $N\text{-}H^+$ 2650-3000 cm^{-1} stretching, and 2500-2650 cm^{-1} overtone/combination bands. In addition, a new band with low intensity emerged at 1623 cm^{-1}, attributed to $N\text{-}H^+$ bending. Bands for protonated amine bending are only observable for primary or secondary amines.

The HRMS analysis, followed by molecular formula prediction of the intermediate and final products (**Table S1 and S2**), revealed that the main difference between them is the number of H atoms: $C_{24}H_{28}N_6^+$ – intermediate; $C_{24}H_{25}N_6^+$ – Ferbamine. Based on the reaction conditions (high temperature, aqueous-organic solvents), the best fit to explain this difference is oxidation and addition reactions followed by proton elimination (**Scheme 2.2**), similar

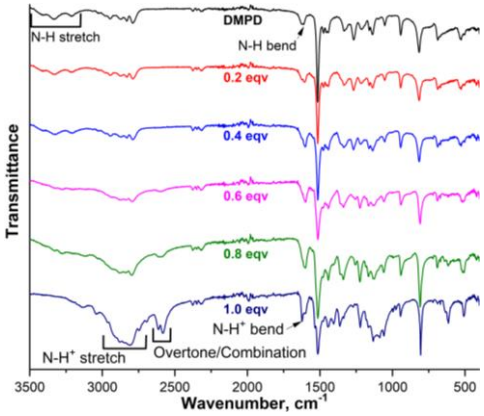
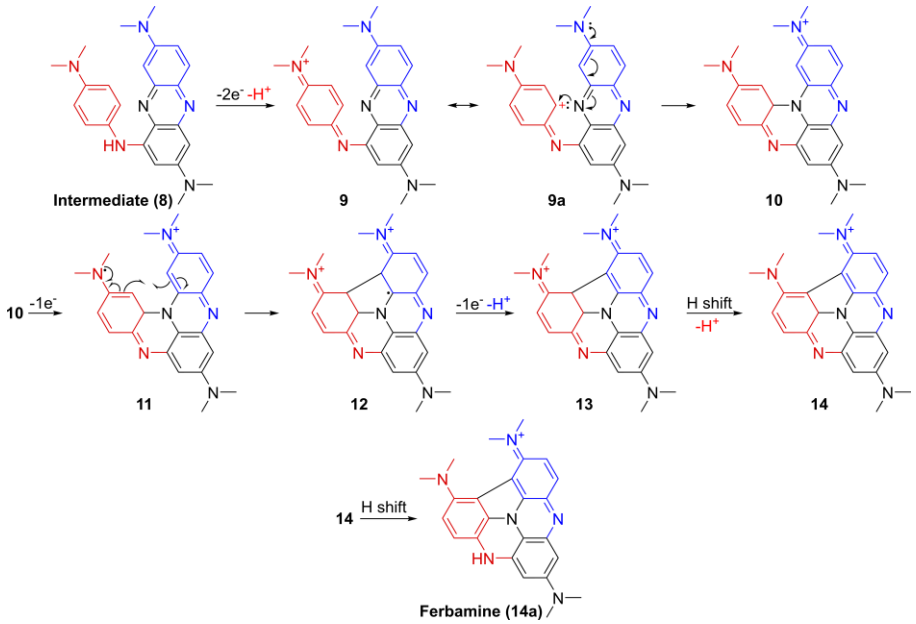


Figure 2.1 ATR-FTIR spectra of Ferbamine intermediate synthesis mixture after adding 0-1.0 eqv of oxidiser.



Scheme 2.2 Proposed mechanism of synthesis from the intermediate to Ferbamine.

to the proposed mechanism for intermediate formation. It is well known that phenylenediamines are susceptible to auto-oxidation initiated by irradiation, oxygen species, ions, unpaired electrons (radicals), or even ultrasound (Guo et al., 2009; Meyer and Fischer, 2015; Kim et al., 2017). We assert that oxidation reactions that occurred during the intermediate conversion to Ferbamine resulted from thermally accelerated autooxidation. Intermediate (**8**) undergoes oxidation with proton elimination to structure **9**. It has a resonance form **9a**, which participates in intermolecular 1,4-nucleophilic addition to produce **10**. It is followed by mono-electronic oxidation, resulting

in radical cation **11**. The stability of phenylenediamine radical cations is relatively high – $DMPD^{\bullet+}$ is commonly employed in oxidative stress and radical-scavenging assays (Verde et al., 2002; Kamer et al., 2019; Busuricu et al., 2008). Based on the structural similarities, it was assumed that conjugated DMPD trimer could also produce a radical cation. **11** reacts in radical addition to the *α*-position (relative to *N*,*N*-dimethyliminium group), creating a new C-C bond (**12**). Radical cation **12** undergoes spontaneous mono-electronic autoxidation with proton elimination **13**, a process reported for other phenylenediamine radical cations (Maleki and Nematollahi, 2013; Meyer and Fischer, 2015). The final reactions are H shifts (**14** and **14a**), which are driven by the thermodynamically favourable increase in the size of the delocalized electron system. The formed Ferbamine molecule is fully conjugated; thus, it has a multitude of resonance forms (not shown) to delocalise and stabilise the positive charge. The proposed mechanism was also supported by ATR-FTIR measurements of the Ferbamine synthesis media, taken at 1 h intervals for 3 h (**Figure 2.2**).

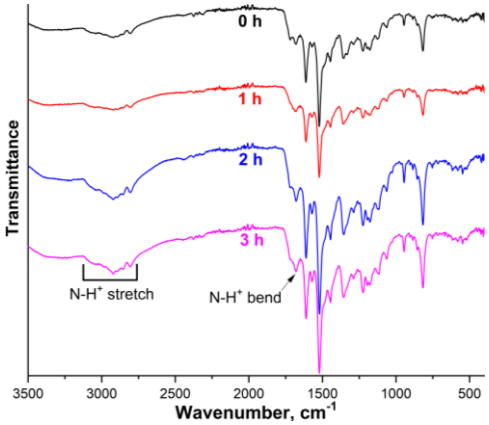
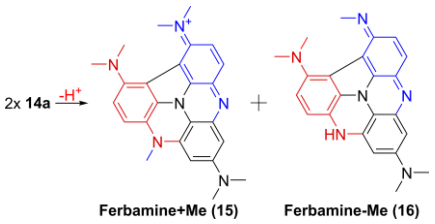


Figure 2.2 ATR-FTIR spectra of Ferbamine synthesis mixture after 0-3 h.

It revealed that the signal intensity in the 3100-3400 cm^{-1} range (N-H stretch) was low and did not show notable changes during the reaction, as expected. Proposed structures of intermediate and Ferbamine molecules have one N-H (secondary) bond; therefore, the N-H band should not have deviated during synthesis. The intensity for the 2750-3100 cm^{-1} range ($N\text{-}H^+$ stretch) band has increased moderately, but no overtone/combination band was observed in the 2500-2700 cm^{-1} range. The 1500-1700 cm^{-1} band ($N\text{-}H^+$ bend) had a slight increase at 1678 cm^{-1}, indicating that protonation was weak or mainly occurred for tertiary amine groups. Another possibility is that water acted as the primary H^+ acceptor, as evidenced by the reaction not occurring in solvents with low water content.

HRMS analysis of Ferbamine has also exposed the presence of two additional compounds – $C_{25}H_{27}N_6^+$ and $C_{23}H_{22}N_6$. We propose that these compounds are products of intramolecular methyl group transfer between two molecules of Ferbamine (**Scheme 2.3**).



Scheme 2.3 Proposed formation of Ferbamine synthesis by-products.

It has been shown that methylated quaternary ammonium and dimethyliminium groups can act as methyl-group donors to nucleophilic amines (Sikora et al., 2020; Sitte et al., 2019). In this case, a secondary amine group acts as a nucleophile, while the dimethyliminium group is the donor. It results in a Ferbamine molecule with an additional methyl group (Ferbamine+Me – **15**) and a Ferbamine molecule without a methyl group and with a positive charge (Ferbamine-Me – **16**). This assumption is consistent with the signal intensities in the HRMS results: the Ferbamine-Me intensity (9.64%) is significantly lower than those of Ferbamine (100%) and Ferbamine+Me (91.6%) because it is not an intrinsic cation.

The exploration of Ferbamine synthesis mechanism has revealed that it mainly follows the established phenylenediamine oligomerisation pattern. The mechanism showed multiple H^+ liberation steps supported by ATR-FTIR analysis. Since the reaction was not supplemented with additional bases, DMPD or its oligomers acted as the base. This could explain why both synthesis steps had such low yields. DMPD and its oligomers act as bases, yielding protonated compounds that are less nucleophilic and more resistant to oxidation. Another observation made in this mechanism was that it slightly deviates from the general phenylenediamine oxidation pathway. We have identified the formation of the dimethyliminium group as the primary cause of this deviation. Conjugated (*α,β*-unsaturated) dimethyliminium has a resonance form with the positive charge on the *β* position, as seen in the **1-1a**, **3-3a**, **5-5a**, and **9-9a** resonance pairs. The charge increases the selectivity of nucleophilic attack at the *β* position, as reported by Erkkila et al. (2007) and List (2009), leading to the formation of Ferbamine. It also implies that using other nucleophiles in DMPD oxidation could open a new, selective pathway for substrate synthesis in laccase functional analysis.

2.1.2. Thermal and pH Stability of Ferbamine

The top priority in developing Ferbamine was to maintain the compound's pH and thermal stability during screening assays. The UV-Vis spectra of native, partly oxidised or reduced Ferbamine solutions (**Fig. S1**) demonstrated that Ferbamine exhibits high absorption in the 550-570 nm range. Partially oxidised Ferbamine exhibited absorption in the shorter wavelengths – between 400 nm and the near-UV range. Based on these observations, UV-Vis spectroscopy was used to assess the stability of Ferbamine (*3.4.1*). In this set of experiments, 7.5 µg ml^{-1} Ferbamine was incubated in 50 mM K-phosphate buffer solution in a range of pH 3.5-8.0 at 20 °C, 30 °C, or 37 °C. The incubation buffer was limited to phosphate-based due to Ferbamine's strong interactions with certain common buffer anions, resulting in water-insoluble salts (data not shown). A solution of Ferbamine in dH_2O (pH 5.7) was used as a reference to pursue the influence of buffer ions. UV-Vis spectra of the solutions were measured once a week. The stability of Ferbamine was calculated as the percentage of the remaining absorption relative to the starting absorption (*3.4.2*). The stability data is presented in **Figure 2.3**.

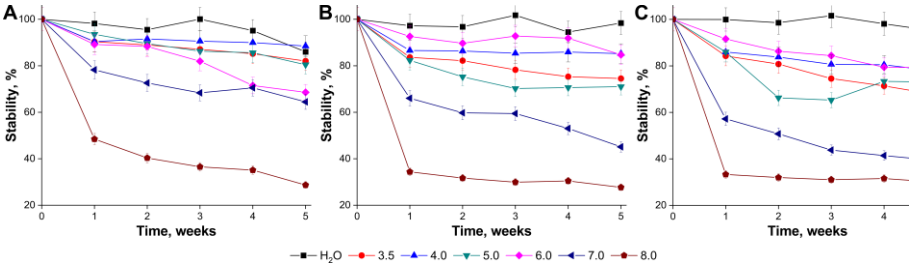


Figure 2.3 Thermal and pH stability of Ferbamine solution. Incubation temperatures: **A** 20 °C, **B** 30 °C, **C** 37 °C.

According to the results, the Ferbamine solutions, after 1 week at pH 3.5-6.0, retained more than 80% of their original absorption. After 5 weeks, it decreased to a 68-85% range. At pH 7.0, the absorption gradually decreased and remained above 60% at 20 °C (64.5%) at the end of incubation; while at 30 °C and 37 °C, it decreased to 45.1% and 39.3%, respectively. At pH 8.0, absorption dropped below 50% after the first week of incubation, reaching 28-30% after five weeks. The absorbance of the Ferbamine solution prepared in dH_2O did not fall below 86% at any temperature. It was clear that buffer ions negatively affected the stability. It is worth noting that the ABTS distributors state that it can be stored in a phosphate-citrate buffer at pH 5.0 for two weeks at 4 °C and for one month at -20 °C (ABTS Sigma-Aldrich®). Another conventional substrate – syringaldazine – requires MeOH to increase its solubility, making it incompatible with microorganisms (Syringaldazine

SIGMA-ALDRICH®, 2009). In essence, the results of this study have revealed that the stability of Ferbamine exceeds that of conventional laccase substrates, and this compound has potential as a substrate for methods requiring long-term incubations at elevated temperatures (Babinskas et al., 2024).

2.1.3. Application of Ferbamine in Agar Plates for Laccase Activity Screenings

Research on the applicability of Ferbamine for screening assays was conducted using Ferbamine-agar plates. Substrate-agar plate methods are very convenient for ascertaining functionality and do not require spectroscopy equipment such as a spectrophotometer or a well plate reader. The investigation was started with the commercially available laccase Novozymes® 51003. The laccase activity for this product was measured using Metol assay at 2.7 U ml^{-1} (*3.5.1*). 1 U was defined as 1 µmol of Metol oxidised per 1 min at pH 5.0 and 20 °C. 1-4 µl of this enzyme was added to the plate containing Ferbamine at a concentration of 4.5 µg ml^{-1} and incubated at 20 °C for 20 h (*3.6.1*) (**Figure 2.4**).

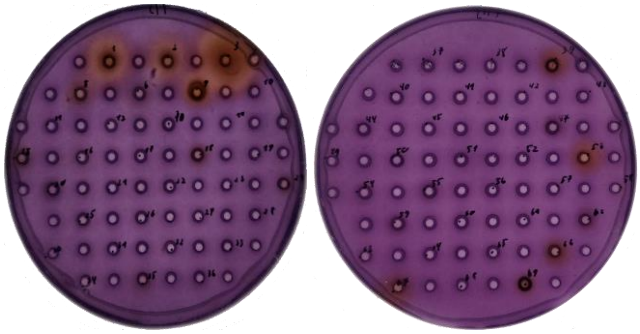


Figure 2.4 Functional analysis of Novozymes® 51003 laccase on the agar plates containing 4.5 µg ml^{-1} Ferbamine. Amount of the enzyme added, from left to right: 1, 2, 3, 4 µl. Incubation conditions: 20 h at 20 °C.

The absorption maximum of the oxidised Ferbamine was in the near-UV (400 nm) range (**Fig. S1**), which was observed as a pale yellow colour in the central area. The colour of the halo varied slightly with the amount of enzyme added, but overall oxidised Ferbamine was easily distinguished from the background by visual inspection.

Further screening with Ferbamine as a substrate was applied to survey laccase activity in extracts from wild terrestrial fungi. This collection of extracts was generously donated by Dr. Jerica Sabotič from the Jožef Stefan Institute (Slovenia) through COST action CA18238 “Ocean4Biotech”. The experiment was performed on 37.5 µg ml^{-1} Ferbamine-agar plates with wells: 2 µl of the extracts were added and incubated at 20 °C for 20 h (*3.6.2*). The obtained laccase activity results were classified into three levels based on the relative intensity of the colour change: +++ significant, ++ moderate, + detectable. In parallel, the spectrophotometric Metol assay screened for laccase activity in the fungal protein extract collection. The results of both screening approaches and previous reports on the presence of laccase in the tested species are presented in **Table 2.1**.

Table 2.1 The results of laccase activity screening in the collection of extracts from terrestrial fungi. The data is sorted according to Metol assay results.



Extract No.	Species	Assays		Previous reports on laccase[b]
		Metol, U ml^{-1}[a]	Ferbamine	
3	*Clitocybe nebularis*	9.00	+++	Yes (Asav, 2021)
39	*Psilocybe cubensis*	5.40	+++	Yes (Lenz et al., 2020)
6	*Cortinarius violaceus*	5.25	+	No (Chen et al., 2003)
2	*Macrolepiota procera*	4.80	+++	Yes (Luis et al., 2004)
50	*Gomphidius glutinosus*	3.90	-	Not tested
53	*Pleurotus eryngii*	2.70	+++	Yes (Guo et al., 2017)
1	*C. nebularis*	2.55	+++	Yes (Asav, 2021)
67	*Rhodocybe gemina*	1.65	+	Not tested
15	*Tricholoma tigrinum*	1.65	+	Not tested
66	*Tricholoma saponaceum*	1.50	++	Yes (Khaund and Joshi, 2014)
33	*Lentinula edodes*	1.13	-	Yes (Yano et al., 2009)
5	*Ganoderma lucidum*	1.05	++	Yes (Jeon et al., 2008)
55	*Gymnopilus penetrans*	0.90	+	No (Marr et al., 1986)
9	*Cortinarius caperatus* (*Rozites caperata*)	0.83	+++	Not tested
62	*Amanita vaginata*	0.83	+	Not tested
47	*Anthurus archeri* (*Clathrus archeri*)	0.75	+	Not tested
18	*Pleurotus ostreatus* (summer strain)	0.75	+	Yes (Park and Park, 2014)
35	*Clitocybe geotropa*	0.68	+	Not tested
54	*Amanita spissa*	0.68	-	No (Chen et al., 2003)
70	*A. vaginata*	0.68	-	Not tested
51	*Tricholomopsis rutilans*	0.68	-	Not tested
59	*Clavariadelphus pistillaris*	0.60	+	Yes (Marr et al., 1986)
40	*Ramaria stricta*	0.53	-	Yes (ABTS, guaiacol), No (syringaldazine) (Erden et al., 2009)
20	*P. ostreatus* (winter strain)	0.45	+	Yes (Park and Park, 2014)
36	*Russula alutacea*	0.45	+	Not tested

Table 2.1 Continuation

57	*Clitocybe geotropa*	0.38	-	Not tested
31	*Paxilllus atrotomentosus*	0.38	-	Not tested
69	*Cortinarius multiformis*	0.30	++	Not tested
32	*Clitocybe gibba*	0.30	-	Not tested
28	*Lactarius necator*	0.23	-	Not tested
63	*Amanita rubescens*	0.15	-	No (Hutchison, 1990)
58	*Craterellus cornucopioides*	0.15	-	Not tested
43	*P. ostreatus*	0.15	-	Yes (Park and Park, 2014)
42	*Xerocomus badius*	0.15	-	No (Hutchison, 1990)
65	*Agaricus bisporus*	0.08	-	Yes (Mayolo-Deloisa et al., 2011)
41	*A. rubescens*	0.08	-	No (Hutchison, 1990)
42	*A. rubescens*	0.08	-	No (Hutchison, 1990)
46	*P. atrotomentosus*	0.08	-	Not tested
24	*Amanita excelsa*	-	+	Not tested
16	*Macrolepiota rachodes*	-	+	No (Luis et al., 2004)
8	*Amanita citrina*	-	-	No (Hutchison, 1990)
61	*A. citrina*	-	-	No (Hutchison, 1990)
64	*A. citrina*	-	-	No (Hutchison, 1990)
37	*A. rubescens*	-	-	No (Hutchison, 1990)
60	*A. spissa*	-	-	No (Chen et al., 2003)
68	*A. spissa*	-	-	No (Chen et al., 2003)
21	*Armillaria borealis*	-	-	Not tested
22	*Boletus badius*	-	-	Not tested
11	*Boletus erythropus*	-	-	Not tested
25	*Coprinus comatus*	-	-	Yes (Bao et al., 2013)
34	*Fomitopsis pinicola*	-	-	Yes (Park and Park, 2014)
23	*Kuehneromyces mutabilis*	-	-	Yes (Gramss, 2020)
14	*L. necator*	-	-	Not tested
19	*L. edodes*	-	-	Yes (Yano et al., 2009)
56	*Lycoperdon perlatum*	-	-	Yes (Harkin et al., 1974)
27	*Sparassis crispa*	-	-	Not tested
10	*Suillus bovinus*	-	-	No (Timonen and Sen, 1998)
38	*Suillus granulatus*	-	-	Yes (Cullings et al., 2008)
17	*Suillus luteus*	-	-	No (Mucha, 2011)
30	*Suillus variegatus*	-	-	Not tested
26	*Tricholoma sulphureum*	-	-	Not tested

[a] 1 U is defined as 1 μmol of Metol oxidased per 1 min, at pH 5.0 and 20 °C.
[b] Yes – laccase gene or activity has been previously reported in the species; No – species has been tested, but laccase genes or activity was not detected; Not tested – species has not been tested for laccase genes or activity.

The lowest laccase activity detected by Ferbamine was 0.30 U ml^{-1} in extract N° 69. Extracts N° 6, N° 33 and N° 50 had high laccase activity in the Metol

assay (1.1-5.3 U ml^{-1}) but were only slightly or not detectable on the Ferbamine plates. N° 16 and N° 24 displayed noticeable activity on Ferbamine plates but showed no activity in the Metol assay. These deviations may have arisen from the enzymes' specificity (e.g., laccase's substrate selectivity) or from a possible dependence on pH or other factors. A similar inconsistency has been documented by Erden et al. (2009) for laccase activity screening in fungi using guaiacol, ABTS, and syringaldazine (N° 40). Out of 40 species presented in **Table 2.1**, laccase activity has been reported for 18 species in the literature. In this survey, eight species exhibited laccase activity, which, in other studies, were reported as laccase-negative. 18 species, to our knowledge, have not been tested before and displayed laccase-like activity using Ferbamine and/or Metol. In summary, Ferbamine displayed persuasive performance in detecting laccase activity in extracts from environmental samples and proved to be a suitable substrate for screening activities on agar plates. The intended application of Ferbamine also included screening live microbial cultures to discover laccases in wild cultures, in metagenomic libraries, or as engineered enzymes. For these reasons, the compatibility of Ferbamine with components of cultivation media and microorganisms had to be evaluated.

In the initial Ferbamine-agar plate preparation, agar powder was added to the Ferbamine solution, which was then autoclaved. This approach worked well, as agar did not affect the substrate, and it was used in testing with Novozymes® 51003 and in fungal extract screening. However, when media components for YEPG (yeast extract-peptone-glycerol) were used, the resulting Ferbamine plates did not exhibit the characteristic purple colouring. Autoclavation of Ferbamine with separate media components (yeast extract, peptone, glycerol) revealed that peptone was solely responsible for the discolouration of Ferbamine (data not shown). This indicated that peptone negatively affected Ferbamine and potentially hindered its application. In the YEPG case, this component could have been substituted with another, but it would have also required *a priori* testing with Ferbamine. Furthermore, many commercially available cultivation media are premixed, meaning that interfering components cannot be substituted. This implied that any interaction between substrate and cultivation components during preparation had to be minimised, regardless of the media type. For these reasons, concentrated Ferbamine and cultivation media solutions were autoclaved separately and then combined to produce the final product – Ferbamine-growth medium agar – without the limitations of the media components. The downside of this approach is that the initial 45 µg ml^{-1} Ferbamine solution is always diluted with the concentrated medium solution. That limits the

maximum Ferbamine concentration in cultivation media-agar at 37.5 μg ml^{-1}. In addition, it was tested that a concentrated medium solution cannot exceed 9% of agar; otherwise, the viscosity is too high to properly mix it with the substrate solution.

Following the establishment of a comprehensive Ferbamine-cultivation agar plate preparation methodology, the substrate's toxicity was another concern requiring examination. Ferbamine is a synthetic, phenazine-type substrate. Currently, compounds with a phenazine framework are being investigated as a new class of antibacterial agents against antibiotic-resistant bacteria (Sousa et al., 2024). Therefore, it was likely that Ferbamine could also inhibit microbial growth. Tests on the toxicity of substrate were performed on strains which are widely used as hosts for gene engineering, gene expression and the creation of genomic or metagenomic libraries (*3.6.2*): two strains of Gram-negative bacteria (*Escherichia coli*, *Pseudomonas putida*), two Gram-positive bacteria (*Rhodococcus erythropolis*, *Bacillus pumilus*) and four strains of yeast (*Kluyveromyces marxianus*, *Kluyveromyces lactis*, *Pichia pastoris*, *Saccharomyces cerevisiae*). Microorganisms were incubated for up to 168 h at different temperatures: *E. coli*, *P. putida*, and *B. pumilus* at 37 °C, and other strains at 30 °C. Ferbamine concentrations in the plates were 4.5 μg ml^{-1}, 22.5 μg ml^{-1}, or 37.5 μg ml^{-1}, and the plate omitting Ferbamine was used as a control (**Figure 2.5**).

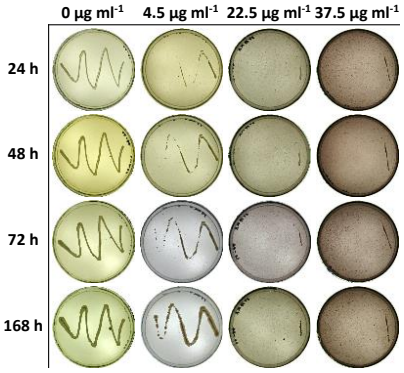


Figure 2.5 Results of Ferbamine concentration influence on the growth of *K. marxianus* on 0-37.5 μg ml^{-1} Ferbamine-YEPG agar plates.

The tests revealed that Ferbamine did not affect the growth of *E. coli* and *P. putida* – colonies were fully grown after overnight incubation (14 h) on the plate with the highest Ferbamine concentration (37.5 μg ml^{-1}). Data for the other strains, represented by results for *K. marxianus*, showed growth inhibition. After 168 h of incubation, little to no growth was observed on plates containing 22.5 μg ml^{-1} and 37.5 μg ml^{-1} of Ferbamine, while it was

protracted on plates with 4.5 μg ml^{-1} concentration. The difference in inhibition between Gram-negative and Gram-positive microorganisms led to an assumption that Gram-negative bacteria were more resistant to Ferbamine. To test it, an experiment was carried out on five Gram-negative bacteria (*Achromobacter denitrificans, Delftia acidovorans, Pseudomonas aeruginosa, Alcaligenes faecalis, Acinetobacter calcoaceticus*) from our own collection (Vilnius University). Microorganisms were grown on 37.5 μg ml^{-1} Ferbamine-nutrient and control (omitting Ferbamine) plates at 37 °C for 48 h (**Figure 2.6**).

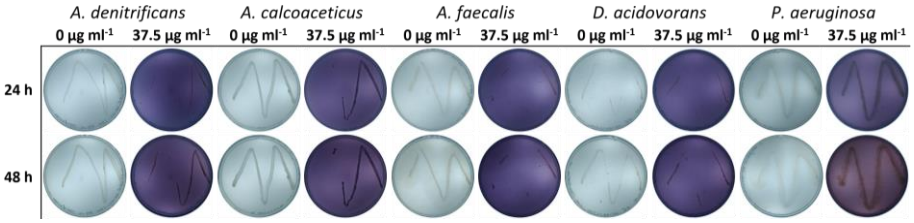


Figure 2.6 Results of Ferbamine concentration influence on the growth of *A. denitrificans*, *A. calcoaceticus*, *A. faecalis, D. acidovorans* and *P. aeruginosa* growth 37.5 μg ml^{-1} Ferbamine-nutrient agar and control plates.

The results revealed that microorganism growth on Ferbamine plates was only marginally slower than on control plates. This observation could be explained by the fact that Gram-negative bacteria are more resistant to chemical agents because their outer membrane acts as an additional barrier to the entry of molecules (Jones, 2017; Zhang et al., 2022).

To sum up, despite some limitations, Ferbamine is a suitable substrate for experiments involving common lab strains and can be applied in high-throughput screening of laccase activity on agar plates.

2.1.4. Screening of Wild-Type Microorganisms from Dinaric Caves

Up to this point, the microorganisms used for Ferbamine testing were pure colonies identified to the species level. Their use enabled the selection of suitable cultivation media and conditions to isolate the substrate's influence on microbial growth. However, the real challenge lay in the screening of unknown microorganisms directly from environmental samples. For the final testing of the Ferbamine application, colony screening was conducted in extreme cave ecosystems. The source of colonies was samples collected during the International speleological and speleodiving expeditions “Ponor Kovači – Izvor Ričine” (Tomislavgrad) in the period from August to September 2022 and the “Balkan Cave Summit (Mostar) 2022”, at seven localities in Bosnia and Herzegovina (*3.7*). Forty samples were collected from

six caves and an abandoned man-made railway tunnel (**Table S3**). Various objects were collected from different habitats, including subterranean fungi, entomophagous fungi, and decaying wood, as potential sources of enzymes involved in decomposition. Most of the samples included microbial biofilm on the cave walls and speleothems collected at different depths within speleological objects, i.e., at different heights above the cave floor. Of special interest was sampling moonmilk, a secondary calcite deposit composed mainly of fine $CaCO_3$ crystals, since the microbial communities in this substrate have been intensively investigated worldwide over the last decade (Portillo and Gonzalez, 2011; Maciejewska et al., 2017; Park et al., 2020). Bat guano and marten faeces samples were collected as a source of microorganisms from the animals' gut biota. In addition, several samples, such as a decaying horn overgrown with the stalkball fungus *Onygena equina*, a cocoon of an unidentified insect overgrown with entomophagous fungi and a deposit on a spider's net, are common finds in speleological objects and were also included in the analysis.

The cultivation of microorganisms from the collected samples was performed by washing a piece of the sample or diluting it with a sterile 0.9% (*w/v*) NaCl solution, streaking it onto cultivation agar media, and incubating the plates until colonies formed, up to 168 h (*3.7*). Two cultivation media types were selected for this study: modified Mueller-Hinton (mHM), which is better suited for bacterial cultivation, and YEPG, which is better suited for yeast and fungal cultivation. Each sample was incubated on two mHM and YEPG plates at 20 °C, 30 °C, or 37 °C, for a total of 160 plates. The cultivation was considered unsuccessful if no microbial growth was observed after 168 hours.

The incubation results showed that in all 40 samples, at least one of the four plates had microbial growth. Nevertheless, after 168 h of incubation, 20 mHM and 36 YEPG plates remained empty. The number of colonies exhibiting a distinct morphology (colour, texture, size, shape, pigmentation) per plate was as follows: 36 plates contained colonies with only one morphology; 41 plates – colonies with two morphologies; 20 plates – three morphologies; 6 plates – four morphologies; 1 plate – five morphologies. The total number of selected colonies was 207 (Babinskas et al., 2025).

The cultivation of microorganisms from subterranean environments yielded 104 agar plates containing 207 microorganisms, ready for functional screening. The screening process for laccase activity was performed using a cultivation medium augmented with 37.5 mg ml^{-1} of Ferbamine. Each microorganism culture exhibiting a distinctive morphology on its cultivation plate was transferred onto an appropriate screening plate and incubated at the

same temperature used for its cultivation. For instance, cultures cultivated on mMH at 20 °C were transferred onto mMH with Ferbamine and incubated at 20 °C. Incubations were performed for up to 168 h, with observations made at 24 h intervals. Notably, 29 of 207 transferred colonies failed to grow on media supplemented with Ferbamine. It was most likely due to substrate toxicity, which has been examined and confirmed in common lab strains of yeast and Gram-positive and Gram-negative bacteria. The most significant observation of potential laccase activity was recorded after 96 hours (**Figure 2.7**, left and middle plates), with three candidates for extremely low laccase activity identified on the YEPG-Ferbamine plate at 30 °C and one candidate on the mMH-Ferbamine plate at 37 °C.

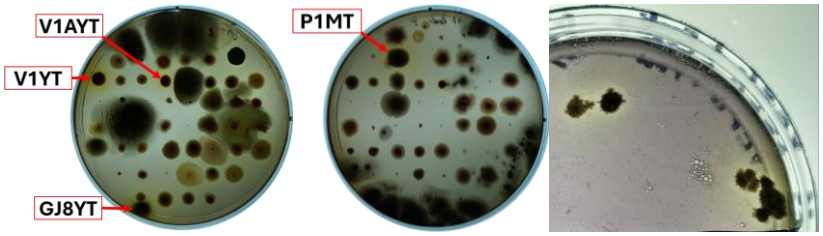


Figure 2.7 Laccase screening results after 96 h incubation. **Left plate** – with YEPG-Ferbamine growth medium; **middle plate** – mMH-Ferbamine growth medium; **right plate** – strain isolated from GJ8YT, after incubation on mHM-Ferbamine agar for 198 h at 37 °C.

The candidate colonies were labelled with their sample code and cultivation plate – YT for YEPG at 30 °C and MT for mMH at 37 °C. These colonies were then transferred and further grown in larger quantities on appropriate media with Ferbamine to confirm the laccase activity (*3.6.2*). The results indicated that GJ8YT growth was unaffected by Ferbamine, but the microorganisms exhibited only minimal laccase activity. Furthermore, colonies V1AYT and V1YT remained unaffected by Ferbamine, but they specifically formed areas of other yellow-coloured compounds rather than Ferbamine oxidation products. In the initial screening phase, these areas were identified as potential sites of laccase activity. The microorganisms from P1MT required 120 h of cultivation to reach a noticeable size and showed no evidence of laccase activity. In short, only one of the four candidate colonies showed a convincing indication of laccase activity. The isolation of laccase-producing microorganisms from the GJ8YT was carried out using the streak plate method on mMH, potato dextrose agar (PDA), Czapek, and YEPG, all supplemented with Ferbamine. After 168 h of incubation, only colonies on mMH-Ferbamine showed significant laccase activity (**Figure 2.7**, right plate). Identification of the 16S rRNA region and RpoB sequences was performed by

Jokūbas Krutkevičius (Sector of Applied Biocatalysis, Institute of Biotechnology, Life Sciences Center, Vilnius University) for all isolated microorganisms from GJ8YT (**Table 2.2**).

Table 2.2 Identified bacterial strains based on 16S rRNA and RpoB gene sequence.

Isolate media	16S rRNA gene sequence length, bp	Highest homology		
		16S rRNA gene sequence		
		nr/nt database[a]	RNA typestrains/16S ribosomal RNA database[a]	RpoB sequence nr/nt database[a]
Czapek	1420	*Bacillus* sp. (100%)	*Bacillus* sp. (100%)	*Bacillus subtilis* MB8_B10 CP045824.1 (100%)
PDA	1386	*Pseudomonas chlororaphis* subsp. *piscium* DSM 21509, CP027707.1 (100%)	*Pseudomonas chlororaphis* subsp. *aurantiaca* NCIB 10068 NR_164626.1 (99.93%)	-
mHM	1395	*Pseudomonas chlororaphis* subsp. *piscium* DSM 21509, CP027707.1 (100%)	*Pseudomonas chlororaphis* subsp. *aurantiaca* NCIB 10068 NR_164626.1 (99.93%)	-
YEPG	1399	*Pseudomonas chlororaphis* subsp. *piscium* DSM 21509, CP027707.1 (100%)	*Pseudomonas chlororaphis* subsp. *aurantiaca* NCIB 10068 NR_164626.1 (99.93%)	-

[a] If multiple BLAST results had the same Query Cover and Pairwise identity at the species level with the sequence of interest, only the first strain listed in the results was included in the table. Additionally, if more than one species in the BLAST results had the same Query Cover and Pairwise identity, the sequence of interest was classified solely at the genus level. The values of Query Cover and Pairwise identity are indicated in brackets. Strain accession numbers are indicated after the strain.

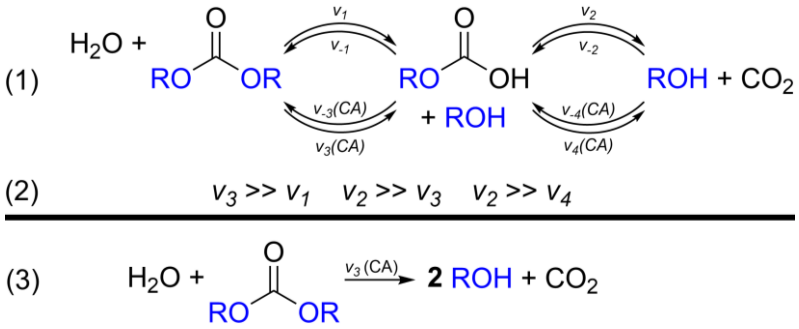
The analysis revealed that the microorganism with prominent laccase activity was identified as *Pseudomonas chlororaphis* by 16S rRNA sequencing (Babinskas et al., 2025). Interestingly, *P. chlororaphis* is known for producing phenazine-type antibiotics for fungal biocontrol (Chin-A-Woeng et al., 2000). Since Ferbamine is a phenazine-class substrate, it may have detected an enzyme with laccase-like activity involved in the antibiotic biosynthetic pathway. Additionally, screening of *Pseudomonas* species by Mandiac et al. (Mandic et al., 2019) has indicated that *P. chlororaphis* B561 exhibits weak laccase activity. In addition to *P. chlororaphis*, *Bacillus* sp. was isolated from GJ8YT, but it did not show laccase activity.

In summary, the effectiveness of Ferbamine in demonstrating laccase-like activity in microorganisms was validated. In addition, the observed inhibition of microbial growth in laboratory strains was less pronounced in wild cultures, with only 14% of the screened colonies failing to proliferate on substrate

plates. Compared to the cultivation effectiveness of microorganisms from environmental samples, the substrate's toxicity was only a minor challenge. Interestingly, the lack of laccase activity in screened microorganisms, especially from decayed wood samples from Vakuf Cave (GS1) and Gornja Jakovljeva Cave (GJ17), implies that prokaryotic laccases may not be so widespread in subterranean environments as they are on the surface (Claus, 2004; Santhanam et al., 2011; Kaur et al., 2022). Laccase-like enzymes were recently reported to be isolated from the saprophytic fungus *Gliomastix murorum* and the entomopathogenic fungus *Conidiobolus thromboides* from a cave in northern Spain (Fernández-Remacha et al., 2022). These findings may indicate a prevalence of eukaryotic laccase-like enzymes of fungal origin relative to those of bacterial origin, as supported by our observations during screening of fungal extracts. On the other hand, it is agreed that microbial diversity within cave ecosystems is largely unknown and is explored significantly more slowly than that of terrestrial and clinically relevant species. Further extensive research of underground ecosystems is required to reinforce these observations.

2.2. Development of the Carbonic Anhydrase Substrates

Carbonate esters are still largely underexplored as substrates for carbonic anhydrase (CA). We propose that they hold the potential to significantly change the landscape of CA functional analysis. This viewpoint is based on the premise that the unique pathways for their catalysed hydrolysis offer distinct advantages over the more commonly used carboxylic esters and hydration assays, as illustrated in **Scheme 2.4**.



Scheme 2.4 Simplified pathways of carbonate ester auto- (v_1/v_{-1}, v_2/v_{-2}) and CA-catalysed (v_3/v_{-3}, v_4/v_{-4}) hydrolysis.

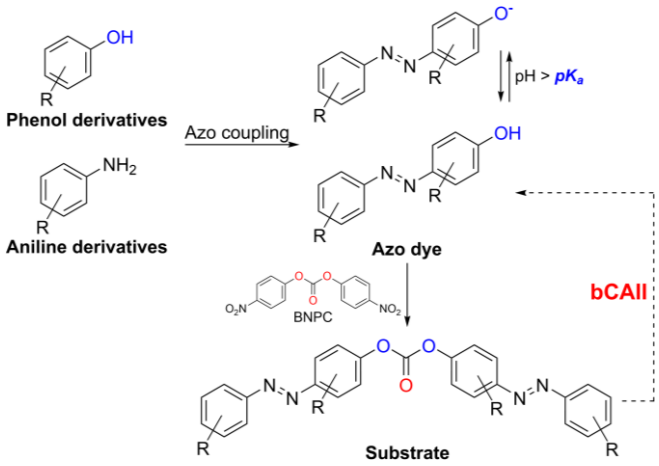
Our hypothesis posits that in an aqueous environment, activated carbonate esters undergo a two-step reversible hydrolysis. The first hydrolysis products, known as hemi-carbonate esters (RO-COOH), are extremely unstable in

aqueous environments with autohydrolysis rate coefficients exceeding 10^8 s^{-1} (Pocker and Guilbert, 1974). The rate of their catalysis (v_4) is negligible compared to the decay rate ($v_2 >> v_4$). This makes the first hydrolysis reaction the rate-limiting step of the process. If the catalytic ester hydrolysis proceeds significantly faster than autohydrolysis ($v_3 >> v_1$) and the initial substrate concentration is in excess, the reverse reaction (v_{-3}) becomes negligible. Under these conditions, the total catalytic rate can be represented by v_3, and a single catalytic cycle produces two ROH molecules, effectively doubling the intensity of the analytical signal. If ROH molecules exhibit different light-absorption properties from the initial carbonate, they can be utilised in spectrophotometric assays for enzyme functional analysis. To our knowledge, no direct spectrophotometric assay using this approach or these types of substrates has been reported. Typically, carbonate ester hydrolysis products are analysed using indirect multi-step enzyme-coupled colourimetric assays or chromatographic methods (Yang et al., 1998).

In this study, we explored phenyl azo dyes and their carbonates as a novel approach for the functional analysis of carbonic anhydrases. The research included the development of synthesis methods for dye carbonate and thiocarbonate esters. Selected compounds were characterised and incorporated into spectrophotometric assays to examine their catalysis rates by a model CA. The study also included CA inhibition experiments to identify the main limiting factors of carbonate and thiocarbonate substrates. Additionally, an *in silico* analysis of both the produced and proposed compounds was conducted to better understand factors influencing substrate properties and interactions with the enzyme, providing insights and highlighting the current limitations of computational mechanistic modelling.

2.2.1. Phenyl Azo Dye Carbonate Substrates: Synthesis and Activity Evaluation

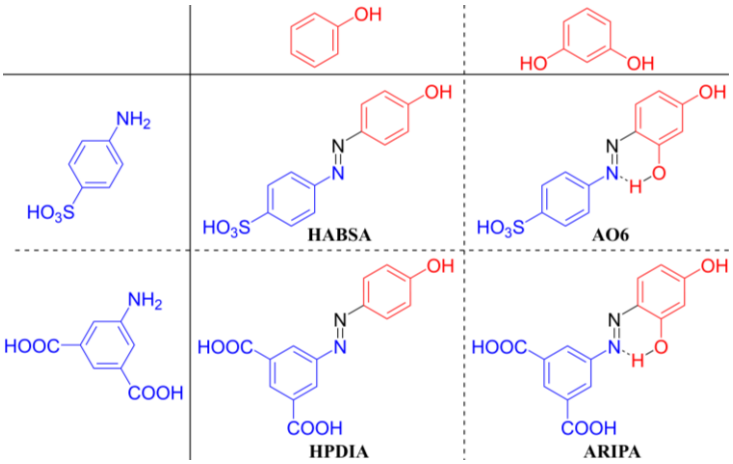
The research approach in this study involved azo coupling between phenols and acidic aniline derivatives to produce a small pool of phenol azo dyes, which would subsequently be converted into carbonate substrates (**Scheme 2.5**). Phenyl azo dyes contain a phenolic group linked to an aromatic system via an azo bridge. They exhibit strong light absorption due to n→π* and π→π* excitations. Deprotonation of the hydroxyl group in the phenolic moiety shifts absorption from near-UV to the visible range (bathochromic shift). It makes these compounds especially useful and attractive for UV-Vis assays. A key example is *p*-nitrophenol esters, which form *p*-nitrophenolate in enzyme assays for esterases, lipases, and phosphatases (Levine et al., 2008; Gil-Rodríguez and Beresford, 2020; Tang et al., 2019). Another concern is



Scheme 2.5 Generalised approach for carbonate substrate synthesis and application.

substrate solubility, which is crucial, as enzymatic assays are performed in aqueous buffers. Robust enzymes, such as lipases, can easily tolerate the presence of organic solvents. However, some water-miscible organic solvents can reduce carbonic anhydrase activity even at low concentrations of 1-2% (Roger Epton et al., 1977; R. Epton et al., 1977). Thus, only dyes exhibiting sufficient water-solubility were considered for their carbonate synthesis through a transcarbonation reaction with commercially available bis(*p*-nitrophenyl) carbonate (BNPC). The use of the produced carbonate esters as substrates was investigated using UV-Vis spectrophotometry. As a widely available and model enzyme, α-carbonic anhydrase II from bovine erythrocytes (bCAII) was selected for this research.

In the production of azo dyes, two types of aniline and phenol compounds were used (*3.3.2*): 4-aminobenzensulfonic acid (sulfanilic acid), 5-aminoisophthalic acid, along with phenol and 3-hydroxyphenol (resorcinol). The initial method for synthesising dye 4-(4-hydroxyphenylazo)benzensulfonic acid (HABSA) was refined into a general procedure by slightly adjusting the ratios of amine, nitrite, and phenol, and by reducing the solvent volume. Following this, high yields of 4-(2,4-dihydroxyphenylazo)benzenesulfonic acid (AO6), 5-(4-hydroxyphenylazo)isophthalic acid (HPDIA), and 5-(2,4-dihydroxyphenylazo)isophthalic acid (ARIPA) were achieved by substituting sulfanilic acid and/or phenol with appropriate components (**Scheme 2.6**). Product purification by recrystallisation was explored for each outcome to achieve higher-quality dyes without the use of time- and labour-intensive chromatography. It enabled the processing of large batches of dyes (2-5 g) in a short time span. For HABSA, recrystallisation in dH_2O rather than the



Scheme 2.6 Synthesised and investigated phenyl azo dye structures and abbreviations.

suggested ethanol increased the yield up to 76% (4% increase). AO6 and ARIPA recrystallisations were also conducted in dH_2O, yielding 50% and 57%, respectively. HPDIA showed lower solubility in water, so its recrystallisation was performed using a 2-propanol/dH_2O (1:4 *v/v*) mixture, yielding 61%. The investigation of various solvents for recrystallisation confirmed that these four dyes were sufficiently water-soluble for their intended applications. Therefore, the next step was to characterise the pK_a of these dyes.

The pK_a is a parameter that indicates the pH at which a functional group is at equilibrium with its deprotonated form. This parameter is particularly important for dyes containing a phenolic group, as deprotonation of the hydroxyl group increases electron density in the aromatic ring. As a result, the energy gap between the highest occupied molecular orbital and the lowest unoccupied molecular orbital is reduced, requiring less energy to excite electrons (Shimizu et al. 2020). In terms of physical properties, the deprotonated form of the compound shows increased water solubility and absorbs light at longer wavelengths. This characteristic makes these dyes more suitable for UV-Vis spectroscopic assays, as it shifts the absorption maximum into the visible range of the UV-Vis spectrum and typically increases the molar extinction coefficient (ε). It is generally advisable to avoid using the UV spectral range when conducting activity assays with protein extracts, concentrated supernatants, or other solutions containing unpurified proteins, as these solutions often show an intrinsically high absorption in the UV range. The pK_a values can be measured using various methods (Han and Priefer, 2023). We chose to use potentiometric titration with a pH meter and conductometer (*3.4.4*). Two compounds were selected for titration to

represent the two types of phenols in the dyes we produced: HABSA, with one hydroxyl group, and AO6, with two. The experiments involved titrating an aqueous HABSA solution with 0.1 M KOH and an alkaline AO6 solution with 0.1 M HCl while stirring. The pH and conductivity (σ) were recorded after the values stabilised for each aliquot of titrant added (**Figure 2.8**).

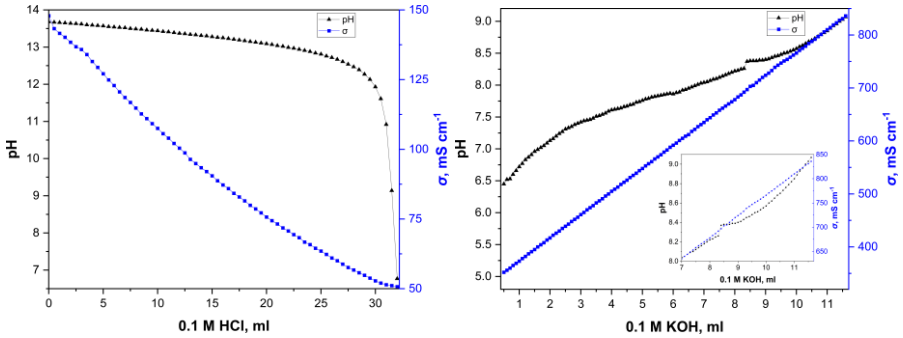


Figure 2.8 Titration pH and conductivity results: **left graph** – AO6; **right graph** – HABSA with insert showing zoomed plot in 7.0-11.7 ml KOH range.

The results indicated that conductivity increased proportionally with the addition of the titrant, but they did not provide information on the analytes' pK_a values. The titration of AO6 was conducted using the dye dissolved in a 0.8 M KOH solution to fully deprotonate both -OH groups. It was anticipated that the individual stages of protonation could be observed during the titration (**Figure S2**). The pH of the solution gradually decreased to around 12 and then, after a few aliquots, sharply dropped below 7, leading to the precipitation of AO6. This compound is known to function as a pH indicator, with an equivalence point near pH 11.8 (Ataman chemicals). The titration confirmed this value, which corresponds to the deprotonation of the second hydroxyl group (pK_{a2}). The first deprotonation (pK_{a1}) could not be determined with the approach employed.

During the HABSA titration, the dye was dissolved in water and titrated with 0.1 M KOH. The pH changes were more erratic compared to AO6, with a sudden increase observed between pH 8.26 and 8.37. The equivalence point corresponding to this increase, at pH 8.32, was attributed to the deprotonation of the phenolic -OH group. To further confirm this observation and to estimate pK_{a1} for AO6, UV-Vis spectra of the dyes were measured across a range of pH to observe the bathochromic shifts (*3.4.5*) (**Figure 2.9**). The AO6 spectra indicated that at pH 5.0, the absorption maximum was at 384 nm, with a broad peak. This peak shape was likely influenced by intramolecular hydrogen exchange between the hydroxy and azo bridge groups (**Scheme 2.6**). As the pH increased, the absorption maximum shifted to 428 nm and narrowed,

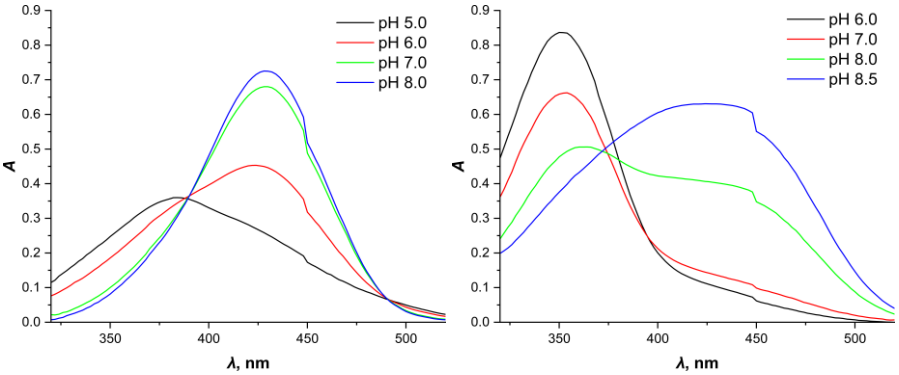
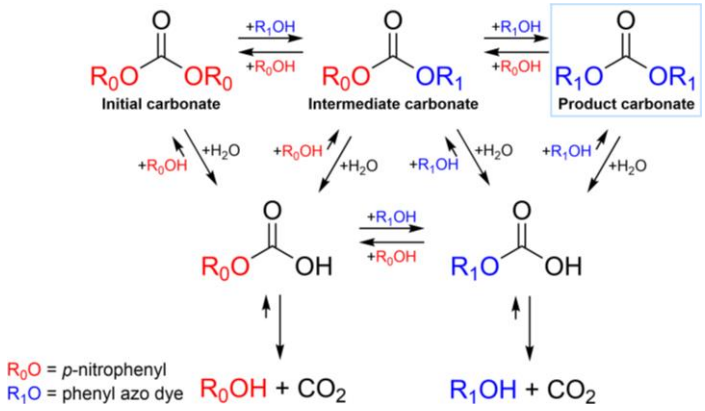


Figure 2.9 UV-Vis spectra of AO6 and HABSA in select pH ranges. **Left spectra** – AO6; **right spectra** – HABSA.

suggesting that the pK_{a1} of AO6 is around 6, as inferred from the changes in the absorption maximum and intensity. For HABSA, the absorption maximum was recorded at 350 nm at pH values below 8.0. By pH 8.5, the maximum shift to 420-440 nm indicated a significant deprotonation of the phenolic group. The titration and spectroscopy results concluded that the pK_a of HABSA is approximately 8.32.

The spectral measurements indicated that a pH of 7.0 was sufficient to induce a bathochromic shift in AO6, whereas HABSA required a pH of 8.5. Notably, after a single deprotonation, both dyes exhibited the same absorption maximum wavelength at 428 nm. The molar extinction coefficients were determined as follows (*3.4.6*): at pH 7.0, ε_{428}(AO6) was 34.0 mM^{-1} cm^{-1}, while at pH 8.5, ε_{428}(HABSA) was 13.4 mM^{-1} cm^{-1}. However, it is important to note that the hydroxyl group in AO6, which is responsible for the bathochromic shift, was not involved in the intended substrate synthesis, as illustrated in **Scheme 2.5**. It suggested that the AO6 carbonate ester could undergo a bathochromic shift without hydrolysis, challenging the rationale behind using this phenyl azo dye. For the other two dyes, HPDIA and ARIPA, only spectral measurements across a range of pH were conducted (data not shown). The bathochromic shift of ARIPA was similar to that of AO6, with its absorption intensity only marginally lower, measured at pH 7.0 as ε_{428}(ARIPA) 27.0 mM^{-1} cm^{-1}. This finding supports the idea that the hydroxyl group at position 2 is the primary factor influencing the spectral properties of dyes containing a 2,4-dihydroxyphenyl functional moiety. In contrast, HPDIA exhibited different behaviour compared to HABSA. At pH 8.5, its absorption maximum shifted into the visible region, while at pH 9.0, both maxima were observed at similar intensities. This indicates that the pK_a of HPDIA is around 9, suggesting that this dye would require a higher pH than the other compounds under investigation.

On an industrial scale, common carbonate esters such as ethylene carbonate, dimethyl carbonate, and glycerol carbonate are produced from appropriate epoxides via heterogeneous metal catalysis by oxidative carbonylation and transcarbonation, a type of transesterification for carbonate esters (Ramesh et al., 2018). These methods are effective when the products are relatively simple and highly stable under high temperatures and pressures. However, when the products contain multiple functional groups or are sensitive to environmental factors, phosgene (Cl-C(O)-Cl) or its analogue, triphosgene (Cl_3C-C(O)-CCl_3), is often used. The hydroxyl group can easily substitute chlorine or perchloroalkanes in these compounds under mild conditions to produce carbonate esters. By controlling the molar ratio of alcohol to phosgene, a mono-substituted product, known as chloroformate, can be isolated. Chloroformates are useful for the production of carbamates or unsymmetrical carbonates. Unfortunately, phosgene is a dual-use and extremely lethal gas, with an LC_{50} of 500 ppm for 1 minute of exposure (CDC 2020). Triphosgene, though considered a safer alternative due to its crystalline form, still poses risks as it exhibits toxic vapour pressure and can release gaseous phosgene or HCl (Li et al., 2014; Cotarca et al., 2017). In this work, we selected the transcarbonation method for synthesising phenyl azo carbonate esters because of safety concerns associated with perchlorinated carbonyls. It posed a challenge to develop a synthesis method that would allow the production of reactive carbonates under mild conditions. One of the main issues with reactive carbonates and their synthesis pathways is presented in **Scheme 2.7**.



Scheme 2.7 Transcarbonation and degradation pathways of carbonate esters.

The transcarbonation reaction relies on the principle that one alcohol compound can reversibly substitute another alcohol in an ester by forming a tetrahedral intermediate. Since carbonate esters contain two alcohol groups,

they can undergo two substitution reactions, as illustrated in the scheme. The key requirement for this reaction is that the attacking hydroxyl group must be more nucleophilic than the leaving alcohol. Fortunately, the nucleophilicity of aromatic hydroxyl groups strongly correlates with their pK_a values, enabling prediction of suitable starting reaction conditions and selection of appropriate initial carbonates. The pK_a values of the synthesised dyes (specifically, pKa_2 for 2,4-dihydroxyphenol groups) ranged from pH 8 to 12. This indicated that the pK_a of the alcohol in the initial carbonate needed to be below 8. Due to the limited availability of commercially viable carbonate esters, the only feasible option was bis(*p*-nitrophenyl) carbonate (BNPC). The pK_a of *p*-nitrophenol is reported to be ~7.15 (Aktaş et al., 2006), which met the necessary requirements. Additionally, this carbonate is one of the few available in bulk as a non-dual-use material, and its applications as a precursor or in other contexts have been well-documented in the literature (Teerawonganan et al., 2024). A significant drawback of the transcarbonation approach is that residual water initiates hydrolysis, forming a hemi-carbonate ester (RO-C(O)OH). These hemi-carbonate compounds can reversibly reform carbonates, but they are extremely unstable under normal conditions, requiring either liquid nitrogen or highly anhydrous environments for preservation (Bernard et al., 2017). Consequently, these hemi-carbonates further decompose into alcohols and CO_2. In summary, the presence of water in the reaction triggers a cascade of hydrolysis, resulting in the complete degradation of the carbonate functional group. Therefore, the objectives of this investigation were to: 1) identify a suitable solvent that would not degrade the initial and product carbonates while facilitating the solvation of the reactants; 2) screen and select an appropriate catalyst (base) to accelerate the synthesis reaction and prevent hydrolysis; 3) explore reaction conditions and product isolation methods; and 4) optimize the molar ratios of the initial carbonate, dye, and catalyst. In the development stage, HABSA was selected as the model dye.

The synthesis began with the selection of a reaction solvent. Experiments were conducted to qualitatively assess changes in the initial carbonate and to observe dye solubility. Examinations were carried out by placing a small amount of material in an Eppendorf tube, followed by the addition of the solvent. The stability of BNPC was assessed by observing CO_2 bubble formation or by monitoring pNP formation using TLC. The dye's solubility was easily evaluated by observing the intensity of the orange colour in the solution. Due to the nature of the transcarbonation reaction, protonic solvents were unsuitable and were not tested. The solvent screening included a range of solvents from aprotic, nonpolar to polar (**Table 2.3**).

Table 2.3 The qualitative results of reaction constituent stability and solubilities in apolar solvents.

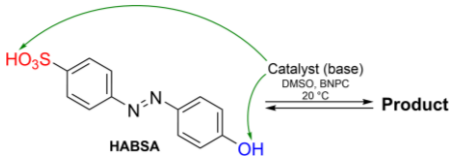
Solvent	BNPC stability[a]	BNPC solubility	Dye solubility	Observations
Hexane	+	+-	-	
Toluene	+	+	-	
Chloroform	+	+	-	
DCM	+	+	-	
THF	±	+	±	BNPC degraded over ~24 h
ACN	±	±	±	
Acetone	n.d.	n.d.	±	BNPC degraded promptly
DMF	n.d.	n.d.	+	BNPC degraded promptly
DMF (anhydrous)	±	+	+	BNPC degraded over ~48 h
DMSO	±	+	+	BNPC degraded over ~1 h
DMSO (anhydrous)[b]	±	+	+	BNPC degraded over ~48 h

[a] Ambient temperature (20 °C), not protected from light.
[b] Dried and stored over 4 Å molecular sieves.

A trend was observed: the stability of BNPC decreased as the solvent polarity increased. The initial assumption was that the hydrolysis rate increased due to the hygroscopic nature of the solvents. To test this hypothesis, anhydrous DMF and DMSO were used. The results showed that BNPC continued to degrade but remained detectable for up to 48 hours, suggesting that BNPC could be used in these solvents as long as anhydrous conditions are maintained and the reactions are concluded within this timeframe. Additionally, HABSA exhibited the highest solubility in highly polar solvents, such as DMF and DMSO.

The second component of the reaction under investigation was the catalyst. Although transcarbonation reactions can occur at higher temperatures without a catalyst (Cattelan et al., 2018), the instability of BNPC, even in anhydrous solvents, indicated that a catalytic reaction at room temperature or lower would be preferable. We chose to explore amine bases as catalysts since the nucleophilicity of the hydroxyl group is significantly enhanced by deprotonation. The experiments were conducted in DMSO containing 85 mM HABSA along with the appropriate amount of catalyst. Reactions were initiated by adding 1 equivalent of BNPC and were stirred for up to 30 hours (**Table 2.4**). The compositions of the reaction mixtures were analysed using TLC. The analysis showed that neither the uncatalyzed reaction nor the use of DABCO or DBU produced any products. In the case of DABCO, white particles precipitated, which were collected through centrifugation and identified as DABCO-H^+ salt by ATR-FTIR analysis. When DBU was added to the initial HABSA solution, the colour changed from the usual orange to

Table 2.4 Catalyst influence on BNPC-HABSA transcarbonation reaction at 20 °C.



Catalyst	Catalyst eqv.[a]	Reaction outcome	Observations
-	-	-	No reaction
DABCO[b]	1	-	White precipitate
Et_3N[c]	2	+	High BNPC conversion
DBU	2	-	BNPC degraded violently
Py[c]	2	±	Traces of the product

[a] 1 eqv. was used to deprotonate the sulfonic acid group.
[b] Has two amine (base) groups. Dried by storing over P_2O_5.
[c] Dried by distillation over KOH pellets and stored over 3 Å molecular sieves.

red, leading to a violent reaction with BNPC. This suggested that DBU was too strong and reactive to serve as a suitable base for the intended reaction. On the other hand, both triethylamine (Et_3N) and pyridine (Py) resulted in product formation. In the reaction involving Py, only trace amounts of product were observed, while Et_3N successfully converted the majority of BNPC in less than 20 min. It is important to note that TLC alone was insufficient to ascertain whether the product was a single or double-substituted HABSA carbonate.

The next step in the synthesis development was to identify the best method for isolating the products from the reaction mixture. Initial attempts using liquid-liquid extraction were unsuccessful, indicating that the produced carbonate had a high affinity for DMSO and was highly polar. Subsequently, a strategy to facilitate product precipitation was explored by reducing the solvent polarity *via* the addition of an antisolvent. The study involved mixing 0.5 ml of the synthesis mixture, which had reacted for 30 min, with 0.5 ml of an anti-solvent to observe any precipitation. The selection of anti-solvents was limited to aprotic non-polar solvents (hexane, toluene) and weakly polar solvents (chloroform, DCM, acetone, THF, ACN) previously used in evaluating BNPC stability. It was found that hexane, toluene, and chloroform did not affect the reaction mixture due to their low miscibility. In contrast, DCM, THF, and ACN successfully induced precipitation. Following this, centrifugation was performed, and particle and liquid analysis were conducted using ATR-FTIR and TLC. The results indicated that using THF and ACN primarily led to the precipitation of unreacted HABSA, while most of the product remained in the liquid phase. In contrast, DCM induced the precipitation of the product carbonate, which was contaminated with HABSA and Et_3N salts. To purify the solid carbonate, it was washed with acetic acid

to react with and remove residual Et_3N, then with MeOH to dissolve and wash out unreacted HABSA, and finally with DCM to remove residual pNP and solvents. NMR analysis of the remaining solid revealed that the product was a doubly substituted bis(HABSA) carbonate, designated as bis(HABSA)c, with a purity of approximately 98%. The overall yield of the process was 32%, confirming that one-pot transcarbonation under mild conditions was feasible for the production of activated carbonate esters. This synthesis approach was also tested with other dyes to determine its applicability to other compounds. Although appropriate carbonate esters were produced, the yields were disappointingly low, ranging from 3% to 10%. This suggested that case-by-case modifications were necessary to achieve adequate production.

The next step was to ascertain the reactant molar ratios to achieve the highest yields. In the initial experiments, it was found that using an excess of base did not improve synthesis yield; instead, it increased BNPC degradation. Therefore, Et_3N was only used to neutralise the sulfonic acid group and fully deprotonate the hydroxyl group. The HABSA-to-BNPC ratio showed a strong correlation with yield. An initial ratio of 2:1 for the chromophore to carbonate produced approximately 30% yield, as previously described. Increasing the amount of carbonate resulted in better yields, with the highest achieved at a 1:1.1 ratio, over 50%. It indicated that BNPC needed to be used in more than a two-fold excess.

The final step of the development process involved making adjustments and optimising the conditions for individual carbonate synthesis. The parameters investigated included solvents (DMF, DMSO), bases (Et_3N, DABCO, Py), temperatures (20 °C, 0 °C, -20 °C), reaction times (up to 48 h), and isolation conditions. The dye-to-BNPC molar ratio was set to 1:1.1. The optimisation criteria were yield and quality. The optimal ascertained conditions (*3.3.3*) for each dye carbonate synthesis are summarised in **Table 2.5**. The results indicated that DMSO was more effective than DMF for transcarbonation reactions involving selected azo dyes. For the synthesis of bis(HABSA)c, only minor adjustments to the initial conditions were necessary – specifically, a secondary reduction in temperature was implemented. This adjustment facilitated product precipitation and slowed its hydrolysis rate. However, the yield could not be increased beyond 50% without compromising the product's purity. The reaction time and temperature for bis(AO6)c were quite similar to those for bis(HABSA)c. In the synthesis of bis(AO6)c and bis(HPDIA)c, DABCO outperformed other amine bases. HPDIA showed poor reactivity in the transcarbonation reaction, requiring 20 h at 0-2 °C to achieve only about a 20% yield. In the case of bis(ARIPA)c, the synthesis yielded up to 50% of the crude product; however, adequate purification through washing

Table 2.5 Summarisation of phenyl azo dye carbonate synthesis conditions.

Carbonate	Solvent[a]	Base[a]	Reaction time and temperature	Anti-solvent	Product washing	Yield
bis(HABSA)c	DMSO	Et_3N	1) 5 min, 20 °C 2) 1 h, 0 °C	DCM	1) AcOH 2) MeOH 3) DCM	50.2%
bis(HPDIA)c	DMSO	DABCO	20 h, 0 °C	Et_2O and DCM	1) Et_2O 2) dH_2O 3) Acetone 4) DCM	19.1%
bis(AO6)c	DMSO	DABCO	1) 10 min, 20 °C 2) 1 h, 0 °C	Et_2O	1) Et_2O 2) MeOH 3) DCM	37.0%
bis(ARIPA)c	DMSO	Py	4 h, 20 °C	TOL	1) DCM 2) cHex	Crude

[a] Anhydrous.

with solvents proved unsuccessful, and rapid product degradation was observed during experiments. Both gravity and dry column vacuum chromatographies were attempted, but product hydrolysis resulted in only traces of the desired product – bis(ARIPA)c was excluded from further investigations.

In summary, the transcarbonation strategy was successful overall, although the production of certain carbonate esters was constrained by their stability. There are only a few published studies that utilised BNPC for the synthesis of symmetrical aromatic carbonates, with yields ranging from 23% to 52% (Brunelle, 1982). This range is similar to our findings; however, the reactions in those studies were typically conducted over 48 hours, whereas our longest production, bis(HPDIA)c, reached its highest yield in just 20 h. In other cases, the majority of the product was obtained within the first 5-10 minutes, with reaction times extended to achieve optimal results. The synthesis processes were quick, easily replicable, and scalable. This facilitated the production of substrates in large quantities, enabling research into their use in spectrophotometric CA activity assays.

With a reliable and easily replicable substrate synthesis procedure established, the next phase of the study focused on developing a spectrophotometric assay utilising these carbonate compounds. The selected model enzyme was commercially available α-carbonic anhydrase II from bovine erythrocytes – bCAII. The development of the assay involved exploring various substrates, buffer types and concentrations, co-solvents, enzyme concentrations, and assay durations.

The initial investigation indicated that only the bis(HABSA)c showed potential as a substrate. The compound bis(AO6)c proved to be incompatible with aqueous media. It demonstrated decent stability in organic solvents but

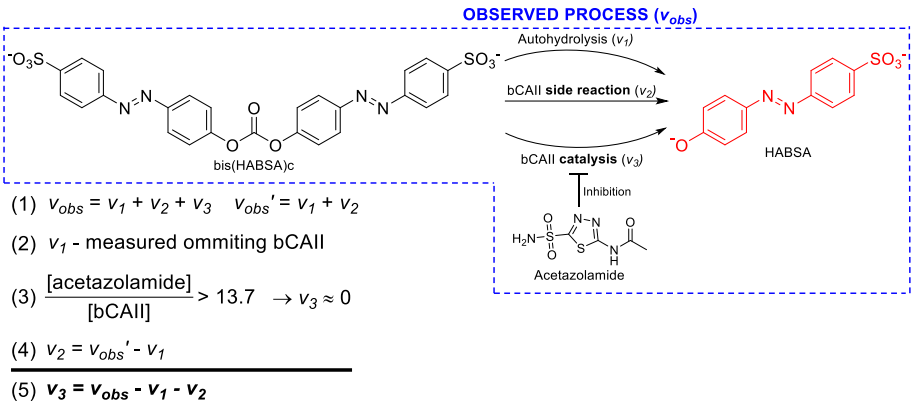
underwent complete hydrolysis within 10 min upon the addition of water. The intrinsic instability of both bis(AO6)c and bis(ARIPA)c suggested that the second, weakly acidic hydroxyl group was responsible for the degradation of the carbonate functional group. Meanwhile, bis(HPDIA)c exhibited extremely poor solubility in both organic and aqueous media, rendering it unsuitable.

The bis(HABSA)c was successfully incorporated into a spectrophotometric assay. The substrate was prepared in DMSO and then added to a 10 mM Tris-HCl buffer (pH 8.5) in the spectrophotometric cuvette. The reaction was initiated by adding the enzyme, and absorbance was monitored at 428 nm for 10 min. Initial results indicated that under these conditions, the substrate was undergoing autohydrolysis, but the rate was significantly lower than that of the enzymatic catalysis. By measuring reaction rates at different initial substrate concentrations (ranging from 0.1 to 1.0 mM), preliminary Michaelis-Menten kinetic parameters were determined using a nonlinear Hill-function fitting method and linear methods, such as the Lineweaver-Burk plot (data not shown). For the validation of the bis(HABSA)c assay, we investigated the inhibition of bCAII by acetazolamide (5-acetamido-1,3,4-thiadiazole-2-sulfonamide). This inhibitor exhibits an extremely high affinity for bCAII (K_i 10^{-7} to 10^{-8} M) (Pocker and Sarkanen, 2006) and is widely used as a model compound in carbonic anhydrase research. This property allowed us to select convenient inhibitor concentrations and easily compare our assay results to published data.

The experiments involved incubating the enzyme with the inhibitor for 30 min at a selected molar ratio of bCAII to acetazolamide, followed by measuring the catalytic rate across a substrate concentration range of 0.1 to 1.0 mM (*3.9.5*). The enzyme concentration in the reaction mixture was maintained at 1 mg ml^{-1} (34.4 μM). In these experiments, a decrease in enzymatic activity was observed, but it was far less than expected; for instance, we measured residual activity of 87% vs the 12% anticipated by Pocker and Stone (1967). These findings suggested that another reaction, in addition to substrate autohydrolysis and catalysis, was occurring at a significant rate.

The most likely source of the unknown side reaction was the enzyme, as the influences of inhibitors and buffers on the substrate were accounted for through control measurements. It was assumed that amino acid side groups not involved in catalysis were reacting with the bis(HABSA)c. To test this hypothesis, we substituted bCAII with bovine serum albumin (BSA), a non-catalytic protein. The results showed a significantly higher reaction rate than that of substrate autohydrolysis, confirming our assumptions.

The observation that bis(HABSA)c reacted with proteins raised concerns about the actual catalytic rates of bCAII. Additionally, the preliminary Michaelis-Menten kinetic parameters were deemed meaningless. To address these questions, an experimental scheme was designed to estimate the reaction rate of each component: substrate autohydrolysis, side reactions, and enzymatic catalysis (**Scheme 2.7**).



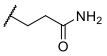
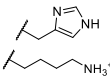
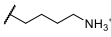
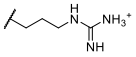
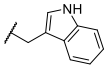
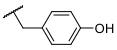
Scheme 2.7 Reactions observed in the bis(HABSA)c assay and workflow on how to calculate their individual rates

During the bis(HABSA)c assay, three main substrate reactions occurred: autohydrolysis (v_1), unknown side reactions with the protein molecule (v_2), and catalytic hydrolysis (v_3). All three reactions resulted in the same outcome, the release of HABSA, so the total process was observed spectrophotometrically as v_{obs}. The autohydrolysis rate (v_1) was always measured as a control by performing the reaction in the absence of the enzyme. To investigate v_2 and v_3, an excessive amount of inhibitor was used to render the catalytic process undetectable ($v_3 \approx 0$), which reduced the total observed reaction rate to v_{obs}'. The ratio of acetazolamide to bCAII at which catalytic activity becomes undetectable is reported to be 13.7 (Pocker and Stone, 1967). In this study, we used a ratio greater than 24 to ensure complete loss of catalytic activity. With this, the rate of the side reaction (v_2) was calculated by subtracting the substrate autohydrolysis rate from the reduced total reaction rate: $v_2 = v_{obs}' - v_1$. The enzymatic catalysis (v_3) was then determined by subtracting the rates of autohydrolysis and the side reaction from the total observed rate: $v_3 = v_{obs} - v_2 - v_1$. Using the presented experimental scheme, the reaction rates for bis(HABSA)c were measured using a 0.5 mM substrate (5% DMSO) and 1 mg ml^{-1} bCAII in 10 mM Tris-HCl buffer at pH 8.5. The measurements were conducted for 10 min at 20 °C. The observed reaction rates and their contributions to the total process were as follows:

autohydrolysis (v_1) – 1.96 μM min^{-1} (36.5%); side reactions (v_2) – 2.63 μM min^{-1} (49.0%); catalytic hydrolysis (v_3) – 0.78 μM min^{-1} (14.5%). It revealed that nearly half of the total observed rate in the bis(HABSA)c assay was attributed to non-catalytic side reactions between the substrate and the enzyme. In contrast, the catalytic reaction accounted for only 14.5% of the overall process, while autohydrolysis represented 36.5%. This data confirmed that bCAII catalyses the hydrolysis of carbonate substrates, but the catalytic reaction was a minor component of the observed process.

The analysis of the reaction rates in the bis(HABSA)c assay implied that this substrate was generally incompatible with proteins. Other substrates proved unsuitable for other reasons, such as stability or solubility issues. Consequently, the only viable option was to minimise interference from side reactions by adjusting the assay conditions. However, to accomplish this, it was crucial to gain a better understanding of the side reactions occurring between the substrate and the amino acids. The primary objective of this experiment was to identify which amino acid side groups were reacting with the substrate. To achieve this, bis(HABSA)c assays were conducted with a selection of individual amino acids (**Table 2.6**). Some of the amino acids included an N_α-acetyl (Ac) or chloroacetyl (AcCl) group to prevent interference from the primary amine.

Table 2.6 The bis(HABSA)c reaction rates with selected amino acids.

Amino acid	Side chain	Reaction rate, μM min^{-1}[a]
Gly	-H	0.68
Gln		0.21
Ser		0.12
N_α-Ac-Cys		26.1
N_α-Ac-His		2.27
N_α-Ac-Lys		0.50
N_α-Ac-Arg		0.05
N_α-Ac-Trp		0.02
N_α-AcCl-Tyr		0.01

[a] 0.5 mM bis(HABSA)c, 0.5 mM amino acid, 5% DMSO, 10 mM Tris-HCl pH 8.5, 10 min, 20 °C. bis(HABSA)c autohydrolysis rate subtracted.

The analysis revealed that amino acids containing nucleophilic groups were the most reactive. This was particularly evident for cysteine, which reacted more than 38-fold faster than glycine. This high reactivity was attributed to the sulfide anion present in its side group. The imidazole ring in histidine also

exhibited increased reactivity, while the reactivity of lysine N_ε was slightly lower than that of glycine N_α. In contrast, glutamine and serine showed only minor reactivity, which could be attributed to their free N_α groups. Reaction rates for tryptophan, arginine, and tyrosine were negligible.

An additional experiment was conducted using bis(HABSA)c and glycine to better understand the nature of the side reactions and their outcomes. A solution containing 67.7 μM of the substrate and glycine was incubated in a buffer at pH 8.5 for 6 h. The reaction had two potential outcomes: 1) the amino acid reacted with the substrate to form a stable carbamate, releasing one dye molecule for each molecule of substrate in the process; or 2) glycine acted as a catalyst, resulting in substrate degradation and the release of two dye molecules per substrate molecule. After incubation, UV-Vis spectra over the range of 320-520 nm were measured for the reaction mixture, followed by measurements for 67.7 μM and 135 μM HABSA solutions at the same pH. The analysis showed that the spectrum of the reaction mixture closely matched that of the 135 μM HABSA solution, indicating that the dye concentration was twice that of the initial substrate. This finding suggested that the amine group catalysed the complete degradation of the substrate's carbonate ester functional group.

Based on the data collected, the most effective strategy to reduce reactions between amino acids and bis(HABSA)c was to lower the buffer pH. Lowering the pH converts cysteine-S^- to -SH and limits the reactivity of amine groups. For this reason, assays were conducted within a pH range of 6.0 to 7.2, using glycine, N_α-Ac-cysteine, and N_α-Ac-histidine. The results indicated that at pH 7.2, the reaction rate with glycine decreased significantly from 0.68 μM min^{-1} to 0.02 μM min^{-1}. However, both N_α-Ac-Cys and N_α-Ac-His continued to exhibit substantial reaction rates of 2.03 μM min^{-1} and 1.29 μM min^{-1}, respectively. For the subsequent measurements, the pH was further lowered to 7.0. At this pH, the reaction with glycine became undetectable, while the reaction rates for the other two amino acids decreased to 1.39 and 1.10 μM min^{-1}. Further decrease in pH resulted in the immediate precipitation of the substrate. It indicated that a pH below 7.0 was unsuitable for bis(HABSA)c. The observed pH dependence of the reaction could be explained by the formation of intermediate carbamates and their degradation pathways (**Figure S3**). Since N_α-blocked cysteine and histidine exhibited the lowest reaction rates with the substrate at pH 7.0, this pH was utilised to determine the reaction rates v_1, v_2, and v_3, as previously described in **Scheme 2.7**. The reactions were monitored at 380 nm, which corresponds to the dye's absorption maximum at pH 7.0. The results obtained are summarised in **Table 2.7**, along with data at pH 8.5 as a reference.

Table 2.7 Constituent reaction rates in the bis(HABSA)c assay at pH 8.5 and 7.0.

	pH	Autohydrolysis (v_1)	Side reactions (v_2)	bCAII catalysis (v_3)
Reaction rate, μM min^{-1}	8.5	1.96	2.63	0.78
	7.0[a]	0.47	1.32	0.10
% of total process (v_{obs})	8.5	36.5%	49.0%	14.5%
	7.0	24.9%	69.8%	5.3%

[a] 0.5 mM bis(HABSA)c, 5% DMSO, 10 mM HEPES pH 7.0, 10 min, 20 °C, ε_{380} 0.0130 μM^{-1} cm^{-1}.

The study demonstrated that lowering the assay pH from 8.5 to 7.0 reduced the rates of the side reactions and autohydrolysis by factors of 2 and 4, respectively. However, this change also led to a near eightfold decrease in the enzymatic rate of catalysis, reducing its contribution to the overall process from 14.5% to 5.3%.

To summarise, we have developed a simple synthesis method to produce activated carbonate esters via transcarbonation. Our investigation into their use as substrates for measuring carbonic anhydrase activity confirmed their potential applications. However, we identified several limitations, including low solubility in both organic and aqueous media, insufficient stability, and inevitable side reactions with protein structures. After exploring the nature of the side reactions and attempting to mitigate them by adjusting assay conditions, the only viable option left was to modify the carbonate group itself.

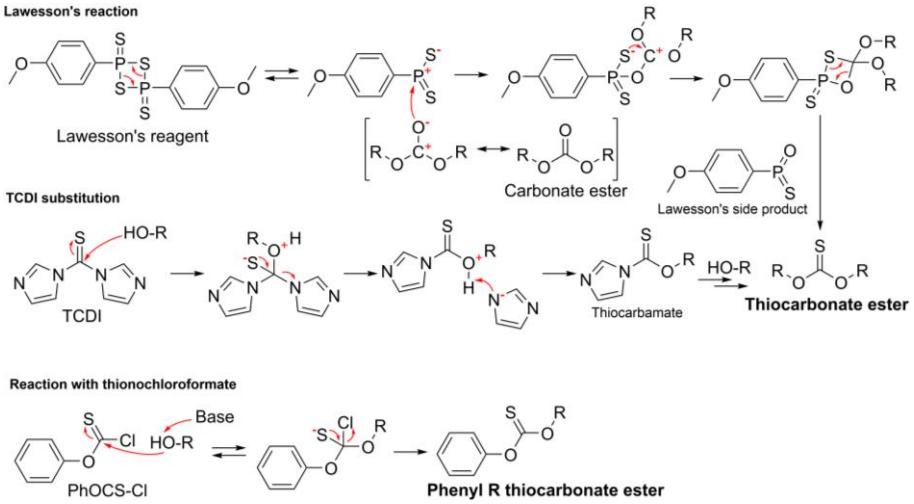
2.2.2. Thiocarbonate Ester Substrates: Synthesis and Evaluation

The thiocarbonate ester functional group is similar to the carbonate ester, but it features sulphur atoms in place of one or more oxygen atoms. These functional groups can exist in various forms, depending on the number of sulphur substitutions: mono-, di-, or tri-thiocarbonates. Additionally, these substitutions can exhibit isomerism; for instance, oxygen can be replaced either in the alcohol oxygen or the carbonyl. In our study, we focused solely on mono-thiocarbonates, in which a sulphur atom substitutes for oxygen in the carbonyl group (-C=S). This approach allowed us to utilise the synthesised dyes without further modifications. To our knowledge, thiocarbonate compounds have not been studied as substrates for CA enzymes, and it was unclear whether their hydrolysis was facilitated by these enzymes.

Common methods for synthesising thiocarbonates typically involve thiophosgene. While it is less lethal than phosgene, thiophosgene is still an extremely dangerous and volatile liquid (Hobson et al., 2019). Other methods for producing thiocarbonyl compounds are not well studied, primarily due to the rarity of this chemical group and its underexploited applications. There are only a few published methods for synthesising symmetrical thiocarbonates

without resorting to extremely hazardous materials, and these methods have only been successfully applied to specific compounds (Onyancha et al., 2009). Our previous approach, transesterification, is not suitable for thiocarbonate synthesis because no commercially available thiocarbonates are suitable as the ester base. Therefore, the main challenge of this study was to develop a synthesis method for activated thiocarbonate substrates without employing transcarbonation.

Thus, we explore three methods for synthesising thiocarbonate esters (*3.3.4*), as illustrated in **Scheme 2.8**: 1) the direct transformation of carbonates into thiocarbonates; 2) the substitution of imidazoles in thiourea compound 1,1-thiocarbonyldiimidazole (TCDI); and 3) the synthesis of unsymmetrical thiocarbonates using *O*-phenyl thionochloroformate (PhO-C(S)-Cl).



Scheme 2.8 Investigated approaches for the synthesis of thiocarbonate ester substrates.

The direct transformation method utilised Lawesson's reaction, which employs appropriately named Lawesson's reagent (LR). This reagent replaces the oxygen atom in the carbonyl group with a sulphur atom. It is a well-established and widely used method in both laboratory and industrial applications due to its high selectivity and yields. Although its application with carbonate esters has not been reported yet. The second strategy employed a thiourea reagent, TCDI. This compound is commonly used to convert amines to isothiocyanates (-NCS), synthesise thioureas, form heterocycles, or create intermediate imidazole-thiocarbamates (RO-C(S)-imidazole) (Schwan and Byers, 2007). Onyancha et al. (2009) have demonstrated that it is possible to produce thiocarbonates using this reagent; however, their success was limited to a single case. The third strategy involved using a commercially

available thionochloroformate compound, PhO-C(S)-Cl. This compound is produced by reacting thiophosgene with phenol in a 1:1 molar ratio, yielding a mono-substituted thiophosgene derivative. The chlorine atom in PhO-C(S)-Cl can be readily substituted with a compound containing a nucleophilic group, such as an amine, hydroxyl, or thiol. A limitation of this strategy is that phenol is not a good leaving group (pK_a ~10), making substitution with our phenyl azo dyes unfavourable.

The investigation of thiocarbonate synthesis used two phenyl azo dyes (HABSA and AO6) and either pNP or its corresponding carbonate ester. The Lawesson reactions were conducted in several solvents (toluene, THF, DCM) at either 20 °C or under reflux of the appropriate solvent, employing a fivefold excess of Lawesson's reagent for 24 hours. The results of the TLC analysis indicated that bis(HABSA)c did not react under any of the tested conditions, while bis(AO6)c completely degraded even under mild conditions. The carbonate derived from pNP, BNPC, exhibited slight reactivity in toluene at reflux temperature, yielding traces of the expected product and Lawesson's reagent byproducts. By applying liquid-liquid extraction followed by chromatographic separation, approximately 0.8 mg of crude thio-BNPC oil was isolated from a 5 g reaction mixture. The reaction yields were extremely low due to BNPC degradation during the process, as evidenced by the high levels of pNP in the reaction mixture. ATR-FTIR analysis supported the identity of the targeted product, but a conclusive confirmation without higher-resolution methods such as NMR could not be achieved. Additionally, the product released a strong odour of sulfides. One significant drawback of Lawesson's reaction is the contamination of the products with sulfides and other byproducts, which are notoriously difficult to remove (Wu et al., 2021). In essence, Lawesson's reaction for converting carbonates to thiocarbonates proved to be inapplicable. The data indicated that only BNPC was reactive enough to undergo transformation, but the yields were exceedingly low, below 0.1%. Additionally, thio-BNPC would have served only as an intermediate compound in the development and production of thiocarbonate dye esters, meaning it would be required in quantities exceeding the microgram scale. Research by Nishio and Ori (2000) examined Lawesson's reagent reactivity with various substituted carbonyls, revealing that electron-rich oxygen in hydroxyls or amides showed high reactivity. In contrast, electron-withdrawing groups, such as carboxylic esters, were found to be the least favourable for the Lawesson's reaction. Extrapolation of their results suggests that carbonate esters may exhibit even lesser reactivity, as supported by our findings and the lack of published successful cases.

The second strategy for synthesising thiocarbonates involved using a thiourea compound, TCDI. In our experiments, we tested the reactions using HABSA, AO6, and pNP in various solvents (toluene, THF, DCM) as well as in solid phase, with and without catalysts (Et_3N, Py, DABCO, imidazole), at various temperatures (20 °C, 40 °C, and reflux). The TLC analysis results showed that HABSA and AO6 were unreactive under all tested conditions. In contrast, pNP readily reacted with TCDI in both solvent and solid-phase reactions, with and without catalysts, and even at ambient temperature. Unfortunately, in this case, the product was not the desired thio-BNPC but rather a thiocarbamate (pNP-C(S)-imidazole). Furthermore, we discovered that this thiocarbamate was unstable and would completely degrade within 24 to 30 hours. Attempts to perform secondary reactions to convert this compound into the thiocarbonate using pNP, HABSA, or AO6 were unsuccessful. In summary, while this strategy showed promise in the reaction between TCDI and pNP, the resulting product was not the target compound and could not be utilised further. The only well-documented application of thiourea in the formation of thiocarbonates is the Corey-Winter-Eastwood olefination (Schwan and Byers, 2007). This method utilises thiophosgene or its analogues, such as TCDI, to convert vicinal diols into thiocarbonates, which subsequently undergo syn-alkene formation. This reaction has been shown to work only with saturated and vicinal hydroxyls. Other examples of successful thiocarbonate formation involved alkyl hydroxyl groups, such as those in 4-trifluoromethylbenzyl alcohol (Onyancha et al., 2009). There has been no documented success with phenolic compounds. Additionally, the mechanisms involved in TCDI reactions are significantly underexplored, restricting further attempts to improve the strategy (Paul-Gorsline, 2024).

The third strategy for synthesising thiocarbonates involved using a commercially available compound, *O*-phenyl thionochloroformate (PhO-C(S)-Cl). The reaction between PhO-C(S)-Cl and HABSA was created based on the bis(HABSA)c synthesis model. To prevent degradation of PhO-C(S)-Cl, DMSO was replaced with DMF, while the reaction was carried out in a similar manner: HABSA and Et_3N were added to the solvent, followed by PhO-C(S)-Cl. The mixture was stirred for 10 min at ambient temperature and then centrifuged to collect the crude product. The solids were washed with dH_2O, MeOH, and DCM, affording 72.5% yield of the target product, PhO-C(S)-HABSA. In short, of the three investigated strategies for the synthesis of thiocarbonate esters, the use of thionochloroformate proved successful. Its straightforward application produced the targeted thiocarbonate in high yields and could be scaled up for high-quantity substrate production.

The newly produced substrate, PhO-C(S)-HABSA, was used in the bCAII activity assay instead of bis(HABSA)c, as previously described for pH 8.5. We calculated the reaction constituent rates both with and without the addition of acetazolamide, following the earlier experimental scheme. The data revealed that the substrate's autohydrolysis rate (v_1) accounted for 8.4% (0.38 μM min^{-1}) of the total observed process, while the non-catalytic reaction rate (v_2) contributed 30.3% (1.37 μM min^{-1}), and the bCAII catalysis rate (v_3) made up 61.3% (2.78 μM min^{-1}). This confirmed the hypothesis that the hydrolysis of thiocarbonates could be catalysed by carbonic anhydrases. Moreover, the catalysis rate of the substrate was 3.5-fold higher than that of bis(HABSA)c, whereas the side reaction and autohydrolysis rates were at least two and five-fold lower, respectively. This suggests that not only can thiocarbonates be used as substrates, but their performance might also exceed that of carbonate esters. Nonetheless, without a direct comparison between carbonate and thiocarbonate esters, such as bis(HABSA)c and its thiocarbonate equivalent, this claim cannot be verified.

2.2.3. In Silico Evaluation of Carbonate and Thiocarbonate Ester Substrates

To address the lack of experimental results, we employed computational methods to simulate the observed reactions. Experimental observation, when correlated with theory-based models, enhances understanding of processes at a fundamental level and provides guidance for future improvements. The first theoretical approach utilised molecular dynamics (MD) simulations involving bCAII and bis(HABSA)c (*3.11.1 and Electronic Supplementary Materials*). The aim of this approach was to simulate the enzyme-substrate complex within a water box at various stages of the reaction. From these simulations, average structures were generated and analysed to identify which amino acids were crucial for substrate-enzyme orientation and to examine their behaviour at different reaction stages. The initial simulation was conducted with the bCAII structure in the absence of a ligand, followed by simulations including bis(HABSA)c, the tetrahedral intermediate of the substrate, and HABSA hemi-carbonate and $HABSA^-$ pair. The ligand structures used for simulations were optimised using a QM density functional theory (DFT) method 6-31G**/M06-2X. The initial bCAII model was sourced from the Protein Data Bank (PDB code 1V9E) (Saito et al., 2004). The main MD simulation parameters were as follows: minimisation time – 0.5 ns; simulation time – 1.0 ns; temperature – 293.15 K; solvent box dimensions – extended 20 Å beyond the protein's bounding box. The average simulation structures were generated after the system had relaxed and reached equilibrium, based on the

root-mean-square deviation (RMSD) of C_α atoms. Typically, this status was reached before the 0.5 ns mark.

The analysis of simulations and average structures indicated that the side groups of Thr197 and Thr198, located within the active site pocket, played a critical role in positioning the OH^- and the substrate. In the free enzyme form, the Thr198 side group alternated between forming hydrogen bonds with OH^- and Thr197 nearby. The average reduced structure from this simulation is shown in **Figure 2.10 A**, with average hydrogen bond lengths of 3.91 Å and 3.83 Å. The enzyme backbone was hidden for visual clarity.

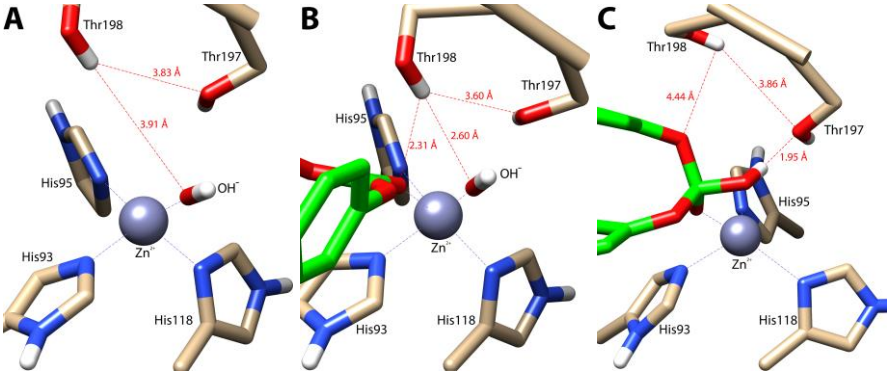


Figure 2.10 The average reduced bCAII MD simulation structures. bis(HABSA)c ligand structures – green; hydrogen bond dotted lines – red. **A** – native enzyme; **B** – with bis(HABSA)c; **C** – with bis(HABSA)c tetrahedral intermediate.

The introduction of the substrate reduced this alteration, directing Thr198 toward the OH^- ion and the O=C (ligand) (**Figure 2.10 B**). The average interaction distances ranged between 2.3 Å and 2.6 Å. The hydrogen bonding distance between Thr198 and Thr197 decreased to 3.6 Å. The next ligand structure was formed by bonding the OH^- ion to the substrate's carboxyl group, resulting in a tetrahedral intermediate. The simulation indicated that the newly formed -OH group exhibited strong hydrogen bonding with Thr197, with an average distance of 1.95 Å (**Figure 2.10 C**). Interestingly, the interactions between Thr198 and the substrate became weaker and longer, whereas the interactions with Thr197 returned close to the enzyme's initial state. The final step of the simulation involved a hemi-carbonate bound to the Zn^{2+} ion, with the $HABSA^-$ anion situated nearby. This model was the least accurate because the complexation of the formed acids with Zn^{2+} in the CA active site is not well understood and, as a result, was not included in the analysis.

Further analysis was undertaken by isolating the substrate and the enzyme's active-site pocket from the generated average structures and

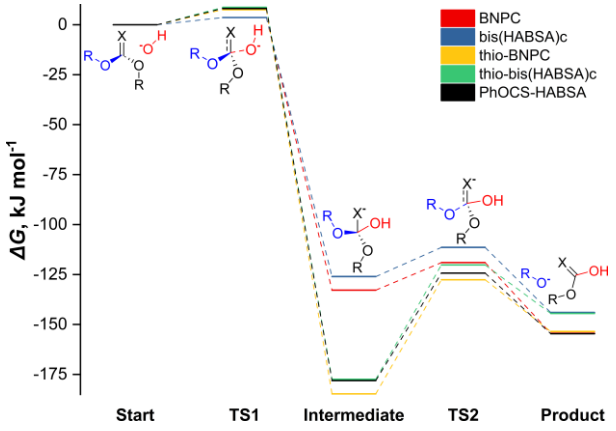
performing QM energy calculations (*3.11.3*). However, these attempts revealed a crucial weak point of metalloenzyme MD simulations: the simulation outcome strongly correlates with the initial metal ion-ligand geometry. The enzyme backbone undergoes dynamic changes, such as relaxation, rotation, and conformational changes, while the bond lengths, bond angles, tetrahedral angles, and electrostatic potential parameters of the metal-ion coordination sphere remain static. This discrepancy arises from the MD algorithm's reliance on predefined datasets for standard amino acids, nucleotides, and common solvents. Any molecule not in these datasets must be manually parameterised using QM calculations, including metal-ion complexes. The drawback is that manual parameterisation for metal complexes covers only a single set of coordinates. When these parameters are fed into the MD software, it results in a rigid set of bond lengths, angles, charges, and other parameters that remain fixed throughout the simulation. This limitation is particularly pronounced in the simulation of enzyme metal complex-substrate interactions. In such cases, the geometry of substrate complexation is constrained, whereas the remainder of the protein structure remains flexible and undergoes fluctuations. In conclusion, the MD simulations of bCAII and bis(HABSA)c provided a broader perspective on the protein structure and on interactions between the active site and ligands. Nonetheless, the QM-level energy calculation could not be applied. The strong correlation between the initial placement of the ligand in the active-site pocket and the simulation outcome could not be resolved using the available tools. This limitation arises because the current software and workflows for metalloenzyme MD simulations rely on rigid parameterisation. The main script, *MCPB.py*, that enables these metalloenzyme MD simulations has only recently become widely accessible (Li and Merz, 2021) and is expected to improve further. For more accurate representations, QM/MM methods could be employed, but their computational resource cost is too great for personal computers.

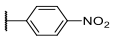
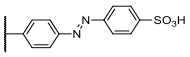
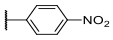
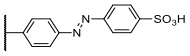
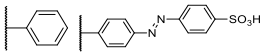
A more advanced methodology than molecular mechanics, semiempirical extended tight-binding (xTB), was utilised at the GFN0, GFN1, and GFN2 levels (*3.11.2*). It has been demonstrated that, in specific cases, the results obtained using the GFN2 methodology closely resemble those from QM computations or experiments, while requiring only a fraction of the computational resources typically needed for QM computations (Bannwarth et al., 2019). We attempted to simulate bCAII either in a water box or using a solvation model; however, the software currently does not support systems with more than a few thousand atoms. The enzyme model consisted of 4049

atoms, excluding ligands and solvent. In addition, this software is not compatible with the QM/MM scheme as a substitute for QM computations.

A theoretical approach to evaluate substrates was undertaken using QM computations (6-311G**/M06-2X) to analyse their autohydrolysis (*3.11.3*). While QM computations face limitations due to model size and high computational resource demands, they are less affected by software choice. Consequently, simulations included only the substrate, the hydroxide ion (OH^-), or their combination, excluding the enzyme. The objective was to correlate the results of the substrate hydrolysis simulations with experimental observations for further theoretical studies. The substrates under investigation included BNPC, thio-BNPC, bis(HABSA)c, thio-bis(HABSA)c, and PhOCS-HABSA. To account for solvation effects, the conductor-like polarizable continuum model (C-PCM) was applied. Transition states (TS1 and TS2) were established by performing constrained bond length optimisations, followed by Hessian matrix and saddle point calculations. For TS1, the constrained bond involved the carbonyl C-OH^-, while TS2 involved the carbonyl C-O leaving alcohol bond. The starting, intermediate, and product structures were confirmed by performing intrinsic reaction coordinate calculations originating from TS1 and TS2. Their final energies were calculated using relaxed optimisations. From the gathered data, we constructed the reaction coordinate diagram for each substrate. The energies depicted in the diagram were normalised to the starting state. Using the computed energies, we estimated the reaction barrier energies ($\Delta G^{\ddagger}$) for both the forward and reverse reactions (**Table 2.8**). The number in the subscript indicates the transition state. The results showed that all compounds reached their highest non-transition-state energy at the initial stage of the reaction. This observation aligns with experimentally observed reactivities. Between carbonates and thiocarbonates, the latter were significantly more stable. In addition, the hydrolysis products of thiocarbonates were at a higher energy level than the tetrahedral intermediates, suggesting hydrolysis as a less favourable outcome. When comparing the R groups, compounds containing HABSA were less stable than those containing pNP or phenol. Interestingly, in the hemi-ester geometry (products), there was a noticeable clustering around specific free energy (ΔG) values: -144 kJ mol^{-1} for HABSA and -154 kJ mol^{-1} for pNP and phenol. The reaction barrier data indicated that the X atom was the primary factor distinguishing the reaction barrier, which aligns with the observed stability trend in the energy diagram. In contrast, substitutions (R groups) had only a minor effect on the energies, directly contradicting the experimental results. The $\Delta G^{\ddagger}$ values, ranging from 3.6 to 14.6 kJ mol^{-1}, are relatively small, comparable to the rotational barriers of

Table 2.8 Reaction coordinate diagram and barrier energies of substrate hydrolysis and reverse reactions.



Substrate	X and R	$\Delta G^{\ddagger}_{1}$, kJ mol^{-1}	$\Delta G^{\ddagger}_{-1}$, kJ mol^{-1}	$\Delta G^{\ddagger}_{2}$, kJ mol^{-1}	$\Delta G^{\ddagger}_{-2}$, kJ mol^{-1}
	X = O; R =				
BNPC		3.6	136.4	13.7	35.4
bis(HABSA)c		3.6	129.6	14.6	32.6
	X = S; R =				
thio-BNPC		7.5	192.2	57.1	25.9
thio-bis(HABSA)c		8.7	186.1	57.2	24.3
PhO-C(S)-HABSA		8.1	181.2	53.8	30.3

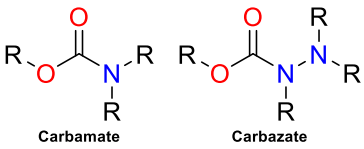
alkanes (Mo, 2011) or to diffusion-limited reactions (Shoup et al., 1981). These activation energies could explain the experimental observations for BNPC, which degraded within a few seconds in a pH 8.5 buffer. However, the bis(HABSA)c was several orders of magnitude more stable, while the calculated $\Delta G^{\ddagger}$ differed by no more than 0.9 kJ mol^{-1}. Assuming that the second hydrolysis step should have even lower activation energies due to known hemi-ester instability, the discrepancies in the computed values implied that the model used was not representative of the actual reaction system. Potential reasons for this could be that hydrolysis follows a different mechanism than predicted or that the C-PCM solvation model is inadequate. Boereboom et al. (2018) demonstrated that a microsolvation model – placing several solvent molecules near the reacting groups – grossly underestimated reactant stabilisation in a nucleophilic reaction. Their study suggested that computations for even simple reactions necessitate the inclusion of fully simulated solvent molecules. Unfortunately, this approach also exponentially increases computational resource requirements and creates challenges in

Hessian calculations and transition-state determination. The use of explicit solvation with QM/MM methods is a possible solution. However, there is currently a lack of developed tools to implement it effectively with limited resources.

To conclude the *in silico* investigations, MD simulations of enzyme-substrate structures provided a better understanding of substrate interactions within the active site. However, further analysis beyond average bonding distances and modes was limited by the capabilities of currently available software and MD methods for metalloenzymes. Results from *ab initio* computations showed that it could compare different substrate states, such as the tetrahedral intermediate and hemi-ester. Nevertheless, a general lack of knowledge in organic carbonate hydrolysis mechanisms and limitations of solvation modelling could not ensure an accurate representation of the entire substrate hydrolysis process.

With this study, our investigation into the application of carbonates and thiocarbonates as substrates was concluded. Both ester types showed promise and worked at a proof-of-concept level, but some unique challenges remain unsolved. Therefore, the focus of consequential studies was shifted to functional groups containing the RO-C(O)-R moiety – carbamates, carbazates and carboxylic esters.

2.2.4. p-Nitrophenyl Carbamate and Carbazate Substrates: Synthesis and Evaluation

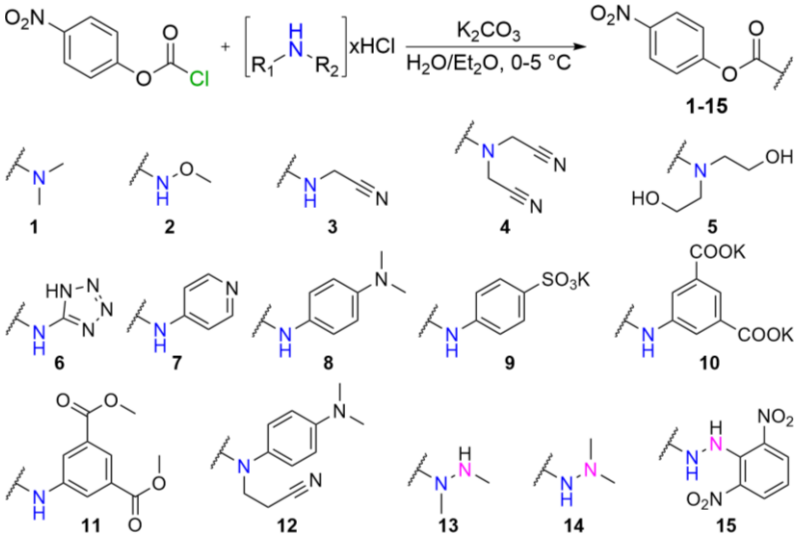


The carbamate functional group consists of an alcohol and an amine bonded to a carbonyl group. Carbazates are closely related to carbamates, with a hydrazine group instead of an amine. Compared with carbonates, these functional groups have similar geometries but significantly different electron densities. Oxygen atoms are highly electronegative, which causes them to withdraw electrons from neighbouring atoms, including the carbonyl group. In contrast, nitrogen has a free electron pair that can be donated to the carbonyl, leading to various resonance forms (Kemnitz and Loewen, 2007). This interaction contributes to the intrinsic stability of these compounds and their resistance to hydrolysis. In the context of carbonic anhydrases, some carbamates have been shown to exhibit inhibitory activity (Yılmaz et al., 2016), but little else is known about their interactions.

In this study, we conducted a rapid screening of selected activated carbamate and carbazate compounds to determine whether their hydrolysis is catalysed by bCAII. We chose *p*-nitrophenol as the dye for this purpose, as its

chloroformate (pNP-C(O)-Cl) is commercially available and readily reacts with compounds containing amine groups. The substrates under investigation were synthesised using a modified method (*3.3.5*) based on Peterson et al. (2006). We assessed the successful synthesis variants using UV-Vis spectroscopy to evaluate their stability in Tris-HCl buffer (pH 7.5), and then examined their catalytic hydrolysis by bCAII (**Table 2.9**).

Table 2.9 Carbamate and carbazate synthesis, isolation, stability in buffer and catalysis outcomes.



Entry	Synthesis	Stability in open air	Stability at pH 7.5[a]	bCAII catalysis[b]
1	+	-	n.t.	n.t.
2	+	+	+	-
3	+	+	-	n.t.
4	+	+	+	-
5	+	-	n.t.	n.t.
6	+	+	-	n.t.
7	+	-	n.t.	n.t.
8	+	+	-	n.t.
9	+	-	n.t.	n.t.
10	+	+	n.t.[c]	n.t.
11	+	+	-	n.t.
12	+	+	+	-
13	+	+	-	n.t.
14	+	-	n.t.	n.t.
15	+	+	+	-

n.t. – not tested.
[a] 0.5 mM of compound, 1% DMSO, 10 mM Tris-HCl, λ 400 nm, ambient temperature, 30 min.
[b] Same as stability measurement, supplemented with 1 mg ml^{-1} of bCAII.
[c] Insoluble in organic and aqueous solvents.

Out of the 15 syntheses performed, all variants were successful. The isolation of successfully synthesised compounds was relatively straightforward;

however, entries N° 1, N° 5, N° 7, N° 9 and N° 14 degraded during drying at ambient temperature in open air. The stability of the remaining nine compounds in a pH 7.5 buffer was examined, showing that four did not undergo rapid autohydrolysis, while N°10 carbamate could not be tested due to its insolubility in both aqueous and organic media. The four stable entries – N° 2, N° 4, N° 12 and N° 15 – under assay conditions were found not to be catalysed by bCAII. The compounds examined included several possible amine variants (hydroxyl, tertiary, or hydrazine); however, none of them showed enzyme-catalysed hydrolysis. This strongly suggested that carbamates and carbazates were unsuitable as substrates for carbonic anhydrases and were not pursued further.

2.2.5. Phenyl Azo Dye Carboxylic Ester Substrates: Synthesis and Evaluation

Some CAs also exhibit esterase-like activity, enabling them to catalyse the hydrolysis of carboxylic acid esters. This property is frequently used to measure activity and enzymatic kinetics and to investigate reaction and inhibition mechanisms. *p*-Nitrophenyl acetate (pNPA) is the most widely used substrate because it is commercially available and assays are easy to adapt, with numerous protocols available. However, it is important to note that this substrate does have certain limitations, including poor water solubility, potential autohydrolysis rates that may exceed catalytic rates for low-activity enzymes, and promiscuity, as its hydrolysis can be catalysed by a wide array of hydrolases, such as chymotrypsin (Verma and Ghosh, 2010), trypsin (Stewart and Ouellet, 1959), carboxylesterases (Ali et al., 1985), hydroxynitrile lyases (Nedrud et al., 2014), lipases (Schmidt and Bornscheuer, 2005) and others (Fecker et al., 2018). This study explored HABSA acetate ester (HABSA-Ac) as a potential substrate. Its characterisation was undertaken by developing a new spectrophotometric CA activity assay, validating it for thermostability and enzyme inhibition, and assessing its performance compared to other CA esterase activity assays. Additionally, an *ad hoc* approach has been proposed and applied to identify potential outliers in Michaelis-Menten kinetic measurements, with the aim of enhancing measurement reliability and parameter estimates.

The selected dye, HABSA, was utilised to synthesise a new substrate, 4-(4-acetoxyphenylazo)benzenesulfonic acid (HABSA-Ac). In brief, the dye was dissolved in DMF and heated with an excess of acetic anhydride (*3.3.6*). Our modified synthesis method involved increasing the temperature from 70 °C to 75 °C, extending the reaction time from "overnight" to 20 h, and incorporating additional washing steps during product isolation to improve

quality. This synthesis successfully produced a high-quality substrate, as confirmed by NMR, achieving a yield of up to 70% and an overall production yield of 53%.

Subsequently, the absorption maximum and molar extinction coefficients for HABSA-Ac and, for comparison, pNP, were assessed (*3.4.6*). The spectral measurements were conducted over the 320-800 nm range on solutions containing 5 µM chromophore, 1% DMSO, 10 mM Tris-HCl pH 8.5 buffer. The 1% DMSO concentration was selected as a sufficient co-solvent for HABSA-Ac based on its ability to maintain the solubility in the aqueous phase while ensuring a negligible effect on the carbonic anhydrases. The spectral measurements indicated that HABSA-Ac exhibited an intrinsic absorption maximum at 428 nm, with a relatively low ε_{428} of approximately 1.3 mM^{-1} cm^{-1}. For reference, HABSA ε_{428} at these conditions was 17.5 mM^{-1} cm^{-1}. The molar extinction coefficient of pNP at its maximum (400 nm) was measured to be 19.1 mM^{-1} cm^{-1}. Since the autohydrolysis of HABSA-Ac began immediately after mixing it with the buffer, the ε_{428} value was measured after a delay of 5 to 10 seconds, resulting in an approximate figure. Nevertheless, the difference between the molar extinction coefficients of HABSA-Ac and HABSA is more than 10-fold.

The last investigated characteristic was the stability of HABSA-Ac. During the course of the determination of its molar extinction coefficient, autohydrolysis was observed within minutes in an aqueous solution. However, the initial solution for these measurements contained only DMSO. The substrate exhibited good stability in solvent, providing consistent results for up to 12 h. So, to assess its long-term stability in DMSO, UV-Vis spectroscopy was carried out to monitor spectral changes in the 0.2 mM solution at 370-800 nm range over a period of seven days under six storage conditions: 20 °C, 4 °C, -20 °C, 40 °C, 60 °C, and 80 °C (*3.4.7*). The results indicated that the differences in absorption after 72 h (3 days) below 80 °C were negligible. After seven days, the difference reached 0.1, suggesting substantial substrate degradation. At 80 °C, substrate quality decreased after 24 h. These observations suggested that the storage solvent, rather than temperature, was the primary driver of substrate degradation. Overall, HABSA-Ac exhibited notable resistance to autohydrolysis in DMSO and maintained effective storage at ambient temperature for 72 h. It is noteworthy that using older solutions may result in diminished performance.

The substrate concentration in the assay reaction must be set to enable enzyme catalysis during the steady-state kinetic phase while maximising assay sensitivity. This concentration is particularly important when the analytical signals of the substrate and product overlap, as observed in the absorption at

428 nm for HABSA and HABSA-Ac. An elevated substrate concentration increases the initial absorption, thereby narrowing the reliable measurement range, which is typically between 0.1 and 1.0 absorption units (Bisswanger, 2014). Using the molar extinction coefficient for HABSA-Ac, it was estimated that a 0.2 mM solution in a 1.0 cm light path cuvette would yield an absorption value of approximately 0.1. Experimental measurements confirmed this finding (*3.8*), demonstrating absorptions of 0.136 at 0.2 mM and 0.080 at 0.1 mM. Consequently, the optimal concentration of HABSA-Ac for activity measurements was determined to be 0.2 mM.

As previously stated, CAs are enzymes that are highly sensitive to environmental conditions, including buffer components. At pH 8.5, several buffers can be used, with Tris-HCl being the most prevalent and well-established in CA research (Li et al., 2024). In order to ascertain the suitability of Tris-HCl for use with HABSA-Ac, an investigation was conducted on substrate catalysis by bCAII in four buffers of 10 mM concentration (*3.8*): Tris-HCl, 2-amino-2-methyl-1,3-propanediol (AMPD), sodium borate ($NaBO_3$), and diethanolamine ($NH(EtOH)_2$). It is known that the borate buffer has the capacity to inhibit the activity of certain CAs (Yusuf et al., 2022), although it does encompass bCAII. Data concerning AMPD and $NH(EtOH)_2$ remains to be elucidated. The reactions were performed in a spectrophotometric cuvette and monitored at 428 nm (**Figure 2.11 A**).

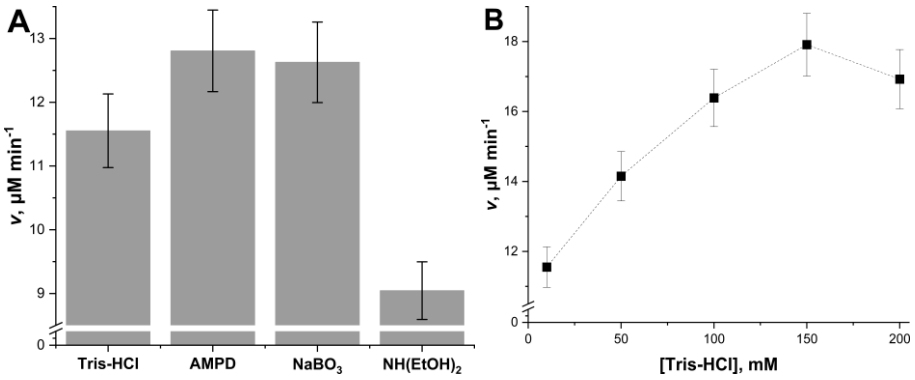


Figure 2.11 Catalysis rates of bCAII in different buffer conditions: **A** – effect of selected buffers (10 mM); **B** – influence of the Tris-HCl buffer concentration (10-200 mM).

The results demonstrated that the bCAII catalysis rate in $NH(EtOH)_2$ was noticeably diminished. Conversely, the reaction rates in the remaining three buffers were relatively consistent, thereby validating the suitability of Tris-HCl for the HABSA-Ac assay. The next phase of buffer optimisation involved identifying its optimal concentration. It is well established that many enzymes,

including CAs, achieve their highest catalytic activity at sufficiently high ionic strength. The ionic strength can be adjusted by adding neutral salts, such as NaCl, or by controlling the buffer concentration. For the present assay, the latter option was selected, and catalysis rates were measured in buffer concentrations ranging from 10 mM to 200 mM (**Figure 2.12 B**). The resulting data showed a gradual increase in reaction rates, peaking at 150 mM. Conversely, higher buffer concentration resulted in decreased activity, likely due to perturbations in protein-solvent interactions.

An important consideration in assay development is the measurement time. In general, spectrophotometric measurements require between one minute and several hours to yield reliable results, depending on the enzyme's catalytic rate and the assay's sensitivity (Baliukynas et al., 2020; Fernández et al., 2018). To estimate the minimum reaction time for the HABSA-Ac assay, reactions were performed for 1, 3, 5, 10, and 20 min (*3.8*). The results showed that 1 minute was too short, as a burst phase occurred within the first 20-30 seconds, reducing the linear slope range by half. Extending the measurement beyond 3 minutes did not improve the slope linear range, so a 3-minute duration was deemed sufficient.

The last factor in assay development involved identifying the optimal enzyme concentration and establishing the limits of quantification and detection. Activity assays are typically designed to yield reliable results while minimising the usage of enzymes. One method to determine the appropriate enzyme concentration is to run reactions with progressively smaller amounts of the enzyme. As the enzyme concentration is reduced, the reaction rates decrease linearly until they begin to deviate at the assay's limit of quantification. The lowest distinguishable reaction rate above the baseline (autohydrolysis) defines the limit of detection. To ascertain these parameters for HABSA-Ac, the hydrolysis was examined at bCAII concentrations in the reaction mixture (cuvette) ranging from 10 $\mu g\ ml^{-1}$ (as used in previous HABSA-Ac experiments) to 0.1 $\mu g\ ml^{-1}$ (*3.8*). At a concentration of 1 $\mu g\ ml^{-1}$ (34.4 nM) of bCAII, the errors in catalysis rates exceeded ± 5.0%, indicating the assay's limit of quantification. At a concentration of 0.1 $\mu g\ ml^{-1}$ (3.44 nM), the difference between autohydrolysis and catalytic rates reached 0.0006 $Abs\ min^{-1}$, representing the minimal measurable difference. These findings suggest that the assay's limit of detection is approximately 3.44 nM of bCAII. For the purpose of enzyme research or routine enzymatic activity measurements, the final concentration of 10 $\mu g\ ml^{-1}$ has been chosen to be sufficient. In summary, the developed HABSA-Ac assay was carried out in 150 mM Tris-HCl (pH 8.5) buffer using 0.2 mM substrate and 10 $\mu g\ ml^{-1}$ enzyme for 3 min at ambient (20 °C) temperature. 1 activity unit (1 U) was

defined as 1 µmol of HABSA-Ac hydrolysed per 1 min at pH 8.5 and 20 °C (*3.8*).

One drawback of pNPA as a substrate is its poor thermal stability. Characterisation of thermo- or hyperthermostable CAs can involve conducting assays at temperatures approaching the boiling point of aqueous media (Yang et al., 2025). Under these conditions, substrate autohydrolysis rates can approach the catalytic rates of enzymes with low esterase activity, thereby reducing measurement resolution, even when side reactions are accounted for. Therefore, the autohydrolysis and catalytic rates of HABSA-Ac were investigated in a temperature range of 30-75 °C using established buffer, substrate, and enzyme concentrations. Temperature equilibration was ensured before and during measurements using a water-jacketed cuvette holder connected to an external water-circulating thermostat. For comparison, measurements with pNPA were performed in parallel using 0.2 mM substrate in 150 mM Tris-HCl (pH 8.5 adjusted at 20 °C) buffer (*3.5.3*). The effect of temperature on reaction rates is summarised in **Figure 2.12**.

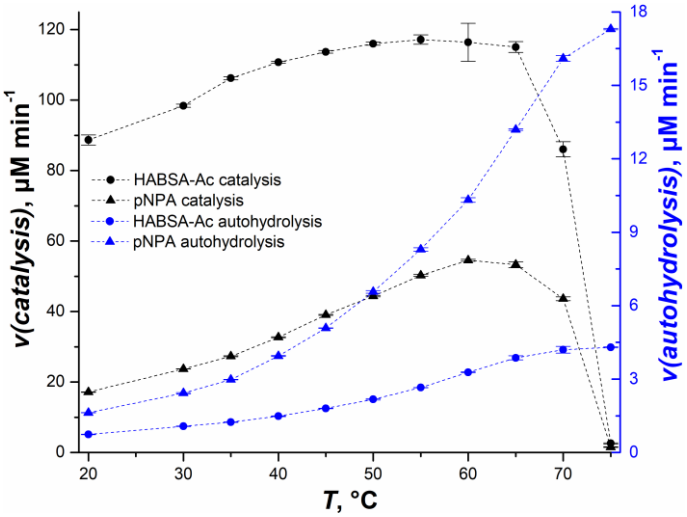


Figure 2.12 HABSA-Ac and pNPA autohydrolysis and catalysis rate dependency on the temperature (150 mM Tris-HCl, pH 8.5, 10 µg ml^{-1} bCAII).

The data showed that catalytic rates steadily increased, peaked at 60 °C, then decreased, and were completely lost at 75 °C. These findings align with the melting temperature of bCAII, which is reported to be 68.8 °C at similar conditions (Ge et al. 2016). The increase in catalytic rate per temperature was comparable for both substrates, while substrate autohydrolysis rates exhibited significantly different profiles. For HABSA-Ac, from 20 °C to 75 °C, the decomposition rate increased by approximately 3.6 µM min^{-1} in total. Meanwhile, pNPA surged more than 10-fold, from 1.6 µM min^{-1} to

17.3 μM min^{-1}, highlighting its sensitivity to environmental conditions. The thermostability of HABSA-Ac is advantageous (Babinskas and Matijošytė, 2026), as autohydrolysis often complicates CA kinetic measurements, particularly at alkaline pH or elevated temperatures. For example, Fredslund et al. reported that thermostable alkaline CA with low esterase activity could not be reliably assayed with pNPA above pH 7.5 due to excessive autohydrolysis (Fredslund et al., 2018).

The collected catalytic reaction data in the range of 30-55 °C were utilised for Arrhenius and transition-state theory (TST) plots and analyses (*3.9.1*). Since the HABSA-Ac and pNPA assays used a substrate concentration of 0.2 mM – significantly below the expected K_M (> 2 mM) – the Arrhenius and TST analyses for enzymatic reactions yielded the specificity constant (k_{cat}/K_M). Analysis of autohydrolysis reactions utilised data from 20 °C to 75 °C. The derived k_{cat}/K_M, $E_{a,obs}$, $\Delta H^{\ddagger}_{obs}$, $\Delta S^{\ddagger}_{obs}$, and $\Delta G^{\ddagger}_{obs}$ are summarised in **Table 2.10**.

Table 2.10 Summary of parameters derived from Arrhenius and TST plots.

Arrhenius plot	Substrate	$E_{a,obs}$, kJ mol^{-1}	ΔH_{obs}, kJ mol^{-1}	k_{obs}, s^{-1} [a]	k_{cat}/K_M, M^{-1} s^{-1} [a]
Autohydrolysis	HABSA-Ac	28.1 ± 1.3	25.6 ± 1.3	(6.34 ± 0.85) × 10^{-5}	
	pNPA	37.6 ± 0.8	35.1 ± 0.8	(1.30 ± 0.02) × 10^{-4}	
Catalysis	HABSA-Ac	6.22 ± 0.86	3.78 ± 0.86		2251 ± 796
	pNPA	25.3 ± 0.5	22.9 ± 0.5		409 ± 78

TST plot	Substrate	$\Delta H^{\ddagger}_{obs}$, kJ mol^{-1}	$\Delta S^{\ddagger}_{obs}$, J mol^{-1}	$\Delta G^{\ddagger}_{obs}$, kJ mol^{-1} [a]	k_{obs}, s^{-1} [a]	k_{cat}/K_M, M^{-1} s^{-1} [a]
Autohydrolysis	HABSA-Ac	25.2 ± 1.3	-239 ± 22	95.3 ± 6.6	(6.43 ± 0.45) × 10^{-5}	
	pNPA	32.4 ± 0.8	-185 ± 36	86.7 ± 10.5	(2.22 ± 0.27) × 10^{-3}	
Catalysis	HABSA-Ac	3.70 ± 0.87	-168 ± 16	53.0 ± 4.7		2249 ± 26
	pNPA	22.1 ± 0.4	-119 ± 2	57.1 ± 0.8		413 ± 4

[a] T = 293.15 K (20 °C).

The computed thermodynamic and kinetic parameters revealed that HABSA-Ac autohydrolysis reaction was less favourable than pNPA. For instance, the reaction rate constants were in a 10^{-5} s^{-1} range and lower by 10^{1}-10^{2}-fold, then compared to pNPA. Meanwhile, the k_{cat}/K_M of HABSA-Ac catalysis were as follows: 2251 ± 796 M^{-1} s^{-1} in Arrhenius analysis and 2249 ± 26 M^{-1} s^{-1} in TST. The analysis of pNPA catalysis yielded 409 ± 78 M^{-1} s^{-1} and 413 ± 4 M^{-1} s^{-1}, which closely agree with published results (Asadi et al., 2019). In summary, this investigation confirmed that HABSA-Ac exhibited substrate properties comparable to, and in some respects superior to, the classical substrate pNPA.

Following the establishment of the conditions for the HABSA-Ac assay and validation for thermodynamic analysis, the subsequent application was the determination of kinetic measurements: Michaelis constant (K_M), maximum catalytic rate (V_{max}), enzyme turnover number (k_{cat}), and substrate specificity constant (k_{cat}/K_M). These involved measuring the catalytic rates of bCAII across a substrate concentration range of 0.1 to 1.0 mM, plotting the data, and calculating the parameters. Initial results showed that within this substrate range, the reaction rates increased linearly and did not approach enzyme saturation. This indicated that the substrate concentration remained below the K_M value while the reaction rates were significantly lower than V_{max}. In such scenarios, the linear Michaelis-Menten equations and plots are utilised, commonly known as the Lineweaver-Burk (L-B), Eadie-Hofstee (E-H), Hanes-Woolf (H-W), and Eisenthal-Cornish-Bowden (E-C-B) methods (*3.9.2* and *3.9.3*). It is noteworthy that although achieving enzyme saturation is not a prerequisite for these analytical methods, experimental errors can significantly affect the outcomes, and these methods are inherently biased, which can lead to overestimation or underestimation of kinetic parameters (Cho and Lim, 2018; Choi et al., 2017). Nonetheless, these analytical methods have been successfully employed to determine the catalytic parameters for the HABSA-Ac-catalysed system, as outlined in **Table 2.11**.

Table 2.11 Individual and average initial kinetic parameters for HABSA-Ac catalysis by bCAII. Estimated using Lineweaver-Burk (L-B), Eadie-Hofstee (E-H), Hanes-Woolf (H-W), and Eisenthal-Cornish-Bowden (E-C-B) methods.

Kinetic parameter	L-B	E-H[b]	H-W[c]	E-C-B
K_M, mM	37.1 ± 28.2	3.03 ± 0.30	12.5	9.5 ± 1.8
V_{max}, μM min^{-1}	1314 ± 1013	117 ± 10	416	334 ± 62
k_{cat}, s^{-1}	63.7 ± 49.1	5.7 ± 0.5	20.1	16.2 ± 3.0
k_{cat}/K_M, M^{-1} s^{-1} [a]	1675 ± 33	1860 ± 9	1614	1697 ± 24

[a] Average and standard errors were calculated using individual k_{cat}/K_M data.
[b] Measurement Nº 3 produced negative kinetic parameters.
[c] Measurements Nº 2 and Nº 3 produced negative kinetic parameters.

The data indicated that the specificity constants were in relatively good agreement across L-B, H-W and E-C-B methods. Meanwhile, the results from E-H and H-W could not be applied to all measurements because some outcomes were negative. Other kinetic parameters showed wide distributions and significant deviations across methods. Especially, one measurement in L-B resulted in considerable deviation from the rest of the results, distorting the K_M, V_{max} and k_{cat} average values and standard error ranges.

These results indicated that the highest HABSA-Ac concentration used in the measurements (1 mM) was substantially lower than the K_M, making the analysis highly sensitive to even minor errors. As a result, the data exhibited

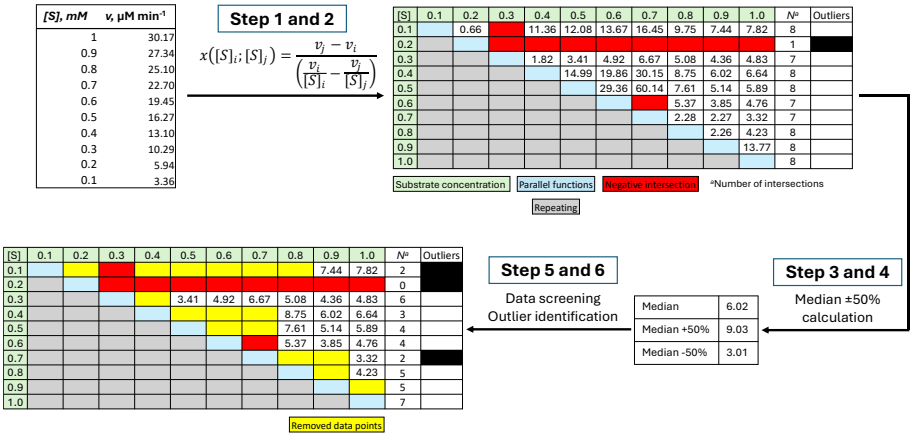
substantial variability, introducing uncertainty in the determination of kinetic parameters. To improve the reliability of the results, an *ad hoc* approach based on the E-C-B method was developed to identify outlier pairs between reaction rate and substrate concentration.

2.2.6. Development of an E-C-B-Based Method for Ad Hoc Identification of Outlying Data Points

While the classical E-C-B method is primarily used to estimate kinetic parameters, it can also facilitate outlier detection through graphical analysis (Eisenthal and Cornish-Bowden, 1974). In 1974 Eisenthal and Cornish-Bowden extended their method by incorporating median values and statistical error minimisation to estimate deviations in kinetic parameters. However, their work relied on simulated datasets with predefined error magnitudes and reaction rates nearing V_{max}. Notably, they did not propose a method for identifying outliers. In contrast, our data exhibited substantially greater errors, with reaction rates reaching only ~10% of V_{max}: observed rate of 34 μM min^{-1} vs approximate V_{max} of 323 μM min^{-1}. Therefore, we expanded on their original approach by developing a simple algorithm to screen velocity measurements and detect erroneous data points (*3.9.4*).

Our proposed data processing approach is fundamentally based on the core principle of the Eisenthal-Cornish-Bowden plot: lines that pass through $(-[S]_i;0)$ and $(0;v_i)$ coordinates intersect at points where the x-coordinates indicate K_M, and the y-coordinates – V_{max}. Primarily, the trajectories of lines depend on the $(0;v_i)$ point, as the substrate concentration $[S]_i$ is independent of the reaction rate measurements. It is important to note that $[S]_i$ can also be affected by systematic errors originating in experimental procedures. Most of the intersection points are clustered, and the median value of these points provides the best estimate of kinetic parameters. Intersection points outside the cluster suggest that one or both lines may be based on erroneous v. Our proposed approach eliminates such intersection points. The remaining number of intersection points reflects the quality of the obtained data. This concept allows for flexibility and adaptation to specific scenarios by adjusting two thresholds: i) which intersection points are considered to be outside the median cluster, and ii) how many intersection points have to remain for data to be designated as reliable. This idea was streamlined into a data-screening algorithm, applied to our data, and the kinetic parameters were then recalculated using previously employed methods, with outlier measurements removed. The iterated thresholds were as follows: clustering – median value iterated with ± 100%, 75%, 50%, and 25%; measurement data confidence – 75%, 50%, 25%, and 10% intersection points remaining after screening. The

clustering threshold shows the boundary between the inside and outside of the cluster. Measurement confidence defines the limit on how many intersection points can be removed before the line (and associated v_i) is considered an unreliable measurement. The data screening workflow is presented in **Scheme 2.9**, and, for illustrative purposes, it includes actual data from a kinetic measurement.



Scheme 2.9 The workflow for the suggested potential outlier identification algorithm based on the E-C-B method.

Step 1 – a generalised function $y(x)_{[S]}$ is employed to generate linear functions for reaction rates v and the corresponding substrate concentration $[S]$ (Cornish-Bowden and Eisenthal, 1974). Step 2 – the x-values (coordinates) of the function intersection points are tabulated. It can be done manually or using the provided formula to solve $x([S]_i;[S]_j)$. Negative intersection coordinates are not included in tabulation. Duplicate values resulting from tabulation symmetry are also excluded. Step 3 – the median x-coordinate is calculated, providing the centre of the intersection cluster. Step 4 – selection of clustering threshold. The example in the scheme uses a clustering threshold of ± 50%. Step 5 – selection of measurement confidence threshold. The example in the scheme uses a threshold of 25 %, meaning that measurements with two or fewer intersection points remaining after screening were designated as unreliable (outliers). Notably, one measurement met this criterion prior to the screening step. Step 6 – data screening and outlier removal from tabulated data. Any measurement below the confidence threshold is removed. Step 7 (not shown) – kinetic parameter re-evaluation. The K_M and V_{max} are recalculated using the L-B, E-H, H-W, and E-C-B methods, excluding outlier data points.

The evaluation of clustering thresholds indicated that the median ± 100% and ± 75% intervals were too lenient, as no additional outliers were detected. In contrast, the median ± 25% interval was overly stringent, resulting in up to 8 of 10 functions being classified as outliers. The mean ± 50% interval provided a more balanced approach for our datasets, identifying two additional outliers, whose corresponding *v* and *[S]* values were excluded from further analysis. Kinetic parameters were then recalculated using the L-B, E-H, H-W and E-C-B methods. Results based on both the initial (raw) and screened (processed) data sets are presented in **Figure 2.13**.

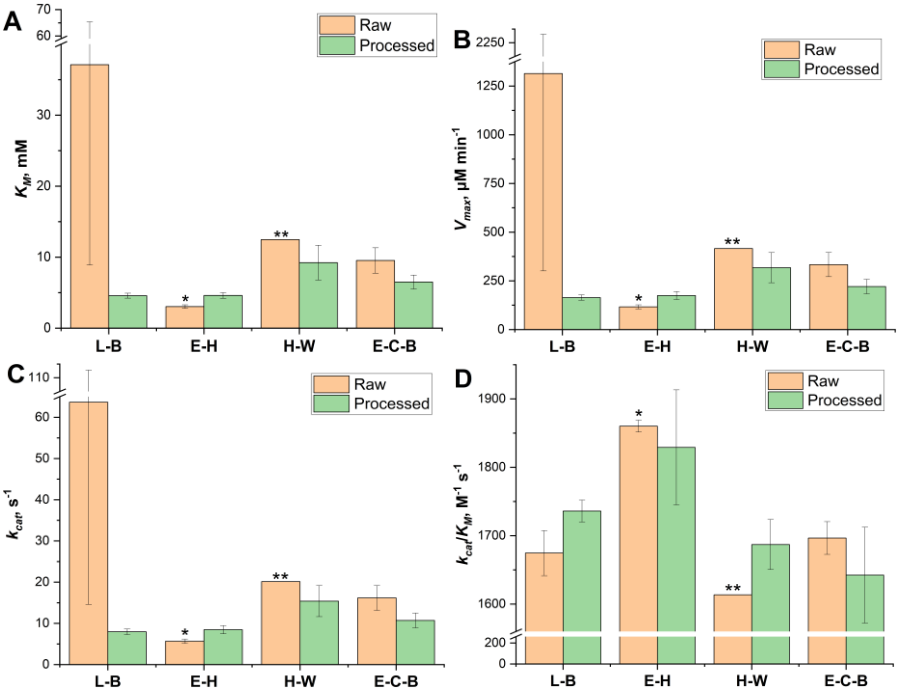


Figure 2.13 Kinetic parameters calculated using raw and processed data following outlier removal. **A** – K_M; **B** – V_{max}; **C** – k_{cat}; **D** – k_{cat}/K_M. Asterisks (* and **) denote the number of negative results in the analysis.

The data processing led to an overall improvement in the calculated kinetic parameters. The E-H and H-W methods successfully produced results for all three measurements. Notably, K_M, V_{max} and k_{cat} values obtained via the E-H method closely matched those from the L-B analysis. Although the H-W results showed significant improvement, they remained higher than L-B values, except for k_{cat}/K_M, which was generally the least affected by data processing. The proposed algorithm improved the estimation of kinetic parameters, but it was insufficient to achieve overall agreement among methods within their respective error ranges. Based on the processed data,

kinetic parameters for the bCAII and HABSA-Ac reaction were estimated as follows: K_M between 4.6 mM and 9.2 mM (mean 6.2 mM), V_{max} between 164 μM min^{-1} and 318 μM min^{-1} (mean 220 μM min^{-1}), k_{cat} between 8.0 s^{-1} and 15.4 s^{-1} (mean 10.7 s^{-1}), and k_{cat}/K_M between 1642 M^{-1} s^{-1} and 1829 M^{-1} s^{-1} (mean 1724 M^{-1} s^{-1}). For comparison, Asadi et al. (2019) reported the kinetic parameters of the bCAII and pNPA reaction under similar conditions (50 mM Tris-HCl, pH 8.0): K_M of 8.9 mM, V_{max} of 42.7 μM min^{-1}, k_{cat} of 3.56 s^{-1}, and k_{cat}/K_M of 399.8 M^{-1} s^{-1}. These results suggest that while HABSA-Ac exhibits a similar affinity for bCAII, its catalytic efficiency is 2 to 7-fold higher. The specificity constants obtained from the thermodynamic approach (Arrhenius – k_{cat}/K_M 2251 ± 796 M^{-1} s^{-1}; TST – 2249 ± 26 M^{-1} s^{-1}) were slightly higher, but not unreasonably. This discrepancy could have arisen from limitations in the HABSA-Ac concentration, fundamentally different theoretical frameworks, or error propagation commonly recognised in linearised models (Doran, 1995). In summary, the proposed algorithm improved the accuracy of kinetic parameter estimation. Based on the available data, the derived kinetic parameter ranges for HABSA-Ac are comparable to those of pNPA, a standard substrate in carbonic anhydrase studies. However, testing under a single set of conditions was insufficient to fully validate the algorithm, even as an *ad hoc* (preliminary) solution tool. To further assess its application and proceed with validation of the HABSA-Ac assay, a bCAII inhibition study was conducted.

One way to evaluate the capabilities and limitations of an enzymatic assay is to study the inhibition of the target enzyme, thereby highlighting the assay's robustness and its performance in low-enzymatic-activity scenarios. The present study selected potassium cyanide (KCN) and acetazolamide based on their high affinity for bCAII (Pocker and Sarkanen, 2006). Enzyme inhibition assays were performed by mixing bCAII with each inhibitor at defined molar ratios and measuring catalytic activity across a range of substrate concentrations, as previously described (*3.8*). Substrate autohydrolysis rates were also assessed in the presence of an inhibitor; however, no significant differences were observed compared to control conditions. Kinetic parameters were calculated from both raw and processed data using L-B, E-H, H-W and E-C-B methods. The V_{max} values for both inhibitors are presented in **Figure 2.14**, while the full set of kinetic parameters (K_M, V_{max}, k_{cat} and k_{cat}/K_M) is provided in **Tables S4 and S5**. The results indicate that data processing substantially improved the quality of results. Only the 1:1 [bCAII]/[Acetazolamide] ratio yielded unsuccessful outcomes, attributed to catalytic rates approaching the assay's detection limit, thereby introducing significant experimental error. In a few cases, data processing increased error

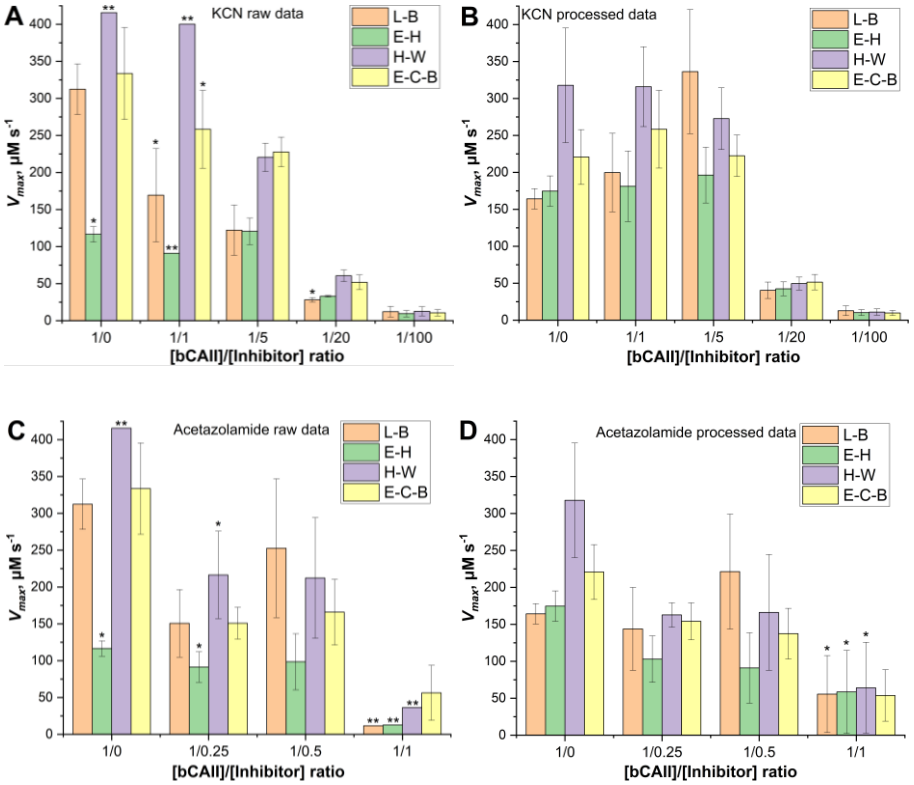


Figure 2.14 Results of V_{max} with various [bCAII]/[Inhibitor] molar ratios, calculated using L-B, E-H, H-W and E-C-B methods for raw and processed datasets: **A** – raw dataset for inhibition by KCN; **B** – processed dataset for inhibition by KCN; **C** – raw dataset for inhibition by acetazolamide; **D** – processed dataset for inhibition by acetazolamide. Ratios 1/0 – uninhibited bCAII (control). Asterisks (* and **) denote the number of negative results in the analysis.

margins or caused a notable shift in mean values. Similar patterns were observed for other kinetic parameters (**see Tables S4 and S5**). Overall, the *ad hoc* approach to identifying and eliminating outliers was effective, reducing extreme values, increasing the number of valid results, and improving the data's overall reliability.

Analysis of the kinetic parameters revealed that bCAII inhibition by KCN became apparent at a [bCAII]/[KCN] molar ratio of 1:5 and higher, as indicated by decreases in both V_{max} and K_M. The k_{cat}/K_M exhibited a gradual decline, beginning with a slight decrease at the 1:1 ratio and continuing as inhibitor concentration increased. In contrast, acetazolamide reduced all kinetic parameters at the lowest tested ratio (1:0.25), except for the K_M, which remained relatively stable across all inhibitor concentrations. These trends suggest that KCN inhibited bCAII via a mixed inhibition mechanism, characterised by concurrent reductions in K_M and V_{max}, whereas acetazolamide

acted via a non-competitive mechanism, as reflected by a decrease in V_{max} without affecting K_M. To confirm these mechanisms and determine inhibition constants, Dixon and Cornish-Bowden (C-B) plots were constructed (*3.9.5*).

The Dixon plot, which estimates the inhibition constant (K_i) by plotting $1/v$ against inhibitor concentration *[I]* at varying substrate levels, yields $-K_i$ at the *x*-intercept of the fitted linear regressions (Cornish-Bowden, 1974). The C-B plot, suited for analysing mixed inhibition, plots *[S]*/*v* versus *[I]*, where the *x*-intercept gives $-K_i'$ (Kanodia et al., 2009). The relative positions of the intersection points in both plots indicate the relationship between *Ki and Ki': if Ki > Ki', the C-B plot intersects above the X-axis and the Dixon plot below the X-axis*, and *vice versa* (Cornish-Bowden, 1974). In non-competitive inhibition ($K_i = K_i'$), both intersections lie on the X-axis. Data points corresponding to the highest inhibitor concentrations were excluded from these analyses because reaction rates fell below the assay's quantification limit. The inhibition constants were calculated following the initial three steps of the data screening algorithm: 1) tabulation of *x*-intercepts from plot intersections, 2) exclusion of positive intersection values, and 3) calculation of the median. Standard deviations and standard errors were then computed based on the tabulated data. The resulting inhibition constants from Dixon and C-B plots are summarised in **Table 2.12**.

Table 2.12 The inhibition constants calculated from raw and processed datasets using Dixon and C-B plots.

	KCN		Acetazolamide	
	Raw	**Processed**	**Raw**	**Processed**
Dixon plot (K_i), μM	3.00 ± 0.14	3.44 ± 0.60	0.105 ± 0.002	0.081 ± 0.035
C-B plot (K_i'), μM	0.88 ± 1.12	1.05 ± 0.58	0.104 ± 0.073	0.254 ± 0.864

The analysis revealed that for KCN, the Dixon plot intersected below the X-axis, while the C-B plot intersected above it, consistent with the calculated K_i and K_i' values and the expected behaviour of mixed inhibition. Among the two methods, the Dixon plot yielded more accurate and consistent results than the C-B plot. Data processing, however, was generally counterproductive for inhibition constant estimation, as it caused slight shifts in median values and significantly increased error margins, except for K_i' for KCN, which showed improved precision.

The previously reported K_i value for KCN inhibition of bCAII at pH 7.55 (Tris-HCl buffer) was 2.6 μM (Pocker and Stone, 1968), which compares reasonably well with the current estimate of 3.44 μM, although differences in pH preclude a direct comparison. The K_i' value has not been previously reported for this system. For acetazolamide, raw dataset analysis showed

excellent agreement between K_i and K_i', supporting the reliability of the results. These values were consistent with literature data (~0.2 μM at pH 8.45 in 9 mM Tris-HCl with 10% (*v/v*) acetonitrile) (Pocker and Stone, 1967). In contrast, the processed dataset for acetazolamide yielded less reliable estimates, with opposing shifts in medians and a standard error for the C-B plot that exceeded its median.

This study demonstrates the use of the HABSA-Ac for analysing bCAII kinetics and inhibition mechanisms by KCN and acetazolamide. The proposed data-processing approach improved the quality of kinetic parameter estimates (K_M, V_{max}, k_{cat}, and k_{cat}/K_M). However, several methodological limitations were noted. The algorithm was tested at low substrate concentrations relative to K_M, and its performance across a broader substrate range remains to be tested. The ± 50% median-based screening threshold may need adjustment depending on the enzyme-substrate system, as its effectiveness is dataset-dependent. Furthermore, the outlier identification criterion may require refinement through empirical evaluation. A large number of measurements is essential, as the number of intersections (N) follows a triangular distribution ($N = n(n-1)/2$). For example, with 10 substrate concentrations, up to 45 intersections were analysed, whereas datasets with only 5-7 measurements (Gibbons and Edsall, 1964; Johansson and Forsman, 1993) would yield just 10-21 intersections, limiting the robustness of the screening. Despite these limitations, the proposed approach demonstrated strong potential for enhancing data quality in enzyme kinetic studies. With further optimisation and tailored implementation, it may serve as a valuable tool for more accurate and confident analysis of enzyme inhibition mechanisms.

2.2.7. Comparative Evaluation of the HABSA-Ac Assay with p-Nitrophenyl Acetate and Indoxyl Acetate Assays

Selectivity is a critical parameter in evaluating enzymatic activity assays. Hydrolases such as esterases and lipases have broad substrate specificity and readily hydrolyse a range of acetate esters. In contrast, CAs display more restricted hydrolytic activity, with only specific isoforms capable of catalysing ester hydrolysis. To evaluate the selectivity of the HABSA-Ac assay, substrate hydrolysis was assessed in the presence of CAs, hydrolases, and non-catalytic proteins. Five commercially available enzymes were used: carbonic anhydrase II (bCAII) from bovine erythrocytes – model CA with high esterase-like activity; a promiscuous recombinant esterase from *Bacillus subtilis*; two highly active lipase preparations (*3.5.5*) – Biorro LPS L and Novozymes Lipolase 100L; and a lysophospholipase product Finizym W as a reference for hydrolases with non-lipase activity. Several other CAs were also included:

human α-carbonic anhydrase IX (hCAIX) catalytic domain, known for its low esterase-like activity and two *β*-CAs from *Pseudomonas aeruginosa* (psCA1 and psCA2) without esterase activity (Del Prete et al., 2014). Bovine serum albumin (BSA) was tested as a negative control. Protein concentrations for BSA, bCAII, esterase, hCAIX, psCA1, and psCA2 in the reaction were standardised to 0.344 μM (*3.5.6*). The two lipase products were diluted due to their exceptionally high hydrolytic activity in the *p*-nitrophenyl palmitate assay. For benchmarking, two established esterase activity assays were used: the pNPA assay (0.2 mM substrate in 150 mM Tris-HCl pH 8.5) (*3.5.3*) and the indoxyl acetate (Indoxyl-Ac) assay (*3.5.4*), scaled from microplate to cuvette format and conducted at room temperature (20 °C) for 10 min (Baliukynas et al., 2020). Reaction rates for all enzymes across the three substrates are summarised in **Table 2.13**.

Table 2.13 The reaction rates (*v*) obtained using HABSA-Ac, pNPA and Indoxyl-Ac assays.

	Assays (v, μM min^{-1})		
Enzyme/control	**HABSA-Ac**	**pNPA**	**Indoxyl-Ac**
Autohydrolysis	0.76	1.67	0.37
BSA[a]	0.02	0.04	0.28
bCAII[a]	6.21	1.21	0.20
Esterase[a]	35.32	41.19	298.57
hCAIX[a]	1.38	0.67	1.65
psCA1[a]	0.05	0.27	0.37
psCA2[a]	0.06	0.33	0.33
LPS L[a]	2.20[b]	39.75	61.84
Lipolase 100L[a]	1.88[b]	6.29	221.45
Finizym W[a]	0.12[b]	0.83	0.83

[a] Results with substrate autohydrolysis rates subtracted.
[b] Protein concentrations in the assay were 10-fold higher than in pNPA and Indoxyl-Ac reactions.

The comparative analysis revealed that HABSA-Ac had a higher autohydrolysis rate than Indoxyl-Ac but was more stable than pNPA. Reaction rates with BSA, psCA1 and psCA2 were negligible (< 0.1 μM min^{-1}), thus indicating the absence of non-specific hydrolysis. Among the tested enzymes, HABSA-Ac was hydrolysed most efficiently by bCAII, while lipases exhibited minimal catalytic activity. To ensure sensitivity and comparability, protein concentrations were increased 10-fold. Despite this adjustment, lipase-catalysed hydrolysis remained the lowest across all three substrates. This suggested that HABSA-Ac is a poor ester substrate for lipases – an advantageous characteristic when analysing complex protein mixtures derived from extraction or fermentation processes. Autohydrolysis of pNPA accounted for nearly half of the total reaction rate observed with bCAII,

highlighting the challenge of background interference. Although psCA1 and psCA2 are generally not associated with esterase activity (Lotlikar et al., 2013), both enzymes showed reaction rates above 0.1 μM min^{-1}. This activity may be attributed to the slightly elevated assay pH (8.5), as previously reported (Simplício et al., 2013; Tekincanli et al., 2015). Indoxyl-Ac showed the lowest autohydrolysis among the substrates, but reacted noticeably with BSA, psCA1 and psCA2, suggesting possible non-catalytic interactions. Interestingly, bCAII catalysis of Indoxyl-Ac was slower than reactions observed with some of these non-catalytic proteins. In contrast, the *B. subtilis* esterase effectively hydrolysed all three substrates, with particularly high activity towards Indoxyl-Ac. Human CAIX exhibited weak esterase-like activity across all substrates (Uda et al., 2015).

The assay sensitivities of HABSA-Ac, pNPA and Indoxyl-Ac were also compared based on the slopes (AU min^{-1}) calculated for hydrolysis catalysed by bCAII. The slope is a suitable parameter because it directly reflects the signal detected by the equipment and is not affected by data extrapolation or the kinetic model framework. In this analysis, the HABSA-Ac assay produced a slope of 0.109 ± 0.003 AU min^{-1}, pNPA – 0.0231 ± 0.0001 AU min^{-1}, and Indoxyl-Ac – 0.0005 ± 0.0001 AU min^{-1}. It demonstrated that the HABSA-Ac hydrolysis produced a 4.7-fold higher signal than pNPA and more than 200-fold higher than Indoxyl-Ac (Babinskas and Matijošytė, 2026).

In summary, HABSA-Ac demonstrated moderate autohydrolysis, high selectivity for carbonic anhydrases, and limited susceptibility to the investigated lipase-catalysed hydrolysis. While its moderate reactivity with *B. subtillus* esterase suggests room for improvement, these characteristics underscore its promise as a selective assay for carbonic anhydrase activity.

3. MATERIALS AND METHODS

3.1. General Procedures

Commercially available reagents were used without additional purification, unless stated otherwise. ^{1}H and ^{13}C NMR spectra were recorded in deuterated solvent using a Bruker Ascened™ 400 MHz spectrometer. Chemical shifts (δ) were given with reference to the solvent signals: DMSO-$_{d6}$: $\delta(^{1}H)$ = 2.50 ppm, $\delta(^{13}C)$ = 39.52 ppm. The abbreviations were used to indicate multiplicity: s – singlet, d – doublet, t – triplet, dd – doublet of doublets, dt – doublet of triplets, td – triplet of doublets, m – multiplet. High-resolution mass spectra (HRMS) were recorded using an Agilent LC/MSD TOF mass spectrometer by electrospray ionisation time-of-flight (ESI-TOF) reflection experiments. Attenuated total reflectance Fourier-transform infrared (ATR-FTIR) spectra were recorded using a Bruker Alpha I spectrophotometer equipped with a Platinum-ATR single reflectance diamond module. 64 cumulative spectra scans with 2 cm^{-1} resolution were measured in the 400-4000 cm^{-1} range for background and analysis. ATR spectra were analysed using OPUS 7.2 and SpectraGryph 1.2 software (Menges, 2016). UV-Vis spectroscopy was performed using a 1.00 cm quartz cuvette at room temperature with an Analytik Jena spectrophotometer Spekol 2000, unless stated otherwise. Synthesis reactions were monitored by thin-layer chromatography (TLC) carried out on 0.2 mm Merck silica plates (60 F_{254}), using UV light and/or iodine vapour for visualisation. Melting points were measured on a hot plate using a thermometer. Column chromatographies were performed with a stationary phase of Silica Gel 60 HR (reinst). DMSO was dried and stored with 4 Å molecular sieves. Et_3N, THF, ACN and Py were distilled over KOH and stored with 3 Å molecular sieves.

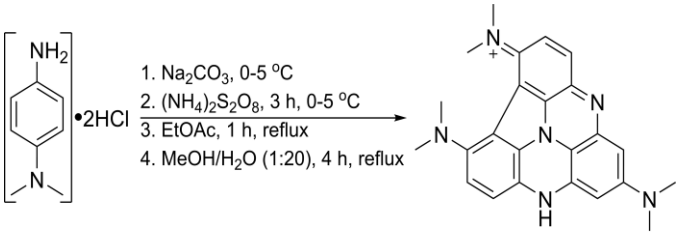
3.2. Materials

Acros Organics: agar; phosphorus pentoxide; tetrahydrofuran; diethyl ether; cyclohexane; sodium hypochlorite, 5%; ethyl acetate; *N*,*N*-dimethylformamide; pork peptone; calcium chloride; *p*-nitrophenol; sodium nitrite; 1,4-diazabicyclo[2.2.2]octane; 1,8-diazabicyclo[5.4.0]undec-7-ene; acrylonitrile; *p*-nitrophenyl carbonate; *p*-nitrophenyl chloroformate; agar; phosphorus pentoxide; ethyl acetate; sodium sulfanilate hydrate; sodium hydroxide; 5-aminoisophthalic acid; 2-propanol; *N*-(2-hydroxyethyl)piperazine-*N*′-2-ethanesulfonic acid; orthophosphoric acid; indoxyl acetate. *Alfa Aesar*: chloroform. *BD*: trypticase soy broth. *DB*: peptone. *Biorro*: Lipase LPS L. *Biosynth*: *N*-chloroacetyl-L-tyrosine. *Carl Roth*: sodium sulfate, boric acid. *Calbiochem*: *N*-*α*-acetyl-L-cysteine. *Chemapol*: potassium cyanide. *Chempur*: potassium hydroxide. *Fisher Scientific*: glycine; *N*,*N*-dimethyl-*p*-phenylenediamine dihydrochloride; sodium salt deoxycholic acid. *Difco*: Czapek-agar; bovine peptone. *Fisher Scientific*: Luria-Bertani broth, Miller; *N*,*N*-dimethyl-*p*-phenylenediamine dihydrochloride. *Fluka*: glycerol, 100%; sodium borohydride; triethylamine; *O*-methylhydroxylamine hydrochloride; *N*,*N*-dimethylhydrazine; *N*,*N*′-

dimethylhydrazine dihydrochloride; 5-aminotetrazole monohydrate; 4-aminopyridine; aminoacetonitrile hydrochloride; phenol; diethanolamine; imidazole; gum arabic. *Lach:ner*: hydrogen peroxide, 30%; pyridine. *Mavis*: ethanol. *Merck*: metol; yeast extract; methanol; sodium carbonate; ammonium persulfate; potassium dihydrogen phosphate; sodium acetate; dipotassium hydrogen phosphate; sodium chloride; peptone; iminodiacetonitrile; dimethyl sulfoxide; concentrated HCl, 36-38%; sodium dihydrogen phosphate dihydrate; disodium hydrogen phosphate dodecahydrate. *Novozymes*: Novozymes® 51003; Lipolase 100 L; Finizym 250 L. *Oxoid*: beef extract; GMO-free soya peptone; nutrient broth. *P-L Biochemicals*: 1,3-amino-2-methyl-2-propanediol. *Roanal*: glucose; L-serine. *Serva*: potato peptone; *N*-*α*-acetyl-L-lysine; *N*-*α*-acetyl-L-arginine dihydrate; glucose; Coomassie Briliant Blue G-250. *Sigma-Aldrich*: potato dextrose agar; toluene; L-glutamine; 2,4-dinitrophenylhydrazine; toluene; α-bovine carbonic anhydrase II; bovine serum albumin; *p*-nitrophenyl acetate; *p*-nitrophenyl palmitate; esterase from *Bacillus subtilis*. *Thermo Scientific*: *N*-acetyl-L-histidine; sodium succinate hexahydrate; *O*-phenyl chlorothionocarbonate; Lawesson's reagent; 1,1-thiocarbonyldiimidazole; tris(hydroxymethyl)aminomethane; 5-acetamido-1,3,4-thiadiazole-2-sulfonamide.
Recombinant enzymes provided by Dr. Lina Baranauskienė and PhD student Tautvydas Kojis from the Department of Biothermodynamics and Drug Design, Institute of Biotechnology, Life Sciences Center, Vilnius University: human α-carbonic anhydrase IX catalytic domain expressed in Chinese hamster ovary (CHO) cell line; *Pseudomonas aeruginosa* carbonic anhydrase 1 expressed in *E. coli* BL21 (DE3) and carbonic anhydrase 2 expressed in *E. coli* Tuner (DE3).

3.3. Synthesis Methods

3.3.1. Ferbamine Using Optimised Conditions



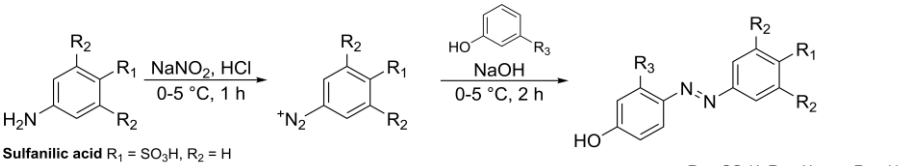
DMPD **Ferbamine**

The solution consisting of 7.53 g (36 mmol) *N*,*N*-dimethyl-*p*-phenylenediamine dihydrochloride (DMPD·2HCl) and 100 ml dH_2O was prepared in a 400 ml beaker with a thermometer and magnetic stirring. Small portions of 3.816 g (36 mmol) Na_2CO_3 were added to the solution to neutralise HCl. The solution was cooled down to 0-5 °C in an ice bath. 8.2 g (36 mmol) of $(NH_4)_2S_2O_8$ was dissolved in 40 ml dH_2O, cooled to 0-5 °C in an ice bath, and added dropwise to the DMPD solution while maintaining temperatures below 5 °C. After 3 h of mixing, the reaction mixture was warmed to 20 °C. Black precipitate was collected using the Büchner filtration system and washed with 4 × 100 ml of dH_2O. The precipitate was dried over P_2O_5 in an

exicator for 24 h. 150 mg of dry precipitate and 150 ml of EtOAc were added to a 250 ml round-bottom flask with an Allihn condenser and magnetic stirring. The slurry was refluxed for 1 h and cooled down to 20 °C. The dark slurry was collected using the Büchner filtration system, washed with 4 × 50 ml of EtOAc, and dried in the open air. 50 mg of dry precipitate and 100 ml of 5% MeOH-dH_2O mixture were added to a 250 ml round-bottomed flask with an Allihn condenser and magnetic stir bar. The mixture was refluxed for 4 h and cooled down to 20 °C. Insoluble residues were filtered using a Büchner filtration system, and Ferbamine was collected by rotovaping the filtrate at 55 °C under reduced pressure.

Black crystals, yield: 0.92%. Melting point (not purified): 160-164 °C (decomposed). ^{1}H NMR (400 MHz, DMSO-d_6) δ (ppm): δ 8.88 (s, 1H), 8.14 (s, 1H), 8.05 (d, 1H, *J* = 9.56 Hz) 7.93 (d, 1H, *J* = 8.72 Hz), 7.69 (d, 2H, *J* = 8.24 Hz), 7.01 (d, 2H, *J* = 8.76 Hz), 6.87 (s, 1H), 3.23 (s, 6H,), 3.06 (s, 6H), 1.23 (s, 6H). ^{13}C NMR (DMSO-d_6, 100 MHz) δ (ppm): 152.03, 151.72, 149.05, 146.10, 140.90, 137.77, 134.23, 132.39, 130.40, 126.25, 125.93, 121.59, 113.04, 112.91, 109.58, 100.37, 34.79, 34.08, 29.46. HRMS *m/z*: calculated 397.2135, found 397.2132 $[M]^+$ ($C_{24}H_{25}N_6^+$); calculated 411.2292, found 411.2289 $[M]^+$ ($C_{25}H_{27}N_6^+$); calculated 383.1978, found 383.1979 $[M+H]^+$ ($C_{24}H_{25}N_6$+H)$^+$. ATR-FTIR (cm^{-1}): 3365, 3227, 3043, 2927, 2811, 1610, 1569, 1520, 1456, 1449, 1339, 1361, 1290, 1226, 1196, 1169, 1129, 1068, 946, 820, 755, 618, 548.

3.3.2. Phenyl Azo Dyes



Sulfanilic acid R_1 = SO_3H, R_2 = H
5-aminoisophthalic acid R_1 = H, R_2 = COOH

HABSA (76.7%) R_1 = SO_3H, R_2 = H, R_3 = H
AO6 (50.2%) R_1 = SO_3H, R_2 = H, R_3 = OH
HPDIA (61.2%) R_1 = H, R_2 = COOH, R_3 = H
ARIPA (56.7%) R_1 = H, R_2 = COOH, R_3 = OH

The general procedure of azo dye synthesis was created by modifying the work of Tang et al (2016). 20 mmol of aniline derivative and 22 mmol of $NaNO_2$ were dissolved in 8 ml of dH_2O and cooled down to 0-5 °C in an ice bath. 16 ml of 19-18% HCl was added dropwise and mixed for 1 h at 0-5 °C. 20.4 mmol of phenol or resorcinol (3-hydroxyphenol recrystallised from toluene) was dissolved in 40 ml 3 M NaOH and cooled down to 0-5 °C in an ice bath. Diazo salt suspension was added dropwise to the phenolate solution and mixed for 2 h at 0-5 °C. Crude product was precipitated by adding 36% HCl to pH 2-3, collected by filtration, and washed with cold dH_2O. Crude product was dried in the open air and purified by recrystallisation.

4-(4-hydroxyphenylazo)benzenesulfonic acid (HABSA). Orange crystals. Recrystallisation solvent: dH_2O. Yield: 4.26 g (77%). Melting point: 282-287 °C decomposed (lit. 282-285 °C decompose). ^{1}H NMR (400 MHz, DMSO-d_6) δ (ppm): 10.35 (s, 1H), 7.82 (d, 2H, *J* = 8.8 Hz), 7.77 (s, 4H), 6.95 (d, 2H, *J* = 8.8 Hz). ^{13}C NMR (100 MHz, DMSO-d_6) δ (ppm): 161.5, 151.80, 149.85, 145.25, 126.64, 124.94, 121.60, 115.98. NMR spectral data match published in the literature (Tang et al.,

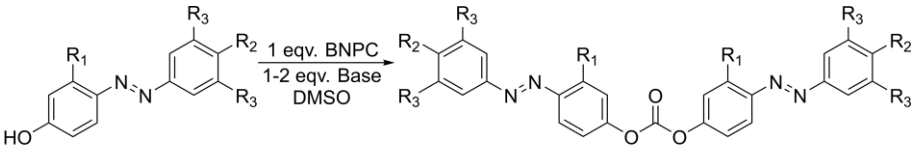
2016). ATR-FTIR (cm^{-1}): 3585, 3502, 3288, 3018, 1619, 1590, 1499, 1461, 1432, 1391, 1363, 1269, 1247, 1184, 1146, 1118, 1101, 1034, 1002, 956, 893, 843, 794, 710, 621, 562, 526, 423.

4-(2,4-dihydroxyphenylazo)benzenesulfonic acid (AO6). Red crystals. Recrystallisation solvent: dH_2O. Yield: 2.92 g (50%). Melting point: 260-268 °C decomposed. ^1H NMR (400 MHz, DMSO-d_6) δ (ppm): 11.51 (s, 1H), 9.73 (s, 1H), 6.86 (dd, 4H, J = 25.6 Hz, 8.4 Hz), 6.79 (d, 1H, J = 8.8 Hz), 5.62 (dd, 1H, J = 8.8 Hz, 2.4 Hz), 5.48 (d, 1H, J = 2.4 Hz). ^{13}C NMR (100 MHz, DMSO-d_6) δ (ppm): 163.20, 156.60, 150.45, 149.35, 132.40, 129.89, 126.73, 121.15, 109.25, 103.03. ATR-FTIR (cm^{-1}): 3461, 3062, 1623, 1589, 1559, 1540, 1506, 1474, 1418, 1397, 1340, 1319, 1223, 1198, 1163, 1118, 1032, 1007, 978, 956, 924, 848, 827, 808, 720, 626, 598, 569, 529, 477, 457. NMR and FTIR spectral data match published in the literature (Noroozi-Pesyan et al., 2009).

5-(4-hydroxyphenylazo)isophthalic acid (HPDIA). Orange crystals. Recrystallisation solvent: 2-propanol and dH_2O (1:4 *v/v*) mixture. Yield: 3.50 g (61%). Melting point: 282-287 °C decomposed. ^1H NMR (400 MHz, DMSO-d_6) δ (ppm): 13.53 (s, 2H), 10.47 (s, 1H), 8.54 (s, 1H), 8.50 (s, 2H), 7.89 (d, 2H, J = 8.4 Hz), 6.97 (d, 2H, J = 8.4 Hz). ^{13}C NMR (100 MHz, DMSO-d_6) δ (ppm): 166.10, 161.76, 152.27, 145.08, 132.61, 130.92, 126.27, 125.43, 116.09. NMR spectral data match published in the literature (Husain et al., 2015). ATR-FTIR (cm^{-1}): 3332, 3082, 2954, 2821, 2575, 2515, 1698, 1650, 1606, 1586, 1504, 1475, 1457, 1418, 1311, 1269, 1243, 1216, 1188, 1147, 1109, 978, 918, 835, 804, 785, 758, 739, 871, 661, 842, 606, 561, 506, 476.

5-(2,4-dihydroxyphenylazo)isophthalic acid (ARIPA). Orange crystals. Recrystallisation solvent: dH_2O. Yield: 3.42 g (57%). Melting point: 255-262 °C decomposed. ^1H NMR (400 MHz, DMSO-d_6) δ (ppm): 13.01 (s, 1H), 8.53 (s, 1H), 8.34 (s, 2H), 7.68 (d, 1H, J = 8.4 Hz), 6.53 (d, 1H, J = 8.4 Hz), 6.4 (s, 1H). ^{13}C NMR (100 MHz, DMSO-d_6) δ (ppm): 191.02, 168.33, 165.26, 157.66, 150.44, 132.73, 131.57, 131.25, 124.24, 110.66, 103.60. ATR-FTIR (cm^{-1}): 3719, 3120, 3047, 2911, 2747, 2597, 1725, 1685, 1627, 1599, 1546, 1500, 1485, 1458, 1386, 1316, 1261, 1229, 1158, 1100, 954, 912, 880, 842, 801, 754, 734, 659, 633, 603, 507, 464, 411.

3.3.3. Phenyl Azo Dye Carbonates



Dyes:
HABSA R_1 = H, R_2 = SO_3H, R_3 = H
AO6 R_1 = OH, R_2 = SO_3H, R_3 = H
HPDIA R_1 = H, R_2 = H, R_3 = COOH
ARIPA R_1 = OH, R_2 = H, R_3 = COOH

Bis-[4-(4-hydroxyphenylazo)benzenesulfonic acid] carbonate (bis(HABSA)c) synthesis was created and developed during this work. 0.75 g (2.5 mmol) of 4-(4-hydroxyphenylazo)benzenesulfonic acid (HABSA), 28.5 ml of dry DMSO and 1.5 ml of Et_3N were added to an oven-dried 50 ml round-bottom flask. 0.8 g (2.625 mmol)

of bis(*p*-nitrophenol) carbonate (BNPC) and 10 ml of DCM were added into a 15 ml Falcon tube and cooled down to 0-4 °C in an ice bath. BNPC was added to HABSA in a single aliquot, mixed for 5 min, and cooled to 0 °C for 1 h. After that, the mixture was allowed to return to ambient temperature (20 °C). Crude product precipitate was filtered and washed with 40 ml of AcOH, followed by 40 ml of MeOH and 40 ml of DCM. The product was left to dry in the open air.

Pale orange powder. Synthesis yield: 0.36 g (50%). Melting point: > 350 °C. ^{1}H NMR (400 MHz, DMSO-d_6) δ (ppm): 8.04 (d, 4H, J = 8.8 Hz), 7.85 (dd, 8H, J = 26.8 Hz, 8.4 Hz), 7.68 (d, 4H, J = 8.8 Hz). ^{13}C NMR (100 MHz, DMSO-d_6) δ (ppm): 153.11, 151.97, 151.50, 151.33, 150.46, 127.25, 124.51, 122.95, 122.71. ATR-FTIR (cm^{-1}): 1785, 1595, 1497, 1399, 1275, 1239, 1185, 1156, 1126, 1103, 1047, 1007, 954, 887, 848, 779, 760, 709, 664, 631, 572, 531, 501, 430.

Bis-[4-(2,4-dihydroxyphenylazo)benzenesulfonic acid] carbonate (bis(AO6)c) synthesis was based on the bis(HABSA)c method. 0.088 g (0.3 mmol) of 4-(2,4-dihydroxyphenylazo)benzenesulfonic acid (AO6), 0.75 ml of dry DMSO and 0.0336 g (0.3 mmol) of DABCO were added into a 2 ml Eppendorf tube. 0.1 g (0.33 mmol) of BNPC and 1 ml of Et_2O were added into a 1.5 ml Eppendorf tube and cooled down to 0-4 °C in an ice bath. BNPC was added to AO6 in a single aliquot, mixed for 10 min, and cooled to 0 °C for 1 h. After that, the mixture was allowed to return to ambient temperature (20 °C). Crude product precipitate was centrifuged at 10000 × g for 10 min at 20 °C. Precipitate was washed with 1.5 ml of Et_2O, 2 × 1.5 ml of MeOH and 1.5 ml of DCM, using 10000 × g centrifugation for 10 min at 4 °C. The product was left to dry in the open air.

Orange powder. Synthesis yield: 0.034 g (37%). Melting point: 240-250 °C (decompose). ^{1}H NMR (400 MHz, DMSO-d_6) δ (ppm): 11.38 (s, 1H), 7.96 (d, 2H, J = 8.4 Hz), 7.84-7.72 (m, 5H). ^{13}C NMR (100 MHz, DMSO-d_6) δ (ppm): 181.00, 151.26, 146.57, 132.45, 126.96, 122.05, 121.46, 120.89, 120.12, 118.18, 117.70. ATR-FTIR (cm^{-1}): 3467, 3065, 3046, 1743, 1654, 1638, 1599, 1578, 1546, 1499, 1407, 1368, 1314, 1256, 1216, 1162, 1135, 1053, 1019, 996, 920, 902, 839, 825, 743, 727, 707, 653, 630, 609, 582, 563, 504, 482, 482, 439.

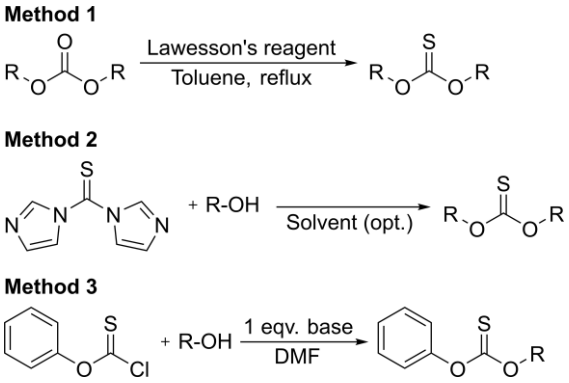
Bis-[5-(4-hydroxyphenylazo)isophthalic acid] carbonate (bis(HPDIA)c) synthesis was based on bis(AO6)c method. 0.229 g (0.8 mmol) of 5-(4-hydroxyphenylazo)isophthalic acid (HPDIA), 0.179 ml (1.6 mmol) of DABCO and 4 ml of dry DMSO were added into a 15 ml Falcon tube. 4.6 ml of Et_2O was added, followed by 0.243 g (0.8 mmol) of BNPC and 4.6 ml of DCM. The tube was stored at 0 °C overnight and allowed to return to ambient temperature (20 °C). Crude product precipitate was centrifuged at 3400 × g, 10 min at 18 °C and washed with 10 ml of Et_2O, dH_2O, acetone and DCM using centrifugation at 3400 × g for 10 min at 4 °C. The product was left to dry in the open air.

Orange powder. Synthesis yield: 0.0457 g (19%). Melting point: > 350 °C. ^{1}H NMR (400 MHz, DMSO-d_6) δ (ppm): 8.40 (td, 1H, J = 8.42 Hz, 2.64 Hz), 8.11 (d, 1H, J = 9.2 Hz), 7.71 (t, 2H, J = 8.88 Hz), 6.99 (t, 1H, J = 8.84 Hz), 6.92 (d, 1H, J = 9.2 Hz). ATR-FTIR (cm^{-1}): 3361, 3112, 3079, 2956, 1739, 1612, 1590, 1521, 1491, 1385,

1345, 1311, 1274, 1191, 1150, 1083, 1053, 1009, 971, 917, 852, 786, 743, 726, 669, 592, 564, 494, 450.

Bis-[5-(2,4-dihydroxyphenylazo)isophthalic acid] carbonate (bis(ARIPA)c) synthesis was based on bis(AO6)c method. 0.0363 g (0.12 mmol) of 5-(2,4-dihydroxyphenylazo)isophthalic acid (ARIPA), 1.5 ml of dry DMSO and 0.0365 g (0.12 mmol) of BNPC were added into a 2 ml Eppendorf tube. The reaction was initiated by adding 50 µl (0.6 mmol) of dry Py, then mixed for 4 h at 20 °C. The reaction mixture was added to 5 ml of toluene; the liquid phase was collected by filtration and rotovaped to remove Py and solvents. Resulting particles were washed with 10 ml of DCM. DCM rotovaped and washed with 10 ml of cHex. The product was left to dry in the open air.

3.3.4. Thiocarbonates



Method 1 – Lawesson's reaction

0.6 g (1.97 mmol) of BNPC, 0.75 g (1.86 mmol) of Lawesson's reagent, and 50 ml of toluene were added to a 150 ml round-bottomed flask and refluxed for 24 h. The reaction mixture was washed with 3 × 50 ml dH_2O, followed by rotovaping to remove toluene.

Method 2 – imidazole substitution in 1,1-thiocarbonyldiimidazole (TCDI)

The synthesis was based on the Onyancha et al. (2009) published method. 0.3336 g (2.4 mmol) of pNP and 0.2403 g (1.35 mmol) of TCDI were added into a 1.5 ml Eppendorf tube with an optional 1 ml of DCM. The tube was heated at 40 °C for 1 h. The monosubstituted product was isolated using dry column vacuum chromatography using Hex-EtOAc with a 2% (5 ml) gradient.

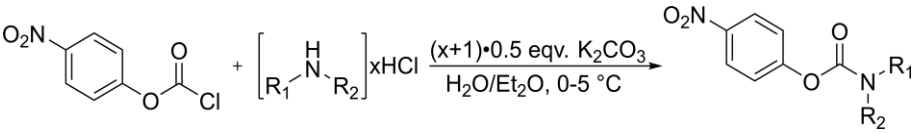
Brown oil. ^{1}H NMR (400 MHz, DMSO-d_6) δ (ppm): 8.12 (dt, 2H, J = 9.2 Hz, 3.2 Hz), 7.04 (s, 1H), 6.93 (dt, 2H, J = 9.2 Hz, 3.6 Hz), 1.35 (s, 2H). ^{13}C NMR (100 MHz, DMSO-d_6) δ (ppm): 164.01, 139.58, 135.14, 126.22, 124.93, 121.63, 115.82, 30.43.

Method 3 – using *O*-phenyl thiochloroformate (PhO-C(S)-Cl)

4-(4-Hydroxyphenylazo)benzenesulfonic acid phenyl thiocarbonate (PhO-C(S)-HABSA) synthesis was created during this work. 33.3 mg (0.12 mmol) of HABSA, 17.6 µl (0.126 mmol) of Et_3N and 1.5 ml of DMF were added into a 2 ml Eppendorf tube. 28.4 µl (0.127 mmol) of phenyl thiochloroformate was added and mixed for

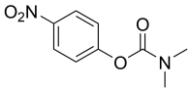
10 min. Crude product precipitate was collected using 10000 × g 10 min 4 °C centrifugation followed by washing with 1.5 ml of dH_2O, MeOH and DCM.
Orange powder. Synthesis yield: 17.5 mg (73%). Melting point: > 350 °C. ^{1}H NMR (400 MHz, DMSO-d_6) δ (ppm): 8.04 (d, 2H, *J* = 8.8 Hz), 7.85 (dd, 4H, *J* = 26.8 Hz, 8.4 Hz), 7.58 (d, 2H, *J* = 8.8 Hz), 7.55-7.51 (m, 2H), 7.39-7.35 (m, 3H). ^{13}C NMR (100 MHz, DMSO-d_6) δ (ppm): 193.99, 155.15, 153.32, 151.75, 150.92, 150.44, 130.15, 127.28, 127.28, 126.96, 124.37, 123.39, 122.48, 121.92. ATR-FTIR (cm^{-1}): 3055, 1669, 1590, 1487, 1456, 1411, 1280, 1235, 1194, 1153, 1131, 1099, 1050, 1008, 931, 858, 785, 768, 723, 693, 648, 600, 576, 530, 527, 498, 474, 420.

3.3.5. Carbamates and Carbazates



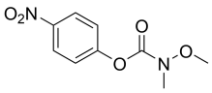
The general synthesis method was modified from Peterson et al (2006). 1.2 mmol of amine (hydrazine) or its salt, 5 ml of Et_2O and 0.5 ml of dH_2O were added into a 25 ml round-bottom flask and mixed for 10 min. The mixture was cooled down to 0-5 °C in an ice bath. An appropriate amount of K_2CO_3 was added to neutralise the acid in the amine salt, and 0.5 eqv. for the reaction. 0.208 g (1 mmol) of *p*-nitrophenyl chloroformate (pNP-C(O)-Cl) was dissolved in 5 ml of Et_2O, cooled down to 0-5 °C and dropwise added to the stirring amine solution. The reaction conditions and product isolation were determined for each product.

4-nitrophenyl *N*,*N*-dimethyl carbamate (**1**)



Amine – dimethylamine hydrochloride; reaction time – 18 h at 0-5 °C. The reaction mixture was diluted with 9 ml of dH_2O and 4 ml of Et_2O. The Et_2O phase was collected and dried using granular $CaCl_2$ by shaking for 2 h. Crude product was isolated by decanting off Et_2O, rotovaping to remove the solvent and residual dimethylamine, and drying in open air. White crystals ATR-FTIR (cm^{-1}): 3112, 3084, 1771, 1616, 1590, 1518, 1489, 1348, 1321, 1291, 1194, 1166, 1126, 1106, 1013, 890, 863, 833, 803, 743, 677, 532, 505, 419.

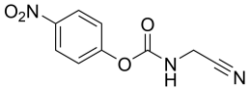
4-nitrophenyl *N*-methoxy-*N*-methyl carbamate (**2**)



Amine – *N*,*O*-dimethylhydroxylamine hydrochloride; reaction time – 5 h at 0-5 °C. The Et_2O phase was collected and dried using granular $CaCl_2$ by shaking for 2 h. Crude product was isolated by decanting Et_2O and rotovaping to remove solvent. The product was recrystallised from cHex and dried at 40 °C in a drying oven. White crystals. Yield: 0.226 g (33%). ^{1}H NMR (400 MHz, DMSO-d_6) δ (ppm): 8.29 (dt, 2H, *J* = 9.2 Hz, 3.2 Hz), 7.48 (dt, 2H, *J* = 9.2 Hz, 3.2 Hz), 3.74 (s, 3H), 3.25 (s, 3H). ^{13}C NMR (100 MHz, DMSO-d_6) δ (ppm): 164.07, 155.74, 144.98, 125.43, 123.13, 61.45, 35.33. ATR-FTIR (cm^{-1}): 3115, 3091, 2998, 2980, 2942, 2844, 2825, 1723, 1611, 1593, 1514, 1469, 1440, 1397, 1343, 1288, 1239, 1201, 1183, 1156, 1106, 1018, 965, 861,

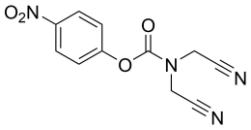
822, 755, 726, 686, 668, 633, 610, 528, 511, 494, 447, 411. NMR and ATR spectral data matches published in the literature (Varjosaari et al., 2016).

4-nitrophenyl *N*-acetonitrile carbamate (**3**)



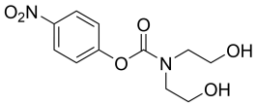
Amine – aminoacetonitrile hydrochloride; reaction time – 3 h at 0-5 °C. Product precipitated during the reaction. Reaction mixture was diluted with 9 ml of dH_2O, followed by crude product filtration and washing with dH_2O. White crystals. ATR-FTIR (cm^{-1}): 3360, 3111, 3079, 2995, 1716, 1618, 1594, 1534, 1511, 1484, 1414, 1349, 1305, 1279, 1249, 1219, 1159, 1131, 1104, 1049, 1010, 965, 925, 893, 856, 825, 762, 711, 687, 668, 623, 605, 528, 490, 435, 409.

4-nitrophenyl *N*,*N*-diacetonitrile carbamate (**4**)



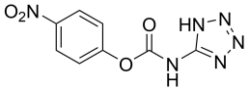
Amine – iminodiacetonitrile; reaction time – 1 h at 0-5 °C. Product precipitated during the reaction. It was collected using filtration, washed with Et_2O, and dried in open air. White crystals. ATR-FTIR (cm^{-1}): 3135, 2982, 2956, 2326, 1739, 1613, 1591, 1518, 1490, 1453, 1402, 1348, 1331, 1308, 1239, 1191, 1157, 1105, 1002, 959, 944, 910, 963, 848, 821, 748, 665, 624, 527, 498, 481, 448.

4-nitrophenyl *N*,*N*-diethanol carbamate (**5**)



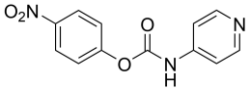
Amine – *N*,*N*-diethanolamine; reaction time – 3 h at 0-5 °C and 18 h at ambient temperature. Product precipitated during the reaction. It was collected using filtration, washed with Et_2O, and dried in open air. White crystals. ATR-FTIR (cm^{-1}): 3484, 3119, 3085, 2948, 2885, 1704, 1614, 1593, 1519, 1498, 1464, 1416, 1340, 1290, 1211, 1164, 1111, 1066, 1052, 954, 858, 821, 692, 667, 631, 533, 495.

4-nitrophenyl 1*H*-tetrazol-5-yl carbamate (**6**)



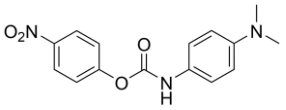
Amine – 5-aminotetrazole monohydrate; reaction time – 4 h at 0-5 °C. Product precipitated during the reaction. It was collected using filtration, washed with Et_2O and MeOH, and dried in open air. White crystals. ATR-FTIR (cm^{-1}): 3245, 3114, 3081, 3060, 2708, 2606, 1727, 1642, 1620, 1592, 1535, 1488, 1410, 1360, 1323, 1245, 1205, 1160, 1125, 1109, 1038, 1017, 987, 884, 856, 789, 755, 728, 696, 979, 631, 541, 485, 411.

4-nitrophenyl 4-pyridine carbamate (**7**)



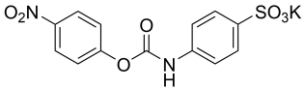
Amine – 4-aminopyridine; reaction time – 2 h at 0-5 °C. Product precipitated during the reaction. It was collected using filtration, washed with Et_2O, and dried in open air. Pale yellow powder. ATR-FTIR (cm^{-1}): 3169, 3112, 3084, 2955, 2896, 2794, 1750, 1693, 1629, 1609, 1590, 1537, 1517, 1489, 1417, 1396, 1352, 1331, 1310, 1245, 1203, 1168, 1109, 995, 903, 857, 817, 775, 744, 703, 687, 667, 624, 572, 532, 493, 464, 407.

4-nitrophenyl *N'*,*N'*-dimethylamino-*N*-phenylenediamine carbamate (**8**)



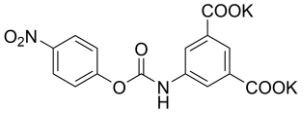
Amine – DMPD·2HCl; reaction time – 18 h at 0-5 °C. Product precipitated during reaction and was collected using filtration and washed with Et_2O. White crystals. ^1H NMR (400 MHz, DMSO-d_6) δ (ppm): 10.39 (s, 1H), 8.30 (dt, 2H, *J* = 9.2 Hz, 3.2 Hz), 7.51 (dt, 2H, *J* = 9.2 Hz, 3.2 Hz), 7.45 (d, 2H, *J* = 8.4 Hz), 7.13 (d, 2H, *J* = 6.8 Hz), 2.95 (s, 6H). ^{13}C NMR (100 MHz, DMSO-d_6) δ (ppm): 164.15, 155.83, 150.93, 144.69, 126.40, 125.45, 123.06, 120.34, 116.02, 42.77. ATR-FTIR (cm^{-1}): 3567, 3366, 3318, 3213, 3110, 3075, 2956, 2557, 2508, 2468, 1744, 1714, 1615, 1685, 1541, 1514, 1486, 1447, 1421, 1407, 1344, 1322, 1198, 1163, 1137, 1107, 1066, 998, 946, 904, 854, 811, 775, 747, 725, 677, 647, 626, 591, 552, 512, 489, 408.

4-nitrophenyl *N*-(4-benzenesulfonate sodium salt) carbamate (**9**)



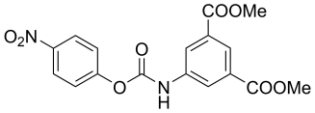
Amine – sodium 4-aminobenzenesulfonate hydrate; reaction time – 45 min at 0-5 °C. The Et_2O phase was collected and dried using Na_2SO_4 by shaking for 2 h. Product was isolated by decanting Et_2O, rotovaping to remove solvent and drying in open air. White crystals. ATR-FTIR (cm^{-1}): 3363, 3116, 3080, 1923, 1772, 1611, 1590, 1511, 1489, 1334, 1292, 1195, 1165, 1135, 1108, 1010, 970, 889, 862, 842, 803, 747, 690, 675, 630, 595, 534, 494, 418.

4-nitrophenyl *N*-(5-isophthalate potassium salt) carbamate (**10**)



Amine – 5-aminoisophthalic acid; reaction time – 18 h at ambient temperature. Product precipitated during the reaction. It was collected using filtration, washed with Et_2O and dried over P_2O_5 in an exicator. White crystals ATR-FTIR (cm^{-1}): 3288, 1696, 1623, 1557, 1454, 1394, 1362, 1322, 1299, 1264, 1243, 1213, 1096, 1070, 982, 958, 894, 802, 764, 722, 681, 584, 542, 478, 447.

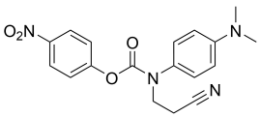
4-nitrophenyl *N*-(5-isophthalate dimethyl ester) carbamate (**11**)



Amine (dimethyl 5-aminoisophthalate) for this reaction was synthesised by refluxing 1.81 g (10 mmol) of 5-aminoisophthalic acid with 3 drops of 96% H_2SO_4 in 10 ml of MeOH for 24 h. The reaction mixture was rotovaped to remove MeOH and dissolved in 50 ml of $CHCl_3$. The organic phase was washed with 2 × 25 ml of 9% $NaHCO_3$ solution, rotovaped and dried in open air. White powder. Synthesis yield: 88.0%. ATR-FTIR (cm^{-1}): 3471, 3378, 2950, 1699, 1630, 1602, 1437, 1350, 1248, 1193, 1130, 1095, 1019, 995, 900, 885, 754, 726, 580, 558, 431, 401. ATR spectral data match published in the literature (Coblentz society inc., 1966).

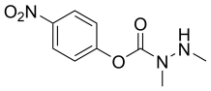
Appropriate carbamate synthesis was performed for 1.5 h at 0-5 °C. Product precipitated during the reaction. It was collected using filtration, washed with Et_2O and dried in open air. White crystals. ATR-FTIR (cm^{-1}): 3315, 3121, 3096, 2959, 2855, 1763, 1731, 1703, 1613, 1557, 1525, 1490, 1457, 1435, 1347, 1323, 1297, 1202, 1165, 1129, 1110, 1034, 1003, 982, 942, 922, 903, 852, 832, 788, 753, 718, 677, 580, 566, 532, 491, 452.

4-nitrophenyl *N*-(*N'*,*N'*-dimethyl-*p*-phenylenediamine)-*N*-propanenitrile carbamate (**12**)



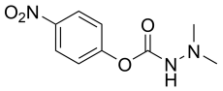
Amine (*N'*,*N'*-dimethylamine-*N*-propanenitrile-*p*-phenylenediamine) for this reaction was synthesised using the method published in J. Babinskas' master thesis (Babinskas, 2020). Carbamate synthesis was performed for 18 h at 0-5 °C. Et_2O phase was collected, dried using granular $CaCl_2$ by shaking for 2 h and rotovaped. Crude product was dissolved in DCM, washed with 1% HCl, dried over Na_2SO_4 and rotovaped. White crystals. ATR-FTIR (cm^{-1}): 3332, 3115, 3082, 2922, 2890, 2855, 2808, 2251, 1722, 1612, 1592, 1517, 1496, 1446, 1396, 1355, 1286, 1215, 1195, 1162, 1128, 1106, 1058, 1008, 963, 945, 903, 856, 818, 749, 731, 688, 664, 629, 601, 579, 552, 533, 495.

4-nitrophenyl *N*,*N'*-dimethyl carbazate (**13**)



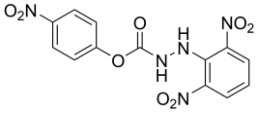
Hydrazine – 1,2-dimethylhydrazine dihydrochloride; reaction time – 3 h at 0-5 °C. Product precipitated during the reaction. It was collected using filtration, washed with Et_2O and dried in open air. White crystals. ATR-FTIR (cm^{-1}): 3116, 3087, 2944, 1758, 1729, 1615, 1593, 1517, 1489, 1466, 1416, 1343, 1217, 1147, 1099, 1006, 956, 935, 851, 819, 753, 736, 712, 670, 625, 533, 492, 416.

4-nitrophenyl *N*,*N*-dimethyl carbazate (**14**)



Hydrazine – 1,1-dimethylhydrazine; reaction time – 3 h at 0-5 °C. Product precipitated during the reaction. It was collected using filtration, washed with Et_2O and dried in open air. ATR-FTIR (cm^{-1}): 3406, 3117, 3084, 1784, 1762, 1640, 1616, 1593, 1519, 1489, 1351, 1326, 1258, 1229, 1195, 1160, 1108, 1009, 891, 857, 837, 746, 724, 696, 675, 612, 531, 492, 450.

4-nitrophenyl 2,6-nitrophenyl carbazate (**15**)



Hydrazine – 2,6-dinitrophenylhydrazine; reaction time – 18 h at 0-5 °C. Product precipitated during the reaction. It was collected using filtration, washed with Et_2O and dried in open air. Yellow crystals. ATR-FTIR (cm^{-1}): 3419, 3342, 3119, 1774, 1642, 1615, 1589, 1512, 1491, 1475, 1421, 1332, 1308, 1285, 1254, 1231, 1202, 1170, 1144, 1127, 1108, 1060, 1005, 924, 910, 864, 834, 779, 739, 707, 872, 652, 625, 644, 630, 497.

3.3.6. 4-(4-hydroxyphenylazo)benzenesulfonic acid acetate (HABSA-Ac)



4-(4-Acetoxyphenylazo)-benzenesulfonic acid (HABSA-Ac) synthesis was adapted from Larsen et al (Larsen et al., 2019). 0.52 g (1.83 mmol) of HABSA, 120 ml of DMF and 20 ml of acetic anhydride were added to a 250 ml round-bottomed flask with an Allihn reflux condenser and magnetic stirring. Acetylation was performed at

75 °C for 20 hours. The precipitate of the crude product was washed with 2 × 50 ml of dH_2O and ethanol. The product was dried in the open air.
Pale orange powder. Yield: 0.367 g (70.6%). Melting point: 198-204 °C (decomposed). ^{1}H NMR (400 MHz, DMSO-d_6) δ (ppm): 7.96 (dt, 2H, J = 8.8 Hz, 2.8 Hz), 7.84 (qd, 4H, J = 8.4 Hz, 2 Hz), 7.37 (dt, 2H, J = 8.8 Hz, 2.8 Hz), 2.31 (s, 3H).^{13}C NMR (100 MHz, DMSO-d_6) δ (ppm): 169.11, 152.92, 151.66, 150.75, 149.62, 126.84, 123.95, 123.05, 122.24, 20.98. NMR spectral data match published in the literature (Suh and Kwon, 1998). ATR-FTIR (cm^{-1}): 3101, 3063, 1763, 1593, 1488, 1368, 1302, 1235, 1183, 1153, 1127, 1102, 1048, 1008, 916, 852, 790, 726, 705, 661, 637, 615, 594, 575, 566, 530, 501.

3.4. Characterisation of Dyes and Substrates

3.4.1. UV-Vis Spectroscopy of Ferbamine Solutions

Ferbamine stock solution was diluted from 45 µg ml^{-1} to 7.5 µg ml^{-1} with dH_2O, 1% NaClO or 0.1 g ml^{-1} $NaBH_4$, and incubated at 20 °C for 30 min. The UV-Vis measurement range was 320-750 nm with 2 nm increments. Reference measurement was performed with dH_2O.

3.4.2. Thermal and pH Stability of Ferbamine

The analysis was performed using UV-Vis spectroscopy. 1 ml of 45 µg ml^{-1} Ferbamine solution was diluted with 5 ml of 60 mM potassium phosphate buffer of pH 3.5, 4.0, 5.0, 6.0, 7.0, 8.0, or dH_2O to set the control solution. The initial UV-Vis spectra were measured, and initial absorption maxima (λ_{Max}) were determined for each solution in the 380-750 nm range. Solutions were divided into three parts (3 × 2 ml) and incubated at three temperatures (20 °C, 30 °C and 37 °C) for 5 weeks. Consecutive UV-Vis spectra measurements were performed every week. Stability was calculated and defined as the percentage of remaining absorption at λ_{Max}.

$$Stability(\%) = \frac{A_0 - A_t}{A_0} * 100\%$$

Where A_0 – initial absorption at λ_{Max}; A_t – absorption after t number of weeks, at the initial λ_{Max}.

3.4.3. ATR-FTIR Analysis of Ferbamine Synthesis Products

1 µl of the reaction mixture sample was applied and evaporated on the ATR crystal at ambient temperature. After that, a full-spectrum measurement was taken, followed by atmospheric compensation and baseline correction.

3.4.4. Determination of pK_as for Phenol Azo Dyes

The pK_a of the dye HABSA and pK_{a2} of AO6 were determined by potentiometric titration using pH (*Mettler Toledo* SevenEasy S20) and electric conductivity (*Mettler Toledo* SevenCompact S230) meters. A 17 mM AO6 solution was prepared by dissolving 0.251 g of the dye in 5 ml of 0.8 M KOH. Titration was performed using a burette with 1 M HCl solution. 5 mM HABSA solution was prepared by dissolving

0.139 g of the dye in 100 ml of Milli-Q H_2O. Titration was performed using a burette with 0.1 M KOH solution. Stable pH and conductivity value measurements were recorded for each 0.1 ml of titrant added.

3.4.5. UV-Vis Spectra of HABSA and AO6

The wavelengths of the absorption maxima (λ_{max}) for HABSA and AO6 were measured across a range of pH values. 5 mM HABSA stock solution was prepared by dissolving 0.139 g of dye in 100 ml of DMSO. 0.5 mM AO6 stock solution was prepared by dissolving 0.0132 g of dye in 90 ml of dH_2O. 16.7 µM HABSA and 20 µM AO6 solutions for spectral measurements were prepared by diluting the stock solution with corresponding 50 mM buffers pH: 3.0 (K-phosphate), 4.0 (Na-succinate), 5.0 (Na-acetate), 6.0 (K-phosphate), 7.0 (HEPES-HCl), 8.0 (HEPES-HCl), 8.5 (Tris-HCl). UV-Vis measurement parameters: reference – dH_2O; range 320-800 nm with 2 nm steps; light path 1.00 cm.

3.4.6. Determination of Molar Extinction Coefficients

The molar extinction coefficient (ε) of HABSA, HABSA-Ac and pNP in 1% DMSO was measured at pH 8.5 and additionally in 100% DMSO for HABSA. 0.5 mM HABSA stock solution was prepared by dissolving 15.9 mg of dye in 15 ml of DMSO and diluting it with DMSO and 10 mM Tris-HCl pH 8.5 buffer to 38.13 µM (1% or 100% DMSO). 50 mM HABSA-Ac DMSO stock was prepared by dissolving 160 mg of substrate in 10 ml of DMSO and diluting it to 0.5 mM (1% DMSO) with pH 8.5 buffer. For *p*-nitrophenol (pNP), a 1 mM stock solution was prepared by dissolving 0.139 g of pNP in 10 ml of DMSO and diluting to 10 µM (1% DMSO) with DMSO and buffer. Absorbance values were measured in triplicate at a 320-800 nm range, with a light path of 1.00 cm. For reference measurements, 100% or 1% DMSO 10 mM pH 8.5 buffer solution was used. The molar extinction coefficients were calculated using the Beer-Lambert law:

$$\varepsilon = \frac{A}{c * l}$$

Where ε – molar extinction coefficient ($\mu M^{-1}\ cm^{-1}$); A – absorption (Abs); c – analyte concentration (µM) l – cuvette light path (cm).

3.4.7. Stability of HABSA-Ac in DMSO

The stability of HABSA-Ac in DMSO was evaluated using UV-Vis spectroscopy. 20 mM HABSA-Ac solution was prepared by dissolving 38.4 mg of the substrate in 6 ml of DMSO and diluting to a final concentration of 0.2 mM. 2 ml of this solution was stored at 20 °C, 4 °C and -20 °C. UV-Vis spectra of each solution were recorded every 24 h for 7 days. Spectroscopy parameters: reference – DMSO; range – 190-800 nm with 1 nm steps; quartz cuvette with 0.50 cm light path.

3.5. Assays

3.5.1. UV-Vis Spectroscopic Laccase Activity with Metol

Laccase activity was measured by observing the formation of the oxidised Metol (*N*-methyl-*p*-aminophenol sulfate) product at 542 nm. Measurement durations were 60 s, with 2 s increments, and the start was delayed by 5 s for mixing. The substrate solution contained 2.0 ml of 50 mM Metol in dH_2O and 0.5 ml of 50 mM pH 5.0 sodium acetate buffer. The reaction was initiated by adding 0.5 ml of enzyme solution to the substrate. Reference measurement was performed by adding 0.5 ml of buffer to the substrate solution. Laccase activity (*U*) was calculated using the formula provided below. One unit (1 U) was defined as 1 µmol of Metol oxidised per 1 min at pH 5.0 and 20 °C.

$$U = \frac{Slope}{\varepsilon_{542} * l} * \frac{V_R}{V_E} * 60 * D_E$$

Where U – laccase activity (U ml^{-1} or µmol ml^{-1} min^{-1}); slope – absorption slope (Abs s^{-1}); ε_{542} – molar extinction coefficient of Metol oxidation product at 542 nm (2 mM^{-1} cm^{-1}) (Lunar et al., 2000); l – cuvette length of light path (cm); V_R – reaction volume in the cuvette (3 ml); V_E – enzyme solution volume in the reaction mixture (0.5 ml); *60* – seconds to minutes conversion factor; D_E – enzyme dilution before the measurement.

3.5.2. Bis(HABSA)c Assays with Amino Acids

The bis(HABSA)c reaction rates with amino acids were evaluated using UV-Vis spectroscopy. 10 mM bis(HABSA)c solution was prepared by dissolving 58.3 mg of the compound in 10 ml of DMSO. 50 mM selected amino acid (Gly, Gln, Ser, N_α-Ac-Cys, N_α-Ac-His, N_α-Ac-Lys, N_α-Ac-Arg, N_α-Ac-Trp, N_α-AcCl-Tyr) solutions were prepared in 10 mM Tri-HCl (pH 8.5) buffer. 2.55 ml of buffer and 0.3 ml of amino acid solution were added to a 1.00 cm light path cuvette. Reaction was initiated with the addition of 0.15 ml of 10 mM bis(HABSA)c solution. The kinetic spectroscopy parameters were as follows: reference – 5% DMSO in 10 mM Tris-HCl buffer; measurement delay – 5 s; wavelength – 428 nm; duration – 600 s; data recording rate – 5 s. Substrate autohydrolysis was measured by omitting amino acids. Bis(HABSA)c reaction rates with amino acids were calculated as follows:

$$v = \frac{Slope_{aa} - Slope_0}{\varepsilon_{428} * 2 * l} * 60$$

Where v – reaction rate (µM min^{-1}); $Slope_{aa}$ – absorption slope in amino acid reactions (Abs s^{-1}); $Slope_o$ – absorption slope in autohydrolysis reaction (Abs s^{-1}); ε_{428} – HABSA molar extinction coefficient (0.0175 μM^{-1} cm^{-1}); 2 – factor to account for two dye molecules; l – cuvette light path (1.00 cm); *60* – factor to convert seconds to minutes.

Bis(HABSA)c reaction with glycine was performed by mixing 0.1 ml of 6.77 mM bis(HABSA)c DMSO solution with 9.9 ml of 68.4 µM gly in 10 mM Tri-HCl (pH 8.5) buffer and incubating for 6 h. Reaction outcome was evaluated using UV-Vis spectroscopy. The spectroscopy parameters were as follows: reference – 1% DMSO

in 10 mM Tris-HCl solution; wavelengths – 320-520 nm; $\Delta\lambda$ – 2 nm. 67.7 µM and 135 µM HABSA solution in 1% DMSO-buffer were measured afterwards.

3.5.3. Esterase Activity Assay with pNPA as the Substrate

20 mM pNPA substrate solution was prepared by dissolving 36.2 mg of pNPA in 10 ml of DMSO. 2.67 ml of 168 mM Tris-HCl (pH 8.5) buffer and 0.03 ml of substrate were combined in the cuvette. The cuvette was placed in a 1.00 cm light path, and reaction measurements were initiated by the addition of 0.3 ml of enzyme solution. Substrate autohydrolysis control measurements were conducted by substituting the enzyme with buffer. The kinetic spectroscopy parameters were as follows: reference – 1% DMSO in 150 mM Tris-HCl solution; measurement delay – 5 s; wavelength – 400 nm; duration – 180 s; data recording rate – 2 s. One activity unit (1 U) is defined as 1 µmol of pNPA hydrolysed per 1 min at pH 8.5 and 20 °C.

$$v = \frac{Slope_E - Slope_o}{\varepsilon_{400} * l} * 60$$

Where v – catalysis rate (µM min^{-1}); $Slope_E$ – absorption slope in enzymatic reaction (Abs s^{-1}); $Slope_o$ – absorption slope in autohydrolysis reaction (Abs s^{-1}); ε_{400} – pNP molar extinction coefficient (0.0191 µM^{-1} cm^{-1}) l – cuvette light path (1.00 cm); 60 – factor to convert seconds to minutes.

3.5.4. Esterase Activity Assay with Indoxyl Acetate as the Substrate

The assay was adapted from a method published by Baliukynas et al. 2020. In brief, the reaction constituents were increased 10-fold, and measurements were performed in a 1 cm light path cuvette. 2.4 ml of 17.5 mM HEPES and 17.5 mM imidazole (pH 7.2) buffer and 0.3 ml of substrate were combined in the cuvette. The reaction was initiated by adding 0.3 ml of an enzyme solution. Substrate autohydrolysis control measurements were conducted by substituting the enzyme with buffer. The kinetic spectroscopic parameters were as follows: reference – 1% EtOH in buffer solution; measurement delay – 5 s; wavelength – 375 nm; duration – 600 s; data recording rate – 5 s. One activity unit (1 U) is defined as the catalysis of 1 µmol of indoxyl acetate hydrolysed per 1 min at pH 7.2 and 20 °C.

$$v = \frac{Slope_E - Slope_o}{\varepsilon_{375} * l} * 60$$

Where v – reaction rate (µM min^{-1}); $Slope_E$ – absorption slope in enzymatic reaction (Abs s^{-1}); $Slope_o$ – absorption slope in autohydrolysis reaction (Abs s^{-1}); ε_{375} – Indoxyl molar extinction coefficient (0.00254 µM^{-1} cm^{-1}) (Pohanka et al., 2011); l – cuvette light path (1.00 cm); 60 – factor to convert seconds to minutes.

3.5.5. Lipase Activity Assay with p-Nitrophenyl Palmitate as the Substrate

The assay was based on a method published by Winkler and Stuckmann (1979). In short, 0.5 mg ml^{-1} substrate solution was prepared by mixing 1 ml of 10 mg ml^{-1} of *p*-nitrophenyl palmitate in 2-propanol with 19 ml of 50 mM pH 8.0 sodium phosphate buffer supplemented with 1 mg ml^{-1} of gum arabic and 2 mg ml^{-1} of sodium deoxycholate. The reaction measurements were initiated with the addition of 0.2 ml

enzyme to 1.8 ml of substrate solution. For substrate autohydrolysis control measurements, the enzyme was substituted with buffer. The kinetic UV-Vis spectroscopy parameters: reference – buffer; measurement delay – 5 s; λ_{max} – 400 nm; duration – 60 s; data recording interval – 2 s. One unit (1 U) – 1 µmol of *p*-nitrophenyl palmitate hydrolysed per 1 minute at pH 8.0 and 20 °C.

$$U = \frac{Slope_E - Slope_0}{\varepsilon_{400} * l} * \frac{V_R}{V_E} * 60$$

Where U – enzyme activity (µM min^{-1} or 1 U ml^{-1}); $Slope_E$ – absorption slope in enzymatic reaction (Abs s^{-1}); $Slope_o$ – absorption slope in autohydrolysis reaction (Abs s^{-1}); ε_{400} – pNP molar extinction coefficient (0.01615 µM^{-1} cm^{-1}); l – cuvette light path (1.0 cm); V_R – total reaction volume (2 ml); V_E – enzyme solution volume (0.2 ml); 60 – seconds to minutes conversion factor.

3.5.6. Bradford Protein Assay

Bradford reagent was prepared according to the original method protocol (Bradford, 1976). The calibration curve was produced using a standard solution of 0.5 mg ml^{-1} bovine serum albumin (BSA) at a final concentration of 1.5-15.0 µg ml^{-1} range and measuring the absorbance. Protein sample measurements used 10-100 µl of sample diluted with 0.15 M NaCl to a final volume of 0.3 ml. Then, 3 ml of Bradford reagent was added, mixed and incubated for 2.0 min at 20 °C. After incubation, the absorbance at 595 nm was measured. The reference measurement used 0.3 ml 0.15 M NaCl and protein sample was omitted. Protein concentration was calculated using the formula below:

$$C_E = \frac{A_{595}}{Slope} * \frac{V_R}{V_E}$$

Where C_E – protein concentration in the initial sample (mg ml^{-1}); A_{595} – absorption at 595 nm; $Slope$ – calibration curve slope; V_R – total reaction volume (3.3 ml); V_E – protein solution volume (ml).

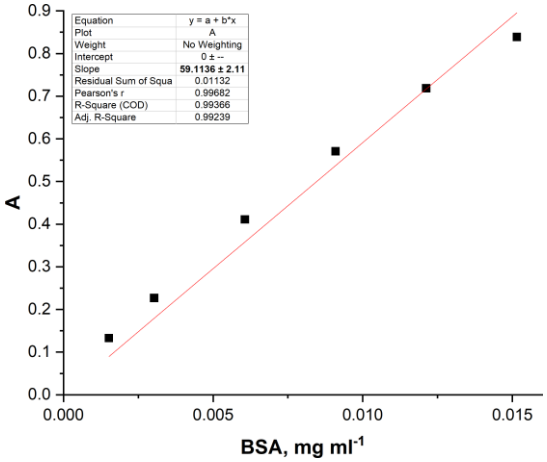


Figure 3.1. Calibration curve for Bradford assay employing BSA.

3.6. Agar Plates for Cultivation and Laccase Activity Screening

3.6.1. Ferbamine-Agar Plate With Wells

9% (*w/w*) agar stock solution was prepared by mixing 0.3 g of agar with 3.4 ml of dH_2O and autoclaving it for 20 min at 121 °C. The agar stock was warmed to 80-85 °C and mixed with 16.6 ml of 45 μg ml^{-1} Ferbamine solution. The mixture was stirred at 80-85 °C until it became homogenous. A polypropylene 200 μl PCR 96-well plate was placed in a Petri dish as a well template. Hot Ferbamine-agar solution was added to the Petri dish and allowed to cool down to ambient temperature. After the agar solidified, the 96-well plate was removed. Ferbamine-agar plate composition: 37.5 μg ml^{-1} Ferbamine, 1.5% agar.

For functional analysis of commercially available Novozymes® 51003 laccase, a plate without wells was prepared. Analysis was performed by adding 1-4 μl of laccase and incubating for 20 h at 20 °C.

3.6.2. Medium-Agar Plates With Various Ferbamine Concentrations for Cultivation and Screening of Microorganisms

General procedure: different volumes of 45 μg ml^{-1} of Ferbamine stock solution were combined with 3.4 ml of medium-agar stock, diluted with sterile dH_2O to 20 ml and mixed at 70-80 °C until the media became homogeneous. Microorganisms cultivation conditions – **Table 3.1**; Ferbamine plate (20 ml) preparation and final compositions – **Table 3.2**.

Table 3.1 Microorganism cultivation conditions

Microorganisms	Media type	Incubation conditions
Escherichia coli DH5-α, *Pseudomonas putida* TBSLT100	LB	10 h, 37 °C
Bacillus pumilus, *Rhodococcus erythropolis* DSMZ 312	TS	168 h, 30 °C
Kluyveromyces marxianus BKM Y-719, *Kluyveromyces lactis* MD2/1, *Pichia pastoris* GS115, *Saccharomyces cerevisiae* AH22-214, colonies from cave samples and GJ8YT plate	YEPG	168 h, 30 °C, 20 °C
Delftia acidovorans, *Alcaligenes faecalis*, *Acinetobacter calcoaceticus* BT8	Nutrient	48 h, 30 °C
Achromobacter denitrificans, *Pseudomonas aeruginosa* A2	Nutrient	48 h, 37 °C
Colonies from cave samples and GJ8YT plate	mHM	168 h, 20 °C, 37 °C
Colonies from GJ8YT plate	PDA	168 h, 30 °C
Colonies from GJ8YT plate	Czapek	168 h, 30 °C

Table 3.2 Medium-agar stocks and 0-37.5 µg ml^{-1} Ferbamine-medium agar plate composition and application.

Medium type	Medium-agar stock, 3.4 ml	Ferbamine stock, ml	Final composition: Ferbamine, µg ml^{-1}	Final composition: Medium-agar
LB	0.5 g LB broth (Miller), 0.3 g agar	16.6	37.5	1% tryptone, 0.5% yeast extract, 1% NaCl, 1.5% agar
		10	22.5	
		2	4.5	
		0	0	
TS	0.6 g trypticase soy broth, 0.3 g agar	16.6	37.5	3% trypticase soy broth, 1.5% agar
		10	22.5	
		2	4.5	
		0	0	
YEPG	0.4 g peptone, 0.1 g yeast extract, 0.47 g 85% glycerol, 0.3 g agar	16.6	37.5	2% peptone, 1% yeast extract, 2% glycerol, 1.5% agar
		10	22.5	
		2	4.5	
		0	0	
Nutrient	0.26 g nutrient broth, 0.3 g agar	16.6	37.5	0.1% lab-lemco, 0.5% peptone, 0.2% yeast extract, 0.5% NaCl, 1.5% agar
		10	22.5	
		2	4.5	
		0	0	
mHM	0.04 g beef extract, 0.1 g yeast extract, 0.35 g soybean peptone, 0.03 g glucose, 0.3 g agar	16.6	37.5	0.2% beef extract, 0.5% yeast extract, 1.75% soybean peptone, 0.15% glucose, 1.5% agar
		0	0	
PDA	0.48 g potato-dextrose broth, 0.3 g agar	16.6	37.5	2.4% potato-dextrose broth, 1.5% agar
		0	0	
Czapek	0.98 g Czapek-agar	16.6	37.5	K_2HPO_4, 0.05% $MgSO_4$, 0.05% KCl, 0.001% $FeSO_4$, 1.5% agar

3.7. Cave Sampling Sites and Their Physical Parameters

The samples were collected during the International speleological and speleodiving expeditions "Ponor Kovači – Izvor Ričine" (Tomislavgrad) in the period from August to September 2022 and the "Balkan Cave Summit (Mostar) 2022", at seven localities in Bosnia and Herzegovina (**Table 3.3**). The samples were collected from the cave entrance zone, the twilight zone, and the transition zone to the dark zone using sterile forceps, transferred into sterile falcon tubes, transported in portable coolers to the laboratory, and kept at 4 °C until analysis. Bat guano deposits were collected with disposable plastic spoons or disposable wooden sticks, with possible removal of soil and sand. Sampling was carried out in compliance with safety regulations, with protective equipment worn; the samples were stored in marked plastic bags and then packed in jars for safe transport. Physical parameters were measured using a combined thermo-hygro-anemometer, the Kestrel 4000 Pocket Weather Meter, and a 4-in-1 environmental meter (luxmeter, sound level meter, thermometer, hygrometer).

Culturing microorganisms from collected samples was performed by placing a piece of the sample, not larger than 1 cm × 1 cm × 1 cm, in a Petri dish, suspending it in 5mL of 0.9% NaCl solution, and streaking the suspension on the agar plate. For each sample, microorganism cultivation was performed on mMH at 20 °C and 37 °C and

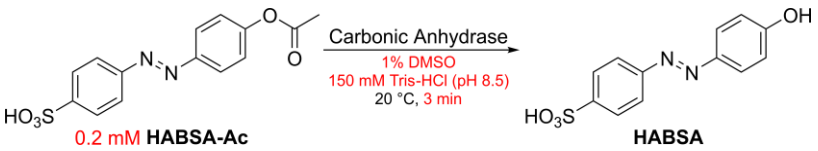
on YEPG plates at 20 °C and 30 °C. Plates were incubated until microbial colonies formed, but not for more than 168 h. Plates containing grown colonies were stored at 4°C until further use.

Table 3.3 Sampling data of selected sampling sites.

	Gornja Jakovljeva Cave	**Donja Mijatova Cave**	**Ponor Kovači**	**Prosječenica Cave**	**Vakuf Cave**	**Čvaljina Tunnel**	**Vjetrenica Cave**
Locality	Dinara Mt.	Vran Mt.	Grabovica Plateau	Podveležje	Gornja Studenčica	Čvaljina, Popovo polje	Zavala, Popovo polje
Latitude	44.050578	43.653268	43.676821	43.26569	43.18007	42.86828	42.504521
Longtitude	16.582166	17.526883	17.187070	17.9402	17.60697	17.9719	17.59168
Air temperature	7.9 °C	7.9 °C	9.6 °C	19.9 °C	17.1 °C	18.2 °C	11.3 °C
Water temperature	7.4 °C	7.7 °C	9.2 °C	-	-	-	11.1 °C
Bedrock temperature	7.5 °C	7.5 °C	9.2 °C	-	-	-	11.2 °C
Relative humidity	100%	100%	99%	85%	97%	-	100%
Altitude (m)	860	1310	868	660	57	307	260
Date of sampling	2022.09.02	2022.08.24	2022.09.01	2022.08.30	2022.08.29	2022.08.31	2022.08.31
Sampling legality[a]	L.L.B; J.B.	L.L.B; J.B.	L.L.B; J.B.	L.L.B; J.B.	L.L.B; J.B.	L.L.B; J.B.	L.L.B; J.B.

[a] L.L.B – Lada Lukić Bilela; J.B. – Justinas Babinskas

3.8. Development of Carbonic Anhydrase Assay With HABSA-Ac as the Substrate



General procedure. 1.602 ml of buffer and 0.018 ml of substrate (in DMSO) were combined in a 0.50 cm cuvette. The enzymatic reaction and kinetic measurements were initiated with the addition of 0.18 ml of enzyme (bCAII) solution, and for substrate autohydrolysis control measurements, the enzyme was substituted with the appropriate buffer. The kinetic spectroscopy parameters are as follows: reference – 1% DMSO solution in the corresponding buffer; measurement delay – 5 s; wavelength – 428 nm; data recording rate – 2 s. The calculation of bCAII catalytic rates is achieved by means of the formula provided below. 1 activity unit (1 U) is defined as the hydrolysis of 1 µmol of HABSA-Ac per 1 min at pH 8.5 and 20 °C.

$$v = \frac{Slope_E - Slope_o}{\varepsilon_{428} * l} * 60$$

Where v – reaction rate (µM min^{-1}); $Slope_E$ – absorption slope in enzymatic reaction (Abs s^{-1}); $Slope_o$ – absorption slope in autohydrolysis reaction (Abs s^{-1}); ε_{428} – HABSA molar extinction

coefficient (0.0175 μM^{-1} cm^{-1}); *l* – cuvette light path (0.50 cm); *60* – factor to convert seconds to minutes.

Optimal initial substrate concentration was established using 0.1-1.0 mM HABSA-Ac solutions in 1% DMSO, 10 mM Tris-HCl (pH 8.5) without enzyme. Assertion of optimal buffer type used 10 mM (pH 8.5) Tris-HCl, 2-amino-2-methyl-1,3-propanediol (AMPD), sodium borate ($NaBO_3$), and diethanolamine ($NH(EtOH)_2$) buffers in the reaction with 10 μg ml^{-1} of bCAII. The optimal buffer concentration of Tris-HCl was determined by conducting assays in 10 mM, 50 mM, 100 mM, 150 mM and 200 mM (pH adjusted to 8.5 using 1 M HCl at 20 °C). Sufficient reaction duration was resolved by measuring 1, 3, 5, 10, and 20 minutes. The optimal bCAII concentration for kinetic investigations and the assay limits of quantification and detection were determined by measuring catalytic rates at final enzyme concentrations of 10 μg ml^{-1}, 1 μg ml^{-1}, and 0.1 μg ml^{-1} (344-3.44 nM) in 150 mM Tris-HCl buffer. The investigation of bCAII inhibition used 34.4 μM (1 mg ml^{-1}) bCAII solutions incubated for 20 minutes with KCN or Acetazolamide at molar ratios of 1:1, 1:5, 1:20, 1:100 for KCN; and 1:0.25, 1:0.5, 1:1 for Acetazolamide. After incubation, bCAII catalysis rates were measured at the final enzyme concentration of 3.44 μM (0.1 mg ml^{-1}).

3.9. Determination of Carbonic Anhydrase Catalytic Parameters

3.9.1. Thermodynamic Parameter Analysis Using Arrhenius and Transitional State Theory (TST) Plots

Observed activation energy ($E_{a,obs}$) and Arrhenius factor (*A*) were estimated from the Arrhenius plots, while observed enthalpy ($\Delta H^{\ddagger}_{obs}$) and entropy ($\Delta S^{\ddagger}_{obs}$) were estimated from the TST linear plots. The Arrhenius and TST plotting data for the linear functions ($y = ax+b$) are provided in **Table 3.4**.

Table 3.4. Variables for L-B, E-H, and H-W plots, as well as calculation of K_M and V_{max} from the plots.

Plot	*y* variable	*x* variable	Derivative parameter
Arrhenius	$\ln(v)$	$1/T$	$a = -E_{a,obs} / R$ $b = \ln A + \ln([S]_0[E]_0)$
TST[a,b]	$\ln(k_{eff} / T)$	$1/T$	$a = -\Delta H^{\ddagger}_{obs} / R$ $b = \ln(k_B / h) + (\Delta S^{\ddagger}_{obs} / R)$

[a] k_{eff} – effective reaction rate $_v$ / $[S]_0$ for substrate autohydrolysis reactions or v / $([E]_0[S]_0)$ for enzymatic catalysis.
[b] *R* – universal gas constant (8.3145 J mol^{-1} K^{-1}); k_B – Boltzmann constant (1.38×10^{-23} J K^{-1}); *h* – Plank constant (6.63×10^{-34} J s).

Further analysis of Arrhenius plot and estimation of parameters:

$$\Delta H_{obs} = E_{a,obs} - \frac{RT}{1000}$$

Where ΔH_{obs} – observed change in enthalpy (kJ mol^{-1}); $E_{a,obs}$ – observed activation energy, derived from the linear function slope in the Arrhenius plot (kJ mol^{-1}); *R* – universal gas constant (8.3145 J mol^{-1} K^{-1}); *T* – temperature (K).

$$k_{obs} = e^{b-ln[S]_0} * e^{-\frac{E_{a,obs}}{RT}} \qquad k_{cat}/K_M = e^{b-ln([S]_0[E]_0)} * e^{-\frac{E_{a,obs}}{RT}}$$

Where k_{obs} – observed autohydrolysis rate constant (s^{-1}); k_{cat}/K_M – specificity constant (M^{-1} s^{-1}); b – linear function intercept in the Arrhenius plot; $[S]_0$ – initial substrate concentration in the reaction (2×10^{-4} M); $[E]_0$ – enzyme concentration in the reaction (3.44×10^{-6} M); $E_{a,obs}$ – observed activation energy, derived from the linear function slope in the Arrhenius plot (J mol^{-1}); R – universal gas constant (8.3145 J mol^{-1} K^{-1}); T – temperature (K).

Further analysis of the TST plot and estimation of parameters:

$$\Delta G^{\ddagger}_{obs} = \Delta H^{\ddagger}_{obs} - T\Delta S^{\ddagger}_{obs}$$

Where $\Delta G^{\ddagger}_{obs}$ – observed change in Gibbs energy (kJ mol^{-1}); $\Delta H^{\ddagger}_{obs}$ – observed change in enthalpy, derived from the linear function slope in the TST plot (kJ mol^{-1}); T – temperature (K); $\Delta S^{\ddagger}_{obs}$ – observed change in entropy, derived from the linear function intercept in the TST plot (kJ mol^{-1} K^{-1}).

$$k_{obs} = \frac{k_B T}{h} e^{-\frac{\Delta G^{\ddagger}_{obs}}{RT}} \qquad k_{cat}/K_M = \frac{k_B T}{h} e^{-\frac{\Delta G^{\ddagger}_{obs}}{RT}}$$

Where k_{obs} – observed autohydrolysis rate constant (s^{-1}); k_{cat}/K_M – specificity constant (s^{-1}); k_B – Boltzmann constant (1.3806×10^{-23} J K^{-1}); T – temperature (K); h – Planck constant (6.6261×10^{-34} J s); $\Delta G^{\ddagger}_{obs}$ – observed change in Gibbs energy (J mol^{-1}); R – universal gas constant (8.3145 J mol^{-1} K^{-1}).

3.9.2. Kinetic Parameter Analysis Using Lineweaver-Burk (L-B), Eadie-Hofstee (E-H) and Hanes-Wolf (H-W) Plots

For each series of Michaelis-Menten kinetics measurements, the values of K_M and V_{max} were calculated from the linear plots. Subsequently, the catalytic constants k_{cat} and k_{cat}/K_M were determined. Data with both initial measurements and outliers removed, using the E-C-B screening method, were utilised for these estimations. The L-B, E-H and H-W plotting data for the linear functions ($y = ax + b$) are provided in **Table 3.5**.

Table 3.5. Variables for L-B, E-H, and H-W plots, as well as calculation of K_M and V_{max} from the plots.

Plot	*y* variable	*x* variable	K_M, mM	V_{max}, µM min^{-1}
L-B	$1 / v$	$1 / [S]$	a / b	1 / b
E-H	v	$v / [S]$	-a	b
H-W	$[S] / v$	$[S]$	1 / a	a · b

Formula for turnover number (k_{cat}) and specificity constant (k_{cat}/K_M) calculations:

$$k_{cat} = \frac{V_{max}}{[E]*60} \qquad k_{cat}/K_M = \frac{k_{cat}}{K_M*1000}$$

Where k_{cat} – enzyme turnover number (s^{-1}); V_{max} – maximum catalysis rate (µM min^{-1}); $[E]$ – bCAII concentration in the reaction (0.344 µM); 60 – minutes to seconds conversion factor; k_{cat}/K_M – substrate specificity constant (M^{-1} s^{-1}); K_M – Michaelis constant (mM); 1000 – mM to M conversion factor.

3.9.3. Kinetic Parameter Analysis Using Eisenthal-Cornish-Bowden (E-C-B) Plot

This method utilised data consisting of initial catalysis rates (v) and corresponding substrate concentrations ($[S]$), which were used in linear function form ($y = ax + b$). The general function:

$$y(x)_{[S]} = \frac{v_{[S]}}{[S]}x + v_{[S]}$$

Where $y(x)_{[S]}$ – linear function for appropriate substrate concentration; $v_{[S]}$ – initial catalysis rate for appropriate substrate concentration (μM^{-1} min^{-1}); $[S]$ – substrate concentration (mM).

To calculate and tabulate the x-coordinates of intersection points, indicating K_M, between two functions, a generalised formula was used:

$$x([S]_i; [S]_j) = \frac{v_j - v_i}{(\frac{v_i}{[S]_i} - \frac{v_j}{[S]_j})}$$

Where $x([S]_i;[S]_j)$ – x-coordinate at the intersection between functions for a pair of $[S]_i$ and $[S]_j$ ($[S]_i \neq [S]_j$); v – initial catalysis rate for appropriate substrate concentration (μM min^{-1}); $[S]$ – substrate concentration (mM).

Note that functions for the same $[S]$ functions are parallel and thus do not intersect. Additionally, the array is symmetric, meaning $x([S]_i;[S]_j)$ yields the same result as $x([S]_j;[S]_i)$; therefore, duplicate results were not included. Any negative intersection values were removed from the array, as negative values are false. Maximum catalysis rate V_{max} was calculated using the x values from the arrays in the relevant $y(x)_{[S]}$ equations. The median K_M and V_{max} determination was followed by calculation of k_{cat} and k_{cat}/K_M.

3.9.4. Adaptation of the E-C-B Plot for Outlier Identification in Kinetic Measurement Data

The array of $x([S]_i;[S]_j)$, tabulated using the generalised formula, was then screened by calculating the median of the x values and applying a ± 50% confidence interval. Any intersection values outside the range of median ± 50% were removed. The K_M for the measurement series was estimated by calculating the median x value of the initial and screened arrays. V_{max} was calculated similarly: the x values from the arrays were used in the relevant $y(x)_{[S]}$ equations, and the median V_{max} (μM min^{-1}) was determined.

Outliers were identified by examining the number of intersections N for each $[S]$ in the screened array. Values of $[S]$ with $N \leq 2$ (below 25% of the maximum possible intersections) were classified as outliers, and these $[S]$ values, along with their associated v, were excluded from subsequent kinetic parameter analysis.

3.9.5. Inhibition Data Analysis

Carbonic anhydrase inhibition by KCN and acetazolamide types and constants K_i and K_i' were determined by analysing Dixon and C-B plots. Variables: Dixon – 1 / v *vs*

[I]; C-B – *[S]* / *v* vs *[I]*. Linear regression functions were plotted for each set of *[S]* used in Michaelis-Menten kinetic measurements (0.1-1.0 mM). Function intersection points *x*-coordinates were tabulated in a matrix. Positive and duplicating values due to tabulation symmetry were excluded. Median values and standard errors were calculated for both plots.

3.10. Statistical Analysis

Examinations involving multiple measurements were performed in independent triplicate – fresh buffer, enzyme solution and substrate stock for each series. Standard deviation and standard errors were estimated using the provided formula:

$$s = \sqrt{\frac{\sum(x_i - \overline{x})^2}{n-1}} \qquad SE = \frac{s}{\sqrt{n}}$$

Where s – sample standard deviation; x_i – sample value; $\overline{x}$ – sample mean; n – number of samples; SE – standard error.

3.11. In silico Methods

Hardware: laptop Acer Nitro 5 (AMD Ryzen 5800H 3.20 GHz, 32 Gb RAM, 2 Tb SSD), Lenovo Y50-70 (Intel Core i7-4720HQ 2.60 GHz, 16 Gb RAM, 1 Tb HHD).
Software: GAMESS-US 2023 R1 intel (Barca et al., 2020); UCSF Chimera 1.12 (Pettersen et al., 2004); wxMacMolPlt 7.7.2 (Bode and Gordon, 1998); Avogadro 1.1.1 (Hanwell et al., 2012); AmberTools24 (Case et al., 2023); Semiempirical Extended Tight-Binding Program Package (xTB) (Bannwarth et al., 2021).
Protein model: crystalline carbonic anhydrase from *Bos taurus* erythrocytes (pdb code: 1V9E) (Saito et al., 2004). Chain B and water molecules were removed from the model.
Ligands: model structures were created using Avogadro and optimised default GAMESS computations at DFT 6-311G**/M06-2X (Zhao and Truhlar, 2008) level of theory.

3.11.1. Amber24 Molecular Dynamics Simulations

The simulation workflow was followed according to the tutorial for metalloenzyme simulations available on the AmberTools24 developer page (Li and Merz, 2015). Simulations used the standard ff99sb force field (Tian et al., 2020) for amino acids supplemented by parametrisation of Zn^{2+} coordination sphere within 2.0 Å (6-311G**/M06-2X). Protein structure ionisation and electrostatic property analysis were carried out using the H++ web server (Anandakrishnan et al., 2012), with pH set to 8.5 and Na^+ and Cl^- neutralising excess charge. Ligands in the enzyme active site were placed manually, avoiding clashes, with coordinating atom distances of 1.8-2.0 Å to Zn^{2+}. Water OPC (Izadi et al., 2014) model solvation box was created using the *tleap* script by adding 20 Å to the protein bounding box. Energy minimisation was performed for 1000 steps with a 2 fs step size. Equilibration was performed using NTP mode (*N* – constant number, *T* – constant temperature 293.15 K, *P* – constant pressure 1 atm). The MD simulations were conducted for a total of 1 ns, with a step size of 2 fs

and conformation output every 1 ps. Simulation trajectories were analysed using UCSF Chimera and the *cpptraj* script. Simulation equilibrium state was confirmed using RMSD analysis of protein backbone, and active site residues (His93, His95, His118, Thr197, Thr198) and ligand interactions. Models representing average equilibrium structures were obtained from 0.5 ns to 1.0 ns range. Average active site structures for *ab initio* calculations used all residues and ligands within 5.0 Å Zn^{2+} coordination sphere. Their single-point energy computations were carried out at 6-311G**/M06-2X level of theory.

3.11.2. Semiempirical Extended Tight Binding (xTB) Computations

xTB simulation of protein structures at GFN2, GFN1 and GFN0 levels was attempted at 293 K for 50 ps with a 1 fs step size, employing average structures generated in Amber24 MD simulations. Water molecules were removed from the initial models and substituted with the alpb water solvation model.

3.11.3. Gamess DFT Computations

All computations were performed at 6-311G**/M06-2X level of theory. Default threshold values were used for geometry and energy convergence. Transition state (TS) was determined using following workflow: 1) constrained optimisation screening of breaking or forming bond to obtain near-TS geometry; 2) Hessian (vibrational analysis) matrix computation to obtain one negative vibrational mode; 3) saddle point (TS structure) calculation using near-TS geometry and its Hessian matrix; 4) Hessian matrix calculation of TS structure; 5) forward and backward intrinsic reaction coordinate (IRC) calculation using TS structure and its Hessian matrix; 5) optimisation of final IRC structures to calculate their energies at higher (default for optimisation) convergence thresholds.

CONCLUSIONS

1. Ferbamine was identified as a chemically stable substrate for laccase assays**,** exhibiting high stability under mildly acidic conditions (pH ≤ 6.0), while its performance was influenced by buffer composition rather than incubation temperature.
2. Ferbamine was successfully validated as a qualitative substrate for laccase screening**,** enabling reliable detection of laccase activity in fungal protein extracts and wild-type microorganism colonies.
3. Four phenol azo dyes with suitable physicochemical and spectroscopic properties were synthesised**,** providing a platform for the development of enzyme substrates.
4. A transcarbonisation-based synthetic strategy was established for the preparation of symmetric phenol azo dye carbonate esters**,** enabling substrate synthesis with minimal optimisation of reaction conditions.
5. Phenyl thionochloroformate-mediated synthesis was identified as the only effective strategy for the preparation of the target thiocarbonate ester substrate.
6. Inhibition-kinetic studies demonstrated that carbonate and thiocarbonate ester substrates are unsuitable for carbonic anhydrase assays because they undergo non-specific reactions with nucleophilic amino acid residues.
7. A novel spectrophotometric assay based on HABSA-Ac was developed and validated for carbonic anhydrase functional characterisation, demonstrating lower non-specific and catalytic interactions with off-target enzymes, and 4.7 and 218-fold higher sensitivity compared with conventional p-nitrophenyl acetate and indoxyl acetate assays, accordingly.

REFERENCES

(1) ABTS Sigma-Aldrich®. 2,2'-azino-bis(3-ethylbenzthiazoline-6-sulfonic acid) diammonium salt product information. *22'-Azino-Bis3-Ethylbenzthiazoline-6-Sulfonic Acid Diammonium Salt*. https://www.sigmaaldrich.com/deepweb/assets/sigmaaldrich/product/documents/360/360/a1888pis.pdf (Accessed February 5, 2024).

(2) Agrawal K, Verma P. (2019) Laccase: Addressing the ambivalence associated with the calculation of enzyme activity. *3 Biotech*. 9:365. doi:10.1007/s13205-019-1895-1.

(3) Ahmed S, Rahman MS, Hasan MM, Paul N, Sajib AA. (2018) Microbial degradation of lignocellulosic biomass: Discovery of novel natural lignocellulolytic bacteria. *BioTechnologia*. 99:137–146. doi:10.5114/bta.2018.75657.

(4) Akocak S, Supuran CT. (2019) Activation of α-, β-, γ- δ-, ζ- and η- class of carbonic anhydrases with amines and amino acids: A review. *J Enzyme Inhib Med Chem*. 34:1652–1659. doi:10.1080/14756366.2019.1664501.

(5) Aktaş AH, Şanlı N, Pekcan G. (2006) Spectrometric determination of pK_a values for some phenolic compounds in acetonitrile – water mixture. *Acta Chim Slov*. 53:214–218.

(6) Alcalde M, Bulter T, Arnold FH. (2002) Colorimetric assays for biodegradation of polycyclic aromatic hydrocarbons by fungal laccases. *SLAS Discov*. 7:547–553. doi:10.1177/1087057102238629.

(7) Aleksejeva O, Mateljak I, Ludwig R, Alcalde M, Shleev S. (2019) Electrochemistry of a high redox potential laccase obtained by computer-guided mutagenesis combined with directed evolution. *Electrochem Commun*. 106:106511. doi:10.1016/j.elecom.2019.106511.

(8) Ali B, Kaur S, James EC, Parmar SS. (1985) Identification and characterization of hepatic carboxylesterases hydrolyzing hydrocortisone esters. *Biochem Pharmacol*. 34:1881–1886. doi:10.1016/0006-2952(85)90302-8.

(9) Ali WB et al. (2020) Enzyme properties of a laccase obtained from the transcriptome of the marine-derived fungus *Stemphylium lucomagnoense*. *Int J Mol Sci*. 21:8402. doi:10.3390/ijms21218402.

(10) Alterio V et al. (2021) Zeta-carbonic anhydrases show CS_2 hydrolase activity: A new metabolic carbon acquisition pathway in diatoms? *Comput Struct Biotechnol J*. 19:3427–3436. doi:10.1016/j.csbj.2021.05.057.

(11) Alvizo O et al. (2014) Directed evolution of an ultrastable carbonic anhydrase for highly efficient carbon capture from flue gas. *Proc Natl Acad Sci*. 111:16436–16441. doi:10.1073/pnas.1411461111.

(12) Amata O, Marino T, Russo N, Toscano M. (2011) Catalytic activity of a ζ-class zinc and cadmium containing carbonic anhydrase. Compared work mechanisms. *Phys Chem Chem Phys*. 13:3468. doi:10.1039/c0cp01053g.

(13) Ambatkar N et al. (2021) Functional screening and adaptation of fungal cultures to industrial media for improved delignification of rice straw. *Biomass Bioenergy*. 155:106271. doi:10.1016/j.biombioe.2021.106271.

(14) Anandabaskar N. (2022) Screening methods for the evaluation of diuretics. In: Lakshmanan, M, Shewade, DG, Raj, GM, eds.*Introduction to basics of pharmacology and toxicology: Volume 3: Experimental pharmacology: Research methodology and biostatistics*. Singapore: Springer Nature, pp. 345–362 doi:10.1007/978-981-19-5343-9_26.

(15) Anandakrishnan R, Aguilar B, Onufriev AV. (2012) H++ 3.0: automating pK prediction and the preparation of biomolecular structures for atomistic molecular modeling and simulations. *Nucleic Acids Res*. 40:W537–W541. doi:10.1093/nar/gks375.

(16) Anastas PT, Warner JC. (2000) Green chemistry: Theory and practice. Oxford University PressOxford doi:10.1093/oso/9780198506980.001.0001.

(17) Arabi MS, Karami C, Taher MA, Ahmadi E. (2020) Fluorescence detection of laccases activity by the photoinduced electron transfer (PET) process. *JBIC J Biol Inorg Chem*. 25:151–159. doi:10.1007/s00775-019-01748-0.

(18) Arakane Y et al. (2009) Molecular and functional analyses of amino ccid decarboxylases involved in cuticle tanning in *Tribolium castaneum**. *J Biol Chem*. 284:16584–16594. doi:10.1074/jbc.M901629200.

(19) Areskogh D, Li J, Gellerstedt G, Henriksson G. (2010) Investigation of the molecular weight increase of commercial lignosulfonates by laccase catalysis. *Biomacromolecules*. 11:904–910. doi:10.1021/bm901258v.

(20) Argyropoulos DDS et al. (2023) Kraft lignin: A valuable, sustainable resource, opportunities and challenges. *ChemSusChem*. 16:e202300492. doi:10.1002/cssc.202300492.

(21) Arregui L et al. (2019) Laccases: Structure, function, and potential application in water bioremediation. *Microb Cell Factories*. 18. doi:10.1186/s12934-019-1248-0.

(22) Asadi V et al. (2019) Novel bovine carbonic anhydrase encapsulated in a metal–organic framework: A new platform for biomimetic sequestration of CO_2. *RSC Adv*. 9:28460–28469. doi:10.1039/C9RA04603H.
(23) Asano T, Seto Y, Hashimoto K, Kurushima H. (2019) Mini-review an insect-specific system for terrestrialization: Laccase-mediated cuticle formation. *Insect Biochem Mol Biol*. 108:61–70. doi:10.1016/j.ibmb.2019.03.007.
(24) Asav E. (2021) Sensitive determination of 3,4-dihydroxyl-L-pheynlalanine by a cloud funnel mushroom (*Clitocybe nebularis* (Batsch), P. Kumm.) homogenate-based amperometric biosensor. *Trak Univ J Nat Sci*. 22:255–262. doi:10.23902/trkjnat.969982.
(25) Aspatwar A et al. (2022) Carbonic anhydrases in metazoan model organisms: molecules, mechanisms, and physiology. *Physiol Rev*. 102:1327–1383. doi:10.1152/physrev.00018.2021.
(26) Ataman chemicals. Chrysoine resocinol. *Ataman Kim*. https://www.atamanchemicals.com/chrysoine-resocinol_u26543/ (Accessed July 10, 2025).
(27) Babinskas J. (2020) Substratų, skirtų lakazės funkcinei analizei, sintezė ir tyrimai. Master thesis, Faculty of Chemistry and Geosciences, Department of Applied Chemistry: Vilnius University https://www.lvb.lt/permalink/370LABT_NETWORK/5bfnq8/alma9912933293108451 (Accessed January 24, 2024).
(28) Babinskas J, Kojis T, Gaubė I, Baranauskienė L, Matijošytė I. (2026) Functional analysis of carbonic anhydrases: comparative methods for hydration and hydrolysis activity. *Biocatal Agric Biotechnol*. 74:104077. doi:10.1016/j.bcab.2026.104077.
(29) Babinskas J, Krutkevičius J, Lukić Bilela L, Bešta-Gajević R, Matijošytė I. (2025) Potential of subterranean microbes: High-throughput screening for industrially relevant enzymatic activities in Dinaric caves. *MicrobiologyOpen*. 14:e70146. doi:10.1002/mbo3.70146.
(30) Babinskas J, Matijošytė I. (2026) A selective phenyl azo acetate substrate for enhanced carbonic anhydrase functional analysis. *Anal Sci Adv*. 7:e70091. doi:10.1002/ansa.70091.
(31) Babinskas J, Matijošytė I. (2025) Laccase functional analysis: Substrates, activity assays, challenges, and prospects. *ChemBioChem*. 26:e202400939. doi:10.1002/cbic.202400939.
(32) Babinskas J, Sabotič J, Matijošytė I. (2024) Synthesis and application of a phenazine class substrate for high-throughput screening of laccase activity. *Appl Microbiol Biotechnol*. 108:66. doi:10.1007/s00253-023-12958-7.
(33) Bach CE et al. (2013) Measuring phenol oxidase and peroxidase activities with pyrogallol, l-DOPA, and ABTS: Effect of assay conditions and soil type. *Soil Biol Biochem*. 67:183–191. doi:10.1016/j.soilbio.2013.08.022.
(34) Bala S, Asthir B, Bains NS. (2016) Syringaldazine peroxidase stimulates lignification by enhancing polyamine catabolism in wheat during heat and drought stress. *Cereal Res Commun*. 44:561–571. doi:10.1556/0806.44.2016.028.
(35) Baliukynas M, Veteikytė A, Kairys V, Matijošytė I. (2020) The hydrolysis of indoxyl acetate: A versatile reaction to assay carbonic anhydrase activity by high-throughput screening. *Enzyme Microb Technol*. 139:109584. doi:10.1016/j.enzmictec.2020.109584.
(36) Baltierra-Trejo E, Márquez-Benavides L, Sánchez-Yáñez JM. (2015) Inconsistencies and ambiguities in calculating enzyme activity: The case of laccase. *J Microbiol Methods*. 119:126–131. doi:10.1016/j.mimet.2015.10.007.
(37) Bannwarth C et al. (2021) Extended tight-binding quantum chemistry methods. *WIREs Comput Mol Sci*. 11. doi:10.1002/wcms.1493.
(38) Bannwarth C, Ehlert S, Grimme S. (2019) GFN2-xTB—an accurate and broadly parametrized self-consistent tight-binding quantum chemical method with multipole electrostatics and density-dependent dispersion contributions. *J Chem Theory Comput*. 15:1652–1671. doi:10.1021/acs.jctc.8b01176.
(39) Bao S, Teng Z, Ding S. (2013) Heterologous expression and characterization of a novel laccase isoenzyme with dyes decolorization potential from *Coprinus comatus*. *Mol Biol Rep*. 40:1927–1936. doi:10.1007/s11033-012-2249-9.
(40) Barca GMJ et al. (2020) Recent developments in the general atomic and molecular electronic structure system. *J Chem Phys*. 152. doi:10.1063/5.0005188.
(41) Batista-García RA et al. (2017) Simple screening protocol for identification of potential mycoremediation tools for the elimination of polycyclic aromatic hydrocarbons and phenols from hyperalkalophile industrial effluents. *J Environ Manage*. 198:1–11. doi:10.1016/j.jenvman.2017.05.010.
(42) Beck S et al. (2018) Characterization of *Trametes versicolor* laccase-catalyzed degradation of estrogenic pollutants: Substrate limitation and product identification. *Int Biodeterior Biodegrad*. 127:146–159. doi:10.1016/j.ibiod.2017.11.020.
(43) Bernard J et al. (2017) Carbonic acid monoethyl ester as a pure solid and its conformational isomerism in the gas-phase. *RSC Adv*. 7:22222–22233. doi:10.1039/C7RA02792C.

(44) Berneth H. (2008) Azine dyes. In: *Ullmann's Encyclopedia of industrial chemistry*. John Wiley & Sons, Ltd doi:10.1002/14356007.a03_213.pub3.
(45) Bidlingmeyer BA, Del Rios JK, Korpi Jack. (1982) Separation of organic amine compounds on silica gel with reversed-phase eluents. *Anal Chem*. 54:442–447. doi:10.1021/ac00240a021.
(46) Bisswanger H. (2014) Enzyme assays. *Perspect Sci*. 1:41–55. doi:10.1016/j.pisc.2014.02.005.
(47) Bode BM, Gordon MS. (1998) Macmolplt: A graphical user interface for GAMESS. *J Mol Graph Model*. 16:133–138. doi:10.1016/s1093-3263(99)00002-9.
(48) Boereboom JM, Fleurat-Lessard P, Bulo RE. (2018) Explicit solvation matters: Performance of QM/MM solvation models in nucleophilic addition. *J Chem Theory Comput*. 14:1841–1852. doi:10.1021/acs.jctc.7b01206.
(49) Boone CD, Pinard M, McKenna R, Silverman D. (2014) Catalytic mechanism of α-class carbonic anhydrases: CO_2 hydration and proton transfer. In: Frost, SC, McKenna, Robert, eds. Subcellular Biochemistry Vol. 75*Carbonic Anhydrase: Mechanism, Regulation, Links to Disease, and Industrial Applications*. Dordrecht: Springer Netherlands, pp. 31–52 doi:10.1007/978-94-007-7359-2_3.
(50) Bradford MM. (1976) A rapid and sensitive method for the quantitation of microgram quantities of protein utilizing the principle of protein-dye binding. *Anal Biochem*. 72:248–254. doi:10.1016/0003-2697(76)90527-3.
(51) Brogioni B et al. (2008) Characterization of radical intermediates in laccase-mediator systems. A multifrequency EPR, ENDOR and DFT/PCM investigation. *Phys Chem Chem Phys*. 10:7284–7292. doi:10.1039/B812096J.
(52) Brunelle DJ. (1982) Novel catalysis of *o*-nitrophenyl carbonates by *p*-dimethlaminonopyridine. *Tetrahedron Lett*. 23:1739–1742. doi:10.1016/S0040-4039(00)86728-3.
(53) Busuricu F, Popescu A, Anghel A. (2008) The evaluation of the wines antioxidant activity. *Innov Romanian Food Biotechnol*. 2:10–17.
(54) Carić D et al. (2015) A multifrequency EPR study of poly(PADPA) synthesized with *Trametes versicolor* laccase from the aniline dimer *p*-aminodiphenylamine (PADPA) in the presence of anionic vesicles. *Curr Appl Phys*. 15:1516–1520. doi:10.1016/j.cap.2015.08.023.
(55) Carroll JJ, Slupsky JD, Mather AE. (1991) The solubility of carbon dioxide in water at low pressure. *J Phys Chem Ref Data*. 20:1201–1209. doi:10.1063/1.555900.
(56) Case DA et al. (2023) AmberTools. *J Chem Inf Model*. 63:6183–6191. doi:10.1021/acs.jcim.3c01153.
(57) Cattelan L, Fiorani G, Perosa A, Maschmeyer T, Selva M. (2018) Two-step synthesis of dialkyl carbonates through transcarbonation and disproportionation reactions catalyzed by calcined hydrotalcites. *ACS Sustain Chem Eng*. 6:9488–9497. doi:10.1021/acssuschemeng.8b02106.
(58) Caulfield B, Abraham J, Christodoulatos C, Prigiobbe V. (2022) Enhanced precipitation of magnesium carbonates using carbonic anhydrase. *Nanoscale*. 14:13570–13579. doi:10.1039/D2NR03199J.
(59) Çavdar H et al. (2012) α-Carbonic anhydrases are sulfatases with cyclic diol monosulfate esters. *J Enzyme Inhib Med Chem*. 27:148–154. doi:10.3109/14756366.2011.629198.
(60) CDC. (2020) Phosgene. https://www.cdc.gov/niosh/idlh/75445.html (Accessed July 10, 2025).
(61) Cen Q et al. (2022) Green production of a yellow laccase by *Coriolopsis gallica* for phenolic pollutants removal. *AMB Express*. 12:96. doi:10.1186/s13568-022-01434-6.
(62) Chegwidden WR. (2021) The carbonic anhydrases in health and disease. In: Chegwidden, WR, Carter, ND, eds. Progress in Drug Research Vol. 75*The carbonic anhydrases: Current and emerging therapeutic targets*. Cham: Springer International Publishing, pp. 1–12 doi:10.1007/978-3-030-79511-5_1.
(63) Chen DM, Bastias BA, Taylor AFS, Cairney JWG. (2003) Identification of laccase-like genes in ectomycorrhizal basidiomycetes and transcriptional regulation by nitrogen in Piloderma byssinum. *New Phytol*. 157:547–554. doi:10.1046/j.1469-8137.2003.00687.x.
(64) Chênevert R, Létourneau M. (1990) Enantioselectivity of carbonic anhydrase catalyzed hydrolysis of mandelic methyl esters. *Can J Chem*. 68:314–316. doi:10.1139/v90-044.
(65) Chin-A-Woeng TFC, Bloemberg GV, Mulders IHM, Dekkers LC, Lugtenberg BJJ. (2000) Root colonization by phenazine-1-carboxamide-producing bacterium *Pseudomonas chlororaphis* PCL1391 is essential for biocontrol of tomato foot and root rot. *Mol Plant Microbe Interact*. 13:1340–1345. doi:10.1094/MPMI.2000.13.12.1340.
(66) Cho Y-S, Lim H-S. (2018) Comparison of various estimation methods for the parameters of Michaelis-Menten equation based on *in vitro* elimination kinetic simulation data. *Transl Clin Pharmacol*. 26:39–47. doi:10.12793/tcp.2018.26.1.39.
(67) Choi B, Rempala GA, Kim JK. (2017) Beyond the Michaelis-Menten equation: Accurate and efficient estimation of enzyme kinetic parameters. *Sci Rep*. 7:17018. doi:10.1038/s41598-017-17072-z.

(68) Choolaei Z, Flick R, Khusnutdinova AN, Edwards EA, Yakunin AF. (2021) Lignin-oxidizing activity of bacterial laccases characterized using soluble substrates and polymeric lignin. *J Biotechnol*. 325:128–137. doi:10.1016/j.jbiotec.2020.11.007.
(69) Christopher LP, Yao B, Ji Y. (2014) Lignin biodegradation with laccase-mediator systems. *Front Energy Res*. 2. doi:10.3389/fenrg.2014.00012.
(70) Claus H. (2004) Laccases: Structure, reactions, distribution. *Micron*. 35:93–96. doi:10.1016/j.micron.2003.10.029.
(71) Coblentz society inc. (1966) 1,3-Benzenedicarboxylic acid, 5-amino-, dimethyl ester. *13-Benzenedicarboxylic Acid 5-Amino- Dimethyl Ester*. https://webbook.nist.gov/cgi/cbook.cgi?ID=C99274&Mask=80 (Accessed June 20, 2025).
(72) Colombo R, Pinelli A. (1981) Determination of the dissociation constant of carbonic anhydrase inhibitors: A computerized kinetic method based on esterase activity assay. *J Pharmacol Methods*. 6:177–191. doi:10.1016/0160-5402(81)90107-8.
(73) Coman C, Hădade N, Pesek S, Silaghi-Dumitrescu R, Moț AC. (2023) Removal and degradation of sodium diclofenac via radical-based mechanisms using *S. sclerotiorum* laccase. *J Inorg Biochem*. 249:112400. doi:10.1016/j.jinorgbio.2023.112400.
(74) Cornish-Bowden A. (1974) A simple graphical method for determining the inhibition constants of mixed, uncompetitive and non-competitive inhibitors. *Biochem J*. 137:143–144. doi:10.1042/bj1370143.
(75) Cornish-Bowden A, Eisenthal R. (1974) Statistical considerations in the estimation of enzyme kinetic parameters by the direct linear plot and other methods. *Biochem J*. 139:721–730. doi:10.1042/bj1390721.
(76) Cotarca L, Geller T, Répási J. (2017) Bis(trichloromethyl)carbonate (BTC, triphosgene): A safer alternative to phosgene? *Org Process Res Dev*. 21:1439–1446. doi:10.1021/acs.oprd.7b00220.
(77) Coulter EM et al. (2007) Activation of human dendritic cells by *p*-phenylenediamine. *J Pharmacol Exp Ther*. 320:885–892. doi:10.1124/jpet.106.113803.
(78) Cui H et al. (2021) Rapid and oriented immobilization of laccases on electrodes via a methionine-rich peptide. *ACS Catal*. 11:2445–2453. doi:10.1021/acscatal.0c05490.
(79) Cullings K, Ishkhanova G, Henson J. (2008) Defoliation effects on enzyme activities of the ectomycorrhizal fungus *Suillus granulatus* in a *Pinus contorta* (lodgepole pine) stand in Yellowstone National Park. *Oecologia*. 158:77–83. doi:10.1007/s00442-008-1119-6.
(80) Dawel G et al. (1997) Structure of a laccase-mediated product of coupling of 2,4-diamino-6-nitrotoluene to guaiacol, a model for coupling of 2,4,6-trinitrotoluene metabolites to a humic organic soil matrix. *Appl Environ Microbiol*. 63:2560–2565. doi:10.1128/aem.63.7.2560-2565.1997.
(81) De Caro JD, Rouimi P, Rovery M. (1986) Hydrolysis of *p*-nitrophenyl acetate by the peptide chain fragment (336–449) of porcine pancreatic lipase. *Eur J Biochem*. 158:601–607. doi:10.1111/j.1432-1033.1986.tb09797.x.
(82) De Luca V, Del Prete S, Supuran CT, Capasso C. (2015) Protonography, a new technique for the analysis of carbonic anhydrase activity. *J Enzyme Inhib Med Chem*. 30:277–282. doi:10.3109/14756366.2014.917085.
(83) De Simone G, Di Fiore A, Capasso C, Supuran CT. (2015) The zinc coordination pattern in the η-carbonic anhydrase from *Plasmodium falciparum* is different from all other carbonic anhydrase genetic families. *Bioorg Med Chem Lett*. 25:1385–1389. doi:10.1016/j.bmcl.2015.02.046.
(84) Del Prete S, De Luca V, Landolo E, Supuran CT, Capasso C. (2015) Protonography, a powerful tool for analyzing the activity and the oligomeric state of the γ-carbonic anhydrase identified in the genome of *Porphyromonas gingivalis*. *Bioorg Med Chem*. 23:3747–3750. doi:10.1016/j.bmc.2015.03.080.
(85) Del Prete S, De Luca V, Supuran CT, Capasso C. (2015) Protonography, a technique applicable for the analysis of η-carbonic anhydrase activity. *J Enzyme Inhib Med Chem*. 30:920–924. doi:10.3109/14756366.2014.990963.
(86) Del Prete S, Vullo D, De Luca V, Supuran CT, Capasso C. (2014) Biochemical characterization of the δ-carbonic anhydrase from the marine diatom *Thalassiosira weissflogii*, TweCA. *J Enzyme Inhib Med Chem*. 29:906–911. doi:10.3109/14756366.2013.868599.
(87) Delacruz J et al. (2010) Detecting extracellular carbonic anhydrase activity using membrane inlet mass spectrometry. *Anal Biochem*. 403:74–78. doi:10.1016/j.ab.2010.04.019.
(88) Deshaies S et al. (2021) Unambiguous NMR structural determination of (+)-catechin—laccase dimeric reaction products as potential markers of grape and wine oxidation. *Molecules*. 26:6165. doi:10.3390/molecules26206165.
(89) Dev B, Bakshi A, Kar S, Balasubramanian P. (2025) Evaluation of potent marine ligninolytic bacteria and its efficiency in seawater-based delignification. *Biomass Conv Bioref*. 15:25795–25807. doi:10.1007/s13399-023-04731-7.
(90) Dias AA, Matos AJS, Fraga I, Sampaio A, Bezerra RMF. (2017) An easy method for screening and detection of laccase activity. *Open Biotechnol J*. 11:89–93. doi:10.2174/1874070701711010089.

(91) Dilmore R et al. (2009) Carbonic anhydrase-facilitated CO_2 absorption with polyacrylamide buffering bead capture. *Int J Greenh Gas Control*. 3:401–410. doi:10.1016/j.ijggc.2009.01.004.
(92) Dong J-W, Cai L, Xing Y, Yu J, Ding Z-T. (2015) Re-evaluation of $ABTS^{\bullet+}$ assay for total antioxidant capacity of natural products. *Nat Prod Commun*. 10:2169–2172. doi:10.1177/1934578X1501001239.
(93) Doran PM, ed. (1995) 11 - Homogeneous reactions. In: *Bioprocess engineering principles*. Academic Press, pp. 257–296 https://doi.org/10.1016/B978-012220855-3/50011-0.
(94) Ducros V et al. (1998) Crystal structure of the type-2 Cu depleted laccase from *Coprinus cinereus* at 2.2 Å resolution. *Nat Struct Biol*. 5:310–316. doi:10.1038/nsb0498-310.
(95) Dwivedi UN, Singh P, Pandey VP, Kumar A. (2011) Structure–function relationship among bacterial, fungal and plant laccases. *J Mol Catal B Enzym*. 68:117–128. doi:10.1016/j.molcatb.2010.11.002.
(96) Ebrahimi KH, Hagedoorn P-L, Jacobs D, Hagen WR. (2015) Accurate label-free reaction kinetics determination using initial rate heat measurements. *Sci Rep*. 5:16380. doi:10.1038/srep16380.
(97) Effendi SSW, Ng I-S. (2019) The prospective and potential of carbonic anhydrase for carbon dioxide sequestration: A critical review. *Process Biochem*. 87:55–65. doi:10.1016/j.procbio.2019.08.018.
(98) Eichlerová I, Homolka L, Nerud F. (2006) Synthetic dye decolorization capacity of white rot fungus *Dichomitus squalens*. *Bioresour Technol*. 97:2153–2159. doi:10.1016/j.biortech.2005.09.014.
(99) Eisenman HC, Casadevall A. (2012) Synthesis and assembly of fungal melanin. *Appl Microbiol Biotechnol*. 93:931–940. doi:10.1007/s00253-011-3777-2.
(100) Eisenthal R, Cornish-Bowden A. (1974) The direct linear plot. A new graphical procedure for estimating enzyme kinetic parameters. *Biochem J*. 139:715–720. doi:10.1042/bj1390715.
(101) Enguita FJ. (2011) Structural biology of fungal multicopper oxidases. In: *Mycofactories*. Bentham Science Publisher, pp. 57–72.
(102) Epton Roger, Hobson ME, Marr G. (1977) A study of carbonic anhydrase covalently bound to a poly(acryloylmorpholine) network in aqueous/organic solvents. *Biochem Soc Trans*. 5:274–276. doi:10.1042/bst0050274.
(103) Epton R., Hobson ME, Marr G. (1977) Synthesis and properties of expanded poly(acryloyl morpholine)/carbonic anhydrase conjugates with catalytic activity in aqueous-organic media. *Polymer*. 18:1203–1207. doi:10.1016/0032-3861(77)90279-8.
(104) Erden E, Ucar MC, Gezer T, Pazarlioglu NK. (2009) Screening for ligninolytic enzymes from autochthonous fungi and applications for decolorization of Remazole Marine Blue. *Braz J Microbiol*. 40:346–353. doi:10.1590/S1517-83822009000200026.
(105) Erkkilä A, Majander I, Pihko PM. (2007) Iminium catalysis. *Chem Rev*. 107:5416–5470. doi:10.1021/cr068388p.
(106) Fecker T et al. (2018) Active site flexibility as a hallmark for efficient PET degradation by *I. sakaiensis* PETase. *Biophys J*. 114:1302–1312. doi:10.1016/j.bpj.2018.02.005.
(107) Felby C, Nielsen BR, Olesen PO, Skibsted LH. (1997) Identification and quantification of radical reaction intermediates by electron spin resonance spectrometry of laccase-catalyzed oxidation of wood fibers from beech (*Fagus sylvatica*). *Appl Microbiol Biotechnol*. 48:459–464. doi:10.1007/s002530051080.
(108) Feng Y et al. (2023) Mechanistic insights into the biodegradation of carbon dots by fungal laccase. *Environ Sci Technol*. 57:11977–11987. doi:10.1021/acs.est.3c02305.
(109) Fernández PA, Roleda MY, Rautenberger R, Hurd CL. (2018) Carbonic anhydrase activity in seaweeds: Overview and recommendations for measuring activity with an electrometric method, using *Macrocystis pyrifera* as a model species. *Mar Biol*. 165:88. doi:10.1007/s00227-018-3348-5.
(110) Fernández-Remacha D et al. (2022) Analysis of laccase-like enzymes secreted by fungi isolated from a cave in northern Spain. *MicrobiologyOpen*. 11:e1279. doi:10.1002/mbo3.1279.
(111) Ferrer FM, Hobart K, Bailey JV. (2020) Field detection of urease and carbonic anhydrase activity using rapid and economical tests to assess microbially induced carbonate precipitation. *Microb Biotechnol*. 13:1877–1888. doi:10.1111/1751-7915.13630.
(112) Fredslund F et al. (2018) Structure of a hyperthermostable carbonic anhydrase identified from an active hydrothermal vent chimney. *Enzyme Microb Technol*. 114:48–54. doi:10.1016/j.enzmictec.2018.03.009.
(113) Gabdulkhakov A et al. (2019) Investigations of accessibility of T2/T3 copper center of two-domain laccase from *Streptomyces griseoflavus* Ac-993. *Int J Mol Sci*. 20:3184. doi:10.3390/ijms20133184.
(114) Gao S et al. (2024) Molecular cloning and functional analysis of 4-coumarate: CoA ligases from *Marchantia paleacea* and their roles in lignin and flavanone biosynthesis. *PLOS ONE*. 19:e0296079. doi:10.1371/journal.pone.0296079.
(115) Ge J, Hua L, Poulose AJ. (2016) Thermostable carbonic anhydrases and methods of use thereof. https://patents.google.com/patent/US9410140B2/en.
(116) Gibbons BH, Edsall JT. (1964) Kinetic studies of human carbonic anhydrases B and C. *J Biol Chem*. 239:2539–2544. doi:10.1016/S0021-9258(18)93884-6.

(117) Gil-Rodríguez AM, Beresford TP. (2020) Lipase inhibitory activity assay for fermented milk. *MethodsX*. 7:100999. doi:10.1016/j.mex.2020.100999.
(118) Glazunova OA, Trushkin NA, Moiseenko KV, Filimonov IS, Fedorova TV. (2018) Catalytic efficiency of basidiomycete laccases: Redox potential versus substrate-binding pocket structure. *Catalysts*. 8:152. doi:10.3390/catal8040152.
(119) Goacher RE et al. (2018) Direct analysis by time-of-flight secondary ion mass spectrometry reveals action of bacterial laccase-mediator systems on both hardwood and softwood samples. *Physiol Plant*. 164:5–16. doi:10.1111/ppl.12688.
(120) Gramss G. (2020) Aspects determining the dominance of *Fomitopsis pinicola* in the colonization of deadwood and the role of the pathogenicity factor oxalate. *Forests*. 11:290. doi:10.3390/f11030290.
(121) Guazzaroni ME et al. (2010) Metagenomic mining of enzyme diversity. In: Timmis, KN, ed.*Handbook of hydrocarbon and lipid microbiology*. Berlin, Heidelberg: Springer Berlin Heidelberg, pp. 2911–2927 doi:10.1007/978-3-540-77587-4_216.
(122) Gunne M, Urlacher VB. (2012) Characterization of the alkaline laccase Ssl1 from *Streptomyces sviceus* with unusual properties discovered by genome mining. *PLOS ONE*. 7:e52360. doi:10.1371/journal.pone.0052360.
(123) Guo C et al. (2017) β-Carotene from yeasts enhances laccase production of *Pleurotus eryngii* var. *ferulae* in co-culture. *Front Microbiol*. 8:1101. doi:10.3389/fmicb.2017.01101.
(124) Guo W-X et al. (2009) An efficient catalyst-free protocol for the synthesis of quinoxaline derivatives under ultrasound irradiation. *J Braz Chem Soc*. 20:1674–1679. doi:10.1590/S0103-50532009000900016.
(125) Gurd FRN, Morrow JS, Keim P, Visscher RB, Marshall R. (1974) ^{13}C NMR studies of the interaction of Hb and carbonic anhydrase with $^{13}CO_2$. In: Friedman, M, ed.*Protein-metal interactions*. Boston, MA: Springer New York, pp. 109–124 doi:10.1007/978-1-4684-0943-7_6.
(126) Hajdok S et al. (2009) The laccase-catalyzed domino reaction between catechols and heterocyclic 1,3-dicarbonyls and the unambiguous structure elucidation of the products by NMR spectroscopy and X-ray crystal structure analysis. *J Org Chem*. 74:7230–7237. doi:10.1021/jo9011915.
(127) Han GE, Priefer R. (2023) A systematic review of various pK_a determination techniques. *Int J Pharm*. 635:122783. doi:10.1016/j.ijpharm.2023.122783.
(128) Hanwell MD et al. (2012) Avogadro: An advanced semantic chemical editor, visualization, and analysis platform. *J Cheminformatics*. 4:17. doi:10.1186/1758-2946-4-17.
(129) Haritos VS, Dojchinov G. (2005) Carbonic anhydrase metabolism is a key factor in the toxicity of CO_2 and COS but not CS_2 toward the flour beetle *Tribolium castaneum* [Coleoptera: Tenebrionidae]. *Comp Biochem Physiol Part C Toxicol Pharmacol*. 140:139–147. doi:10.1016/j.cca.2005.01.012.
(130) Harkin JM, Larsen MJ, Obst JR. (1974) Use of syringaldazine for detection of laccase in sporophores of wood rotting fungi. *Mycologia*. 66:469–476. doi:10.2307/3758490.
(131) Hilgers R, Vincken J-P, Gruppen H, Kabel MA. (2018) Laccase/mediator systems: Their reactivity toward phenolic lignin structures. *ACS Sustain Chem Eng*. 6:2037–2046. doi:10.1021/acssuschemeng.7b03451.
(132) Hirakawa Y et al. (2021) Characterization of a novel type of carbonic anhydrase that acts without metal cofactors. *BMC Biol*. 19:105. doi:10.1186/s12915-021-01039-8.
(133) Hobson ST et al. (2019) Development of an acute, short-term exposure model for phosgene. *Toxicol Mech Methods*. 29:604–615. doi:10.1080/15376516.2019.1636170.
(134) Hoegger PJ, Kilaru S, James TY, Thacker JR, Kües U. (2006) Phylogenetic comparison and classification of laccase and related multicopper oxidase protein sequences. *FEBS J*. 273:2308–2326. doi:10.1111/j.1742-4658.2006.05247.x.
(135) Hoopes JT, Dean JFD. (2001) Staining electrophoretic gels for laccase and peroxidase activity using 1,8-diaminonaphthalene. *Anal Biochem*. 293:96–101. doi:10.1006/abio.2001.5112.
(136) Höst G, Mårtensson L-G, Jonsson B-H. (2006) Redesign of human carbonic anhydrase II for increased esterase activity and specificity towards esters with long acyl chains. *Biochim Biophys Acta BBA - Proteins Proteomics*. 1764:1601–1606. doi:10.1016/j.bbapap.2006.07.010.
(137) Hullo M-F, Moszer I, Danchin A, Martin-Verstraete I. (2001) CotA of *Bacillus subtilis* is a copper-dependent laccase. *J Bacteriol*. 183:5426–5430. doi:10.1128/jb.183.18.5426-5430.2001.
(138) Husain A, Parveen R, Dastidar P. (2015) New series of Zn^{II}/Cd^{II} mixed ligand coordination polymers: Toward the design of metallogels. *Cryst Growth Des*. 15:5075–5085. doi:10.1021/acs.cgd.5b01044.
(139) Hutchison LJ. (1990) Studies on the systematics of ectomycorrhizal fungi in axenic culture. III. Patterns of polyphenol oxidase activity. *Mycologia*. 82:424–435. doi:10.2307/3760013.
(140) Iizuka R et al. (2024) Sulfur assimilation using gaseous carbonyl sulfide by the soil fungus *Trichoderma harzianum*. *Appl Environ Microbiol*. 90:e02015-23. doi:10.1128/aem.02015-23.
(141) Ilyasov IR, Beloborodov VL, Selivanova IA, Terekhov RP. (2020) ABTS/PP decolorization assay of antioxidant capacity reaction pathways. *Int J Mol Sci*. 21:1131. doi:10.3390/ijms21031131.

(142) Innocenti A et al. (2008) Investigations of the esterase, phosphatase, and sulfatase activities of the cytosolic mammalian carbonic anhydrase isoforms I, II, and XIII with 4-nitrophenyl esters as substrates. *Bioorg Med Chem Lett*. 18:2267–2271. doi:10.1016/j.bmcl.2008.03.012.
(143) Innocenti A, Supuran CT. (2010) Paraoxon, 4-nitrophenyl phosphate and acetate are substrates of α- but not of β-, γ- and ζ-carbonic anhydrases. *Bioorg Med Chem Lett*. 20:6208–6212. doi:10.1016/j.bmcl.2010.08.110.
(144) Iracheta-Cárdenas MM, Rocha-Peña MA, Galán-Wong LJ, Arévalo-Niño K, Tovar-Herrera OE. (2016) A *Pycnoporus sanguineus* laccase for denim bleaching and its comparison with an enzymatic commercial formulation. *J Environ Manage*. 177:93–100. doi:10.1016/j.jenvman.2016.04.008.
(145) Islam STA et al. (2022) Isothermal titration calorimetric assessment of lignin conversion by laccases. *Biotechnol Bioeng*. 119:493–503. doi:10.1002/bit.27991.
(146) Itoh N et al. (2021) Construction and characterization of a functional chimeric laccase from metagenomes suitable as a biocatalyst. *AMB Express*. 11:90. doi:10.1186/s13568-021-01248-y.
(147) Izadi S, Anandakrishnan R, Onufriev AV. (2014) Building water models: A different approach. *J Phys Chem Lett*. 5:3863–3871. doi:10.1021/jz501780a.
(148) Jafari M et al. (2020) Molecular level insight into stability, activity, and structure of laccase in aqueous ionic liquid and organic solvents: An experimental and computational research. *J Mol Liq*. 317:113925. doi:10.1016/j.molliq.2020.113925.
(149) Jain A, Jain R, Jain S. (2020) Basic techniques in biochemistry, microbiology and molecular biology: Principles and techniques. New York (NY): Springer US doi:10.1007/978-1-4939-9861-6.
(150) Jamshidinia Z et al. (2017) Investigation of direct and mediated electron transfer of laccase-based biocathode. *J Electrochem Sci Technol*. 8:87–95. doi:10.5229/JECST.2017.8.2.87.
(151) Jensen EL, Clement R, Kosta A, Maberly SC, Gontero B. (2019) A new widespread subclass of carbonic anhydrase in marine phytoplankton. *ISME J*. 13:2094–2106. doi:10.1038/s41396-019-0426-8.
(152) Jeon J-R, Murugesan K, Kim Y-M, Kim E-J, Chang Y-S. (2008) Synergistic effect of laccase mediators on pentachlorophenol removal by *Ganoderma lucidum* laccase. *Appl Microbiol Biotechnol*. 81:783–790. doi:10.1007/s00253-008-1753-2.
(153) Jia W, Zhang X, Wang H, Liang Z. (2023) Study on the polymerization and mechanism of amino acid catalyzed by laccase. *J Nat Fibers*. 20:2198277. doi:10.1080/15440478.2023.2198277.
(154) Jia Y, Huang Q, Zhu L, Pan C. (2022) Characterization of a recombinant laccase B from *Trametes hirsuta* MX2 and its application for decolorization of dyes. *Molecules*. 27:1581. doi:10.3390/molecules27051581.
(155) Jiang J et al. (2020) On-line monitoring of transient radicals and oligomers: *o*-Phenylenediamine electrooxidation mechanism study by mass spectrometry. *Microchem J*. 153:104390. doi:10.1016/j.microc.2019.104390.
(156) Johansson I-M, Forsman C. (1993) Kinetic studies of pea carbonic anhydrase. *Eur J Biochem*. 218:439–446. doi:10.1111/j.1432-1033.1993.tb18394.x.
(157) Jonas S, Hollfelder F. (2008) Mechanism and catalytic promiscuity: Emerging mechanistic principles for identification and manipulation of catalytically promiscuous enzymes. In: Lutz, S, Bornscheuer, UT, eds.*Protein engineering handbook*. Darmstadt: Wiley, pp. 47–79 doi:10.1002/9783527634026.ch3.
(158) Jones S. (2017) Permeability rules for antibiotic design. *Nat Biotechnol*. 35:639–639. doi:10.1038/nbt.3919.
(159) Jones SM, Solomon EI. (2015) Electron transfer and reaction mechanism of laccases. *Cell Mol Life Sci*. 72:869–883. doi:10.1007/s00018-014-1826-6.
(160) Jordaan J, Leukes WD. (2003) Isolation of a thermostable laccase with DMAB and MBTH oxidative coupling activity from a mesophilic white rot fungus. *Enzyme Microb Technol*. 33:212–219. doi:10.1016/S0141-0229(03)00116-9.
(161) Juárez-Hernández J et al. (2021) Isolation of fungi from a textile industry effluent and the screening of their potential to degrade industrial dyes. *J Fungi*. 7:805. doi:10.3390/jof7100805.
(162) Jutinico-Shubach LM et al. (2022) A novel basydiomycete isolated from mangrove swamps in the Colombian Caribbean shows promise in dye bioremediation. *Bioremediation J*. 26:179–197. doi:10.1080/10889868.2021.1964426.
(163) Kamer G, Demirata B, Bayraktar R, Ozyurt D, Apak R. (2019) Nanoceria-based reactive species scavenging activity of antioxidants using *N*,*N*-dimethyl-*p*-phenylenediamine (DMPD) probe. *Anal Methods*. 11:1908–1915. doi:10.1039/C8AY02561D.
(164) Kameshwar AKS, Qin W. (2017) Qualitative and quantitative methods for isolation and characterization of lignin-modifying enzymes secreted by microorganisms. *BioEnergy Res*. 10:248–266. doi:10.1007/s12155-016-9784-5.
(165) Kanodia S et al. (2009) Biochemical characterization of alanine racemase- a spore protein produced by *Bacillus anthracis*. *BMB Rep*. 42:47–52. doi:10.5483/BMBRep.2009.42.1.047.

(166) Karler R, Woodbury DM. (1963) Modified manometric method for determination of carbonic anhydrase in tissues. *Anal Biochem*. 6:381–392. doi:10.1016/0003-2697(63)90091-5.
(167) Kashima K et al. (2019) Effect of template type on the *Trametes versicolor* laccase-catalyzed oligomerization of the aniline dimer *p*-aminodiphenylamine (PADPA). *ACS Omega*. 4:2931–2947. doi:10.1021/acsomega.8b03441.
(168) Kaur R, Salwan R, Sharma V. (2022) Structural properties, genomic distribution of laccases from *Streptomyces* and their potential applications. *Process Biochem*. 118:133–144. doi:10.1016/j.procbio.2022.04.015.
(169) Kazancıoğlu EA, Güney M, Şentürk M, Supuran CT. (2012) Simple methanesulfonates are hydrolyzed by the sulfatase carbonic anhydrase activity. *J Enzyme Inhib Med Chem*. 27:880–885. doi:10.3109/14756366.2011.637202.
(170) Kemnitz CR, Loewen MJ. (2007) "Amide eesonance" correlates with a breadth of C−N rotation barriers. *J Am Chem Soc*. 129:2521–2528. doi:10.1021/ja0663024.
(171) Kenzom T, Srivastava P, Mishra S. (2014) Structural insights into 2,2′-azino-bis(3-ethylbenzothiazoline-6-sulfonic acid) (ABTS)-mediated degradation of Reactive blue 21 by engineered *Cyathus bulleri* laccase and characterization of degradation products. *Appl Environ Microbiol*. 80:7484–7495. doi:10.1128/AEM.02665-14.
(172) Khalifah RG. (1971) The carbon dioxide hydration activity of carbonic anhydrase: I. Stop-flow kinetic studies on the native human isoenzymes B and C. *J Biol Chem*. 246:2561–2573. doi:10.1016/S0021-9258(18)62326-9.
(173) Khaund P, Joshi SR. (2014) Enzymatic profiling of wild edible mushrooms consumed by the ethnic tribes of India. *J Korean Soc Appl Biol Chem*. 57:263–271. doi:10.1007/s13765-013-4225-z.
(174) Kiiskinen L-L, Rättö M, Kruus K. (2004) Screening for novel laccase-producing microbes. *J Appl Microbiol*. 97:640–646. doi:10.1111/j.1365-2672.2004.02348.x.
(175) Kikutani S et al. (2016) Thylakoid luminal θ-carbonic anhydrase critical for growth and photosynthesis in the marine diatom *Phaeodactylum tricornutum*. *Proc Natl Acad Sci*. 113:9828–9833. doi:10.1073/pnas.1603112113.
(176) Kim H, Lee K-J, Han Y-K, Ryu JH, Oh SM. (2017) A comparative study on the solubility and stability of *p*-phenylenediamine-based organic redox couples for non-aqueous flow batteries. *J Power Sources*. 348:264–269. doi:10.1016/j.jpowsour.2017.03.019.
(177) Kim JH, Jo BH. (2022) A colorimetric CO_2 hydration assay for facile, accurate, and precise determination of carbonic anhydrase activity. *Catalysts*. 12:1391. doi:10.3390/catal12111391.
(178) Kimura N, Kamagata Y. (2016) A thermostable bilirubin-oxidizing enzyme from activated sludge isolated by a metagenomic approach. *Microbes Environ*. 31:435–441. doi:10.1264/jsme2.ME16106.
(179) Kocabas DS, Bakir U, Phillips SEV, McPherson MJ, Ogel ZB. (2008) Purification, characterization, and identification of a novel bifunctional catalase-phenol oxidase from *Scytalidium thermophilum*. *Appl Microbiol Biotechnol*. 79:407–415. doi:10.1007/s00253-008-1437-y.
(180) Koester MK, Pullan LM, Noltmann EA. (1981) The *p*-nitrophenyl phosphatase activity of muscle carbonic anhydrase. *Arch Biochem Biophys*. 211:632–642. doi:10.1016/0003-9861(81)90499-9.
(181) Kontro J et al. (2020) Applicability of recombinant laccases from the white-rot fungus *Obba rivulosa* for mediator-promoted oxidation of biorefinery lignin at low pH. *Front Bioeng Biotechnol*. 8:604497. doi:10.3389/fbioe.2020.604497.
(182) La TV, Sung BH, Kim S. (2023) Biocatalytic characterization of *Hericium erinaceus* laccase isoenzymes for the oxidation of lignin derivative substrates. *Int J Biol Macromol*. 241:124658. doi:10.1016/j.ijbiomac.2023.124658.
(183) Labus K, Maniak H. (2023) Colourimetric plate assays based on functionalized gelatine hydrogel useful for various screening purposes in enzymology. *Int J Mol Sci*. 24:33. doi:10.3390/ijms24010033.
(184) Lähdetie A, Liitiä T, Tamminen T, Pere J, Jääskeläinen A-S. (2009) Activation of thermomechanical pulp by laccases as studied by UV-Vis, UV resonance Raman and FTIR spectroscopy 10th EWLP, Stockholm, Sweden, August 25–28, 2008. *Holzforschung*. 63:745–750. doi:10.1515/HF.2009.125.
(185) Larsen D, Bjerre PM, Beeren SR. (2019) Light-controlled out-of-equilibrium assembly of cyclodextrins in an enzyme-mediated dynamic system. *Chem Commun*. 55:15037–15040. doi:10.1039/C9CC08452E.
(186) Lee C, Yoon J. (2008) UV direct photolysis of 2,2′-azino-bis(3-ethylbenzothiazoline-6-sulfonate) (ABTS) in aqueous solution: Kinetics and mechanism. *J Photochem Photobiol Chem*. 197:232–238. doi:10.1016/j.jphotochem.2007.12.030.
(187) Lenz C et al. (2020) Injury-triggered blueing reactions of *Psilocybe* "magic" mushrooms. *Angew Chem Int Ed*. 59:1450–1454. doi:10.1002/anie.201910175.
(188) Levine MN, Lavis LD, Raines RT. (2008) Trimethyl lock: A stable chromogenic substrate for esterases. *Molecules*. 13:204–211. doi:10.3390/molecules13020204.

(189) Li A et al. (2014) Pulmonary primary cells cocultured in a novel cell culture system, the integrated discrete multiple cell–type coculture system (IdMOC)* pulmonary cytotoxicity of eight cigarette smoke condensates and nicotine. In: *Inhalation toxicology*., pp. 328–336 doi:10.1201/b16781-16.
(190) Li F et al. (2023) Molecular-scale investigation on the formation of brown carbon aerosol via iron-phenolic compound reactions in the dark. *Environ Sci Technol*. 57:11173–11184. doi:10.1021/acs.est.3c04263.
(191) Li P, Merz KM. (2015) Building Bonded Model for A Ligand Binding Metalloprotein with MCPB.py. https://ambermd.org/tutorials/advanced/tutorial20/mcpbpy.php (Accessed December 1, 2024).
(192) Li P, Merz KM. (2021) Parameterization of a dioxygen binding metal site using the MCPB.py program. In: Chen, YW, Yiu, C-PB, eds. Methods in Molecular Biology*Methods in Molecular Biology*. New York, NY: Springer US, pp. 257–275 doi:10.1007/978-1-0716-0892-0_15.
(193) Li T et al. (2013) Synthesis, characterization, and properties of aniline-*p*-phenylenediamine copolymers. *High Perform Polym*. 25:348–353. doi:10.1177/0954008312465451.
(194) Li X et al. (2020) Applications of oxidases in modification of food molecules and colloidal systems: Laccase, peroxidase and tyrosinase. *Trends Food Sci Technol*. 103:78–93. doi:10.1016/j.tifs.2020.06.014.
(195) Li X et al. (2024) Properties of carbonic anhydrase-containing active coatings for CO_2 capture. *Processes*. 12:810. doi:10.3390/pr12040810.
(196) Li Y, Tu C, Wang H, Silverman DN, Frost SC. (2011) Catalysis and pH control by membrane-associated carbonic anhydrase IX in MDA-MB-231 breast cancer cells. *J Biol Chem*. 286:15789–15796. doi:10.1074/jbc.M110.188524.
(197) Liberato A et al. (2018) Pitfalls in the ABTS peroxidase activity test: Interference of photochemical processes. *Inorg Chem*. 57:14471–14475. doi:10.1021/acs.inorgchem.8b02525.
(198) List B, ed. (2009) Asymmetric organocatalysis. 1st ed. Berlin, Heidelberg: Springer Berlin Heidelberg doi:10.1007/978-3-642-02815-1.
(199) Liu Y, Huang J, Zhang X. (2009) Decolorization and biodegradation of remazol brilliant blue R by bilirubin oxidase. *J Biosci Bioeng*. 108:496–500. doi:10.1016/j.jbiosc.2009.06.001.
(200) Lonergan G, Mew E, Schliephake K, Baker WL. (1997) Phenolic substrates for fluorometric detection of laccase activity. *FEMS Microbiol Lett*. 153:485–490. doi:10.1111/j.1574-6968.1997.tb12614.x.
(201) Lopes P et al. (2019) *Bacillus licheniformis* CotA laccase mutant: Electrocatalytic reduction of O_2 from 0.6 V (SHE) at pH 8 and in seawater. *ChemElectroChem*. 6:2043–2049. doi:10.1002/celc.201900363.
(202) Lopez M et al. (2011) Promiscuity of carbonic anhydrase II. Unexpected ester hydrolysis of carbohydrate-based sulfamate inhibitors. *J Am Chem Soc*. 133:18452–18462. doi:10.1021/ja207855c.
(203) Lotlikar SR et al. (2013) Three functional β-carbonic anhydrases in *Pseudomonas aeruginosa* PAO1: Role in survival in ambient air. *Microbiology*. 159:1748–1759. doi:10.1099/mic.0.066357-0.
(204) Luis P, Walther G, Kellner H, Martin F, Buscot F. (2004) Diversity of laccase genes from basidiomycetes in a forest soil. *Soil Biol Biochem*. 36:1025–1036. doi:10.1016/j.soilbio.2004.02.017.
(205) Lunar L, Sicilia D, Rubio S, Pérez-Bendito D, Nickel U. (2000) Degradation of photographic developers by Fenton's reagent: Condition optimization and kinetics for metol oxidation. *Water Res*. 34:1791–1802. doi:10.1016/S0043-1354(99)00339-5.
(206) Maciejewska M et al. (2017) Assessment of the potential role of *Streptomyces* in cave moonmilk formation. *Front Microbiol*. 8:1181. doi:10.3389/fmicb.2017.01181.
(207) Maleki A, Nematollahi D. (2013) Mechanism diversity in anodic oxidation of *N*,*N*-dimethyl-*p*-phenylenediamine by varying pH. *J Electroanal Chem*. 704:75–79. doi:10.1016/j.jelechem.2013.06.002.
(208) Mallerman J, Itria R, Babay P, Saparrat M, Levin L. (2019) Biodegradation of nonylphenol polyethoxylates by litter-basidiomycetous fungi. *J Environ Chem Eng*. 7:103316. doi:10.1016/j.jece.2019.103316.
(209) Mander GJ et al. (2006) Use of laccase as a novel, versatile reporter system in filamentous fungi. *Appl Environ Microbiol*. 72:5020–5026. doi:10.1128/AEM.00060-06.
(210) Mandic M et al. (2019) Identification and characterization of new laccase biocatalysts from *Pseudomonas* species suitable for degradation of synthetic textile dyes. *Catalysts*. 9:629. doi:10.3390/catal9070629.
(211) Mao Y-H, Guan Y, Song Q, Zheng Q-K, Wang X-X. (2015) Application of laccase and lipopeptide in rinsing procedure of cotton fabric dyed with reactive dye. *Fibers Polym*. 16:2202–2214. doi:10.1007/s12221-015-4876-y.
(212) Marjasvaara A, Torvinen M, Vainiotalo P. (2004) Laccase-catalyzed mediated oxidation of benzyl alcohol: The role of TEMPO and formation of products including benzonitrile studied by

nanoelectrospray ionization Fourier transform ion cyclotron resonance mass spectrometry. *J Mass Spectrom*. 39:1139–1146. doi:10.1002/jms.691.
(213) Marr CD, Grund DW, Harrison KA. (1986) The taxonomic potential of laccase and tyrosinase spot tests. *Mycologia*. 78:169–184. doi:10.2307/3793162.
(214) Martorana A, Vazquez-Duhalt R, Aguila SA, Basosi R, Baratto MC. (2014) Spectroscopic characterization of 2,6-dimethoxyphenol radical intermediates in the *Coriolopsis gallica* laccase-mediator system. *J Mol Catal B Enzym*. 107:100–105. doi:10.1016/j.molcatb.2014.05.023.
(215) Martorell MM, Pajot HF, de Figueroa LIC. (2012) Dye-decolourizing yeasts isolated from Las Yungas rainforest. Dye assimilation and removal used as selection criteria. *Int Biodeterior Biodegrad*. 66:25–32. doi:10.1016/j.ibiod.2011.10.005.
(216) Mate DM, Alcalde M. (2017) Laccase: A multi-purpose biocatalyst at the forefront of biotechnology. *Microb Biotechnol*. 10:1457–1467. doi:10.1111/1751-7915.12422.
(217) Mattinen M-L et al. (2005) Laccase-catalyzed polymerization of tyrosine-containing peptides. *FEBS J*. 272:3640–3650. doi:10.1111/j.1742-4658.2005.04786.x.
(218) Mattos GJ et al. (2022) Electrochemical characterization of the laccase-catalyzed oxidation of 2,6-dimethoxyphenol: An insight into the direct electron transfer by enzyme and enzyme-mediator system. *Appl Biochem Biotechnol*. 194:4348–4361. doi:10.1007/s12010-022-03838-3.
(219) Mayolo-Deloisa K, Machín-Ramírez C, Rito-Palomares M, Trejo-Hernández MR. (2011) Oxidation of polycyclic aromatic hydrocarbons using partially purified laccase from residual compost of *Agaricus bisporus*. *Chem Eng Technol*. 34:1368–1372. doi:10.1002/ceat.201000205.
(220) McConnell IL, Badger MR, Wydrzynski T, Hillier W. (2007) A quantitative assessment of the carbonic anhydrase activity in photosystem II. *Biochim Biophys Acta BBA - Bioenerg*. 1767:639–647. doi:10.1016/j.bbabio.2007.01.019.
(221) Mehra R, Muschiol J, Meyer AS, Kepp KP. (2018) A structural-chemical explanation of fungal laccase activity. *Sci Rep*. 8:17285. doi:10.1038/s41598-018-35633-8.
(222) Meldrum NU, Roughton FJW. (1933) Carbonic anhydrase. Its preparation and properties. *J Physiol*. 80:113–142. doi:10.1113/jphysiol.1933.sp003077.
(223) Menges F. (2016) Spectragryph - optical spectroscopy software, Version 1.2.16.1, 2022. http://www.effemm2.de/spectragryph/.
(224) Mesbah NM, Sarmiento F. (2016) Editorial: Enzymes from extreme environments. *Front Bioeng Biotechnol*. 4. doi:10.3389/fbioe.2016.00024.
(225) Meyer A, Fischer K. (2015) Oxidative transformation processes and products of *para*-phenylenediamine (PPD) and *para*-toluenediamine (PTD) — A review. *Environ Sci Eur*. 27:11. doi:10.1186/s12302-015-0044-7.
(226) Miller AG, Espie GS, Canvin DT. (1989) Use of carbon oxysulfide, a structural analog of CO_2, to study active CO_2 transport in the cyanobacterium *Synechococcus* UTEX 625 1. *Plant Physiol*. 90:1221–1231. doi:10.1104/pp.90.3.1221.
(227) Mirjafari P, Asghari K, Mahinpey N. (2007) Investigating the application of enzyme carbonic anhydrase for CO_2 sequestration purposes. *Ind Eng Chem Res*. 46:921–926. doi:10.1021/ie060287u.
(228) Mo Y. (2011) Rotational barriers in alkanes. *WIREs Comput Mol Sci*. 1:164–171. doi:10.1002/wcms.22.
(229) Modestov AD, Gun J, Savotine I, Lev O. (2004) On-line electrochemical–mass spectrometry study of the mechanism of oxidation of *N*,*N*-dimethyl-*p*-phenylenediamine in aqueous electrolytes. *J Electroanal Chem*. 565:7–19. doi:10.1016/j.jelechem.2003.09.023.
(230) Mogalisetti P, Walt DR. (2016) Enzyme kinetics in femtoliter arrays. In: Vol. 581*Methods in enzymology*. Elsevier, pp. 541–560 doi:10.1016/bs.mie.2016.08.017.
(231) Molina-Fernández C, Luis P. (2021) Immobilization of carbonic anhydrase for CO_2 capture and its industrial implementation: A review. *J CO2 Util*. 47:101475. doi:10.1016/j.jcou.2021.101475.
(232) More SS et al. (2011) Isolation, purification, and characterization of fungal laccase from *Pleurotus* sp. *Enzyme Res*. 2011:e248735. doi:10.4061/2011/248735.
(233) Moshtaghioun SM et al. (2011) Direct spectrophotometric assay of laccase using diazo derivatives of guaiacol. *Anal Chem*. 83:4200–4205. doi:10.1021/ac200501w.
(234) Mucha J. (2011) Changes in hyphal morphology and activity of phenoloxidases during interactions between selected ectomycorrhizal fungi and two species of *Trichoderma*. *Antonie Van Leeuwenhoek*. 100:155–160. doi:10.1007/s10482-011-9556-3.
(235) Munk L, Andersen ML, Meyer AS. (2017) Direct rate assessment of laccase catalysed radical formation in lignin by electron paramagnetic resonance spectroscopy. *Enzyme Microb Technol*. 106:88–96. doi:10.1016/j.enzmictec.2017.07.006.
(236) National Institutes of Health. (2010) ImageJ. *ImageJ*. https://imagej.net/ij/index.html (Accessed January 15, 2025).
(237) Nedrud DM et al. (2014) Uncovering divergent evolution of α/β-hydrolases: A surprising residue substitution needed to convert *Hevea brasiliensis* hydroxynitrile lyase into an esterase. *Chem Sci*. 5:4265–4277. doi:10.1039/C4SC01544D.

(238) Nguyen K, Iliuta I, Pasquier L-C, Bougie F, Iliuta MC. (2024) Enzymatic CO_2 capture in intensified packed-bed column bioreactors: A techno-economic assessment. *Appl Energy*. 376:124207. doi:10.1016/j.apenergy.2024.124207.
(239) Nishio T, Ori M. (2000) Sulfur-containing heterocycles: Facile synthesis of 4*H*-1,3-thiazines by the reaction of 3-*N*-acylamino ketones with Lawesson's reagent. *HETEROCYCLES*. 52:111. doi:10.3987/COM-99-S34.
(240) Nishita T, Deutsch HF. (1986) Acylation and carbamylation of equine muscle carbonic anhydrase (CA-III) upon reaction with *p*-nitrophenyl esters and carbamoyl phosphate. *Int J Biochem*. 18:319–325. doi:10.1016/0020-711X(86)90037-6.
(241) Noroozi-Pesyan N, Khalafy J, Malekpoor Z. (2009) Can be azo dyes obtained by grinding under solvent-free conditions? *J Chin Chem Soc*. 56:1018–1027. doi:10.1002/jccs.200900148.
(242) Nurul-Aliyaa YA, Awang NA, Mohd MH. (2023) Characterization of white rot fungi from wood decayed for lignin degradation. *Lett Appl Microbiol*. 76:ovad118. doi:10.1093/lambio/ovad118.
(243) Onyancha D, Nyamori V, McCleland CW, Imrie C, Gerber TIA. (2009) Solvent-free reactions of *N*,*N*′-thiocarbonyldiimidazole with ferrocenylcarbinols. *J Organomet Chem*. 694:207–212. doi:10.1016/j.jorganchem.2008.10.023.
(244) Palanisamy S et al. (2017) A novel laccase biosensor based on laccase immobilized graphene-cellulose microfiber composite modified screen-printed carbon electrode for sensitive determination of catechol. *Sci Rep*. 7:41214. doi:10.1038/srep41214.
(245) Palmer AE, Randall DW, Xu F, Solomon EI. (1999) Spectroscopic studies and electronic structure description of the high potential type 1 copper site in fungal laccase: Insight into the effect of the axial ligand. *J Am Chem Soc*. 121:7138–7149. doi:10.1021/ja991087v.
(246) Papudeshi B et al. (2017) Optimizing and evaluating the reconstruction of metagenome-assembled microbial genomes. *BMC Genomics*. 18:915. doi:10.1186/s12864-017-4294-1.
(247) Paramjeet S, Manasa P, Korrapati N. (2018) Characterization of thermophilic fungi producing extracellular lignocellulolytic enzymes for lignocellulosic hydrolysis under solid-state fermentation. *Bioresour Bioprocess*. 5:31. doi:10.1186/s40643-018-0216-6.
(248) Pardo I, Chanagá X, Vicente AI, Alcalde M, Camarero S. (2013) New colorimetric screening assays for the directed evolution of fungal laccases to improve the conversion of plant biomass. *BMC Biotechnol*. 13:90. doi:10.1186/1472-6750-13-90.
(249) Park HJ et al. (2021) Involvement of laccase-like enzymes in humic substance degradation by diverse polar soil bacteria. *Folia Microbiol (Praha)*. 66:331–340. doi:10.1007/s12223-020-00847-9.
(250) Park N, Park S-S. (2014) Purification and characterization of a novel laccase from *Fomitopsis pinicola* mycelia. *Int J Biol Macromol*. 70:583–589. doi:10.1016/j.ijbiomac.2014.06.019.
(251) Park S et al. (2020) Microbial diversity in moonmilk of Baeg-nyong cave, Korean CZO. *Front Microbiol*. 11:613. doi:10.3389/fmicb.2020.00613.
(252) Parra-Cruz R, Lau PL, Loh H-S, Pordea A. (2020) Engineering of *Thermovibrio ammonificans* carbonic anhydrase mutants with increased thermostability. *J CO2 Util*. 37:1–8. doi:10.1016/j.jcou.2019.11.015.
(253) Paul-Gorsline BJ. (2024) Development of a mechanism-based kinetic model and process optimization incorporating imidazole autocatalysis in a 1,1′-thiocarbonyldiimidazole-mediated thiocarbonyl transfer. *Org Process Res Dev*. 28:2481–2487. doi:10.1021/acs.oprd.4c00099.
(254) Peirce S et al. (2018) Kinetic characterization of carbonic anhydrase immobilized on magnetic nanoparticles as biocatalyst for CO_2 capture. *Biochem Eng J*. 138:1–11. doi:10.1016/j.bej.2018.06.017.
(255) Peng J et al. (2021) Anthraquinone removal by a metal-organic framework/polyvinyl alcohol cryogel-immobilized laccase: Effect and mechanism exploration. *Chem Eng J*. 418:129473. doi:10.1016/j.cej.2021.129473.
(256) Peng S, Wang Y, Yang J, Wang L. (2023) Simple and rapid photometry for measuring low dosage of periodate with bromide ion-catalyzed oxidation of ABTS. *J Environ Chem Eng*. 11:111456. doi:10.1016/j.jece.2023.111456.
(257) Peng Y, Fu S, Liu H, Lucia LA. (2016) Accurately determining esterase activity via the isosbestic point of *p*-nitrophenol. *BioResources*. 11:10099–10111. doi:10.15376/biores.11.4.10099-10111.
(258) Perna V, Agger JW, Andersen ML, Holck J, Meyer AS. (2019) Laccase induced lignin radical formation kinetics evaluated by electron paramagnetic resonance spectroscopy. *ACS Sustain Chem Eng*. 7:10425–10434. doi:10.1021/acssuschemeng.9b00723.
(259) Peterson MA, Shi H, Ke P. (2006) A simple and efficient biphasic method for the preparation of 4-nitrophenyl *N*-methyl- and *N*-alkylcarbamates. *Tetrahedron Lett*. 47:3405–3407. doi:10.1016/j.tetlet.2006.03.075.
(260) Pettersen EF et al. (2004) UCSF Chimera—A visualization system for exploratory research and analysis. *J Comput Chem*. 25:1605–1612. doi:10.1002/jcc.20084.

(261) Pieczul K et al. (2020) The activity of β-glucosidase and guaiacol peroxidase in different genotypes of winter oilseed rape (*Brassica napus* L.) infected by Alternaria black spot fungi. *Acta Physiol Plant*. 42:142. doi:10.1007/s11738-020-03125-w.
(262) Pocker Y, Deits TL. (1984) Active-site mechanisms of the carbonic anhydrases. *Ann N Y Acad Sci*. 429:76–83. doi:10.1111/j.1749-6632.1984.tb12316.x.
(263) Pocker Y, Guilbert LJ. (1974) Carbonic anhydrase catalyzed hydrolysis and decarboxylation. Kinetic studies of enzyme-catalyzed decomposition of mono- and disubstituted derivatives of carbonic acid. *Biochemistry*. 13:70–78. doi:10.1021/bi00698a012.
(264) Pocker Y, Guilbert LJ. (1972) Catalytic versatility of erythrocyte carbonic anhydrase. Kinetic studies of the enzyme-catalyzed hydrolysis of methyl pyridyl carbonates. *Biochemistry*. 11:180–190. doi:10.1021/bi00752a007.
(265) Pocker Y, Sarkanen S. (2006) Carbonic anhydrase: Structure, catalytic versatility, and inhibition. In: Meister, A, ed.*Advances in enzymology - and related areas of molecular biology*. Hoboken, NJ, USA: John Wiley & Sons, Inc., pp. 149–274 doi:10.1002/9780470122921.ch3.
(266) Pocker Y, Sarkanen S. (1978) Oxonase and esterase activities of erythrocyte carbonic anhydrase. *Biochemistry*. 17:1110–1118. doi:10.1021/bi00599a027.
(267) Pocker Y, Stone JT. (1967) The catalytic versatility of erythrocyte carbonic anhydrase. III. Kinetic studies of the enzyme-catalyzed hydrolysis of *p*-nitrophenyl acetate. *Biochemistry*. 6:668–678. doi:10.1021/bi00855a005.
(268) Pocker Y, Stone JT. (1968) The catalytic versatility of erythrocyte carbonic anhydrase. VI. Kinetic studies of noncompetitive inhibition of enzyme-catalyzed hydrolysis of *p*-nitrophenyl acetate. *Biochemistry*. 7:2936–2945. doi:10.1021/bi00848a034.
(269) Pohanka M, Hrabinova M, Kuca K, Simonato J-P. (2011) Assessment of acetylcholinesterase activity using indoxylacetate and comparison with the standard Ellman's method. *Int J Mol Sci*. 12:2631–2640. doi:10.3390/ijms12042631.
(270) Pointing SB. (1999) Qualitative methods for the determination of lignocellulolytic enzyme production by tropical fungi. *Fungal Divers*. 2:17–33.
(271) Polyakov KM, Gavryushov S, Fedorova TV, Glazunova OA, Popov AN. (2019) The subatomic resolution study of laccase inhibition by chloride and fluoride anions using single-crystal serial crystallography: Insights into the enzymatic reaction mechanism. *Acta Crystallogr Sect Struct Biol*. 75:804–816. doi:10.1107/S2059798319010684.
(272) Portillo MC, Gonzalez JM. (2011) Moonmilk deposits originate from specific bacterial communities in Altamira cave (Spain). *Microb Ecol*. 61:182–189. doi:10.1007/s00248-010-9731-5.
(273) Power IM, Harrison AL, Dipple GM. (2016) Accelerating mineral carbonation using carbonic anhydrase. *Environ Sci Technol*. 50:2610–2618. doi:10.1021/acs.est.5b04779.
(274) Prillinger H, Molitoris HP. (1979) Genetic analysis in wood-decaying fungi I. Genetic variation and evidence for allopatric speciation in *Pleurotus ostreatus* using phenoloxidase zymograms and morphological criteria. *Physiol Plant*. 46:265–277. doi:10.1111/j.1399-3054.1979.tb06533.x.
(275) Ramesh S, Indukuri K, Riant O, Debecker DP. (2018) Synthesis of carbonate esters by carboxymethylation using $NaAlO_2$ as a highly active heterogeneous catalyst. *Org Process Res Dev*. 22:1846–1851. doi:10.1021/acs.oprd.8b00333.
(276) Ranocha P et al. (1999) Biochemical characterization, molecular cloning and expression of laccases – a divergent gene family – in poplar. *Eur J Biochem*. 259:485–495. doi:10.1046/j.1432-1327.1999.00061.x.
(277) Ray AS, Rajasekaran M, Uddin M, Kandasamy R. (2023) Laccase driven biocatalytic oxidation to reduce polymeric surface hydrophobicity: An effective pre-treatment strategy to enhance biofilm mediated degradation of polyethylene and polycarbonate plastics. *Sci Total Environ*. 904:166721. doi:10.1016/j.scitotenv.2023.166721.
(278) Ren J, Danchana K, Sasaki K, Kaneta T. (2023) Fluorometric assay of laccase in mushroom extracts and comparisons with absorption spectrophotometry. *J Food Compos Anal*. 123:105627. doi:10.1016/j.jfca.2023.105627.
(279) Reymond J. (2008) Colorimetric and fluorescence-based screening. In: Lutz, S, Bornscheuer, UT, eds.*Protein engineering handbook*. Darmstadt: Wiley, pp. 669–711 doi:10.1002/9783527634026.ch28.
(280) Rodríguez-Escribano D, De Salas F, Pardo I, Camarero S. (2017) High-throughput screening assay for laccase engineering toward lignosulfonate valorization. *Int J Mol Sci*. 18:1793. doi:10.3390/ijms18081793.
(281) Rose KD, Bryant RG. (1980) Oxygen-17 NMR studies of carbonic anhydrase. *J Am Chem Soc*. 102:21–24. doi:10.1021/ja00521a005.
(282) Rowlett RS. (2010) Structure and catalytic mechanism of the β-carbonic anhydrases. *Biochim Biophys Acta BBA - Proteins Proteomics*. 1804:362–373. doi:10.1016/j.bbapap.2009.08.002.

(283) Rühl M, Majcherczyk A, Kües U. (2013) Lcc1 and Lcc5 are the main laccases secreted in liquid cultures of *Coprinopsis cinerea* strains. *Antonie Van Leeuwenhoek*. 103:1029–1039. doi:10.1007/s10482-013-9883-7.
(284) Saha R, Mukhopadhyay M. (2022) Time-dependent electrochemical characteristics of a phenolic and non-phenolic compound in the presence of laccase/ABTS system. *PLOS ONE*. 17:e0275338. doi:10.1371/journal.pone.0275338.
(285) Saito K, Kato T, Tsuji Y, Fukushima K. (2005) Identifying the characteristic secondary ions of lignin polymer using ToF−SIMS. *Biomacromolecules*. 6:678–683. doi:10.1021/bm049521v.
(286) Saito R, Sato T, Ikai A, Tanaka N. (2004) Structure of bovine carbonic anhydrase II at 1.95 Å resolution. *Acta Crystallogr D Biol Crystallogr*. 60:792–795. doi:10.1107/s0907444904003166.
(287) Santhanam N, Vivanco JM, Decker SR, Reardon KF. (2011) Expression of industrially relevant laccases: Prokaryotic style. *Trends Biotechnol*. 29:480–489. doi:10.1016/j.tibtech.2011.04.005.
(288) Schirmann JG, Dekker RFH, Borsato D, Barbosa-Dekker AM. (2018) Selective control for the laccase-catalyzed synthesis of dimers from 2,6-dimethoxyphenol: Optimization of 3,3',5,5'-tetramethoxy-biphenyl-4,4'-diol synthesis using factorial design, and evaluation of its antioxidant action in biodiesel. *Appl Catal Gen*. 555:88–97. doi:10.1016/j.apcata.2018.02.015.
(289) Schmidt M, Bornscheuer UT. (2005) High-throughput assays for lipases and esterases. *Biomol Eng*. 22:51–56. doi:10.1016/j.bioeng.2004.09.004.
(290) Schoonen L et al. (2017) Alternative application of an affinity purification tag: Hexahistidines in ester hydrolysis. *Sci Rep*. 7:14772. doi:10.1038/s41598-017-15310-y.
(291) Schulze M, Geisler L, Majcherczyk A, Rühl M. (2019) Signal peptide replacement resulted in recombinant homologous expression of laccase Lcc8 in *Coprinopsis cinerea*. *AMB Express*. 9:36. doi:10.1186/s13568-019-0761-1.
(292) Schwan AL, Byers JH. (2007) 1,1′-Thiocarbonyldiimidazole. In: *Encyclopedia of reagents for organic synthesis*. John Wiley & Sons, Ltd doi:10.1002/9780470842898.rt094.pub2.
(293) Senthilvelan T, Kanagaraj J, Panda RC. (2017) Enhanced biodegradation of lignin by laccase through HOBT mediator: Mechanistic studies supported by FTIR and GCMS studies. *Environ Process*. 4:201–217. doi:10.1007/s40710-017-0209-z.
(294) Sharan AA et al. (2024) Functional screening pipeline to uncover laccase-like multicopper oxidase enzymes that transform industrial lignins. *Bioresour Technol*. 393:130084. doi:10.1016/j.biortech.2023.130084.
(295) Sherif M et al. (2013) Biochemical studies of the multicopper oxidase (small laccase) from *Streptomyces coelicolor* using bioactive phytochemicals and site-directed mutagenesis. *Microb Biotechnol*. 6:588–597. doi:10.1111/1751-7915.12068.
(296) Shimizu A et al. (2020) HOMO–LUMO energy-gap tuning of π-conjugated zwitterions composed of electron-donating anion and electron-accepting cation. *J Org Chem*. 86:770–781. doi:10.1021/acs.joc.0c02343.
(297) Shleev S et al. (2005) Direct electron transfer reactions of laccases from different origins on carbon electrodes. *Bioelectrochemistry*. 67:115–124. doi:10.1016/j.bioelechem.2005.02.004.
(298) Shoup D, Lipari G, Szabo A. (1981) Diffusion-controlled bimolecular reaction rates. The effect of rotational diffusion and orientation constraints. *Biophys J*. 36:697–714. doi:10.1016/S0006-3495(81)84759-5.
(299) Sikora K, Nowacki A, Liberek B, Dmochowska B. (2020) Methyl transfer in quaternary alkylammonium salts, derivatives of 1,4:3,6-dianhydrohexitols. *J Mol Struct*. 1206:127701. doi:10.1016/j.molstruc.2020.127701.
(300) da Silva Vilar D et al. (2022) Lignin-modifying enzymes: A green and environmental responsive technology for organic compound degradation. *J Chem Technol Biotechnol*. 97:327–342. doi:10.1002/jctb.6751.
(301) Silverman DN. (1982) [35] Carbonic anhydrase: Oxygen-18 exchange catalyzed by an enzyme with rate-contributing proton-transfer steps. In: Purich, DL, ed. Enzyme kinetics and mechanism - part C: Intermediates, stereochemistry, and rate studies Vol. 87*Methods in enzymology*. Academic Press, pp. 732–752 doi:10.1016/S0076-6879(82)87037-7.
(302) Silverman DN. (1973) Carbonic anhydrase catalyzed oxygen-18 exchange between bicarbonate and water. *Arch Biochem Biophys*. 155:452–457. doi:10.1016/0003-9861(73)90136-7.
(303) Simonsson I, Jonsson B-H, Lindskog S. (1979) A ^{13}C nuclear-magnetic-resonance study of CO_2-HCO_3^- exchange catalyzed by human carbonic anhydrase C at chemical equilibrium. *Eur J Biochem*. 93:409–417. doi:10.1111/j.1432-1033.1979.tb12837.x.
(304) Simplício AL, Coroadinha AS, Gilmer JF, Lamego J. (2013) A methodology for detection and quantification of esterase activity. In: Volpi, N, Maccari, F, eds.*Capillary electrophoresis of biomolecules: Methods and protocols*. Totowa, NJ: Humana Press, pp. 309–319 doi:10.1007/978-1-62703-296-4_22.

(305) Sitte NA, Bursch M, Grimme S, Paradies J. (2019) Frustrated Lewis pair catalyzed hydrogenation of amides: Halides as active Lewis base in the metal-Free hydrogen activation. *J Am Chem Soc*. 141:159–162. doi:10.1021/jacs.8b12997.
(306) Smirnovienė J, Smirnovas V, Matulis D. (2017) Picomolar inhibitors of carbonic anhydrase: Importance of inhibition and binding assays. *Anal Biochem*. 522:61–72. doi:10.1016/j.ab.2017.01.022.
(307) Solano F, Lucas-Elío P, López-Serrano D, Fernández E, Sanchez-Amat A. (2001) Dimethoxyphenol oxidase activity of different microbial blue multicopper proteins. *FEMS Microbiol Lett*. 204:175–181. doi:10.1111/j.1574-6968.2001.tb10882.x.
(308) Sousa AC, Martins LO, Robalo MP. (2013) Laccase-catalysed homocoupling of primary aromatic amines towards the biosynthesis of dyes. *Adv Synth Catal*. 355:2908–2917. doi:10.1002/adsc.201300501.
(309) Sousa AC, Oliveira MC, Martins LO, Robalo MP. (2014) Towards the rational biosynthesis of substituted phenazines and phenoxazinones by laccases. *Green Chem*. 16:4127–4136. doi:10.1039/C4GC00901K.
(310) Sousa CA, Ribeiro M, Vale F, Simões M. (2024) Phenazines: Natural products for microbial growth control. *hLife*. 2:100–112. doi:10.1016/j.hlife.2023.11.005.
(311) Spulber M et al. (2014) Poly(*N*-vinylpyrrolidone)-poly(dimethylsiloxane)-based polymersome nanoreactors for laccase-catalyzed biotransformations. *Biomacromolecules*. 15:1469–1475. doi:10.1021/bm500081j.
(312) Stewart JA, Ouellet L. (1959) The trypsin catalysed hydrolysis of *p*-nitrophenyl acetate. *Can J Chem*. 37:751–759. doi:10.1139/v59-102.
(313) Stimler K, Berry JA, Yakir D. (2012) Effects of carbonyl sulfide and carbonic anhydrase on stomatal conductance. *Plant Physiol*. 158:524–530. doi:10.1104/pp.111.185926.
(314) Suh J, Kwon WJ. (1998) Artificial metalloesterases constructed by site-directed attachment of oximinato metal centers to [oly(ethylenimine) containing β-Cyclodextrin. *Bioorganic Chem*. 26:103–117. doi:10.1006/bioo.1998.1090.
(315) Sun X et al. (2013) Laccase-catalyzed oxidative polymerization of phenolic compounds. *Appl Biochem Biotechnol*. 171:1673–1680. doi:10.1007/s12010-013-0463-0.
(316) Sun X, Zhang R, Zhang Y. (2004) Production of lignocellulolytic enzymes by *Trametes gallica* and detection of polysaccharide hydrolase and laccase activities in polyacrylamide gels. *J Basic Microbiol*. 44:220–231. doi:10.1002/jobm.200310376.
(317) Supuran CT. (2016) Structure and function of carbonic anhydrases. *Biochem J*. 473:2023–2032. doi:10.1042/BCJ20160115.
(318) Syringaldazine SIGMA-ALDRICH®. (2009) Enzymatic assay of laccase (EC 1.10.3.2). *Enzym Assay Laccase EC 11032*. https://www.sigmaaldrich.com/LT/en/technical-documents/protocol/protein-biology/enzyme-activity-assays/enzymatic-assay-of-laccase (Accessed April 18, 2019).
(319) Sýs M, Metelka R, Frangu A, Vytřas K, Arbneshi T. (2017) Electrochemical study of *Trametes versicolor* laccase compatibility to different polyphenolic substrates. *Chemosensors*. 5:9. doi:10.3390/chemosensors5010009.
(320) Talekar S, Jo BH, Dordick JS, Kim J. (2022) Carbonic anhydrase for CO_2 capture, conversion and utilization. *Curr Opin Biotechnol*. 74:230–240. doi:10.1016/j.copbio.2021.12.003.
(321) Tang Q et al. (2016) An environmentally friendly, photocontrollable and highly recyclable catalyst for use in a one-pot three-component Mannich reaction. *J Mol Catal Chem*. 421:37–44. doi:10.1016/j.molcata.2016.05.006.
(322) Tang Z, Chen H, He H, Ma C. (2019) Assays for alkaline phosphatase activity: Progress and prospects. *TrAC Trends Anal Chem*. 113:32–43. doi:10.1016/j.trac.2019.01.019.
(323) Taylor EL, Meriwether BP, Park JH. (1963) The hydrolysis of *p*-nitrophenyl acetate catalyzed by 3-phosphoglyceraldehyde dehydrogenase crystallized from yeast. *J Biol Chem*. 238:734–740. doi:10.1016/S0021-9258(18)81328-X.
(324) Teerawonganan P et al. (2024) Synthesis, cytotoxicity, and mechanistic evaluation of tetrahydrocurcumin-amino acid conjugates as LAT1-targeting anticancer agents in C6 glioma cells. *Int J Mol Sci*. 25:11266. doi:10.3390/ijms252011266.
(325) Tekincanli MA, Akatin MY, Colak A. (2015) Purification and characterization of a novel thermostable esterase from *Thermus* sp. NCCB 100425^T. *Turk J Biochem*. 40:116–124. doi:10.5505/tjb.2015.13008.
(326) Téllez-Téllez M, Sánchez C, Loera O, Díaz-Godínez G. (2005) Differential patterns of constitutive intracellular laccases of the vegetative phase of *Pleurotus* species. *Biotechnol Lett*. 27:1391–1394. doi:10.1007/s10529-005-3687-4.
(327) Terrón MC et al. (2004) Tannic acid interferes with the commonly used laccase-detection assay based on ABTS as the substrate. *Biochimie*. 86:519–522. doi:10.1016/j.biochi.2004.07.013.

(328) Thorslund A, Lindskog S. (1967) Studies of the esterase activity and the anion inhibition of bovine zinc and cobalt carbonic anhydrases. *Eur J Biochem*. 3:117–123. doi:10.1111/j.1432-1033.1967.tb19504.x.
(329) Tian C et al. (2020) ff19SB: Amino-acid-specific protein backbone parameters trained against quantum mechanics energy surfaces in solution. *J Chem Theory Comput*. 16:528–552. doi:10.1021/acs.jctc.9b00591.
(330) Tian Z et al. (2019) A far-red fluorescent probe for sensing laccase in fungi and its application in developing an effective biocatalyst for the biosynthesis of antituberculous dicoumarin. *Chem Commun*. 55:3951–3954. doi:10.1039/C9CC01579E.
(331) Timonen S, Sen R. (1998) Heterogeneity of fungal and plant enzyme expression in intact Scots pine–*Suillus bovinus* and –*Paxillus involutus* mycorrhizospheres developed in natural forest humus. *New Phytol*. 138:355–366. doi:10.1046/j.1469-8137.1998.00103.x.
(332) Tiwari N, Santhiya D, Sharma JG. (2024) Significance of landfill microbial communities in biodegradation of polyethylene and nylon 6,6 microplastics. *J Hazard Mater*. 462:132786. doi:10.1016/j.jhazmat.2023.132786.
(333) Toker SK, Evlat H, Koçyiğit A. (2021) Screening of newly isolated marine-derived fungi for their laccase production and decolorization of different dye types. *Reg Stud Mar Sci*. 45:101837. doi:10.1016/j.rsma.2021.101837.
(334) Tomar JS, Shen J. (2020) Characterization of carbonic anhydrase *in vivo* using magnetic resonance spectroscopy. *Int J Mol Sci*. 21:2442. doi:10.3390/ijms21072442.
(335) Tominaga M, Takatori T, Togami M, Tsushida M. (2023) Nanocarbon-assisted carbon-nanotube-based composite electrodes for improved laccase bio-electrocatalysis. *Sens Mater*. 35:4721. doi:10.18494/SAM4407.
(336) Trivedi TJ, Lee JH, Lee HJ, Jeong YK, Choi JW. (2016) Deep eutectic solvents as attractive media for CO_2 capture. *Green Chem*. 18:2834–2842. doi:10.1039/C5GC02319J.
(337) Tsujimura S et al. (2001) Bioelectrocatalytic reduction of dioxygen to water at neutral pH using bilirubin oxidase as an enzyme and 2,2′-azinobis(3-ethylbenzothiazolin-6-sulfonate) as an electron transfer mediator. *J Electroanal Chem*. 496:69–75. doi:10.1016/S0022-0728(00)00239-4.
(338) Uda NR et al. (2015) Esterase activity of carbonic anhydrases serves as surrogate for selecting antibodies blocking hydratase activity. *J Enzyme Inhib Med Chem*. 30:955–960. doi:10.3109/14756366.2014.1001754.
(339) Umashankar N, Meghashree HM, Benherlal PS, Chavan M. (2018) Isolation and screening of lignin degrading bacteria from different natural and organic sources. *Int J Curr Microbiol Appl Sci*. 7:609–617. doi:10.20546/ijcmas.2018.712.075.
(340) Uygun M et al. (2015) Micromotor-based biomimetic carbon dioxide sequestration: Towards mobile microscrubbers. *Angew Chem Int Ed*. 54:12900–12904. doi:10.1002/anie.201505155.
(341) Varjosaari SE, Suating P, Adler MJ. (2016) One-pot synthesis of *O*-aryl carbamates. *Synthesis*. 48:43–47. doi:10.1055/s-0035-1560726.
(342) Verde V et al. (2002) Use of *N*,*N*-dimethyl-*p*-phenylenediamine to evaluate the oxidative status of human plasma. *Free Radic Res*. 36:869–873. doi:10.1080/1071576021000005302.
(343) Verma SK, Ghosh KK. (2010) α-Chymotrypsin catalyzed hydrolysis of *p*-nitrophenyl acetate in cationic microemulsions. *Colloids Surf Physicochem Eng Asp*. 368:154–158. doi:10.1016/j.colsurfa.2010.07.030.
(344) Verpoorte JA, Mehta S, Edsall JT. (1967) Esterase activities of human carbonic anhydrases B and C. *J Biol Chem*. 242:4221–4229. doi:10.1016/S0021-9258(18)95800-X.
(345) Volkova N, Ibrahim V, Hatti-Kaul R. (2012) Laccase catalysed oxidation of syringic acid: Calorimetric determination of kinetic parameters. *Enzyme Microb Technol*. 50:233–237. doi:10.1016/j.enzmictec.2012.01.005.
(346) Wang S, Li W, Liu L, Qi H, You H. (2022) Biodegradation of decabromodiphenyl ethane (DBDPE) by white-rot fungus *Pleurotus ostreatus*: Characteristics, mechanisms, and toxicological response. *J Hazard Mater*. 424:127716. doi:10.1016/j.jhazmat.2021.127716.
(347) Wang T, Xiang Y, Liu X, Chen W, Hu Y. (2017) A novel fluorimetric method for laccase activities measurement using Amplex Red as substrate. *Talanta*. 162:143–150. doi:10.1016/j.talanta.2016.10.006.
(348) Wang T-Z, Li W-P, Wan H-W, Zhou P-J, Qu S-S. (2000) Assay for laccase activity by microcalorimetry: Laccase was extracted from China lacquer of *Rhus vernicifera*. *J Biochem Biophys Methods*. 45:57–63. doi:10.1016/S0165-022X(00)00098-1.
(349) Wilbur KM, Anderson NG. (1948) Electrometric and colorimetric determination of carbonic anhydrase. *J Biol Chem*. 176:147–154. doi:10.1016/S0021-9258(18)51011-5.
(350) Winkler UK, Stuckmann M. (1979) Glycogen, hyaluronate, and some other polysaccharides greatly enhance the formation of exolipase by *Serratia marcescens*. *J Bacteriol*. 138:663–670. doi:10.1128/jb.138.3.663-670.1979.

(351) Wistrand PJ. (1981) The importance of carbonic anhydrase B and C for the unloading of CO_2 by the human erythrocyte. *Acta Physiol Scand*. 113:417–426. doi:10.1111/j.1748-1716.1981.tb06918.x.
(352) Wu K et al. (2021) A chromatography-free and aqueous waste-free process for thioamide preparation with Lawesson's reagent. *Beilstein J Org Chem*. 17:805–812. doi:10.3762/bjoc.17.69.
(353) Xia Z, Yoshida T, Funaoka M. (2003) Enzymatic degradation of highly phenolic lignin-based polymers (lignophenols). *Eur Polym J*. 39:909–914. doi:10.1016/S0014-3057(02)00357-9.
(354) Xu F. (1996) Oxidation of phenols, anilines, and benzenethiols by fungal laccases: Correlation between activity and redox potentials as well as halide inhibition. *Biochemistry*. 35:7608–7614. doi:10.1021/bi952971a.
(355) Xu X et al. (2018) Inhibition of metal ions on *Cerrena* sp. laccase: Kinetic, decolorization and fluorescence studies. *J Taiwan Inst Chem Eng*. 84:1–10. doi:10.1016/j.jtice.2017.12.028.
(356) Yadav R et al. (2010) Immobilized carbonic anhydrase for the biomimetic carbonation reaction. *Energy Fuels*. 24:6198–6207. doi:10.1021/ef100750y.
(357) Yang C et al. (2025) Ancestral carbonic anhydrase with significantly enhanced stability and activity for CO_2 capture and utilization. *Bioresour Technol*. 419:132054. doi:10.1016/j.biortech.2025.132054.
(358) Yang Y-L, Ramaswamy SG, Jakoby WB. (1998) Enzymatic hydrolysis of organic cyclic carbonates*. *J Biol Chem*. 273:7814–7817. doi:10.1074/jbc.273.14.7814.
(359) Yano A, Kikuchi S, Nakagawa Y, Sakamoto Y, Sato T. (2009) Secretory expression of the non-secretory-type *Lentinula edodes* laccase by *Aspergillus oryzae*. *Microbiol Res*. 164:642–649. doi:10.1016/j.micres.2008.12.001.
(360) Yılmaz S et al. (2016) Synthesis and inhibitory properties of some carbamates on carbonic anhydrase and acetylcholine esterase. *J Enzyme Inhib Med Chem*. 31:1484–1491. doi:10.3109/14756366.2016.1149477.
(361) Yoshimoto M, Schweizer T, Rathlef M, Pleij T, Walde P. (2018) Immobilization of carbonic anhydrase in glass micropipettes and glass fiber filters for flow-through reactor applications. *ACS Omega*. 3:10391–10405. doi:10.1021/acsomega.8b01517.
(362) Yu L et al. (2024) Analysis of the electron transfer pathway in small laccase by EPR and UV–vis spectroscopy coupled with redox titration. *Magn Reson Lett*. 4:200116. doi:10.1016/j.mrl.2024.200116.
(363) Yusuf ZS et al. (2022) The inhibitory effect of boric acid on hypoxia-regulated tumour-associated carbonic anhydrase IX. *J Enzyme Inhib Med Chem*. 37:1340–1345. doi:10.1080/14756366.2022.2072837.
(364) Zavarzina AG et al. (2018) Laccase production and humic acids decomposition by microscopic soil fungi. *Microbiology*. 87:308–316. doi:10.1134/S0026261718030153.
(365) Zeebe RE, Wolf-Gladrow DA. (2001) CO_2 in seawater: Equilibrium, kinetics, isotopes. Amsterdam; New York: Elsevier doi:10.1016/S0422-9894(01)80011.
(366) Zeng Xiangkang et al. (2011) Decolorization of synthetic dyes by crude laccase from a newly isolated *Trametes trogii* strain cultivated on solid agro-industrial residue. *J Hazard Mater*. 187:517–525. doi:10.1016/j.jhazmat.2011.01.068.
(367) Zhang S et al. (2022) Enzymatic hydrolysis of corn stover lignin by laccase, lignin peroxidase, and manganese peroxidase. *Bioresour Technol*. 361:127699. doi:10.1016/j.biortech.2022.127699.
(368) Zhao Y, Truhlar DG. (2008) The M06 suite of density functionals for main group thermochemistry, thermochemical kinetics, noncovalent interactions, excited states, and transition elements: Two new functionals and systematic testing of four M06-class functionals and 12 other functionals. *Theor Chem Acc*. 120:215–241. doi:10.1007/s00214-007-0310-x.
(369) Zimbardi ALRL et al. (2016) A high redox potential laccase from *Pycnoporus sanguineus* RP15: Potential application for dye decolorization. *Int J Mol Sci*. 17:672. doi:10.3390/ijms17050672.
(370) Zippilli C et al. (2021) Laccase-catalyzed 1,4-dioxane-mediated synthesis of belladine *N*-oxides with anti-influenza a virus activity. *Int J Mol Sci*. 22:1337. doi:10.3390/ijms22031337.

SUPPLEMENTARY MATERIALS

Additional Electronic Supplementary Materials available at:
https://doi.org/10.18279/MIDAS.556412

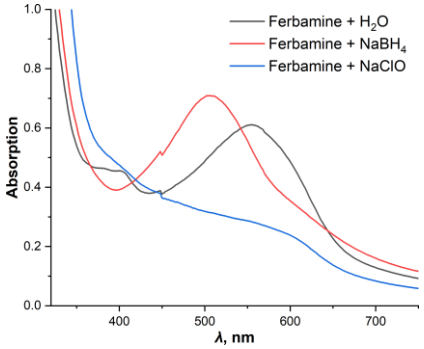


Figure S1 UV-Vis spectra of partially reduced (Ferbamine + $NaBH_4$), oxidised (Ferbamine + NaClO) and control (Ferbamine + H_2O) Ferbamine solutions.

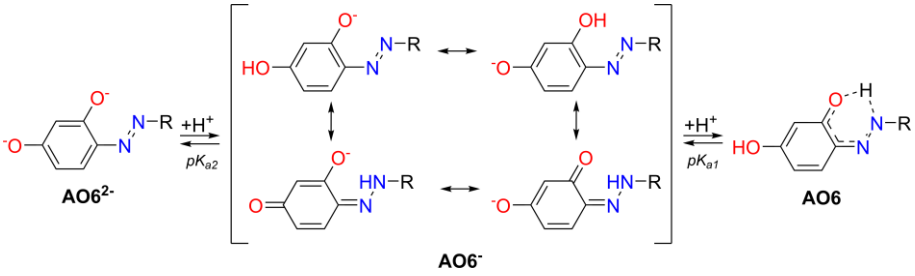


Figure S2 AO6 protonation states.

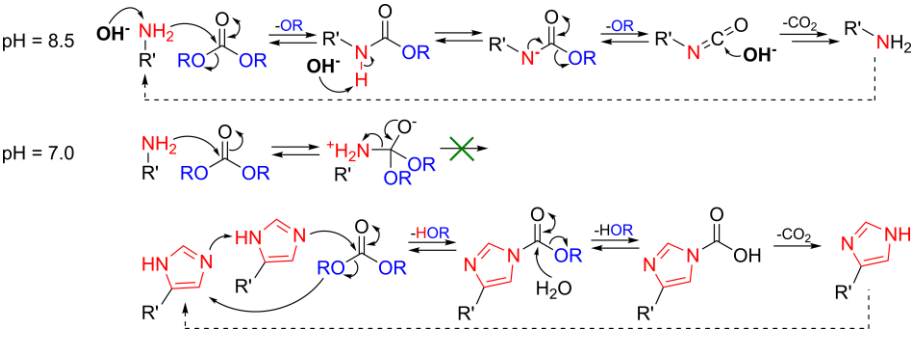
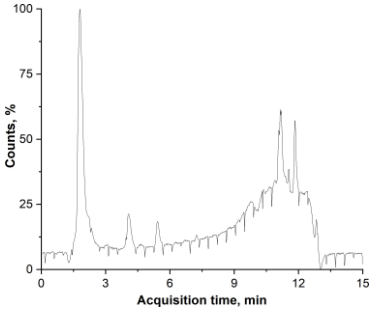


Figure S3 Proposed primary amine and histidine-catalysed carbonate ester degradation mechanisms.

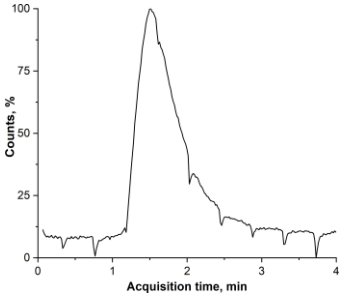
Table S1 Results of the Ferbamine intermediate synthesis product LC-HRMS analysis.



t_R, min	m/z[a]	Counts, %[b]	M chemical formula[c]	Error, ppm
1.802	401.2448	100	$C_{24}H_{28}N_6$	-0.05
	200.6220	15.39	$C_{24}H_{28}N_6$[d]	-0.50
2.235	411.2296	100	$C_{25}H_{26}N_6$	1.04
	295.1916	37.14	$C_{18}H_{22}N_4$	-0.42
	200.6215	21.97	$C_{24}H_{28}N_6$[d]	-2.99
	401.2420	18.10	$C_{24}H_{28}N_6$	-7.05
	417.2381	16.96	$C_{24}H_{28}N_6O$	-3.93
	397.2131	12.84	$C_{24}H_{24}N_6$	-1.06
4.099	389.2446	100	$C_{23}H_{28}N_6$	-0.57
	405.2377	45.49	$C_{23}H_{28}N_6O$	-5.04
	421.2340	25.77	$C_{23}H_{28}N_6O_2$	-1.55
	403.2239	14.73	$C_{23}H_{26}N_6O$	-0.46
5.431	415.2122	100	$C_{25}H_{26}N_4O_2$	-1.58
	460.2695	46.18	$C_{27}H_{33}N_5O_2$	-2.62
	555.3176	45.57	$C_{31}H_{38}N_8O_2$	-2.61
	437.1936	15.79	$C_{22}H_{24}N_6O_4$	0.96
	569.3200	12.28	$C_{28}H_{40}N_8O_5$	-1.94
11.075	282.2792	100	-	-
	121.0509	22.87	-	-
11.824	443.3157	100	-	-
	465.2975	10.51	-	-

[a] Signals of molecules with heavier isotopes were not included.
[b] Intensities were normalised to the highest value for each t_R.
[c] M formulas were calculated for $[M+H]^+$ type ionisation.
[d] M formulas were calculated for $[M+H]^{2+}$ type ionisation.

Table S2 Results of the final Ferbamine synthesis product LC-HRMS analysis.



t_R, min	m/z[a]	Counts, %[b]	M chemical formula[c]	Error, ppm
1.515	397.2132	100	$C_{24}H_{25}N_6$	-0.81
	411.2289	91.55	$C_{25}H_{27}N_6$	-0.66
	383.1979	9.64	$C_{23}H_{22}N_6$[e]	0.08
2.235	397.2134	100	$C_{24}H_{25}N_6$	-0.31
	411.2294	32.58	$C_{25}H_{27}N_6$	0.56
	383.1976	8.80	$C_{23}H_{22}N_6$[d]	-0.71

[a] Signals of molecules with heavier isotopes were not included.
[b] Intensities were normalised to the highest value for each t_R.
[c] M formulas were calculated for $[M]^+$ type ionisation.
[d] M formulas were calculated for $[M+H]^+$ type ionisation.

Table S3 The sample codes and types.

Sampling location	Sample code	Sample type	Sampling location	Sample code	Sample type
Gornja Jakovljeva cave	GJ1-2, GJ7, GJ12-16	Microbial biofilm	Prosječenica cave	P1	Bat guano
				P2	Cave soil
	GJ3-4	*Unidentified*	Vakuf cave	GS1	Piece of wood
	GJ5	Sediment		GS2	Guano with fungi
	GJ6, GJ8	Moonmilk		GS3	Deposits on spider net
	GJ9	Clay		GS4	Cocoon with fungi
	GJ11	Fungi on faeces		GS5	Bat guano
	GJ17	Wood	Čvaljina tunnel	TČ1	Dry bat guano
Ponor Kovači cave	PK1	Wood		TČ2	Guano with soil
	PK2	Soil	Vjetrenica cave	V1A	Soil and sediment
	PK3	Fungi		V1	Lake sediment
	PK4	Biofilm		V2	Unidentified
	PK5	Fungi on insect *Stenophylax* sp.	Donja Mijatova cave	DM1	Horn with fungi
	PK6	Fungi on Opiliones		DM2	Fungi
	PK7	Faeces (*Martes martes*)		DM3	Wood
	PK8	Fungi on roots		DM4	Stalagmite

Table S4 Results of K_M, V_{max}, k_{cat} and k_{cat}/K_M with different [bCAII]/[KCN] molar ratios, calculated using L-B, E-H, H-W and E-C-B methods for raw and processed datasets. Ratios 1/0 – uninhibited bCAII (control). Asterisks (* and **) denote the number of negative results in the analysis.

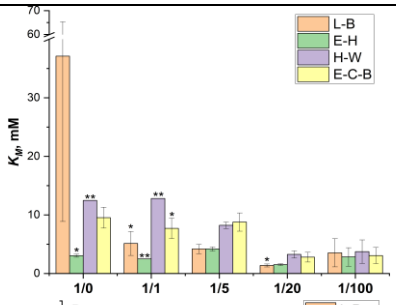
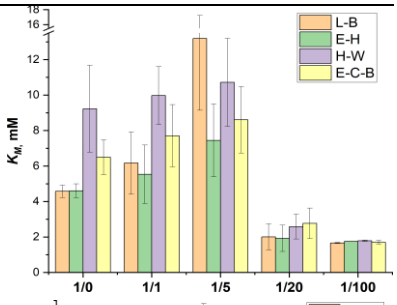
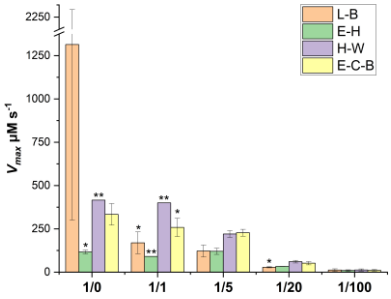
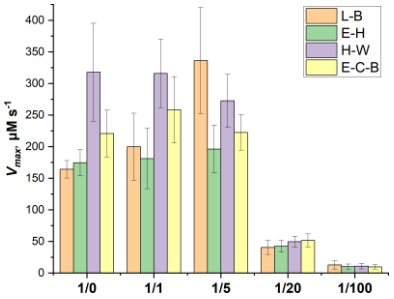
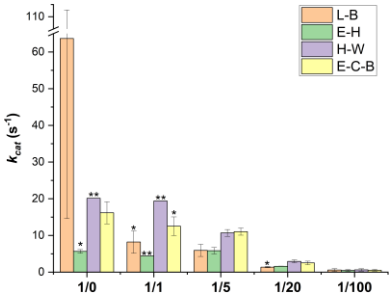
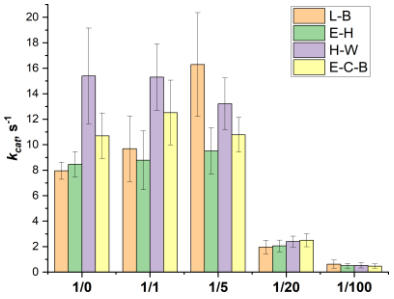
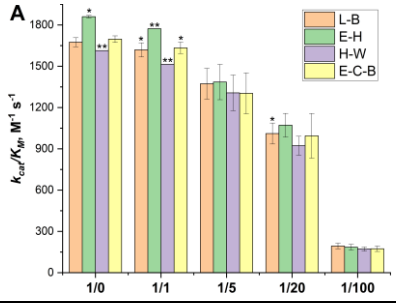
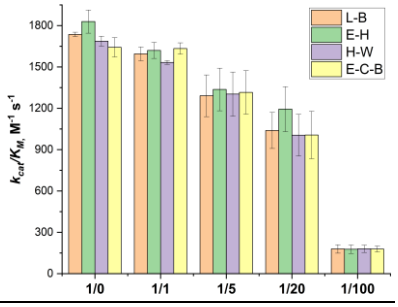
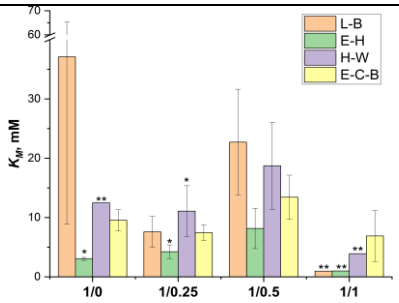
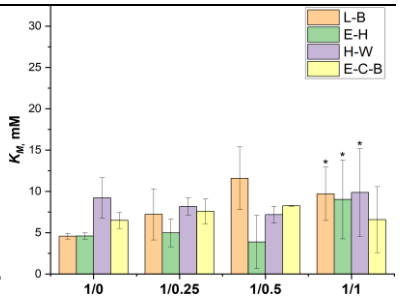
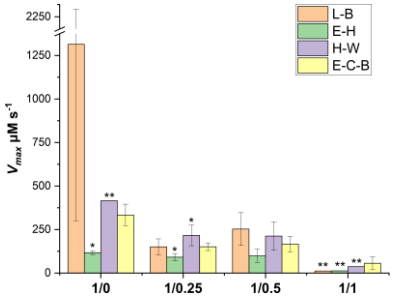
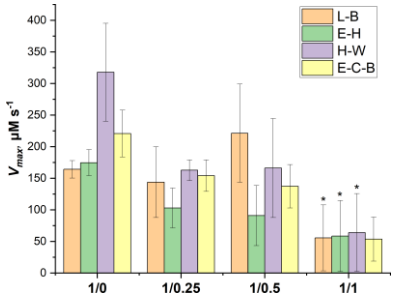
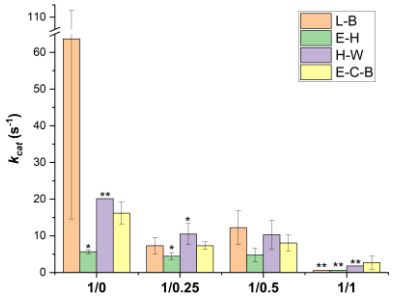
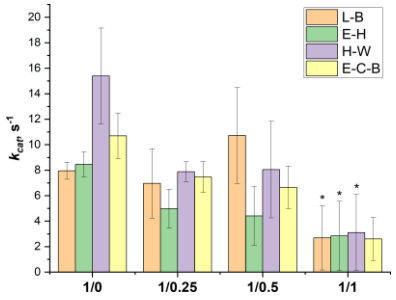
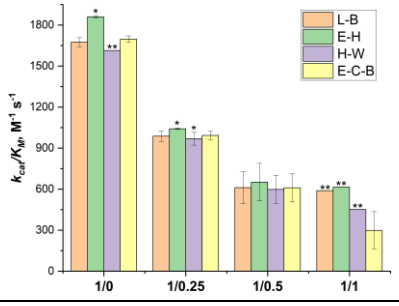
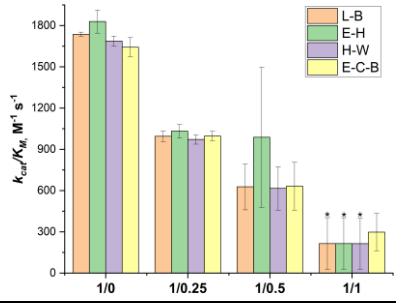
Parameter	Raw datasets	Processed datasets
K_M		
V_{max}		
k_{cat}		
k_{cat}/K_M		

Table S5 Results of K_M, V_{max}, k_{cat} and k_{cat}/K_M with different [bCAII]/[Acetazolamide] molar ratios, calculated using L-B, E-H, H-W and E-C-B methods for raw and processed datasets. Ratios 1/0 – uninhibited bCAII (control). Asterisks (* and **) denote the number of negative results in the analysis.

Parameter	Raw datasets	Processed datasets
K_M		
V_{max}		
k_{cat}		
k_{cat}/K_M		

SANTRAUKA

Įvadas

Naujų biokatalizatorių identifikavimas ir charakterizavimas, bei jų tyrimai ir vystymas technologiniuose procesuose yra paremti funkcine analize. Funkcinės analizės metu yra aptinkami cheminių arba fizikinių savybių skirtumai tarp substrato ir fermento katalizuojamos reakcijos metu susidariusio produkto (Reymond, 2008). Šiuos skirtumus apima oksidacinis potencialas, šviesos absorbcijos savybės, elektroninis tankis, cheminių ryšių virpesių dažniai ir kitos savybės. Analizės metu taip gali būti aptinkami reakcijos metu sukelti fiziniai reiškiniai, tokie kaip chemiliuminescencija arba laisvosios energijos (šilumos) pokyčiai. Funkcinės analizės metodai gali būti skirstomi į kokybinius ir kiekybinius, pagal gaunamų rezultatų formą (Babinskas and Matijošytė, 2025). Visgi, nepriklausomai nuo taikomo metodo, substratas yra esminė biokatalizatorių funkcinės analizės dalis.

Lakazės yra multi-vario oksidazės (EC 1.10.3.2), kurių aktyvųjį centrą sudaro T1, T2 and T3 vario kompleksai. Šie biokatalizatoriai tyrinėjami jau daugiau nei 100 metų, per kuriuos buvo surinkta daugybė informacijos apie jų katalitinį mechanizmą sudarančius procesus, redokso potencialus, šių fermentų šaltinius ir potencialias pritaikymo sritis (Jones and Solomon, 2015). Lakazės katalizuoja unikalią aromatinių alkoholių, aminų ir tiolių oksidaciją panaudojant molekulinį deguonį kaip ko-substratą ir susidarant vandeniui kaip šalutiniam produktui (Jones and Solomon, 2015). Ši reakcija yra itin dominanti maisto, tekstilės, popieriaus, biokuro, kosmetikos, dažų, baldų industrijas bei jos taikymas organinės sintezės, nanobiotechnologijų ar bioremiadiacijos technologijose (Mate and Alcalde, 2017). Papildomų mediatorių taikymas leidžia praplėsti lakazių substratų spektrą ir pakeisti agresyvius cheminius oksidatorius naudojamus industriniuose procesuose. Tačiau, realus šių fermentų taikymas susiduria su daugybe problemų, tokių kaip žemas stabilumas, mažas komercinių preparatų pasirinkimas bei didelė kaina, neefektyvios fermentų biosintezės sistemos ir imobilizacijos metodai. Vienas iš veiksnių limituojančių naujų lakazių atradimus su geresnėmis savybėmis yra nepakankamai platus substratų pasirinkimas aukšto našumo atrankos metodams. Šiuo metu ABTS yra pagrindinis substratas naudojamas lakazių funkcinėje analizėje (Babinskas and Matijošytė, 2025). Spektrofotometriniuose metoduose jo veikimas yra patenkinamas (Mander et al., 2006), tačiau, šis junginys pasižymi žemu temperatūriniu ir pH stabilumu, yra nespecifinis ir ganėtinai brangus.

Karboanhidrazės (CA) yra metalo-fermentų šeima (EC 4.2.1.1), kuri katalizuoja grįžtamąją CO_2 hidrataciją. Šie fermentai plačiai paplitę gamtoje dėl jų funkcijos dalyvaujant CO_2 transportavime ir pH homeostazėje (Aspatwar et al., 2022). Karboanhidrazės yra intensyviai tyrinėjamos kaip farmaciniai taikiniai, bet pastaruoju metu susilaukė daug dėmesio kaip potencialūs katalizatoriai CO_2 fiksavimo technologijose (Effendi and Ng, 2019). Jų katalizuojama CO_2 hidratacija yra laikoma viena iš greičiausių žinomų biokatalizinių reakcijų, todėl šie fermentai yra patrauklus pasirinkimas. Deja, šiuo metu žinomos laukinio tipo CA arba modifikuoti variantai yra nepakankamai stabilūs industrinėmis sąlygomis. Tyrėjai bando įvairias strategijas, pasitelkiant genų inžinerija, fermentų imobilizaciją ir kitus metodus, tobulinti ir stabilizuoti šiuos fermentus. Nepaisant to, vienas iš aspektų limituojančių šių strategijų taikymą ir tyrimus yra nepakankamai patikimi fermentinio aktyvumo matavimo metodai.

Darbo tikslas buvo sukurti naujus sintetinius substratus ir analitines metodologijas fermentų funkcinei analizei, pasitelkiant lakazes bei karboanhidrazes kaip modelinius biokatalizatorius.

Darbo uždaviniai:

1. Sukurti ir optimizuoti ferbamino sintezę bei pritaikomumą aukšto našumo lakazinio aktyvumo patikrai naudojant agaro lėkštelių metodus.
2. Įvertinti ferbamino tinkamumą lakazės aktyvumui aptikiti įvairiose biologinės kilmės ir aplinkos mėginių matricose.
3. Susintetinti ir struktūriškai charakterizuoti fenolio azodažų seriją.
4. Išvystyti fenolio azo dažų karbonatų ir tiokarbonatų substratų sintezės metodus.
5. Ištirti fenolio azodažų karbonatų, tiokarbonatų, acetato ir susijusių esterių substratų pritaikomumą karboanhidrazių charakterizavimui.

Darbo naujumas

Šiame darbe buvo sprendžiamas ilgalaikis didelio našumo metodų, skirtų lakazės aktyvumui aptikti, trūkumas pasitelkiant **naują fenazino tipo substratą ferbaminą**, skirtą agaro lėkštelių metodams. Kitaip nei įprasti lakazės substratai, ferbaminas buvo specialiai sukurtas įgalinti greitą, vizualinį ir didelio našumo lakazės aktyvumo aptikimą neapdirbtuose biologiniuose mėginiuose bei mikroorganizmų kolonijose. **Nauja ferbamino sintezės strategija** buvo sukurta modifikuojant klasikinę metileno mėlynojo sintezę, paremtą *N*,*N*-dimetil-*p*-fenilendiamino (DMPD) reakcijomis. Reakcijos sąlygų optimizacija davė atsikartojantį sintezės procesą su 0,92 % išeiga. Išsamus sintezės tarpinių junginių ir produktų struktūrinis

charakterizavimas, pasitelkiant HRMS, BMR ir ATR-FTIR metodus, leido pasiūlyti **anksčiau neaprašytą ferbamino susidarymo mechanizmą**. Šis mechanizmas ne tik paaiškina tikslinio substrato susidarymą, bet ir pagilina fenilendiaminų oligomerizacijos procesų supratimą bei pasiūlo potencialių fenazino-tipo substratų sintezės kelią su geresnėmis analitinėmis savybėmis. Ferbamino, kaip lakazės substrato, pritaikomumas buvo išsamiai patvirtintas atliekant fizikocheminį charakterizavimą, biologinio suderinamumo vertinimą ir didelio masto atranką. Substratas pasižymėjo aukštu terminiu stabilumu rūgštinėse sąlygose, o lakazinio aktyvumo aptikimas puikiai koreliavo su spektrofotometriniu metolio metodo rezultatais. Ferbamino veikimas buvo papildomai patvirtintas naudojant 65 grybų baltymų ekstraktus, atstovaujančius 42 rūšis, įskaitant 26 rūšis, kurios anksčiau nebuvo tirtos dėl lakazės aktyvumo. Be to, substratas leido atlikti didelio našumo 207 aplinkos izoliatų iš dinarinių urvų atranką, kurioje identifikuotas *Pseudomonas chlororaphis* kamienas pasižymintis ženkliu lakaziniu aktyvumu. Šie rezultatai pademonstruoja ferbamino tinkamumą fermentų atradimui ir mikrobų biožvalgybai.

Siekiant funkciškai charakterizuoti karboanhidrazes (CA), šiame darbe buvo tyrinėjamos **nepakankamai išnaudojamos karbonatų ir tiokarbonatų esterių substratų klasės**. Jų įtraukimas išplečia sintetinių substratų, skirtų CA katalizei tirti, pasirinkimą. Buvo sukurtos ir optimizuotos naujos transkarbonizacijos metodikos, skirtos susintetinti aktyvuotų azodažų karbonato esterių seriją. Tarp jų bis(HABSA)c pasirodė kaip perspektyvus substratas spektrofotometriniams tyrimams. Tačiau netikėta jo sąveika su baltymų struktūromis atskleidė **anksčiau nežinomą aktyvuotų karbonatų esterių apribojimą** fermentinio aktyvumo matavimams. Siekiant įveikti šį iššūkį, buvo sukurta **nauja eksperimentinė strategija**, pagrįsta selektyvia fermento inhibicija su acetazolamidu, leidžianti atskirti substrato hidrolizės katalizinį komponentą nuo nekatalizinių procesų ir tiksliau įvertinti fermentų aktyvumą. Šiame darbe taip pat pateikiamas **pirmasis sisteminis azodažų tiokarbonato esterių**, kaip karboanhidrazių substratų, tyrimas. Išbandžius tris sintezės metodus, buvo sėkmingai sukurtas fenilo HABSA tiokarbonato gamybos būdas. Gautasis substratas pasižymėjo geresne katalizuojama hidrolize, palyginus su karbonato analogu, ir pademonstravo tiokarbonato esterių potencialą karboanhidrazės funkciniams tyrimams. Siekiant pagilinti eksperimentinių stebėjimų rezultatus, buvo naudojamas molekulinis (MD) modeliavimas. MD atskleidė šiuolaikinių skaičiavimo metodų, skirtų metalofermentų modeliavimui, apribojimus bei įžvalgas parodančias šių metodų platesnius trūkumus. Lygiagrečiai buvo susintetinti karbamato ir karbazato junginiai ir įvertinti kaip potencialūs karboanhidrazės substratai.

Buvo parodyta, kad šios junginių klasės netinka karboanhidrazės katalizuojamai hidrolizei, tokiu būdu susiaurinant būsimų substratų kūrimo kriterijus. Pagrindinis šio darbo metodologinis proveržis buvo **acetilinto HABSA substrato** sukūrimas, kuris peržengė karbonatų pagrindu pagamintų junginių apribojimus. Šis substratas pasižymėjo geresniais rezultatais kinetiniuose, termodinaminiuose ir inhibicijos tyrimuose, palyginus su įprastais karboanhidrazės substratais, *p*-nitrofenil acetatu ir indoksilo acetatu. Šis junginys yra **naujas bei patobulintas analitinis įrankis karboanhidrazės funkcinei analizei**. Be to, buvo sukurtas naujas *ad hoc* statistinis metodas klaidingiems kinetiniams duomenų taškams nustatyti, pagerinantis Michaelis-Menten analizės patikimumą bei prisidedantis prie tikslesnių fermentinių katalizinių parametrų apskaičiavimo.

Ginamieji teiginiai:

1. Ferbaminas yra naujas fenazino pagrindu pagamintas substratas lakazės aktyvumui nustatyti, pasižymintis dideliu terminiu stabilumu, mažu toksiškumu ir tinkamumu ilgalaikiams, didelio našumo tyrimams įvairiose biologinėse ir aplinkos matricose.
2. Siūlomas ferbamino susidarymo mechanizmas praplečia supratimą apie fenilendiaminų oligomerizaciją ir suteikia pagrindą racionaliam naujų fenazino pagrindo substratų kūrimui.
3. Karbonilo funkcinės grupės struktūra yra pagrindinis veiksnys lemiantis jautrumą karboanhidrazės katalizuojamai hidrolizei: karbonato ir tiokarbonato esteriai fermentiniu būdu yra hidrolizuojami substratai, o karbamato ir karbazato analogai yra atsparūs fermentinei katalizei.
4. 4-(4-hidroksifenilazo)benzensulfonrūgšties acetatas (HABSA-Ac) yra naujos kartos karboanhidrazės substratas, pasižymintis didesniu termodinaminiu stabilumu, minimalia nefermentine autohidrolize ir didesniu selektyvumu, palyginti su įprastiniais esterių pagrindo metodais.
5. Sintetinių karboanhidrazės substratų funkcinį veikimą lemia ne tik jų cheminis reaktyvumas, bet ir sąveika su baltymų struktūromis, išryškinanti, kad substratų kūrimo metu reikia atsižvelgti tiek į jautrumą fermentinei katalizei, tiek į nekatalizines sąveikas su baltymais.

REZULTATAI IR DISKUSIJA

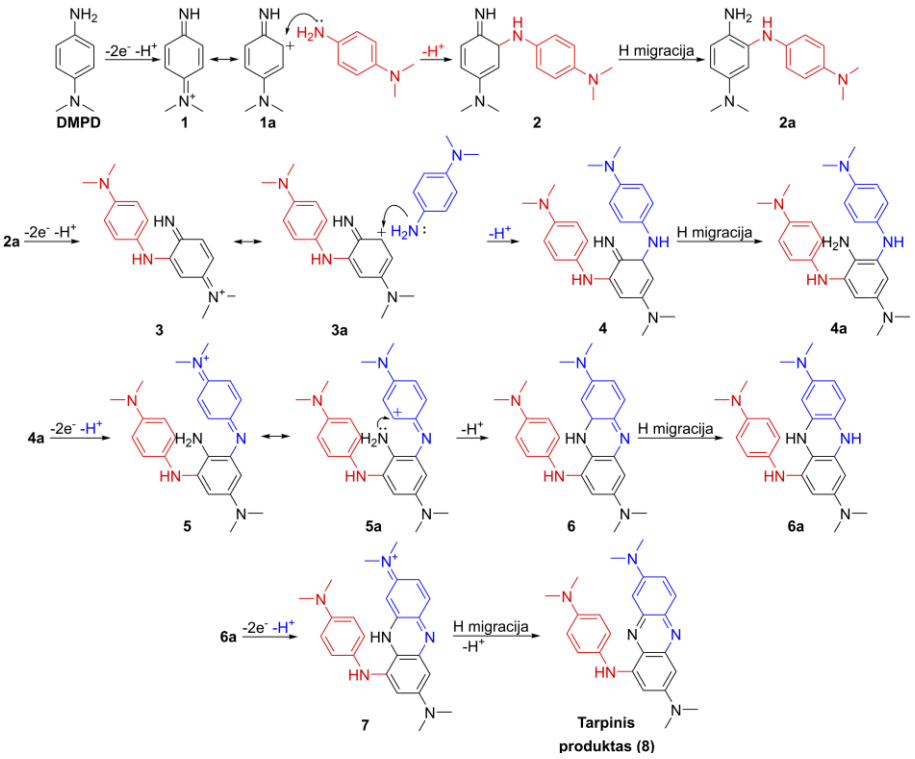
Ferbamino sintezės optimizacija

Pirminis ferbamino (*N*-(4,9-bis(dimetilamino)-3a^2,7,11-triazanafto[3,2,1,8-*mnoa*]aceanfrilen-3(7*H*)-iliden)-*N*-metilmetanoamonis) sintezės variantas buvo paremtas metileno mėlynojo dažo sintezės principu. Šio dažo sintezės metu yra atliekama *N*,*N*-dimetil-*p*-fenilendiamino (DMPD) oksidacija, reakcijos mišinyje esant tiosulfatui. Ferbamino sintezės atveju nukleofilas nebuvo naudojamas, todėl vietoje jo neoksiduotas DMPD atliko nukleofilinę ataką. Tai lėmė DMPD oligomerizaciją, kuri antrajame sintezės žingsnyje buvo pratęsiama pakeliant temperatūrą. Pirminė ferbamino sintezės varianto išeiga siekė tik 0,27 %, todėl buvo atlikta optimizacija, keičiant DMPD-oksidatoriaus santykį, tobulinant pašalinių junginių pašalinimą, nustatant geriausią organinių tirpiklių ir/arba mišinių pritaikymą termo-oksidacijoje bei įvertinant tinkamą oligomerizacijos trukmę. Optimizacijos metu buvo nustatyta, kad DMPD ir oksidatoriaus santykis 1:1 buvo geriausias, nes mažesni oksidatoriaus kiekiai lėmė žemesnę išeigą, o didesni – papildomų pašalinių junginių susidarymą. Toliau buvo nustatyta, kad pašaliniai produktai buvo ganėtinai efektyviai pašalinami tarpinį produktą virinant etilacetate (EtOAc). Oligomerizacijos reakcijai pabaigti geriausios sąlygos buvo 4 val virinimas 5 % metanolio (MeOH) vandeniniame tirpale. Po sintezės optimizacijos, išeiga pasiekė 0,92 %. Galutinė produktų sudėtis ir priemaišų kiekiai buvo įvertinti naudojant analizinę aukšto našumo skysčių chromatografiją (HPLC) su dr. Andriaus Sakalausko pagalba (Amiloidų tyrimų sektorius, Vilniaus universitetas). Analizėje aptikti trys panašių koncentracijų produktai ir nedidelis kiekis priemaišų ($\leq$ 5 %). Kadangi ferbamino taikymas buvo numatytas kokybiniams tyrimams agaro lėkštelėse, o ne kiekybinėms analizėms, šis rezultatas buvo patenkinamas. Tarpiniai ir galutiniai produktai buvo identifikuoti pasitelkiant skysčių chromatografiją kombinuotą su aukštos raiškos masių spektrometrija (LC-HRMS), atliktą Martyno Malikėno (Organinės Chemijos Katedra, Chemijos ir Geomokslų fakultetas, Vilniaus Universitetas).

Ferbamino sintezės mechanizmo analizė

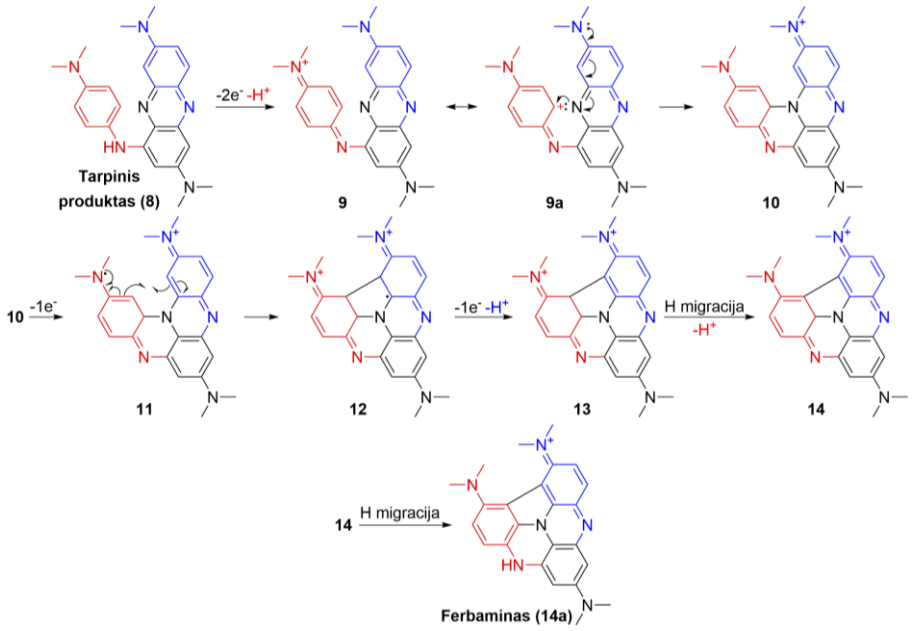
Siekiant prisidėti prie fenilendiaminų oligomerizacijos mechanizmo supratimo, buvo atlikta ferbamino sintezės analizė, pasiūlyti tarpinių bei galutinių produktų susidarymo mechanizmai. Mechanizmams sudaryti buvo atlikta ATR-FTIR, BMR analizės, pasiremta LC-HRMS bei publikuotais DMPD (Molina-Fernández and Luis, 2021) ir *o*-fenilendiamino

elektrocheminės oksidacijos ir oligomerizacijos duomenimis (Trivedi et al., 2016). Tarpinių (oksidacijos žingsnio) produktų susidarymo mechanizmo schema pateikta **Schemoje 1**, o galutinio **Schemoje 2**.



Schema 1. Pasiūlytas ferbamino tarpinio produkto sintezės mechanizmas.

Šio mechanizmo esmė yra trys pasikartojantys žingsniai: 1) DMPD fragmento oksidacija; 2) DMPD nukleofilinė ataka į oksiduotą DMPD fragmentą; 3) struktūros persitvarkymas ir stabilizavimasis. DMPD fragmento oksidacijos metu susidaro benzochinono diiminio fragmentas (**1**, **3**, **5**, **7**), kurio *meta* padėtyje, dimetiliminio grupės atžvilgiu, rezonansinės struktūros (**1a**, **3a**, **5a**) turi teigiamą krūvį. Šis dalinis krūvis selektyviai nukreipia atakuojantį DMPD į šią padėtį. Po nukleofilinės atakos seka H atomo migracija (**2a**, **4a**, **6a**, **8**), kurią lemia struktūros stabilizacija susidarant didesnei delokalizuotų π-elektronų sistemai (aromatizacija). Oligomerizacija sulėtėja ties ferbamino tarpinio produkto susidarymu **8**, nes susidaręs junginys išsėda iš vandeninės reakcijos terpės. HRMS analizėje aptikti aukštesnės molekulinės masės fragmentai parodė, kad nedidelė dalis oligomerų lieka ištirpusi ir dalyvauja tolimesnėse reakcijose.



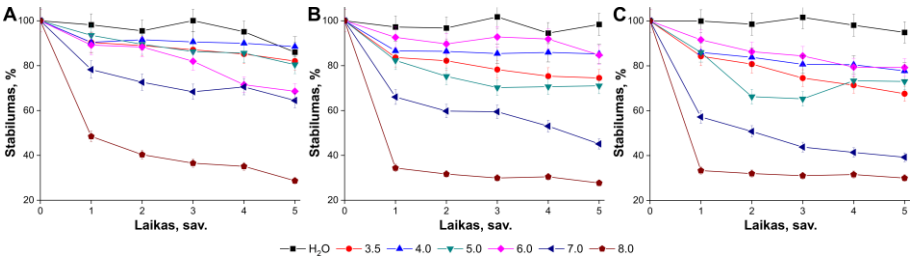
Schema 2. Pasiūlytas sintezės mechanizmas iš tarpinio produkto į ferbaminą.

Remiantis surinktais duomenimis, ferbamino tarpinio junginio virtimas galutiniu produktu yra termiškai pagreitintos autooksidacijos pasekmė. Šis procesas vyksta tokiu pačiu principu iki **10** susidarymo, kaip ir **Schemoje 1**. Po to, vyksta monoelektroninė oksidacija, dėl kurios susidaro radikalkatijonas **11**. Šis junginys reaguoja radikalinio prijungimo būdu prie *α* padėties (*N*,*N*-dimetiliminiumo grupės atžvilgiu), sudarydamas naują C-C jungtį (**12**). Paskutinis etapas yra H poslinkis (**14** ir **14a**) lemiamas termodinamiškai palankaus delokalizuotos elektronų sistemos dydžio padidėjimo. Susidariusi ferbamino molekulė yra pilnai konjuguota; taigi, ji turi daugybę rezonansinių formų (neparodyta), delokalizuojančių ir stabilizuojančių teigiamą krūvį.

Ferbamino savybių ir taikymo tyrimai

Pagrindinis keliamas reikalavimas naujam lakazės substratui buvo sąlyginai aukštas pH ir temperatūrinis stabilumas. Šios savybės reikalingos atliekant ilgesnės trukmės mėginių inkubacijas ant agaro siekiant aptikti fermentinį aktyvumą. Pirmojo eksperimento metu buvo išmatuoti natyvaus ir oksiduoto, bei redukuoto ferbamino tirpalų UV-Vis spektrai. Jie parodė, kad ferbamino absorbcijos maksimumas yra ties ~550 nm, o oksiduotas substratas pasižymi plačiu spektru su maksimumu ties ~350 nm. Kadangi ši spektroskopija leido kiekybiškai išreikšti substrato oksidacinį būvį, sekančio tyrimo metu ji buvo pasitelkta ištirti pH ir temperatūros įtaką ferbamino stabilumui. Substratas 50 mM koncentracijos pH 3,5-8,0 buferiuose buvo

inkubuojamas 20 °C, 30 °C ir 37 °C, iki penkių savaičių. Vandeninis ferbamino tirpalas naudotas kaip kontrolė jonų įtakai. Junginio stabilumas buvo įvertinamas procentaliai, pagal absorbcijos reikšmės pokytį lyginant su pradiniu tirpalu atitinkamame pH ir bangos ilgyje. Rezultatai pateikti **1 pav.**



1 pav. Ferbamino tirpalų pH ir temperatūrinis stabilumas. Inkubavimo temperatūros: **A** 20 °C, **B** 30 °C, **C** 37 °C.

Duomenys parodė, kad ferbamino stabilumas stipriai priklauso nuo pH, bet ne nuo temperatūros. Visais atvejais po pirmos savaitės, ties pH 8,0, buvo stebimas stiprus stabilumo nukritimas iki 30-50 %. Ties pH 7,0, stabilumas buvo didesnis ir labiau priklausė nuo temperatūros – keliant temperatūrą stabilumas krito greičiau. Kitose pH reikšmėse pokyčiai buvo mažesni. Taip pat buvo pastebėta, kad buferio jonai turėjo neigiamos įtakos substrato stabilumui. Palyginimui, ABTS platintojai deklaruoja, kad ABTS pH 5,0 buferyje galima laikyti 4 °C dvi savaites, o -20 °C – penkias (ABTS Sigma-Aldrich®). Kitam tipiniam lakazės substratui, siringaldazinui, ištirpinti reikia MeOH, todėl yra nesuderinamas su agaro lėkštelių metodais ir mikroorganizmais (Syringaldazine SIGMA-ALDRICH®, 2009).

Ferbamino taikymo tyrimai buvo atliekami pasitelkiant substrato-agaro lėkšteles. Jų metu, ferbamino-agaro lėkštelių panaudojimas buvo testuojamas didinant mėginių kompleksiškumą: 1) komercinis lakazės produktas su patvirtintu lakaziniu aktyvumu; 2) baltymų ekstraktų kolekcija su daug potencialių lakazės kandidatų; 3) mikroorganizmų kultivavimas, kurie gali turėti lakazinį aktyvumą. Pirmojo etapo metu buvo patvirtinta, kad lakazė katalizuoja ferbamino oksidaciją. Tam panaudotas komercinis lakazės produktas Novozymes® 51003, kuris parodė, kad substrato katalizės metu spalva pasikeičia iš violetinės į gelsvą ir šį pokyti galima įvertinti vizualiai. Sekančio etapo metu buvo vertinamas ferbamino veikimas atpažįstant lakazinį aktyvumą baltymų ekstraktuose. Šiam tyrimui naudota 65 baltymų mėginių iš 42 grybų rūšių kolekcija buvo padovanota dr. Jerica Sabotič iš Jozefo Stefano instituto (Slovėnija), bendradarbiaujant per COST veiklą CA18238 „Ocean4Biotech“. Eksperimento metu buvo paruoštos agaro lėkštelės su 37,5 μg ml^{-1} ferbamino koncentracija ir šulinėliais. Į šulinėlius įpilta po 2 μl

baltymų ekstrakto ir lėkštelės inkubuotos 20 °C, 20 val. Paraleliai, lakazinis aktyvumas ekstraktuose buvo išmatuotas naudojant metolio UV-Vis spektrofotometrinį metodą (**Lentelė 1**).

Lentelė 1. Lakazinio aktyvumo rezultatai grybų ekstraktų kolekcijoje. Duomenų eiliškumas pateiktas pagal metolio metodo rezultatus.

Ekstrakto Nr.	Rūšis	Metodas		Puklikuoti duomenys apie lakazę[b]
		Metolis, U ml^{-1}[a]	Ferbaminas	
3	*Clitocybe nebularis*	9.00	+++	Taip (Asav, 2021)
39	*Psilocybe cubensis*	5.40	+++	Taip (Lenz et al., 2020)
6	*Cortinarius violaceus*	5.25	+	Ne (Chen et al., 2003)
2	*Macrolepiota procera*	4.80	+++	Taip (Luis et al., 2004)
50	*Gomphidius glutinosus*	3.90	-	Netestuota
53	*Pleurotus eryngii*	2.70	+++	Taip (Guo et al., 2017)
1	*C. nebularis*	2.55	+++	Taip (Asav, 2021)
67	*Rhodocybe gemina*	1.65	+	Netestuota
15	*Tricholoma tigrinum*	1.65	+	Netestuota
66	*Tricholoma saponaceum*	1.50	++	Taip (Khaund and Joshi, 2014)
33	*Lentinula edodes*	1.13	-	Taip (Yano et al., 2009)
5	*Ganoderma lucidum*	1.05	++	Taip (Jeon et al., 2008)
55	*Gymnopilus penetrans*	0.90	+	Ne (Marr et al., 1986)
9	*Cortinarius caperatus* (*Rozites caperata*)	0.83	+++	Netestuota
62	*Amanita vaginata*	0.83	+	Netestuota
47	*Anthurus archeri* (*Clathrus archeri*)	0.75	+	Netestuota
18	*Pleurotus ostreatus* (summer strain)	0.75	+	Taip (Park and Park, 2014)
35	*Clitocybe geotropa*	0.68	+	Netestuota
54	*Amanita spissa*	0.68	-	Ne (Chen et al., 2003)
70	*A. vaginata*	0.68	-	Netestuota
51	*Tricholomopsis rutilans*	0.68	-	Netestuota
59	*Clavariadelphus pistillaris*	0.60	+	Taip (Marr et al., 1986)
40	*Ramaria stricta*	0.53	-	Taip (ABTS, gujakolis), Ne (syringaldazinas) (Erden et al., 2009)
20	*P. ostreatus* (winter strain)	0.45	+	Taip (Park and Park, 2014)
36	*Russula alutacea*	0.45	+	Netestuota
57	*Clitocybe geotropa*	0.38	-	Netestuota
31	*Paxilllus atrotomentosus*	0.38	-	Netestuota
69	*Cortinarius multiformis*	0.30	++	Netestuota
32	*Clitocybe gibba*	0.30	-	Netestuota
28	*Lactarius necator*	0.23	-	Netestuota

Lentelė 1. Tęsinys

63	*Amanita rubescens*	0.15	-	Ne (Hutchison, 1990)
58	*Craterellus cornucopioides*	0.15	-	Netestuota
43	*P. ostreatus*	0.15	-	Taip (Park and Park, 2014)
42	*Xerocomus badius*	0.15	-	Ne (Hutchison, 1990)
65	*Agaricus bisporus*	0.08	-	Taip (Mayolo-Deloisa et al., 2011)
41	*A. rubescens*	0.08	-	Ne (Hutchison, 1990)
42	*A. rubescens*	0.08	-	Ne (Hutchison, 1990)
46	*P. atrotomentosus*	0.08	-	Netestuota
24	*Amanita excelsa*	-	+	Netestuota
16	*Macrolepiota rachodes*	-	+	Ne (Luis et al., 2004)
8	*Amanita citrina*	-	-	Ne (Hutchison, 1990)
61	*A. citrina*	-	-	Ne (Hutchison, 1990)
64	*A. citrina*	-	-	Ne (Hutchison, 1990)
37	*A. rubescens*	-	-	Ne (Hutchison, 1990)
60	*A. spissa*	-	-	Ne (Chen et al., 2003)
68	*A. spissa*	-	-	Ne (Chen et al., 2003)
21	*Armillaria borealis*	-	-	Netestuota
22	*Boletus badius*	-	-	Netestuota
11	*Boletus erythropus*	-	-	Netestuota
25	*Coprinus comatus*	-	-	Taip (Bao et al., 2013)
34	*Fomitopsis pinicola*	-	-	Taip (Park and Park, 2014)
23	*Kuehneromyces mutabilis*	-	-	Taip (Gramss, 2020)
14	*L. necator*	-	-	Netestuota
19	*L. edodes*	-	-	Taip (Yano et al., 2009)
56	*Lycoperdon perlatum*	-	-	Taip (Harkin et al., 1974)
27	*Sparassis crispa*	-	-	Netestuota
10	*Suillus bovinus*	-	-	Ne (Timonen and Sen, 1998)
38	*Suillus granulatus*	-	-	Taip (Cullings et al., 2008)
17	*Suillus luteus*	-	-	Ne (Mucha, 2011)
30	*Suillus variegatus*	-	-	Netestuota
26	*Tricholoma sulphureum*	-	-	Netestuota

[a] 1 U apibrėžtas kaip 1 μmol metolio oksiduoto per 1 min, esant pH 5.0 ir 20 °C.
[b] Taip – lakazės genas arba aktyvumas yra patvirtinti rūšyje; Ne – rūšis buvo testuota, bet lakazės genas arba aktyvumas nebuvo aptikti; Netestuota – lakazės genai arba aktyvumas netirti rūšyje.

Tyrimas pademonstravo, kad ferbamino ir metolio rezultatai stipriai koreliuoja bei abu metodai leidžia aptikti fermentinius aktyvumus, kurie nebuvo identifikuoti kitais metodais arba iki šiol nebuvo tirti šiose grybų rūšyse. Penkiuose mėginiuose rezultatai išsiskyrė. Šešiuose mėginiuose yra

publikuota duomenų apie lakazės geną arba aktyvumą, bet metolis ir ferbaminas neaptiko fermentinio aktyvumo. Šie nesutapimai galėjo atsirasti dėl skirtingo fermentų specifiškumo, itin mažo fermento kiekio arba analizės sąlygų. Šiais eksperimentais buvo patvirtintas ferbamino tinkamumas aptikti lakazinį aktyvumą baltymų produktuose ir ekstraktuose, todėl toliau buvo einama prie aukštesnio kompleksiškumo – aktyvumo identifikavimas mikroorganizmuose.

Vienas iš svarbių aspektų taikant substratus agaro lėkštelėse yra jų suderinamumas su terpės komponentais. Testuojant dvi terpes, Luria-Bertani (LB) ir mielių ekstrakto-peptono-gliceriolio (YEPG), buvo identifikuota, kad autoklavuojant ferbaminą su peptonu, substratas yra oksiduojamas. Kad būtų išvengta šios, bei galimų nepageidaujamų sąveikų su kitais komponentais, buvo nustatytas geriausias būdas kaip paruošti ferbamino-agaro lėkšteles su mitybiniais komponentais. Mitybinės terpės komponentai, įskaitant agarą, autoklavuojami koncentruotame tirpale ir po to praskiedžiami autoklavuotu ferbamino tirpalu iki reikiamos koncentracijos. Šis principas minimalizuoja nereikalingas sąveikas, bet taip pat turi ir kelis trūkumus. Dėl didėjančios klampos mitybinės terpės koncentrate, agaro koncentracija koncentrate negali viršyti 9 %. Taip pat, ferbaminas yra praskiedžiamas, todėl sumažėja jo didžiausia galima koncentracija. Nepaisant to, šis principas leido ferbaminą naudoti su bet kokiu terpės tipu, nepriklausomai nuo jo sudėties.

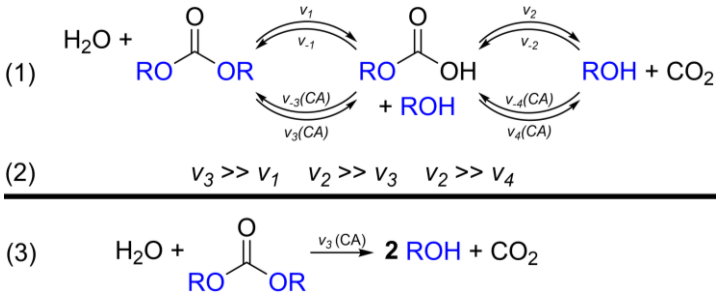
Sekančio etapo metu buvo įvertinama ferbamino įtaka mikroorganizmų augimui. Tam buvo pasirinkta kultivuoti įprastai laboratorijose naudojamus mielių kamienus *Kluyveromyces marxianus*, *Kluyveromyces lactis*, *Pichia pastoris*, *Saccharomyces cerevisiae*, bei Gram-teigiamas bakterijas *Rhodococcus erythropolis*, *Bacillus pumilus* ir Gram-neigiamas *Escherichia coli*, *Pseudomonas putida* ant mitybinių agaro lėkštelių papildytų 37,5 μg ml^{-1}, 22,5 μg ml^{-1}, 4,5 μg ml^{-1} ir 0 μg ml^{-1} (kontrolė) ferbaminu. Mikroorganizmų kultivavimai buvo vykdomi iki 168 val. Eksperimento rezultatai parodė, kad substratas visiškai nepaveikė *E. coli* ir *P. putida* augimo – po naktinio auginimo (~14 val) ant 37,5 μg ml^{-1} lėkštelių mikroorganizmų augimas nesiskyrė nuo kontrolės. Šis pastebėjimas buvo patvirtintas su dar penkiais Gram-neigiamais kamienais. Tuo tarpu, mielės bei Gram-teigiamios bakterijos su didesne nei 4,5 μg ml^{-1} ferbamino koncentracija net ir po 168 val nepasiekė kontrolėje matomo prieaugio. Šie pastebėjimai išryškino, kad ferbaminas turėjo įtakos mikroorganizmų augimui, bet pasirinkus tinkamą laboratorinį kamieną arba substrato koncentraciją, yra suderinamas su mikroorganizmų kultivavimu.

Įvertinus ferbamino suderinamumą su mikroorganizmais, substrato veiksmingumas aptinkant lakazinį aktyvumą buvo testuojamas naudojant

organizmų kolekciją iš aplinkos mėginių. Ši kolekcija buvo sudaryta iš 207 mikroorganizmų, kurie buvo užauginti iš urvų mėginių surinktų speleologinėje ekspedicijose „Ponor Kovači – Izvor Ričine“ (Tomislavgradas) ir „Balkanų urvų susitikimas“ (Mostaras), vykusiose Bosnijoj ir Hercegovinoj 2022 metais. Lakazinis aktyvumas buvo ieškomas pasitelkiant agarizuotas mitybines terpes (YEPG ir modifikuota Muller-Hinton) papildytas 37,5 μg ml^{-1} ferbaminu ir inkubuojant lėkšteles atitinkamose temperatūrose (20 °C, 30 °C arba 37 °C) iki 196 val. Iš sėkmingai kultivuotų 207 mikroorganizmų kolonijų, 29 neaugo ant terpių su ferbaminu, kuomet keturios kolonijos parodė silpną spalvos pokytį aplink augimo zoną. Šios kolonijos buvo perkeltos ir išsėtos dideliu kiekiu patvirtinti fermentiniam aktyvumui. Viena kolonija neparodė lakazinio aktyvumo, o kitos dvi augimo metu gamino geltonos spalvos junginius, kurie nebuvo ferbamino oksidacijos produktai. Paskutinioji kolonija, išskirta iš karbonatinių mineralų biofilmo vadinamo *moonmilk*, parodė teigiamą lakazinį aktyvumą. Mikroorganizmai iš šios kolonijos buvo išgryninti persėjimo metodu ir identifikuoti pagal 16S RNR ir RpoB geno sekas – atliko dokt. Jokūbas Krutkevičius (Taikomosios biokatalizės sektorius, Vilniaus universitetas). Pagal 100 % ir 99,93 % 16s RNR sutapimą dviejose duomenų bazėse, teigiamą lakazinį aktyvumą parodęs mikroorganizmas buvo priskirtas *Pseudomonas chlororaphis* rūšiai. Šios rūšies atstovai yra žinomi fenazino-tipo antibiotikų gamintojai (Chin-A-Woeng et al., 2000). Kadangi ferbaminas yra fenazino-tipo junginys, jis galėjo aptikti fermentus dalyvaujančius šių junginių biosintezės kelyje. Be to, yra publikuotų duomenų patvirtinančių *P. chlororaphis* rūšies atstovus turinčius silpną lakazinį aktyvumą (Mandic et al., 2019).

Fenilo azo dažų karbonatų substratai

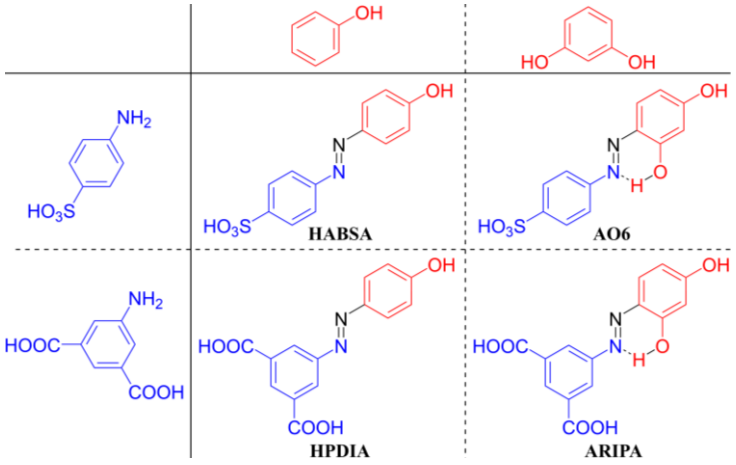
Karbonatų esteriai yra mažai ištyrinėti kaip substratai karboanhidrazės (CA) funkcinei analizei. Tuo tarpu, šie junginiai pasižymi unikalia savybe sujungti dvi dažų molekules karbonilo esterine jungtimi (**Schema 3**).



Schema 3. Supaprastinta karbonatų esterių auto- (v_1/v_{-1}, v_2/v_{-2}) ir CA-katalizuojama (v_3/v_{-3}, v_4/v_{-4}) hidrolizė.

Katalizuojant šios jungties hidrolizę (v_3), susidaro dažo karbonato hemi-esteris, kuris yra itin nestabilus standartinėmis sąlygomis ir suskyla į CO_2 bei atpalaiduoja antrąją dažo molekulę (v_2). Su sąlyga, kad fermentiškai katalizuojama hidrolizė vyksta ženkliai lėčiau negu savaiminė hemi-esterio hidrolizė, vienas fermentinės reakcijos ciklas išlaisvina dvi dažo molekules. Šis efektas pasireiškia dvigubu analitinio signalo intensyvu stebint katalizės procesą, t.y. dvigubu jautrumu. Deja, organinių karbonatų sintezėje ne retai naudojamos itin pavojingos medžiagos, todėl tyrimo metu buvo atliekama sintezės metodų kūrimas bei tobulinimas.

Naujų CA substratų kūrimas buvo pradėtas nuo fenolinių azo dažų sintezės. Šie junginiai buvo pasirinkti naudoti kaip dažai dėl savo gerų UV-Vis spektroskopinių savybių, patenkinamų tirpumų vandeninėje terpėje ir galimybės nesunkiai kombinuoti struktūrinius fragmentus didesniam junginių pasirinkimui. Šiuo atveju buvo pasirinkti fenolis ir resorcinolis (3-hidroksifenolis) bei 4-aminobenzensulfoninė rūgštis ir 5-aminoizoftalio rūgštis. Juos kombinuojant azo derinimo reakcijoje buvo sėkmingai pagaminti keturi dažai: 4-(4-hidroksifenilazo)benzensulfoninė rūgštis (HABSA), 4-(2,4-dihidroksifenilazo)benzensulfoninė rūgštis (AO6), 5-(4-hidroksifenil)isoftalio rūgštis (HPDIA), 5-(2,4-dihidroksifenilazo)isoftalio rūgštis (ARIPA), pavaizduoti **2 pav**.

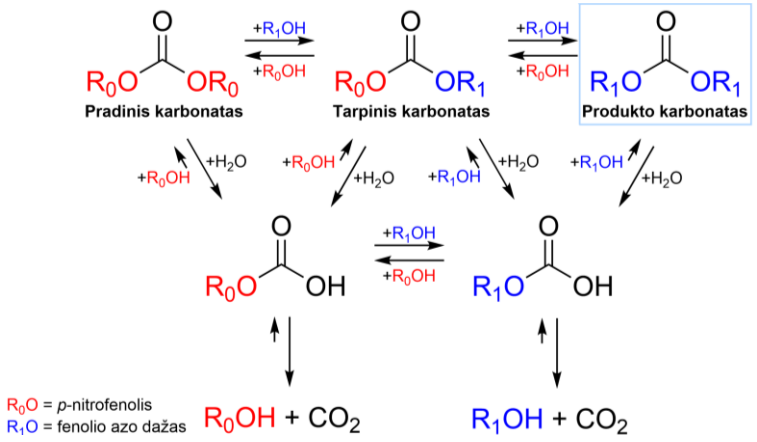


2 pav. Sėkmingai susintetinti azo dažai.

Atlikus šių dažų charakterizavimą buvo įvertinta fenolinių grupių pK_a, medžiagų tirpumas vandenyje ir spektroskopinės savybės. Nustatyta, kad junginiai turintys resorcinolio fragmentą (AO6 ir ARIPA) pasižymi žemu pK_a dėl pirmos -OH grupės vandenilinio ryšio su azo tilteliu – apie 7,0. Kuomet junginiai turintys tik 4-hidroksi grupę (HABSA ir HPDIA) aukštesniu pK_a – 8,32 ir apie 9,0, atitinkamai. Šių junginių moliniai ekstinkcijos koeficientai,

po batochrominio poslinkio dėl fenolinės grupės deprotonizacijos, buvo 13-34 mM^{-1} cm^{-1} ruože ties 428 nm maksimumu.

Sekančio etapo metu buvo kuriama karbonatų esterių sintezės strategija pasitelkiant transkarbonizacijos metodą. Šis metodas remiasi panašiais principais kaip ir transesterifikacija – vienas junginys su -OH grupe gali pakeisti kitą esantį esteryje (**Schema 4**).



Schema 4. Karbonatų transesterifikacijos ir degradacijos keliai.

Transkarbonizacijoje yra itin svarbu palaikyti bevandenę aplinką, kad būtų išvengtas hemi-karbonato susidarymas, kuris veda į karbonato grupės degradaciją. Pradiniu karbonatu buvo pasirinktas bis(*p*-nitrofenilo) karbonatas (BNPC), nes šis junginys yra komerciškai prieinamas, o *p*-nitrofenoliatas yra gerai nueinanti grupė dėl žemo pK_a (7,15) (Peng et al., 2016). Pagrindinis šio karbonato trūkumas yra jo reaktingumas su vandeniu – esant nedideliam drėgmės kiekiui jis skyla į *p*-nitrofenolį (pNP) ir CO_2. Taigi, karbonatų sintezės sukūrimui ir optimizavimui buvo iškelti šie uždaviniai: 1) identifikuoti tirpiklį, kuris būtų tinkamas reagentams ir nesuskaldytų BNPC bei produktų; 2) išsirinkti tinkamiausią amino katalizatorių; 3) nustatyti geriausias reakcijos sąlygas ir produkto išskyrimo būdą; 4) optimizuoti BNPC, dažų ir katalizatoriaus molinius santykius. Pirminiams tyrimams kaip modelinis dažas buvo pasirinkta naudoti HABSA.

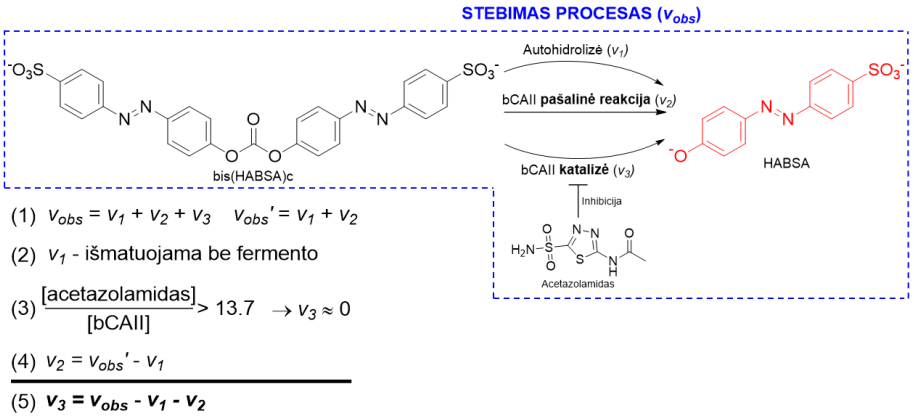
Tirpiklių testavime buvo naudojami tik aprotoniniai tirpikliai, kadangi protoniniai gali dalyvauti pačioje transkarbonizacijoje. Iš testuotų devynių tirpiklių, BNPC stabilumas mažėjo didėjant tirpiklio poliškumui. Buvo iškelta hipotezė, kad stabilumas mažėjo dėl didėjančio tirpiklių higroskopiškumo. Tai buvo patvirtinta naudojant molekuliniais sietais džiovintus DMSO ir DMF – BNPC išliko pilnai nesuskilęs iki 48 val. Iš tirtų keturių amino katalizatorių, DABCO ir DBU netiko, o su piridinu transkarbonizacijos reakcijos vyko itin

lėtai. Trietilaminas (Et_3N) buvo nustatytas kaip geriausias katalizatorius – pagal plonasluoksnės chromatografijos (TLC) rezultatus po 20 min BNPC buvo nebeaptinkamas ir susidarė daug naujo junginio. Produkto išskyrimui iš reakcijos mišinio pasitvirtino anti-tirpiklio pridėjimas, kuris sumažino poliškumą ir išsodino produktą. Geriausias rezultatas gautas pridedant dichlorometano (DCM), nuosėdas surenkant centrifuguojant ir praplaunant su acto rūgštimi, MeOH ir DCM. BMR analizė patvirtino, kad produktas buvo di-pakeistas bis-HABSA karbonatas (trumpinamas [bis(HABSA)c]), gautas 32 % išeiga ir ≤ 98 % grynumu. Tai įrodė, kad reaktingų karbonatų di-esterius galima gauti transkarbonizaciją atliekant vieno-puodo principu ir švelniomis sąlygomis. Paskutinio etapo metu buvo keičiami reagentų moliniai santykiai. Geriausias rezultatas gautas naudojant dažas : katalizatorius : BNPC santykiu 1 : 2 : 1,1. Nustačius optimalius bis(HABSA)c sintezės parametrus (išeiga 50 %), jie buvo adaptuoti kitiems fenilo azo dažams: bis(HPDIA)c išeiga 19 %, bis(AO6)c – 37 %, o b(ARIPA)c – išeiga nenustatyta dėl medžiagos nestabilumo. Lyginant su kitais publikuotais simetrinių karbonatų sintezės rezultatais, naudojančiais BNPC (Brunelle, 1982), išeigos buvo panašios, o reakcijos ženkliai trumpesnės.

Sukūrus gerai atsikartojančius karbonatų sintezės metodus, buvo pereita prie šių junginių taikymo CA aktyvumo matavimuose. Kaip modelinį fermentą buvo pasirinkta naudoti komerciškai prieinamą α klasės CA II išskiriamą iš jaučio (*Bos taurus*) eritrocitų – bCAII. Atlikus pirminius testus buvo nustatyta, kad tik bis(HABSA)c buvo potencialiai tinkamas kaip substratas. bis(AO6)c ir bis(ARIPA)c itin greitai skilo esant vandeninėje terpėje, o bis(HPDIA)c pasižymėjo labai mažu tirpumu vandeninėje terpėje ir organiniuose tirpikliuose. Su bis(HABSA)c buvo atlikta aktyvumo matavimo reakcijos sąlygų optimizacija; nustatytos geriausios sąlygos: 5 % DMSO 10 mM Tris-HCl pH 8,5 buferyje ir 0,2 mM substrato; reakcija stebima 428 nm bangos ilgyje 10 min. Keičiant substrato koncentracijas 0,1-1,0 mM ruože buvo nustatyti preliminarūs bCAII Michaelis-Menten kinetinio modelio parametrai, pasitelkiant regresinę analizę bei tiesines transformacijas.

Siekiant validuoti bis(HABSA)c metodą, buvo atliktas bCAII inhibicijos tyrimas. Jo metu bCAII buvo inkubuojamas su skirtingomis acetazolamido (5-acetamido-1,3,4-tiaziazolo-2-sulfonamidas) koncentracijomis. Šis junginys pasižymi itin dideliu afiniškumu bCAII (K_i 10^{-7}-10^{-8} eilės) ir yra gerai ištyrinėtas kaip modelinis inhibitorius. Aktyvumo matavimo metu buvo keičiamos substrato koncentracijos ir lyginami Michaelis-Menten kinetiniai parametrai. Pirminiai rezultatai parodė, kad su pasirinkta acetazolamido koncentracija fermentas išlaikė 87 % aktyvumo, kuomet, pagal publikuotus duomenis, tikėtasi 12 % (Pocker and Stone, 1967). Testuojant kitas

inhibitoriaus koncentracijas, taip pat buvo nustatyti reikšmingi neatitikimai. Paaiškinti šiems rezultatams buvo iškelta hipotezė, kad substratas reagavo su baltymais ne fermentinės hidrolizės reakcijose. Patvirtinimas buvo gautas aktyvumo matavimą atlikus su nekataliziniu baltymu – jaučio serumo albuminu. Šie duomenys iškėlė fundamentinį klausimą: koks iš tikrųjų yra bCAII katalizinis greitis bis(HABSA)c atveju? Nustatyti reakcijoje vykstančių atskirų greičių indėlį buvo sudaryta eksperimentinė **Schema 5**.



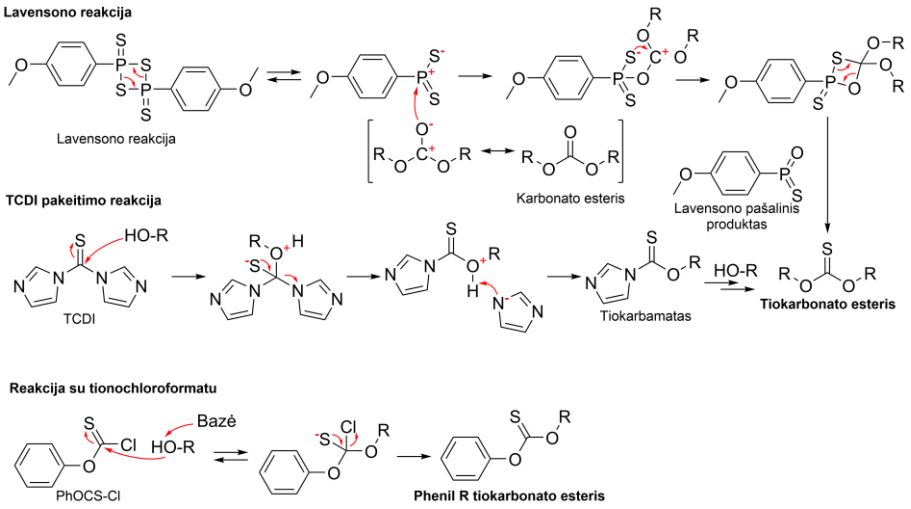
Schema 5. Bis(HABSA)c hidrolizėje vykstantys procesai ir būdas apskaičiuoti jų individualius greičius.

Jos esmė yra, kad visi reakcijoje vykstantys procesai veda į tą pačią baigtį – 2 HABSA molekulių atpalaidavimą, kurio greitis yra v_{obs}. v_1 visada išmatuojamas standartiškai dėl substrato autohidrolizės įvertinimo. $v_2 + v_3$ gaunamas stebint reakciją su aktyviu fermentu, o v_2 – fermentą pilnai inhibavus. Tuomet, v_3 gaunamas iš v_{obs} atimant v_1 ir v_2. Remiantis šiuo eksperimentiniu modeliu buvo nustatyta, kad autohidrolizė sudarė 36,5 %, pašalinės reakcijos su baltymu 49,0 %, o katalizinė reakcija tik 14,5 % viso stebimo bis(HABSA)c hidrolizės proceso. Siekiant nustatyti kas baltymų molekulėse reaguoja su substratu, bis(HABSA)c aktyvumo matavimas buvo atliktas su pasirinktomis N_α-blokuotomis amino rūgštimis. Matavimų rezultatai parodė, kad amino rūgštys su nukleofilinėmis šoninėmis grupėmis ties pH 8,5 (cisteinas, lizinas ir histidinas), yra reaktingiausios. Eksperimentai su glicinu taip pat atskleidė, kad substratas buvo veikiamas katalitiškai, t.y. nesusidaro stabilūs junginiai ir substratas suskaidomas iki laisvų dažų. Sumažinus reakcijos terpės pH iki 7,0, pastebėta, kad bis(HABSA)c nebereagavo su glicinu, o su histidinu ir cisteinu greičiai sumažėjo. Pakartojus substrato eksperimentus su bCAII pagal **Schemą 5**, esant pH 7,0, gauti tokie proceso rezultatai: v_1(autohidrolizė) – 25 %; v_2(pašalinės reakcijos) – 70 %; v_3(katalizė) – 5 %. Pastebėta, kad sumažinus pH sulėtėjo autohidrolizė bei

pašalinės reakcijos, bet bCAII katalizinis greitis tapo itin mažas. Tuo metu nesant kitiems reakcijų sąlygų arba dažų pakeitimo variantams, buvo nuspręsta modifikuoti pačią karbonato funkcinę grupę.

Tiokarbonatų substratai

Tiokarbonatų esterinė funkcinė grupė yra tokia pati kaip karbonatų esteris, tačiau vienas, du arba visi trys deguonies atomai pakeisti į sierą. Taip pat, mono- ir di-tiokarbonatų variantai gali turėti skirtingus izomerus, priklausomai nuo sieros padėties funkcinėje grupėje. Šiam tyrimui buvo pasirinkti mono-tiokarbonatai, kuriuose sieros atomas yra vietoje karbonilinės grupės deguonies (-C=S). Tai leido naudoti sukurtus dažus be papildomų modifikacijų. Iki šiol, tiokarbonatai nebuvo tirti kaip CA substratai ir nebuvo žinoma ar šie fermentai gali katalizuoti jų hidrolizę. Tiesioginė tiokarbonatų sintezės taip pat remiasi pavojingų junginių, tokių kaip tiofosgenas, naudojimu, todėl šiame darbe buvo bandomos trys kitos strategijos (**Schema 6**): i) karbonatų pavertimas tiokarbonatais, pasitelkiant Lavensono reakciją; ii) aminų pakeitimas tiourėjos junginyje tiokarbonildiimidazolas (TCDI); iii) nesimetrinių tiokarbonatų sintezė, naudojant komerciškai prieinamą fenilo tionochloroformatą (PhO-C(S)-Cl).

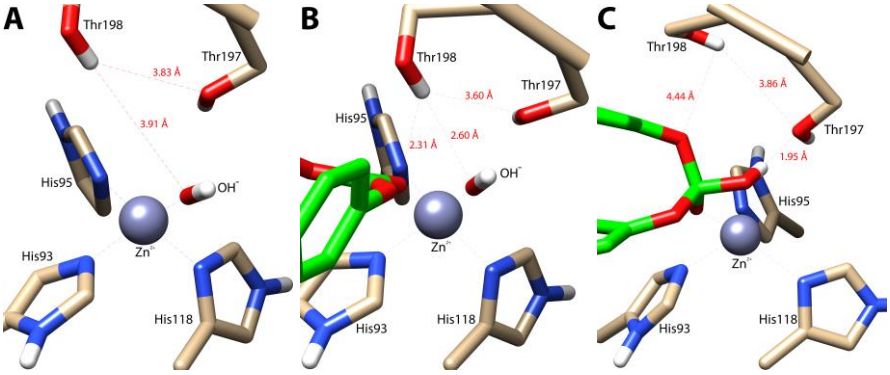


Schema 6. Tirtos tiokarbonatų sintezės strategijos.

Lavensono reakcijoje buvo gautas tik analitiškai aptinkamas bis-(*p*-nitrofenilo) tiokarbonato kiekis, mažesne nei 0,1 % išeiga. Dėl gaunamo produkto itin mažo kiekio ir nestabilumo, jo sudėties nepavyko patvirtinti BMR metodu. Pakeitimo reakcijoje su TCDI reagavo tik pNP, bet susidaręs junginys buvo tiokarbamatas (pNP-C(S)-imidazolas), kuris pasižymėjo žemu

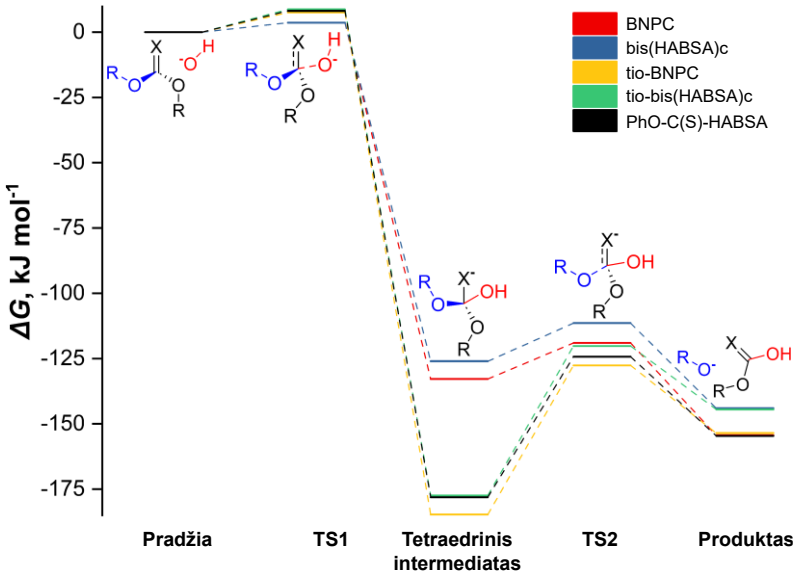
stabilumu ir nedalyvavo tolimesnėse pakeitimo reakcijose. Paskutinė strategija, naudoti tionochloroformato esterį pasitvirtino. Optimizavus reakciją su HABSA, buvo gautas produktas (PhO-C(S)-HABSA) 72,5 % išeiga. Toliau, šis junginys buvo taikytas analogiškai eksperimentui **Schemoje 5** ir suskaičiuoti reakcijos greičių komponentai v_1, v_2 ir v_3. Duomenys parodė, kad šio junginio autohidrolizė (v_1) sudarė 8,4 %, pašalinės reakcijos su bCAII (v_2) – 30,3 %, o katalizinė hidrolizė (v_3) – 61,3 %. Šio substrato katalizinis greitis taip pat buvo didesnis negu bis(HABSA)c: 2,78 μM min^{-1} lyginant su 0,78 μM min^{-1}. Tai ne tik patvirtino, kad karboanhidrazės gali katalizuoti tiokarbonatų esterių hidrolizę, bet šie junginiai, potencialiai, yra geresni CA substratai negu karbonatų esteriai.

Eksperimentinių pastebėjimų papildymui bei gilesniam supratimui, kaip vyksta (tio)karbonatų hidrolizės procesai, buvo pasitelkti *in silico* metodai. Molekulinės dinamikos (MD) simuliacijose buvo stebima kurios amino rūgštys bCAII aktyviajame centre dalyvauja bis(HABSA)c ir OH^- jono pozicionavime prie Zn^{2+}. Simuliacijos trijuose reakcijos etapuose – natyvus fermentas, fermento-substrato kompleksas ir fermento-substrato tarpinis junginys – atskleidė, kad dvi treonino grupės (Thr197 irThr198) atlieka svarbų vaidmenį nukreipiant OH^- ir substratą per vandenilinius ryšius (**3 pav.**).



3 pav. Vidutinės bCAII MD simuliacijų struktūros. Bis(HABSA)c – žalias; vandeniliniai ryšiai – raudoni punktyrai. **A** – natyvus aktyvusis centras; **B** – su bis(HABSA)c; **C** – su bis(HABSA)c tetraetriniu intermediatu.

Buvo bandyta pritaikyti kvantinės mechanikos (QM) skaičiavimus šioms struktūroms, bet dėl MD naudojamų statinių aktyviojo centro parametrų, QM rezultatai nekoreliavo su simuliacijos baigtimi. Todėl, buvo pasirinkta QM taikyti bandant sumodeliuoti kaip vyksta substratų autohidrolizė, dalyvaujant OH^-. Modeliavimas parodė, kad substratų stabilumą stipriai lemia prie karbonilo esantis atomas – O arba S (**4 pav.**).



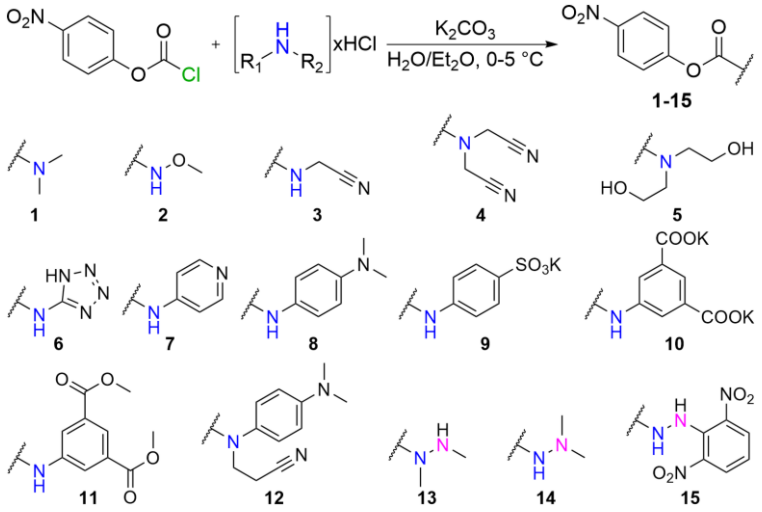
4 pav. Substratų hidrolizės proceso koordinačių diagrama.

Tačiau, apskaičiavus reakcijos barjerų energijas buvo pastebėta, kad barjerai buvo neproporcingai maži (3,6-8,7 kJ mol^{-1}), o esteryje esančios alkoholių grupių įtaka buvo beveik nereikšminga. Šie rezultatai tiesiogiai prieštaravo eksperimentiniams pastebėjimams. Pagrindine šių neatitikimų priežastimi buvo identifikuotas nepakankamas solvatacinio modelio efektas (Boereboom et al., 2018).

Karbamatų ir karbazatų substratai

Karbamato funkcinę grupę sudaro alkolis ir aminas sujungtas per karbonilą – RO-C(O)-NR. Karbazatas yra analogiška grupė, tačiau vietoje amino yra hidrazinas – RO-C(O)-NRNR. Karbonilo grupė šiuose junginiuose turi panašią geometriją kaip karbonatuose, tačiau ženkliai kitokį elektroninį tankį dėl amino (hidrazino) donorinių savybių. Tai suteikia šiems junginiams didesnį stabilumą ir atsparumą hidrolizei. Šiame tyrime buvo susintetinti 12 karbamatų ir 3 karbazatai, pasitelkiant *O*-(*p*-nitrofenilo) chloroformatą (**Lentelė 2**). Iš jų, 5 junginiai suskilo ore po jų išskyrimo, kiti 5 greitai hidrolizavosi pH 7,5 buferyje ir vienas buvo netirpus organiniuose tirpikliuose bei vandeninėje terpėje. Likusieji 4 junginiai (antrinis, du tretiniai karbamatai ir karbazatas) testuoti reakcijoje su bCAII. Nei vieno iš šių junginių hidrolizė nebuvo katalizuojama fermento, todėl tyrimai su karbamatais ir karbazatais nebuvo tęsiami.

Lentelė 2. Karbamatų ir karbazatų sintezės, išskyrimo, stabilumo ir katalizės rezultatai.



Junginys	Sintezė	Stabilumas ore	Stabilumas pH 7.5[a]	bCAII katalizė[b]
1	+	-	nt.	nt.
2	+	+	+	-
3	+	+	-	nt.
4	+	+	+	-
5	+	-	nt.	nt.
6	+	+	-	nt.
7	+	-	nt.	nt.
8	+	+	-	nt.
9	+	-	nt.	nt.
10	+	+	nt.[c]	nt.
11	+	+	-	nt.
12	+	+	+	-
13	+	+	-	nt.
14	+	-	nt.	nt.
15	+	+	+	-

nt. – netestuota.
[a] 0.5 mM junginio, 1 % DMSO, 10 mM Tris-HCl, λ 400 nm, 20 °C, 30 min.
[b] Taip pat kaip stabilumo stebėjime papildyta 1 mg ml^{-1} bCAII.
[c] Netirpus organiniuose tirpikliuose ir vandeninėje terpėje.

Karboksirūgščių esterių substratai

Karboksilo rūgščių esteriai yra gerai žinomi kaip CA substratai ir yra taikomi įvairiuose šių fermentų tyrimuose. Pagrindinis naudojamas junginys yra *p*-nitrofenil acetatas (pNPA) nes yra komerciškai prieinamas ir publikuota daugybė protokolų. Tačiau, jis yra nespecifinis CA substratas ir katalizuojamas daugybės kitų fermentų (Babinskas et al., 2026). Taip pat, jo

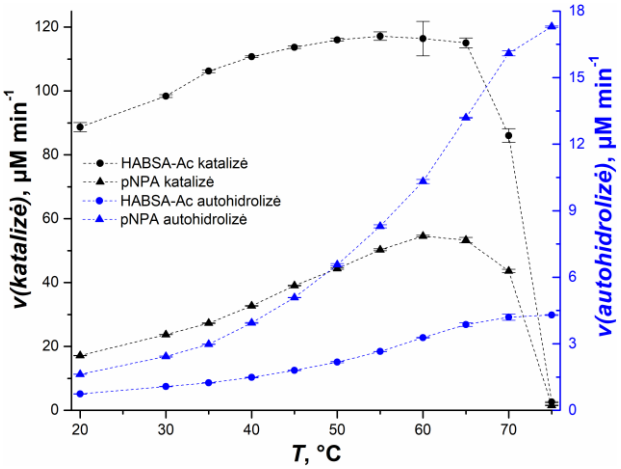
tirpumas vandenyje ir terminis stabilumas apriboja kai kuriuos tyrimus; pvz., CA katalizinių reakcijų greičių tyrimus aukštesnėse temperatūrose.

Šiame tyrime buvo pasirinkta atlikti HABSA acetilinimą ir ištirti jo veikimą bCAII katalizuojamoje hidrolizėje. Dažo acetilinimas atliktas su acto anhidridu, gaunant HABSA-Ac su 70 % išeiga. Išmatavus šio junginio spektroskopines savybes ties pH 8,5 nustatyta, kad jo molinis ekstinkcijos koeficientas ties 428 nm buvo 1,3 mM cm^{-1}, kuomet HABSA – 17,5 mM cm^{-1}. Tai parodė, kad substrato absorbcija tokiomis pačiomis sąlygomis buvo daugiau nei 10 kartų mažesnė negu atpalaiduojamo dažo. Įvertinus HABSA-Ac tirpumą vandenyje, buvo pasirinkta šį junginį ruošti DMSO tirpiklyje dėl didelio tirpumo. Fermentinėje reakcijoje šio tirpalo buvo įdedamas mažas kiekis (1 %) į buferį, išvengiant ženklaus organinio tirpiklio poveikio fermentui. Įvertinus HABSA-Ac stabilumą DMSO tirpiklyje buvo nustatyta, kad žemiau 80 °C substrato skilimas nebuvo aptinkamas iki 3 dienų.

HABSA-Ac metodo kūrimą CA aktyvumo matavimams sudarė keturi etapai: 1) optimalios substrato koncentracijos nustatymas; 2) buferio tipo ir jo koncentracijos parinkimas; 3) matavimų trukmės įvertinimas; ir 4) fermento kiekio minimalizavimas. Pagal žinomą HABSA-Ac molinį ekstinkcijos koeficientą ir atlikus UV-Vis spektroskopiją, optimalia substrato koncentracija buvo pasirinkta 0,2 mM, naudojant 1 cm kiuvetę. Stebint substrato hidrolizę, katalizuojamą bCAII skirtinguose 10 mM buferiuose (Tris-HCl, 2-amino-2-metil-1,3-propandiolio ir natrio borato), reakcijos greičiai buvo panašūs, kuomet dietanolamino buferyje reakcija buvo ženkliai lėtesnė. Kadangi Tris-HCl buferis yra tinkamas ir plačiai naudojamas CA tyrimuose, pasirinkta jį naudoti ir HABSA-Ac aktyvumo matavimo metode. Keičiant buferio koncentraciją 10-200 mM ruože, bCAII aktyvumo maksimumas pasiektas ties 150 mM koncentracija. HABSA-Ac hidrolizę atliekant nuo 1 iki 20 minučių, 3 minutės buvo pakankama laiko trukmė gauti kokybišką tiesinį absorbcijos pokytį per laiką. Testuotos fermento koncentracijos buvo 10-0,1 μg ml^{-1} ruože (reakcijos mišinyje). Rezultatai parodė, kad su 1 μg ml^{-1} bCAII buvo pasiekta metodo kiekybinio įvertinimo riba, o su 0,1 μg ml^{-1} – aktyvumo aptikimo riba. Tolimesniuose tyrimuose, kaip reakcijos koncentraciją, pasirinkta naudoti 10 μg ml^{-1} bCAII (0,344 μM). Taigi, optimalios karboanhidrazinio aktyvumo matavimų su HABSA-Ac sąlygos buvo tokios: 0,2 mM substrato, 1 % DMSO, 150 mM Tris-HCl pH 8,5 buferis ir 10 μg ml^{-1} fermento, reakciją stebint 428 nm bangos ilgyje 3 minutes, 20 °C temperatūroje. Vienas fermentinio aktyvumo vienetas (1 U) buvo apibrėžtas kaip 1 μmol HABSA sudarymas per 1 minutę, esant pH 8,5 ir 20 °C.

HABSA-Ac taikymo tyrimai

Pagrindinis klasikinio CA substrato pNPA trūkumas yra jo limituotas termostabilumas vandeninėje terpėje. Siekiant ištirti ar HABSA-Ac pasižymi geresnėmis savybėmis, buvo atliktas autohidrolizės ir bCAII katalizuojamos reakcijos greičių priklausomybės nuo reakcijos temperatūros stebėjimas, 20-75 °C intervale. Palyginimui, matavimai buvo atlikti analogiškai su pNPA: 0,2 mM substrato; 1 % DMSO 150 mM Tris-HCl pH 8,5 buferis; stebima 400 nm absorbcijos pokytis 3 minutes (**5 pav.**).



5 pav. HABSA-Ac ir pNPA autohidrolizės ir katalizės greičių priklausomybė nuo temperatūros (reakcijos sąlygos: 0,2 mM substrato; 150 mM Tris-HCl pH 8,5; 0.344 µM bCAII).

Rezultatai pademonstravo, kad HABSA-Ac katalizinės hidrolizės greitis buvo ženkliai didesnis negu pNPA. Tuo tarpu, HABSA-Ac autohidrolizės greitis buvo mažesnis ir keliant temperatūrą didėjo, bet ne taip drastiškai kaip pNPA. Reakcijų greičių priklausomybės nuo temperatūros duomenys buvo panaudoti apskaičiuojant termodinaminius parametrus remiantis Arenijaus ir pereinamosios būsenos teorijomis (TST) – pateikta **Lentelėje 3**. Šios analizės parodė, kad HABSA-Ac autohidrolizės greičio konstanta (k_{obs}) buvo mažesnė 10^1 eile, negu pNPA. Tai patvirtino, kad pNPA pasižymi didesniu autohidrolizės greičiu negu HABSA-Ac. Fermentinės katalizės atveju,

Lentelė 3. Iš Arenijaus ir TST gautų parametrų suvestinės.

Arenijaus analizė	Substratas	$E_{a,obs}$, kJ mol^{-1}	ΔH_{obs}, kJ mol^{-1}	k_{obs}, s^{-1} [a]	k_{cat}/K_M, M^{-1} s^{-1} [a]
Autohidrolizė	HABSA-Ac	28,1 ± 1,3	25,6 ± 1,3	(6,34 ± 0,85) × 10^{-5}	
	pNPA	37,6 ± 0,8	35,1 ± 0,8	(1,30 ± 0,02) × 10^{-4}	
Katalizė	HABSA-Ac	6,22 ± 0,86	3,78 ± 0,86		2251 ± 796
	pNPA	25,3 ± 0,5	22,9 ± 0,5		409 ± 78

TST analizė	Substratas	$\Delta H^{\ddagger}_{obs}$, kJ mol^{-1}	$\Delta S^{\ddagger}_{obs}$, J mol^{-1}	$\Delta G^{\ddagger}_{obs}$, kJ mol^{-1} [a]	k_{obs}, s^{-1} [a]	k_{cat}/K_M, M^{-1} s^{-1} [a]
Autohidrolizė	HABSA-Ac	25,2 ± 1,3	-239 ± 22	95,3 ± 6,6	(6,43 ± 0,45) × 10^{-5}	
	pNPA	32,4 ± 0,8	-185 ± 36	86,7 ± 10,5	(2,22 ± 0,27) × 10^{-3}	
Katalizė	HABSA-Ac	3,70 ± 0,87	-168 ± 16	53,0 ± 4,7		2249 ± 26
	pNPA	22,1 ± 0,4	-119 ± 2	57,1 ± 0,8		413 ± 4

[a] T = 293.15 K (20 °C).

termodinaminė analizė pateikė specifiškumo konstantas (k_{cat}/K_M), kurios buvo 409-413 M s^{-1} ir 2251-2249 M s^{-1}, atitinkamai pNPA ir HABSA-Ac.

Sekanti tirta HABSA-Ac taikymo sritis buvo fermentų kinetinių parametrų nustatymas. Šiame tyrime bCAII kataliziniai greičiai buvo matuojami substrato koncentraciją keičiant nuo 0,1 mM iki 1,0 mM. Iš gautų duomenų kinetiniai parametrai buvo suskaičiuojami, taikant tiesinius Michaelis-Menten skaičiavimo metodus: Linewear-Burk (L-B), Eadie-Hofstee (E-H), Hanes-Wolf (H-F); ir Eisenthal-Cornish-Bowden (E-C-B) – **Lentelė 4**.

Lentelė 4. bCAII kataliuojamos HABSA-Ac hidrolizės kinetiniai parametrai.

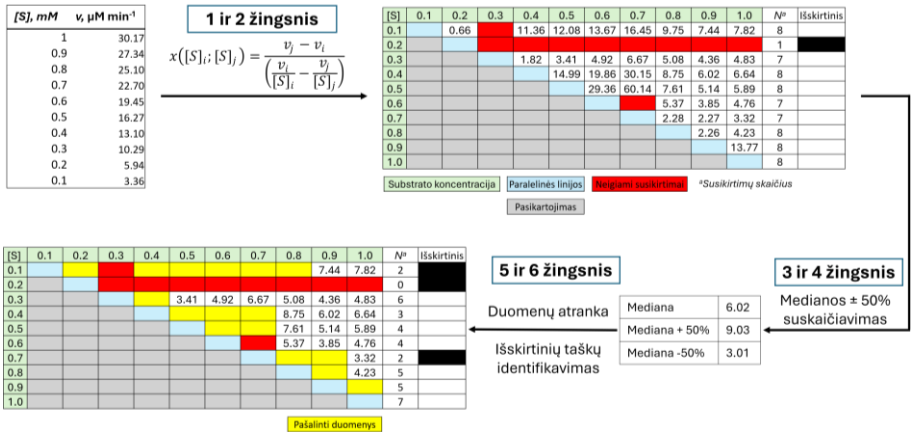
Kinetinis parametras	L-B	E-H[b]	H-W[c]	E-C-B
K_M, mM	37,1 ± 28,2	3,03 ± 0,30	12,5	9,5 ± 1,8
V_{max}, µM min^{-1}	1314 ± 1013	117 ± 10	416	334 ± 62
k_{cat}, s^{-1}	63,7 ± 49,1	5,7 ± 0,5	20,1	16,2 ± 3,0
k_{cat}/K_M, M^{-1} s^{-1} [a]	1675 ± 33	1860 ± 9	1614	1697 ± 24

[a] Vidurkis ir paklaidos buvo apskaičiuotos naudojant individualius k_{cat}/K_M rezultatus.
[b] Matavimo Nr. 3 kinetiniai parametrai buvo neigiami.
[c] Matavimo Nr. 2 ir Nr. 3 kinetiniai parametrai buvo neigiami.

Duomenys parodė, kad k_{cat}/K_M buvo pakankamai panašūs tarp visų metodų, tačiau kiti kinetiniai parametrai skyrėsi ženkliai. Tai ypač matėsi L-B metodo rezultatuose nes vienas iš trijų matavimų buvo nukrypęs, todėl iškreipė vidurkį ir standartinių paklaidų intervalą. Gauti parametrai taip pat pademonstravo, kad aukščiausia testuota ir galima HABSA-Ac koncentracija (1 mM) buvo ženkliai žemesnė negu K_M. Dėl šios priežasties, matavimo paklaidos turėjo itin reikšmingą efektą duomenų analizėje. Siekiant pagerinti duomenų kokybę ir identifikuoti klaidingus matavimus, buvo sudarytas *ad hoc* statistinis metodas kinetinių matavimų kokybės vertinimui.

E-C-B analizės metodas yra paremtas principu, kad per taškus ($-[S]_i$;0) ir (0;v_i) galima nubrėžti tiesę, kurios visi taškai koordinačių plokštumos kvadrate I duoda visas K_M ir V_{max} kombinacijas, tenkinančias Michaelio-Menten lygtį. Atidedant tieses iš matavimų su skirtingomis substrato koncentracijomis, idealiu atveju, jos susikerta taške (K_M; V_{max}), kuris atitinka kinetinius parametrus tenkinančius visus matavimus. Realiuose eksperimentuose tiesių susikirtimai yra išsibarstę, todėl jų mediana geriausiai

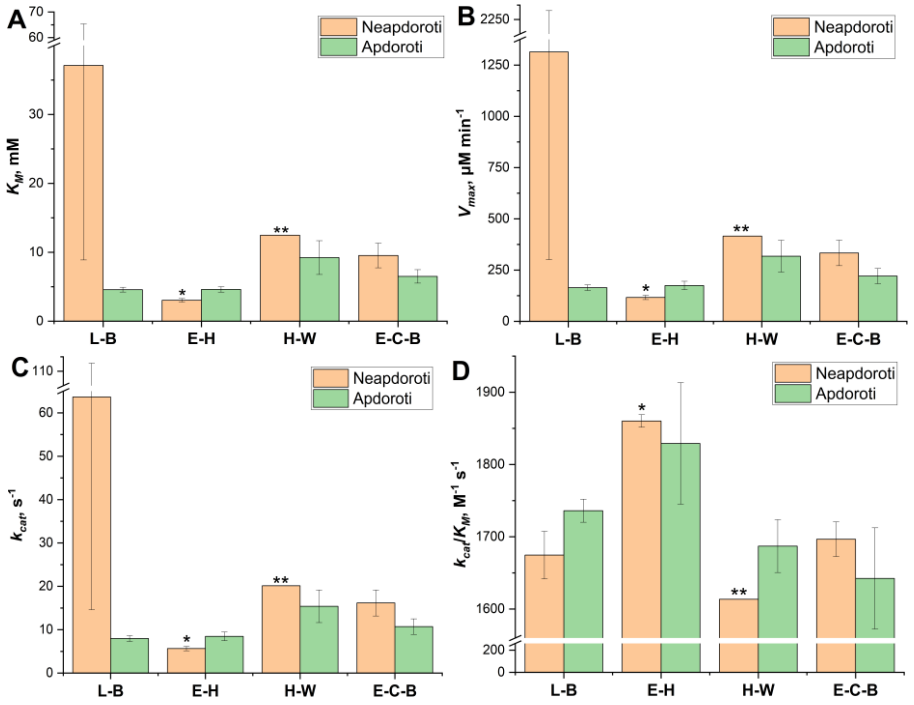
atspindi analizės rezultatus. Remiantis tuo, jeigu vienos tiesės susikirtimo taškai yra labiau nukrypę nuo likusiųjų, galima įtarti, kad šis matavimas buvo klaidingas arba mažiau tikslus. Šis blogų matavimų identifikavimas yra taikomas vizualiai analizuojant grafiką, tačiau šiame darbe buvo atliktas šio principo formalizavimas ir automatizavimas. Tai buvo atlikta apibrėžiant rodiklius, kurie skaitiškai įvertina matavimus, sudarant paprastą algoritmą leidžiantį duomenis analizuoti pasitelkiant eilinę programinę įrangą. Išskirti du rodikliai, leidžiantys keisti ribas pagal kurias matavimai priskiriami potencialiai klaidingiems. Tai suteikia galimybę duomenų atranką kontroliuoti atsižvelgiant į turimą duomenų kokybę (**Schema 7**).



Schema 7. Siūlomas potencialiai klaidingų matavimų identifikavimo algoritmas.

Pasiūlytą algoritmą sudarė septyni žingsniai. 1 žingsnis – apskaičiuojamos susikirtimų taškų *x*-koordinatės pagal pateiktą formulę arba rankiniu būdu. 2 žingsnis – susikirtimų taškų *x*-koordinatės sudedamos į lentelę. Neigiamos reikšmės neįtraukiamos nes jos neturi fizikinės prasmės. Taip pat, dėl susikirtimų simetrijos neįtraukiamos pasikartojančios reikšmės. 3 žingsnis – suskaičiuojama susikirtimų *x*-koordinačių mediana. 4 žingsnis – pasirenkama susikirtimo taškų išsibarstymo riba. Ši reikšmė parodo ribą už kurios nuo medianos nutolę susikirtimo taškai priskiriami potencialiai klaidingam matavimui. Schemoje pateikiama kaip ± 50 % nuo medianos reikšmės, tačiau galima keisti pagal poreikį. 5 žingsnis – duomenų atranka. Susikirtimo taškų reikšmės, nepatenkančios į pasirinktą išsibarstymo ribą, pašalinamos iš lentelės. 6 žingsnis – pasirenkama matavimų patikimumo riba. Ji apibrėžia kiek linija einanti per $(-[S]_i;0)$ ir $(0;v_i)$ porą turi turėti susikirtimų su kitomis linijomis, kad būtų priskiriama teisingam matavimui. Schemoje pateiktame pavyzdyje buvo naudota 25 %, t.y. nuo daugiausiai galimų 9 susikirtimų, linijos su 2 arba mažiau susikirtimų buvo priskirtos išskirtinėms reikšmėms –

klaidingas matavimas. 7 žingsnis (neparodytas) – perskaičiuojami kinetiniai parametrai, neįtraukiant matavimų priskirtų išskirtinėms reikšmėms. Remiantis pateiktu algoritmu, buvo atlikta bCAII katalizuojamos HABSA-Ac hidrolizės duomenų apdorojimas ir perskaičiuoti kinetiniai parametrai (**6 pav.**).

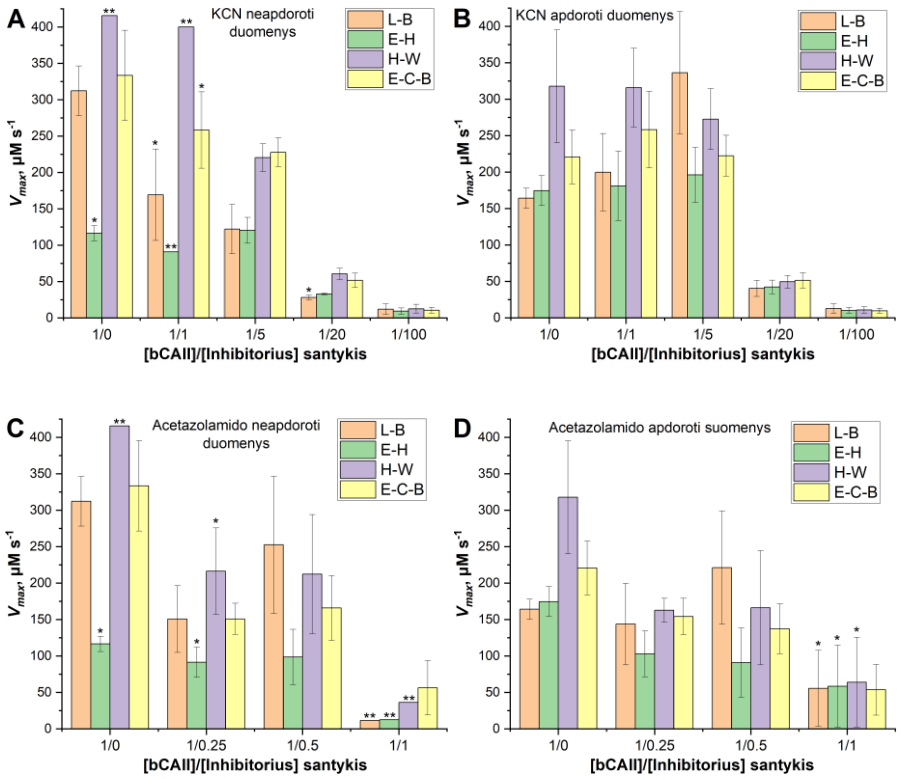


6 pav. Apskaičiuoti kinetiniai parametrai naudojant neapdorotus ir neįtraukus išskirtinių reikšmių (apdoroti) duomenis. **A** – K_M; **B** – V_{max}; **C** – k_{cat}; **D** – k_{cat}/K_M. Žvaigždutės (* ir **) žymi analizės neigiamų rezultatų skaičių.

Iš termodinaminių duomenų gautos specifiškumo konstantos buvo didesnės, galimai, dėl paklaidų arba fundamentiškai kitokio teorinio modelio. Palyginimui, bCAII substrato pNPA (50 mM Tris-HCl pH 8,0) atpažinimas yra panašus (K_M 8,9 mM), tačiau katalizės reakcija lėtesnė ir ne tokia efektyvi – k_{cat} 3,56 s^{-1} ir k_{cat}/K_M 399,8 M^{-1} s^{-1}. Iš esmės, šie rezultatai pademonstravo, kad pasiūlytas algoritmas padidina kinetinių parametrų tyrimų duomenų patikimumą.

HABSA-Ac metodo validacija buvo tęsiama, atliekant bCAII inhibicijos tyrimus su gerai žinomais inhibitoriais – kalio cianidu (KCN) ir acetazolamidu. Eksperimentų metu fermentas buvo inkubuojamas 30 min su įvairiais fermento ir inhibitoriaus ([bCAII]/[inhibitorius]) moliniais santykiais, išmatuojami katalizės greičiai keičiant HABSA-Ac koncentraciją 0,1-1,0 mM ruože ir apskaičiuojami kinetiniai parametrai. Iš neapdorotų ir

apdorotų duomenų maksimalūs katalizės greičiai (V_{max}) su abejais inhibitoriais pateikti **7 pav**.



7 pav. V_{max} priklausomybė nuo fermento ir inhibitoriaus molinių santykių, suskaičiavus naudojant L-B, E-H, H-W ir E-C-B metodais su neapdorotais ir apdorotais duomenimis: **A** – KCN inhibicijos rezultatai su neapdorotais duomenimis; **B** – KCN inhibicijos rezultatai su apdorotais duomenimis; **C** – acetazolamido inhibicijos rezultatai su neapdorotais duomenimis; **D** – acetazolamido inhibicijos rezultatai su apdorotais duomenimis. Santykis 1/0 – neinhibuotas bCAII (kontrolė). Žvaigždutės (* ir **) žymi analizės neigiamų rezultatų skaičių.

Tyrimo rezultatai parodė, kad duomenų apdorojimas pagerino rezultatų kokybę – visi kinetinių parametrų rezultatai, išskyrus 1:1 [bCAII]/[Acetazolamidas], davė teigiamus rezultatus. Iš surinktų duomenų buvo sudaryti Dixon ir Cornish-Bowden (C-B) grafikai siekiant patvirtinti inhibicijos mechanizmus bei nustatyti konstantas. Gauti rezultatai apibendrinti **Lentelėje 5**. Iš grafikų gautos inhibicijos konstantos, bei tiesių susikirtimo padėtys patvirtino, kad bCAII ir HABSA-Ac reakciją KCN inhibavo per mišraus tipo mechanizmą, kuomet acetazolamidas veikė pagal nekonkurencinį inhibicijos mechanizmą. Taip pat, buvo pastebėta, kad duomenų apdorojimas neigiamai veikė konstantų patikimumą, išskyrus KCN su C-B metodu. Suskaičiuotos inhibicijos konstantos yra ganėtinai panašios į

Lentelė 5 Inhibicijos konstantos suskaičiuotos iš neapdorotų ir apdorotų duomenų, naudojantis Dixon ir C-B grafikais.

	KCN		Acetazolamidas	
	Neapdoroti	**Apdoroti**	**Neapdoroti**	**Apdoroti**
Dixon grafikas (K_i), μM	3.00 ± 0.14	3.44 ± 0.60	0.105 ± 0.002	0.081 ± 0.035
C-B grafikas (K_i'), μM	0.88 ± 1.12	1.05 ± 0.58	0.104 ± 0.073	0.254 ± 0.864

žinomas literatūroje (Pocker and Stone, 1967, 1968), tačiau dėl HABSA-Ac metodo sąlygų neatitikimo su publikuotais darbais, pilno palyginimo nebuvo galima atlikti. Apibendrinant, atlikti kinetinių parametrų bei inhibicijos tyrimai pademonstravo, kad HABSA-Ac yra puikiai tinkamas substratas CA biocheminių savybių tyrimams. Taip pat, sukurtas algoritmas biokatalizinių reakcijų greičių duomenų apdorojimui pademonstravo puikius rezultatus ir leido susiaurinti rezultatų neapibrėžtumus, gaunamus taikant skirtingas Michaelio-Menten lygties linerizacijas. Tačiau, šių eksperimentų metu buvo identifikuotas ir papildomi trūkumai. Algoritmas buvo išbandytas substrato koncentracijai esant ženkliai žemiau K_M. Siekiant suprasti ar duomenų apdorojimas yra tinkamas visais atvejais, reikia išbandyti daugiau duomenų rinkinių. Taip pat, susikirtimo taškų bei išskirtinių taškų atrinkimo ribos lieka priklausomos nuo pradinių duomenų kokybės ir matavimų skaičiaus, t.y. nuo tiriamų substratų koncentracijų kiekio. Nepaisant šių apribojimų, pasiūlytas algoritmas parodė didelį potencialą duomenų kokybės pagerinime ir toliau jį vystant gali tapti puikiu įrankiu fermentų funkcinės analizės tyrimuose.

HABSA-Ac, *p*-nitrofenilo acetato ir indoksilo acetato metodų palyginimas

Substratų selektyvumas yra vienas iš esminių rodiklių vertinant fermentų aktyvumo matavimo metodus. Todėl, siekiant įvertinti HABSA-Ac, buvo pasirinkta atlikti aktyvumo matavimus su 9 baltymais, bei palyginti rezultatus gautus su kitais dviem esterazinio aktyvumo metodais – pNPA ir indoksilo acetatu (Indoksil-Ac) (**Lentelė 6**). Metodų palyginimas atskleidė, kad HABSA-Ac autohidrolizė buvo lėtesnė nei pNPA, bet greitesnė nei Indoksil-Ac. Reakcijos su BSA, dvejomis *Pseudomonas aeruginosa* CA (psCA1 ir psCA2) HABSA-Ac hidrolizė buvo žemiau patikimo aptikimo ribos (< 0,1 μM min^{-1}). Žmogaus CA IX (hCAIX), kuri yra žinoma dėl savo žemo esterazinio aktyvumo, HABSA-Ac ir Indoksil-Ac katalizinės hidrolizės greičiai buvo panašūs. Lipazės (LPS L ir Lipolase 100L) bei lizofosfolipazė Finizym W prasčiausiai katalizavo HABSA-Ac hidrolizę – fermento kiekiai buvo padidinti net 10 kartų, kad pavyktų adekvačiai įvertinti reakcijos greičius. Nespecifinė esterazė iš *Bacillus subtilis* efektyviai katalizavo visus substratus, ypač Indoksil-Ac.

Lentelė 6. Reakcijų greičiai (μM min^{-1}) gauti naudojant HABSA-Ac, pNPA ir Indoksil-Ac metodus.

	Metodas (v, μM min^{-1})		
Fermentas/kontrolė	**HABSA-Ac**	**pNPA**	**Indoksil-Ac**
Autohidrolizė	0,76	1,67	0,37
BSA[a]	0,02	0,04	0,28
bCAII[a]	6,21	1,21	0,20
Esterazė[a]	35,3	41,2	298,6
hCAIX[a]	1,38	0,67	1,65
psCA1[a]	0,05	0,27	0,37
psCA2[a]	0,06	0,33	0,33
LPS L[a]	2,20[b]	39,75	61,84
Lipolase 100L[a]	1,88[b]	6,29	221,45
Finizym W[a]	0,12[b]	0,83	0,83

[a] Substrato autohidrolizės greitis atimtas.
[b] Baltymų koncentracija buvo 10 kartų didesnė nei pNPA ir Indoksil-Ac reakcijose.

Apibendrinant, HABSA-Ac pademonstravo vidutinį jautrumą autohidrolizei, didelį selektyvumą CA ir žemus reakcijos greičius su lipazėmis. Deja, reakcija su nespecifine esteraze rodo, kad šis junginys nėra išskirtinai CA substratas, bet tai nesumažina jo vertės ir pasirinkimo kaip substrato karboanhidrazių katalizinių savybių tyrimuose, ypač aplinkos mėginiuose.

IŠVADOS

1. Ferbaminas buvo identifikuotas kaip chemiškai stabilus substratas lakazės tyrimams, pasižymintis dideliu stabilumu švelniai rūgštinėje aplinkoje (pH ≤ 6,0) ir labiau veikiamas buferio sudėties negu inkubacijos temperatūros.
2. Ferbaminas buvo sėkmingai patvirtintas kaip kokybinis substratas lakazės atrankai, leidžiantis patikimai aptikti lakazės aktyvumą grybų baltymų ekstraktuose ir laukinio tipo mikroorganizmų kolonijose.
3. Buvo susintetinti keturi fenolio azodažai su tinkamomis fizikocheminėmis ir spektroskopinėmis savybėmis, suteikiantys pagrindą fermentų substratų kūrimui.
4. Buvo sukurta transkarbonizacija pagrįsta sintezės strategija gauti simetriniams fenolio azodažų karbonato esteriams ir leidžianti sintetinti substratus minimaliai optimizuojant reakcijos sąlygas.
5. Fenil tionochloroformiato naudojimu paremta sintezė buvo identifikuota kaip vienintelė efektyvi tikslinio tiokarbonato esterio substrato gavimo strategija.
6. Naudojantis kinetikos-inhibicijos tyrimais buvo pademonstruota, kad karbonato ir tiokarbonato esterio substratai yra netinkami karboanhidrazių aktyvumui tirti dėl nespecifinių reakcijų su nukleofilinėmis aminorūgščių liekanomis.
7. Buvo sukurtas ir patvirtintas naujas spektrofotometrinis HABSA-Ac metodas karboanhidrazės funkciniam charakterizavimui, pasižymintis silpnesnesnėmis nespecifinėmis ir katalizines sąveikomis su netiksliniais fermentais bei 4.7 ir 218-kartų didesnį jautrumą negu įprasti *p*-nitrofenilacetato ir indoksilo acetato metodai.

ACKNOWLEDGEMENTS

First of all, I would like to thank my family and friends very much for their unwavering support throughout this ordeal. I do not think I could have made it without your constant questions, such as “So, what do you do?” “When are you going to defend your thesis?” and “Where can you get a job after you finish your studies?”

Secondly, this whole thing would have not been possible without my supervisor, Dr. Inga Matijošytė. She took me under her wing early in my bachelor years, and I could not be more proud to still be part of the Sector of Applied Biocatalysis. And of course, this extends to colleagues and students in our sector, who taught and scolded me on how to work as a team and for all the fun activities we have done.

And lastly, I want to thank local and international collaborators: Jokūbas Krutkevičius for work on genome sequencing and analysis; Dr. Aivaras Vaškevičius for performing NMR spectroscopy and countless hours of discussion; Dr. Andrius Sakalauskas for HPLC analysis and consultations; Martynas Malikėnas for LC-HRMS analysis; Tautvydas Kojis and Dr. Lina Baranauskienė for donating carbonic anhydrase samples; Dr. Jerica Sobtič for donating a collection of fungi protein extracts; Dr. Lada Lukić Bilela for inviting me to the Balkans and introducing the wonders of caves and speleology; and everyone else for their informal contributions – thank you!

LIST OF PUBLICATIONS

1. **Babinskas J.**, Matijošytė I. A selective phenyl azo acetate substrate for enhanced carbonic anhydrase functional analysis. *Analytical Science Advances*, **2026**, 7, e70091. DOI: 10.1002/ansa.70091
2. **Babinskas J.**, Kojis T., Gaubė I., Baranauskienė L., Matijošytė I. Functional analysis of carbonic anhydrases: comparative methods for hydration and hydrolysis activity. *Biocatalysis and Agricultural Biotechnology*, **2026**, 74, 104077. DOI: 1016/j.bcab.2026.104077
3. **Babinskas J.**, Krutkevičius J., Lukić Bilela L., Bešta-Gajević R., Matijošytė I. Potential of subterranean microbes: High-throughput screening for industrially relevant enzymatic activities in Dinaric caves. *MicrobiologyOpen*, **2025**, 14, 1. DOI: 10.1002/mbo3.70146
4. **Babinskas J.**, Matijošytė I. Laccase functional analysis: Substrates, activity assays, challenges, and prospects. *ChemBioChem*, **2025**, 26, e202400939. DOI: 10.1002/cbic.202400939
5. **Babinskas J.**, Sabotič J., Matijošytė I. Synthesis and application of phenazine class substrate for high-throughput screening of laccase activity. *Applied Microbiology and Biotechnology*, **2024**, 108 (66), 1-12. DOI: 10.1007/s00253-023-12958-7

Other publications:

1. Daunoraitė D., N.R. de Souza N. R. D., **Babinskas J.**, Cherubini F., Vares L., Matijošytė I. Unlocking nature's sweet secret for citric acid production from wood sugars: Evaluation of microbial strains and environmental impacts. *Journal of Cleaner Production*, **2024**, 467, 142914. DOI: 10.1016/j.jclepro.2024.142914

CONFERENCE LIST

Oral presentations (presenter)

1. **Babinskas J.**, Kojis T., Ožiūnaitė I., Baranauskienė L., Matijošytė I. BioCarbonates: Investigation of enzymatic carbonate synthesis and applications. *ESAB E-Congress 2024*, Online.
2. **Babinskas J.** From Lab to caves: Exploring high-throughput screening method for laccase activity. *Final Ocean4Biotech conference in Riga*, 2024, Riga, Latvia.

Oral presentations (co-author)

1. Lukić Bilela L., Bešta Gajević R., Matijošytė I., Krutkevičius J., **Babinskas J.**, Calvalho Maria F. Subterranean habitats of the dinaric karst: Biodiversity treasure leads to biotechnological challenges. *WEPSD 2023*, Tirana, Albania.
2. Matijošytė I., **Babinskas J.**, Sabotič J., Lukić Bilela L., Daunoraitė D., Krutkevičius J. Discovery of biocatalyst and the paths for their identification. *ABMBBIH Conference 2023*, Sarajevo, Bosnia and Herzegovina.

Poster presentations (presenter)

1. **Babinskas J.**, Kojis T., Gaubė I., Baranauskienė L., Matijošytė I. A new phenyl azo acetate substrate for spectrophotometric investigation of thermostable carbonic anhydrases. *RRB 2026*, Leuven, Belgium.
2. **Babinskas J.**, Paulauskaitė M., Matijošytė I. Investigation of novel lignocellulosic feedstock pre-treatment & fractionation method. *RRB 2023*, Riga, Latvia.
3. **Babinskas J.**, Sabotič J., Matijošytė I. Ferbamine – novel substrate for the functional analysis of the famous laccases. *OxiZymes 2022*, Siena, Italy.
4. **Babinskas J.**, Sabotič J., Matijošytė I. Stability and toxicity investigation of a novel aromatic amine for laccase screening on high-throughput agar plates. *Open Readings 2022*, Vilnius, Lithuania (Online).
5. **Babinskas J.**, Sabotič J., Matijošytė I. Synthesis and investigation of a novel aromatic amine for laccase activity screening on high-throughput agar plates. *Biotrans 2021*, Graz, Austria (Online).
6. **Babinskas J.**, Sabotič J., Matijošytė I. Synthesis and investigation of oligomerized aromatic amine for laccase activity assay. *Open Readings 2021*, Vilnius, Lithuania (online).

Poster presentations (co-author)

1. Matijošytė I., **Babinskas J.** Novel phenyl azo acetate substrate for spectrophotometric activity assay of carbonic anhydrase. *Biotrans 2025*, Bazel, Switzerland.
2. Gaubė I., Kojis T., Lukauskaitė E., **Babinskas J.**, Baranauskienė L., Matijošytė I. Biocarbonates: Recombinant β-carbonic anhydrases for enzymatic synthesis of cyclic carbonates. *Biotrans 2025*, Bazel, Switzerland.
3. Matijoštė I., Gaubė I., **Babinskas J.**, Gallucci A. M. Development and application of sustainable fractionation approaches for beach wrack biomass. *ECMNP 2025*, Piran, Slovenia.
4. Valaitis K., **Babinskas J.**, Matijošytė I. Investigation of lipase imobilisation by cross-linked enzyme aggregate (CLEA) method. *OpenReadings 2024*, Vilnius, Lithuania.
5. Valaitis K., **Babinskas J.**, Matijošytė I. Tailor-made modifications for enzyme immobilisation using the CLEA method. *The COINS 2024*, Vilnius, Lithuania.
6. Paulauskaitė M., **Babinskas J.**, Matijošytė I. Investigation of deep eutectic solvents for lignocellulosic biomass pre-treatment. *OpenReadings 2023*, Vilnius, Lithuania.
7. Matijošytė I., Vares L., Dias de Souza N. R., **Babinskas J.**, Daunoraitė D. Citric acid production from wood sugars: Fermentation and LCA. *Biotrans 2023*, La Rochelle, France.
8. Paulauskaitė M., **Babinskas J.**, Matijošytė I. Investigation of cellulase thermal stability in deep eutectic solvents. *The COINS 2023*, Vilnius, Lithuania.
9. Vaitkus L., **Babinskas J.**, Matijošytė I. Why bother with carrier? Enzyme immobilisation *via* simple carrier-free method. *The COINS 2021*, Vilnius, Lithuania (Online).

CURRICULUM VITAE

Education

- 2020.10 – 2024.09 **Doctoral studies** (Chemical Engineering T005), Sector of Applied Biocatalysis, Institute of Biotechnology, Life Sciences Center, Vilnius University.
- 2018.09 – 2020.06 **Chemistry Master** studies (Thesis: *Synthesis and investigation of substrates for laccase functional analysis*), Faculty of Chemistry and Geosciences, Vilnius University.
- 2014.09 – 2018.06 **Chemistry Bachelor** studies (Thesis: *Investigation of laccase substrate oxidation at T1 Cu site by quantum chemistry methods*), Faculty of Chemistry and Geosciences, Vilnius University.

Work and project experience

- 2025.10 – Current **Investigator** at Sector of Applied Biocatalysis, Institute of Biotechnology, Life Sciences Center, Vilnius University.
- 2024.10 – Current **Junior researcher** at Sector of Applied Biocatalysis, Institute of Biotechnology, Life Sciences Center, Vilnius University in LMT MIP project "BioCarbonates: Investigation of Enzymatic Carbonate Synthesis and Applications " Lithuanian Research Council, ^{13}th Call for the Implementation of Researcher Groups Projects.
- 2023.10 – 2025.09 **Junior researcher** at Sector of Applied Biocatalysis, Institute of Biotechnology, Life Sciences Center, Vilnius University.
- 2024.01 – 2024.09 **Junior researcher** at Sector of Applied Biocatalysis, Institute of Biotechnology, Life Sciences Center, Vilnius University in HORIZON-CSA project "BIOCONNECT: Developing the Action Plan to Foster Baltic Region Innovation Ecosystem in Biotechnology and Synthetic Biology" funded by HORIZON-EIE-2023-CONNECT-01.
- 2023.03 – 2024.03 **Project specialist** at Sector of Applied Biocatalysis, Institute of Biotechnology, Life Sciences Center, Vilnius University in research project "Novel High-performance Polymers From Lignocellulosic Feedstock" funded by Baltic Research Programme, Research Council of Lithuania.
- 2020.10 – 2023.09 **Investigator** at Institute of Biotechnology, Life Sciences Center, Vilnius University.
- 2018.1 – 2019.08 **Lab assistant** at Sector of Applied Biocatalysis, Institute of Biotechnology, Life Sciences Center, Vilnius University in contractual research project MTS-600000-2032.

Supervision of final thesis works

- Kristupas Valaitis, VU Molecular biotechnology bachelor thesis "Investigation of tailor-made modifications for enzyme immobilisation using the CLEA method“, **2024**.
- Monika Paulauskaitė, VU Biochemistry bachelor thesis "Investigation of chemo-enzymatic method for lignocellulose fractionation“, **2023**.
- Laurynas Vaitkus, VU Biochemistry bachelor thesis "Investigation of lipase precipitation, and its immobilization by CLEA method, and solvent-protein interaction simulation by molecular dynamics“, **2021**.

Educational activities

- 2022.01.04 **Laboratory work for National Student Academy**.
- 2022.09.27, 2023.09.27, 2024.10.02, 2025.04.15, 2025.10.02 **Laboratory work for school children “Enzymatic ester synthesis”**.
- 2022.09.28, 2023.09.27, 2025.09.30, 2025.10.02, 2025.09.30 **Events for European Biotech Week**.
- 2022.09.28, 2023.09.26, 2024.10.03 **Excursion at LSC laboratories**.
- 2022.11.29 **Presentation of polyol technology for VU promotional video "*Advanced material solutions at Vilnius University*"**.
- 2022.10.26, 2023.04.25, 2023.10.27, 2024.10.22, 2025.10.23, 2026.04.21 **Vilnius University program for school children “Studentas vienai dienai”**.
- 2023.06.15-2023.07.13 **Supervision of Aras Kaufmann from Hillsdale College (USA)**.

NOTES

Vilniaus universiteto leidykla
Saulėtekio al. 9, III rūmai, LT-10222 Vilnius
El. p. info@leidykla.vu.lt, www.leidykla.vu.lt
bookshop.vu.lt, journals.vu.lt
Tiražas 15 egz.